Surface aspects of some sulphur-vulcanised elastomers, with particular reference to surface modification, as studied by ESCA

Hayat, Umar

SURFACE ASPECTS OF SOME SULPHUR-VULCANISED ELASTOMERS, WITH PARTICULAR REFERENCE TO SURFACE MODIFICATION, AS STUDIED BY ESCA

by

UMAR HAYAT, B.Sc., M.Sc.
(University of Lancaster)

A candidate for the Degree of Doctor of Philosophy

Department of Chemistry
University of Durham

September 1983

To my parents

****

ACKNOWLEDGEMENTS

I am deeply indebted to my supervisor, Professor D.T. Clark, for his invaluable guidance, encouragement and enthusiasm towards the work of this thesis, and my sincere gratitude is due to him. Equally, sincere thanks are due to my colleagues for their various contributions and continued mental stimulation, in particular to Dr. H.S. Munro (Durham) and Dr. P.J. Stephenson (Canada) for providing limited solid state ^{13}C NMR data.

Gratitude is also expressed to the Science Research Council for the provision of an S.E.R.C./CASE Studentship Award, and to Dr. M.C. Kirkham and Mr. P.J. Corish (Dunlop Limited, Research Centre, Birmingham) for providing samples.

Finally, I would like to thank Mrs. E.M. Nevins for her help in the preparation of some of the figures and Miss J. Eccleston for her great patience and secretarial skill in typing this manuscript.

ABSTRACT

X-ray photoelectron spectroscopy (ESCA) has been used to investigate the surface chemistry of a variety of elastomers, as a function of cure conditions.

The surface composition of thickness on a depth scale in the range < 50Å depends on the cure conditions and the bulk formulations of polyisoprene (Natsyn 2200), styrene/butadiene (Solprene 1204) and acrylonitrile/butadiene (Krynac 34/50) elastomers. In all cases, higher levels of antioxidant and accelerators have been detected at the surface than in the bulk, whilst the level of zinc for Natsyn 2200 and Solprene 1204 systems increases with ESCA depth profile into the bulk. The samples of Krynac 34/50 indicated higher levels of zinc and cadmium in the surface regions and, in one case, the level of zinc at the surface is approximately the same as in the bulk. Zinc and cadmium in the surface regions are predominantly present as sulphides. A use of the 'swelling' data has been made, in conjunction with the ESCA data, to estimate the sulphur functionality.

Particular emphasis has been placed on the elaboration of surface crosslink functionality, using inductively coupled radio-frequency glow discharges, excited in oxygen and hydrogen. Model studies to establish the changes in surface chemistry as a function of reaction time in plasmas have been carrried out in conjunction with the type 1, Natsyn 2200, elastomers. The results show that the reactions with oxygen and hydrogen plasmas are by no means simple. Modification by the oxygen containing plasmas is extensive but confined to the outermost

monolayer or so. The rate and extent of oxidation is a strong function of the initial surface chemistry of the samples. The level of sulphur in di- and trisulphide models is essentially the same before and after oxygen plasma treatments and the tetrasulphide model indicated a loss of sulphur by a factor of two. The optimum cured type 1, Natsyn 2200, sample did not indicate any tendency for a loss of sulphur under comparable conditions. For hydrogen plasmas, the level of sulphur in a disulphide model system remains essentially the same, whereas the trisulphide model and the type 1, Natsyn 2200 systems indicated a loss of sulphur.

A thermal oxidation study has also been carried out on the optimum cured type 1, Natsyn 2200, elastomers and the results are complementary in some respects to oxygen plasma treatments.

Finally, the 'sulphur-vulcanised' elastomers have been treated with the thiol-amine reagents for determining the relative proportion of mono-, di- and polysulphide cross-links but the results are additionally complicated by the incorporation of thiol and amine into the elastomers.

MEMORANDUM

The work described in this thesis was carried out at the University of Durham between October 1980 and September 1983. It has not been submitted for any other degree and is the original work of the author, except where acknowledged by reference.

CONTENTS

CHAPTER ONE

THE CHEMISTRY OF ELASTOMERS

1.1 Introduction

Elastomers have been known for several centuries, but it was only in the early 1800's that the materials gained universal acceptance after the discovery of the vulcanisation process by Goodyear and Hancock.[1] The rubbers were mainly used for domestic purposes such as water-proofing and foot-wear, etc. However, it was never considered to be entirely satisfactory. The rubber had a tendency to melt in the summer, freeze hard in the winter, and develop offensive odours over a relatively short period of time.[1]
(Vulcanisation is a process by which the elastomeric materials are generally prepared. The resulting elastomers retract forcibly to their approximately original length after applied force.)

The rubber materials, developed from the formulation of Goodyear and Hancock, were far from optimum properties that large amounts of sulphur and relatively long curing times were needed. Over-vulcanisation, which results in a marked deterioration of physical properties, was a serious problem. The vulcanisates were highly coloured, prone to sulphur blooming (diffusion of sulphur to the surface), and exhibited poor age resistance. Apart from the many different sulphidic crosslinks, the vulcanisates contained a large proportion of main chain modifications such as a cyclic sulphide, conjugated unsaturation, a cis/trans isomerisation of the double bond.

The next break-through in the subject of vulcanisation chemistry came with the discovery of organic accelerators in the early 1900's.[2] Apart from the increased rate of

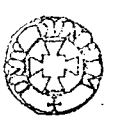

vulcanisation, the use of organic accelerators allowed the vulcanisation temperature to be lowered and the cure times to be reduced. Consequently, the possibility of thermal and oxidative degradation was minimised. Furthermore, the level of sulphur could be reduced, whilst retaining the optimum physical properties of the vulcanisates. This resulted in a reduction of sulphur blooming and far superior aging properties, compared to the vulcanisates of Goodyear and Hancock formulation. In terms of network features, the network derived from accelerated sulphur vulcanisation was found to be far simpler than obtained with only sulphur. It has now been recognised that the chemistry of sulphur vulcanisation is very complex.

Three major classes of accelerators were developed after the First World War and, are still used extensively.[2] These may be classed as: (i) the vulcanising agent - usually sulphur but sometimes a 'sulphur donor' such as a tetra-alkylthiuram disulphide, or dithiobismorpholine; (ii) organic accelerators of vulcanisation - these are generally derivatives of 2-mercaptobenzothiazole, or dialkyldithiocarbamic acids; (iii) activators of vulcanisation - these include metal oxides (zinc oxide), the higher fatty acids, and nitrogen bases. The structures of these classes are shown in Table 1.1.

A history of successive modifications and improvements of the method of curing natural rubber have brought to a high degree of refinement and versatility, whereby the natural rubber and some other synthetic rubbers (Table 1.2) can be vulcanised in various forms at temperatures ranging from

Table 1.1

Organic accelerator

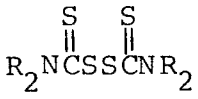

Tetra-alkylthiuram disulphide

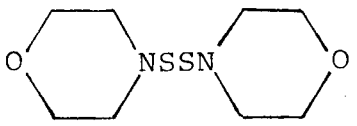

Dithiobismorpholine

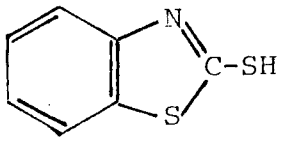

2-Mercaptobenzothiazole

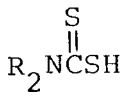

Dialkyldithiocarbamic acid

Table 1.2

Sulphur vulcanisable elastomers

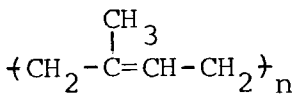

Natural rubber

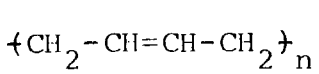

Polybutadiene

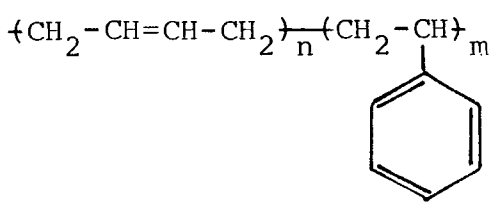

Styrene-butadiene rubber

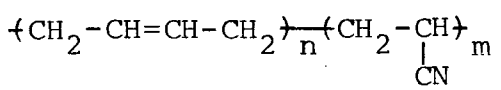

Nitrile rubber

ambient to 200°C. The vulcanisation is effective in the presence of many compounding ingredients such as organic accelerators, zinc oxide, stearic acid and sulphur, which have been incorporated into the Natsyn 2200 (polyisoprene) substrate for a study in this thesis. A conventional high sulphur - low accelerator system produces a high percentage of poly-sulphide crosslinks, which imparts excellent strength and fatique properties at the expense of resistance to compression set, cure reversion, and thermal and oxidative aging (chapter eight). Efficient vulcanising (EV) systems using high accelerator to sulphur ratios (or sulphur donors) yield networks with mainly mono- or disulphide crosslinks possessing a greater resistance to cure reversion aging but inferior strength properties.[1,2] A satisfactory compromise between these features can usually be arranged and, the so called semi-EV systems are currently becoming more popular.

The characteristic changes in physical properties during vulcanisation are known, due to the covalent interlinking of the polymer chains. After the preparation of the rubber 'mix', just prior to vulcanisation, these chains form a mesh of randomly coiled structure, entangled and interwined but chemically discrete. Consequently, deformation of this mesh leads to a slow disentanglement and a partial alignment of the molecules and also to a fairly degree of plastic flow but only with a very limited elastic recovery, when the deforming force is removed. During vulcanisation, the individual chains are crosslinked to form a three dimensional network, in which, some molecular alignment on deformation is still possible but

being resistant to lateral movement and disentanglement. A rapid and a nearly complete elastic recovery is, therefore, obtained on removal of the deforming force. The concentration of intermolecular crosslinks required to form such a network is relatively small. The main reason for this rather low value is that the chain entanglements present in the unvulcanised rubber become trapped when the polymer molecules are crosslinked and, hence, contribute to the elastic properties of the network, thus, greatly enhancing the effect of the actual crosslinks. However, this feature makes difficult for the determination of chemical crosslink density, which is essential for any structural analysis of the network in chemical terms. The estimates of the crosslink density can be treated as approximate only, although their relative accuracy may be quite high.

1.2 Structure of Sulphur Vulcanisates

The application of analytical methods (infrared, ultraviolet, and nuclear magnetic resonance spectroscopy)[106,107,115-127] combined with chemical methods[91,95-97] to a variety of accelerated-sulphur curing systems has shown that the generalised structural features of a natural vulcanisate network is as depicted in Figure 1.1 for the two extreme types of curing systems. Both A and B systems form networks of the same type at the very initial stage of cure, containing accelerator-terminated pendent groups and relatively few crosslinks, which are mainly polysulphides. As the curing time is increased, the rubber chains become modified by

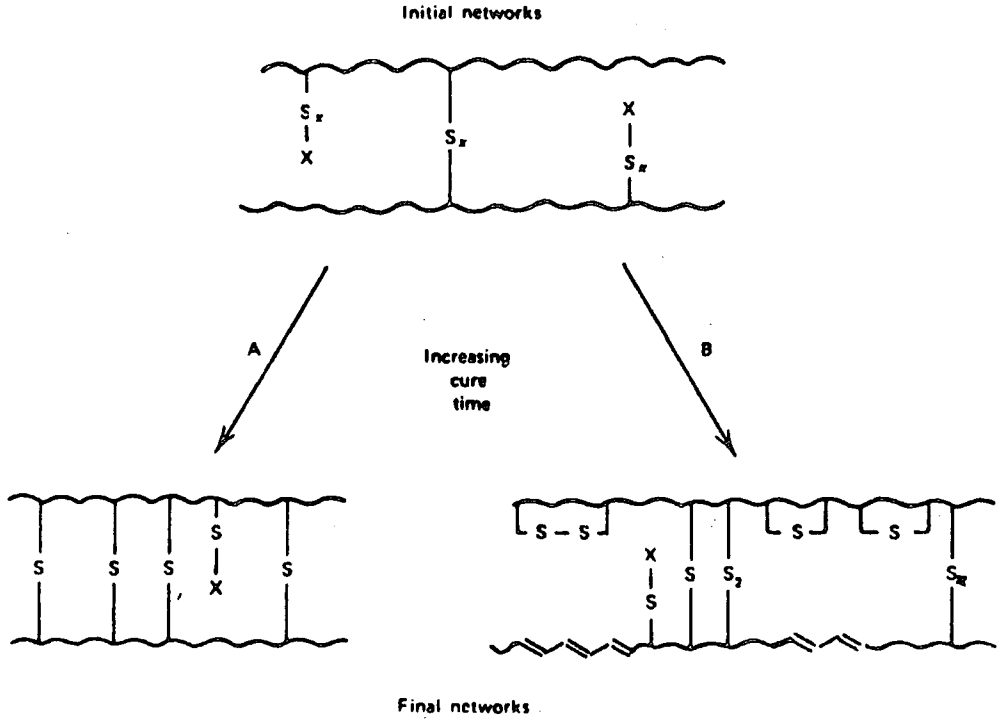

Figure 1.1. Schematic representation of the network structure on vulcanisation conditions. A: high [accelerator/sulphur]; B: low [accelerator/sulphur] (X = accelerator residue; x > 3).

cyclic mono- and disulphide groups, by accelerator-terminated pendent groups and by conjugated diene groups. System A with a high effective concentration of accelerator relative to sulphur, eventually leads to a simple network structure with a high proportion of monosulphide crosslinks and a number of residual pendent groups. The network structure derived from system B is more complex than system A. Polysulphide crosslinks are replaced progressively by mono- and disulphide crosslinks, and the main chains become more and more modified

by olefinic and sulphur-containing groups. The effect of increasing the cure temperature, apart from inducing changes equivalent to increasing the cure time, causes the type A to behave more like system B. The vulcanised structure depends markedly on the accelerator-sulphur ratio, which are, in turn, reflected in changes of physical properties and aging behaviour.[2,3,30]

1.3 Chemistry of Vulcanisation

Although natural rubber has been the oldest polymer known and extensively exploited commercially, the mechanism of sulphur vulcanisation is not yet fully understood. A knowledge of the mechanism has been exclusively derived from studies of the sulphuration of model olefins,[31] resembling the structure of polymer chains. The nature of the products produced from reactions of sulphur with olefins is a function of temperature, the structure of olefins and vulcanising ingredients.

1.3.1 Unaccelerated sulphur vulcanisation

The chemistry of unaccelerated vulcanisation is yet uncertain. The reactions of sulphur with olefins below 130°C are extremely slow leading to a variety of products. The literature indicates that free-radicals[4-7] and ions[8] are involved, as are shown in schemes 1 and 2.

The postulation of the cyclic persulphonium intermediates 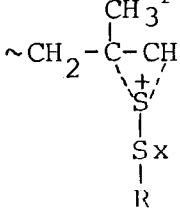 and 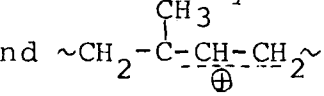 was necessary to explain the fact that models gave both unsaturation products with sulphur atoms connected to secondary and tertiary carbon atoms.

Scheme 1

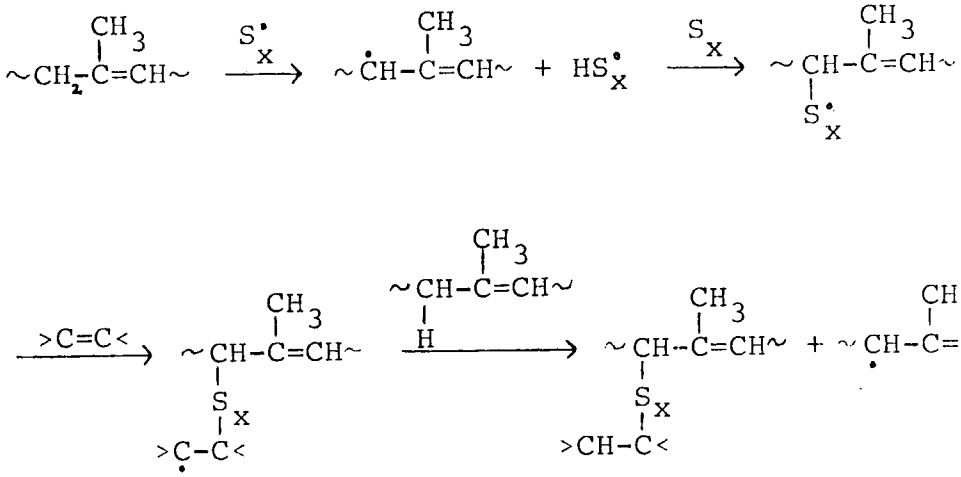

Scheme 2

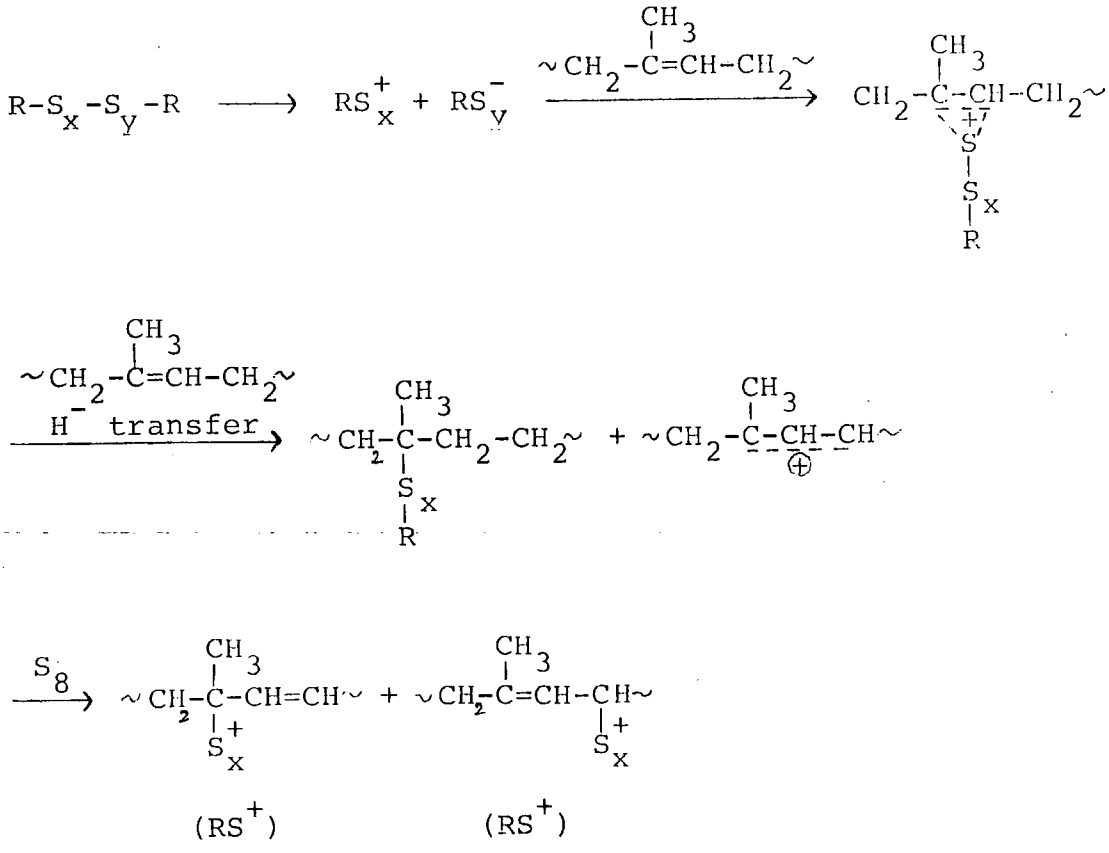

1.3.2 Accelerated sulphur vulcanisation

Sulphuration of olefins in the presence of accelerator-

activator systems proceeds much more rapidly than when sulphur alone is used, and leads to simpler products. The most widely accepted explanation for the mechanism of accelerated sulphur vulcanisation[9,10,11] may be summarised, as follows:

(a) Reaction of accelerator and activator

Scheme 3

$$\left.\begin{matrix} XSH \\ XSSX \\ XSNR_2 \end{matrix}\right\} \xrightarrow[RCOOH]{ZnO} XSZnSX \xrightarrow{\text{Ligand (L)}} XS\overset{\overset{L}{\downarrow}}{Zn}\underset{\underset{L}{\uparrow}}{}SX \qquad (1.1)$$

$$L = \overset{\backslash\,|\,/}{\underset{\cdot\cdot}{N}} \text{ or } \underset{\cdot\cdot}{O} \text{ of } Zn(OCOR)_2$$

$$X = Me_2N\overset{\overset{S}{\|}}{C}-, \quad \text{ 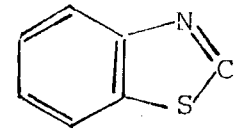 }, \text{ etc.}$$

The accelerator reacts with zinc activators to form a zinc thiolate, made soluble by complexing with primary or secondary amines or with zinc carboxylates.[12-18] The zinc carboxylate results from the excess of zinc oxide and carboxylic acid present in the vulcanising system.[19,21,22]

(b) Reaction of the zinc accelerator complex with sulphur

Scheme 4

$$XSZnSX + S_8 \rightleftharpoons XSS_aZnS_bSX \qquad (1.2)$$

$$S_8 \xrightarrow{\text{amine}} {}^{\bullet}SSSSSSS^{\bullet} \qquad (1.3)$$

The zinc perthiolate complexes are thought to be formed in a series of equilibrium reactions, which lie well on the side of the thiolate complex.[23-25] The average values of a and

b are, therefore, dependent on the relative concentrations of reactive sulphur and soluble zinc complex. The cleavage of cyclooctasulphur by nitrogen base should result in more formation of zinc perthiolate complex than elemental sulphur.[26-29] Consequently, a high ratio of accelerator/sulphur implies low values of a and b in (1.2) and which, in turn, short sulphide crosslinks are produced at all stages of the subsequent sulphuration. Conversely, a low ratio of accelerator: sulphur implies more polysulphide crosslinks.

In the tetramethylthiuram disulphide-zinc oxide vulcanising system, where there is no free sulphur, the zinc perthiolate complex is formed by interchange reactions between tetramethylthiuram polysulphides and zinc dimethyldithiocarbamate, which are formed in a rapid ionic reaction, illustrated in scheme 5. Further reaction of the thiuram trisulphide with zinc oxide leads to higher thiuram poly-

Scheme 5

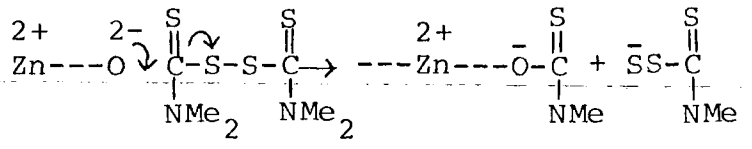

(1.4)

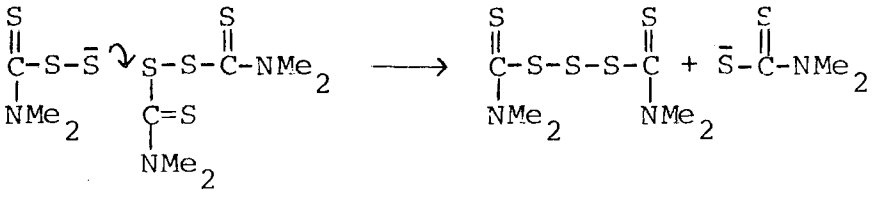

(1.5)

sulphides and, eventually, molecular sulphur. The interchange reaction, viewed in (1.6) leads to smaller values of a and b in the zinc perthiolate complex, and, hence, form short

sulphide crosslinks by feeding to the olefins.[30]

$$Me_2NC(S)S_4(S)CNMe_2 + ZDMDC \rightleftharpoons TMTD + Me_2NC(S)S_a\text{-}Zn\text{-}S_bC(S)NMe_2 \quad (1.6)$$

The other main type of sulphur donor is from morpholine, normally used in conjunction with an accelerator of the sulphenamide since the action is relatively slow, when used alone.

(c) Formation of the rubber-bound intermediate

It is now generally accepted that the precursor to the formation of crosslinks in accelerated sulphur vulcanisation is the rubber-bound intermediate,[10,32,33] although, the

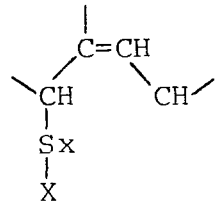

(X = accelerator fragment)

mechanism for the formation of the intermediate is still subject to argument. The Natural Rubber Producers' Research Association (NRPRA)[31] group suggest a polar, largely concerted, mechanism (scheme 6) via a cyclic transition for the reaction between the active sulphurating agent in (1.6) and olefin or olefinic rubber, RH (where H is an α-methylenic or α-methylic hydrogen atom). The essential features of the mechanism

Scheme 6

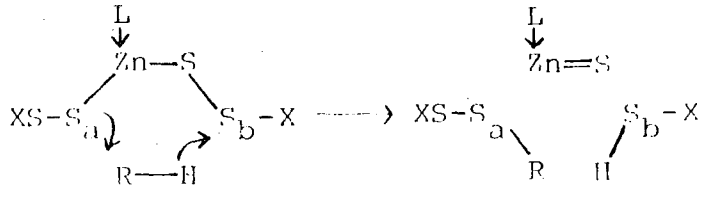

(1.7)

involve a nucleophilic attack of a perthiolate ion on the allylic carbon atom, thus forming a rubber-bound intermediate, together with concomitant displacement hydrogen as an 'incipient hydride ion' and the formation of zinc sulphide. Bateman and his co-workers[31] argued that the coordination of electron donating ligands such as amines or fatty acids to the zinc atom increases the electron density on the terminal sulphur (XS) moieties of the sulphurating agent, which, in turn, facilitates the C-S bond formation by increasing the nucleophilicity of the attacking (XSS_a) group, but hinders the cleavage C-H bond by reducing the electrophilicity of the receiving XS_b group.

The above mechanism is inconsistent with less substituted olefins,[34] where allylic rearrangement and cis/trans-isomerisation of the double bonds occur to a large extent during sulphuration that a free allylic ion or radical is probably involved. However, these isomerisations can, alternatively, be explained by considering thermal rearrangements;[35,36] which, with sulphides of suitable structure may lead to allylic rearrangement as well as to cis/trans-isomerisation and racemisation.

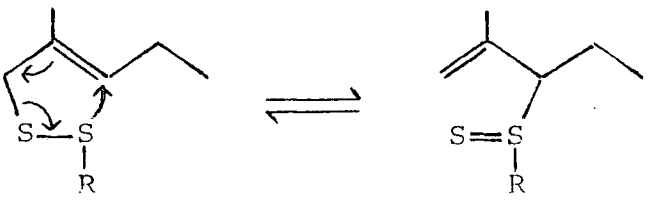

(1.8)

The rubber bound intermediate is converted into crosslinks by two reaction pathways; namely, a simple disproportionation (1.9) either catalysed by a zinc-accelerator-thiolate

complex[20,37] or other nucleophile, or effected by a thermal free radical chain reaction and, the other route involves one molecule of rubber-bound intermediate (RS_aSX) and one molecule of olefin which could proceed via exchange of RS_aSX with zinc complex in (1.1). The crosslinks formed at the

Scheme 7

$$2RS_a.SX \longrightarrow RS_xR + XS.S_{2a-x}.SX \qquad (1.9)$$

$$RS_aSX + XSS_a\overset{L}{\downarrow}Zn.S_bSX \longrightarrow RS_a.\overset{L}{\downarrow}Zn.S_b.SX + XS.S_a.SX \qquad (1.10)$$

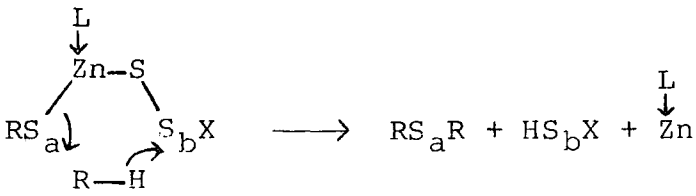

(1.11)

very short cure time are generally polysulphide in nature. The HS_bX species produced in (1.7) and (1.11) react with zinc oxide, forming fresh sulphurating zinc complex:

$$2XS_bH + Zn \longrightarrow XS_b.ZnS_b.X + H_2O \qquad (1.12)$$

(d) Reactions of polysulphide crosslinks

The di- and polysulphide crosslinks produced during the course of vulcanisation are subject to further reactions in the presence of accelerators, activators, and their transformation products, eventually leading to thermally stable monosulphide structure. The most important reactions are as follows:

(i) S-S bond interchange - appear to occur by a free-radical chain mechanism initiated by thermal homolysis of S-S bonds or by an

anionic chain mechanism, initiated by nucleophiles such as zinc-accelerator-thiolate complexes;[20]

(ii) Desulphuration - is catalysed by zinc-accelerator-thiolate complexes, which are able to form new crosslinks from sulphur so removed.[10] Consequently, a high concentration of accelerators and activators relative to

$$RS_xR + XSZnSX \longrightarrow RSR + XSS_a\overset{L}{\underset{\downarrow}{Z}}nS_bSX \xrightarrow{RH} RS_yH \quad (1.13)$$

sulphur lead to a stable monosulphide crosslinked network with a high degree of crosslinks (Figure 1.1A). Conversely, a low concentration of accelerator or of zinc compounds will result in a high concentration of polysulphide crosslinks, which will decompose to a lower degree of crosslinks and lead to increasing modification of the chains by cyclic sulphide and olefinic groups (Figure 1.1B);

(iii) Decomposition - is an uncatalysed thermal process, giving rise to cyclic mono- and disulphide groups, to conjugated diene and triene groups - thus increasing the susceptibility of rubber to oxidation,[39] and to zinc sulphide.[10] Desulphurisation competes with decomposition and, therefore, a rapid desulphurisation leads to reduced degradation of the network.

The principal consecutive and competing reactions, indicated in Figure 1.2 proceed at broadly comparable rates in the normal temperature range of vulcanisation (140 - 180^{o}C) and, hence, none of the step is completed before succeeding steps are well under way. A mixture of products is always obtained, whatever the combination of cure time and temperature is employed. However, the rates are dependent on the composition of the vulcanising system and on cure temperature.

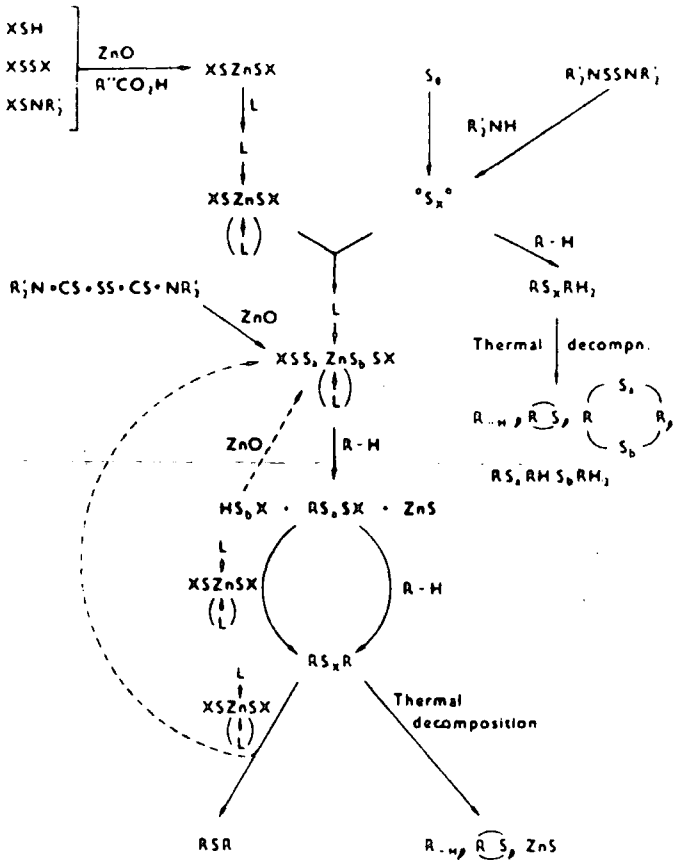

Figure 1.2. Overall course of sulphur vulcanisation of olefinic rubbers [R-H = rubber hydrocarbon in which H is an α-methylenic or α-methylic hydrogen atom; X = accelerator residue and L = ligand.

The influence of vulcanised structures on physical and mechanical properties has been well documented.[39-48]

1.4 Vulcanisation by Peroxides

Vulcanisation results from interaction of the polymer with the free radicals formed by decomposition of peroxides (dicumyl peroxide employed in the system gives cumyloxyl and methyl radicals).[49] The vulcanisation of butadiene or isoprene is initiated either by the abstraction of a hydrogen atom from the allylic position of the elastomer molecule or by the addition of the derived radical to a double bond,[50-51] as are shown in scheme 8. The presence of methyl group in

Scheme 8

$$\text{Peroxide} \longrightarrow 2R^{\bullet} \qquad (1.14)$$

$$R^{\bullet} + -\underset{\displaystyle H}{\overset{\displaystyle |}{CH}}-\overset{\displaystyle |}{C}=\overset{\displaystyle |}{C}- \longrightarrow \overset{\displaystyle \bullet}{C}H-\overset{\displaystyle |}{C}=\overset{\displaystyle |}{C}- + RH \qquad (1.15)$$

$$R^{\bullet} + -CH_2-\overset{\displaystyle |}{C}=\overset{\displaystyle |}{C}- \longrightarrow -CH_2-\overset{\displaystyle R}{\overset{\displaystyle |}{C}}-\overset{\displaystyle \bullet}{\overset{\displaystyle |}{C}}- \qquad (1.16)$$

$$2\text{-}\overset{\displaystyle \bullet}{C}H-\overset{\displaystyle |}{C}=\overset{\displaystyle |}{C}- \longrightarrow -\underset{\displaystyle -CH-C=C-}{\overset{\displaystyle |}{CH}}-\overset{\displaystyle |}{C}=\overset{\displaystyle |}{C}- \qquad (1.17)$$

isoprene rubber directs the attack of a radical to the methylene group nearest it and, thus, the abstraction route predominates over the radical addition. The two polymeric free radicals in (1.17) generated from the attack of free radicals then unite to give a crosslink.

Alternatively, the continuous regeneration of free radicals in a chain propagation step in scheme 9 leads to the addition

of polymeric radicals to double bonds,[53-55] without loss of the free radical, before the termination occurs.

Scheme 9

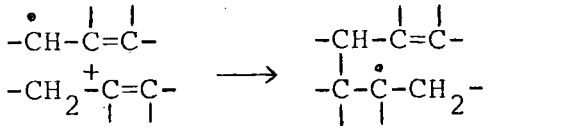

(1.18)

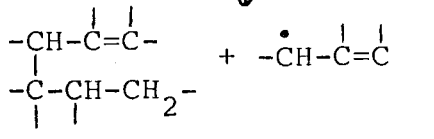

(1.19)

Termination can occur by radical coupling or by unproductive processes; for example, a polymeric radical combines with a radical derived from the peroxide. A scission of chains occur when a polymeric radical decomposes to give a vinyl group and regenerates a new polymeric radical.[59-61] One 'mole' of crosslinks is produced in isoprene rubber per mole of dicumyl peroxide, thus indicating the crosslinking mainly by the coupling of two polymeric radicals.[56-58]

For butadiene and styrene-butadiene rubbers, the efficiency of crosslinking is greater than isoprene; and, this indicates a chain reaction for the crosslink formation.

1.5 Cure and Accelerator Activity

1.5.1 Cure

Technical terms used in industries for discussion of vulcanisation in combination with Mooney Scorch and stress-strain relaxation are summarised with reference to Figure 1.3, as follows:

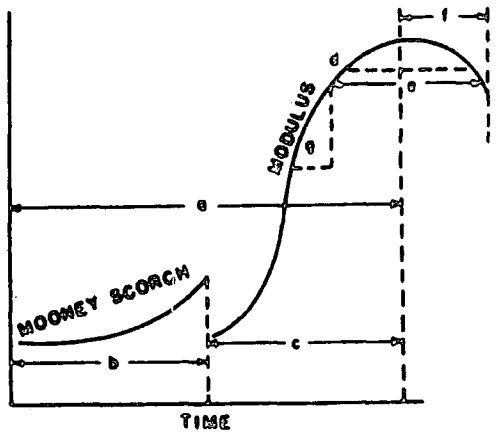

(a) Cure time
(b) Scorch time
(c) Vulcanisation
(d) Optimum cure
(e) Plateau effect
(f) Reversion
(g) Rate of cure

Figure 1.3. Vulcanisation parameters.

(a) Cure time - is the time required to reach optimum cure.

(b) Scorch time - is the time interval from the beginning of the cycle to the beginning of cure.

(c) Vulcanisation time - is the time interval from beginning of cure to optimum cure.

(d) Optimum cure - is usually taken as the time required to reach some point near the maximum of the property plotted. In Figure 1.3, the optimum cure time would be near point (d).

(e) Plateau effect - the curve levels off as the maximum is approached, and the stress remains relatively

constant for a period of time.

(f) Reversion - particularly sulphur vulcanisate subjected to heat longer than required to obtain optimum leads to deterioration, especially of modulus.

(g) Rate of cure - is taken as the slope of the vulcanisation curve during the period of fast reaction. Vulcanisation time is an estimation of the relative rate of cure. The rate of cure and the induction period varies with the type of accelerator. The length of the induction period is directly proportional to the scorch time.

1.5.2 Effect of accelerator structure on activity[2,62,63]

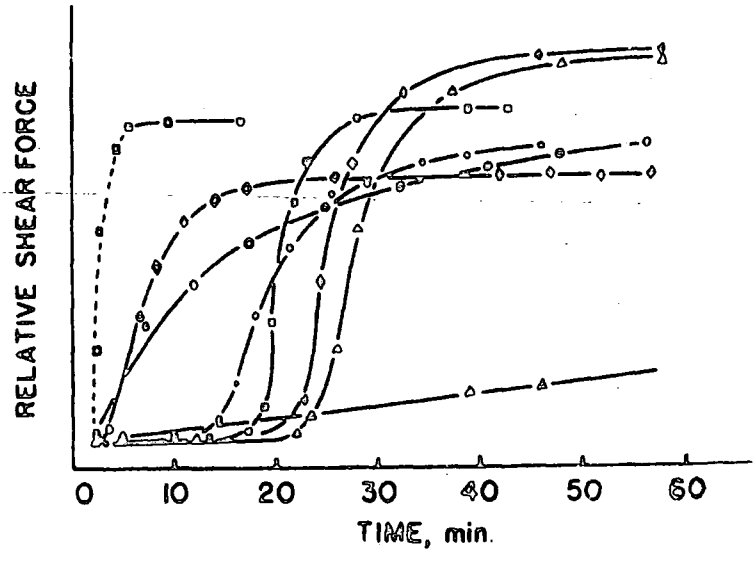

Figure 1.4. Comparison of accelerator cure characteristics.

Δ No accelerator

O Diphenylguanidine (DPG) 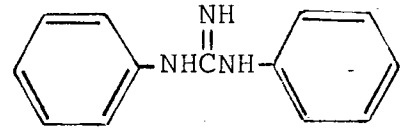

□ Zinc dimethyl-dithiocarbamate (ZDMDC) 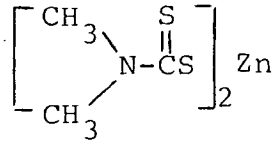

◇ Mercaptobenzthiozole (MBT) 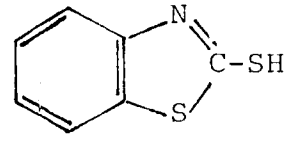

⊙ Dibenzthiazyl disulphide (MBTS) 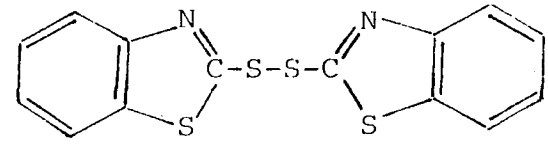

▨ N-Cyclohexylbenzothiazole-2-sulphenamide (NCBS)

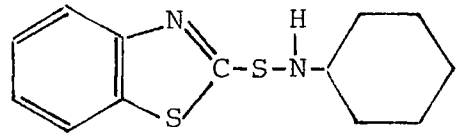

◈ N-t-butylbenzothiazole-2-sulphenamide (NtBBS)

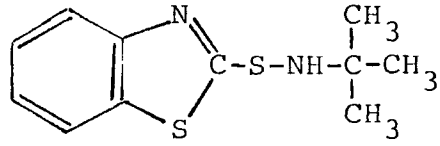

△ N-butylbenzothiazole-2-sulphenamide (NBBS)

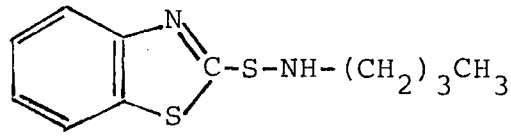

Figure 1.4 illustrates the effects of accelerators on the rate of cure and on the induction period. ZDMDC, an ultra-accelerator, vulcanises the system without revealing any induction period (scorch time), and the rate of cure is extremely rapid; whereas, MBTS, NCBS, NBSS and Nt-BBS have a much longer induction period and a slow rate of cure. From the technological point of view, the accelerators are selected to give significantly safer calendering, extrusion and mould injection.

1.6 Characterisation of Vulcanisate Structure

Perhaps, the most important and fascinating aspect of current affairs in the chemistry of vulcanisation is the problem of determining the structure of rubber vulcanisates since it not only allows the overall efficiency of the cross-linking process to be established but also can be used to estimate the relative proportions of different types of crosslinks. In this context, a distinction between the degree of chemical crosslinking and the physically effective degree of crosslinking is necessary for the characterisation of vulcanisates. The latter generally includes positive contributions from trapped entanglements as well as actual crosslinks. It may also include negative contributions from free chain ends and intramolecular loops, both of which impair the effect of associated crosslinks (Figure 1.5).[64]

Conversely, Figure 1.6 shows the different types of chemical crosslinks for sulphur vulcanisate, which may act physically as one crosslink only or as a crosslink of functionality greater than four.

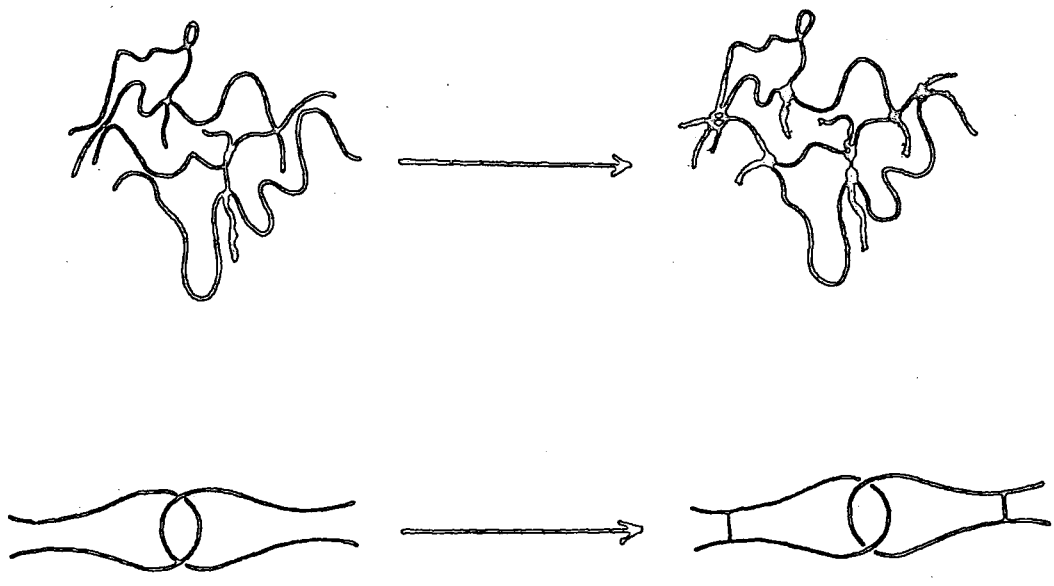

Figure 1.5. Schematic representation of changes in structure during vulcanisation.

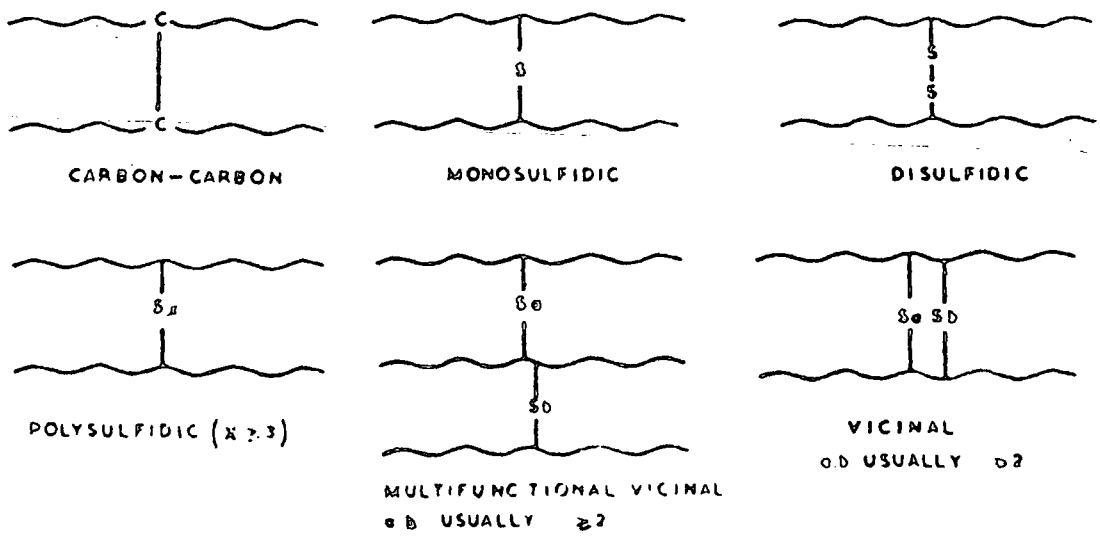

Figure 1.6. Different types of chemical crosslinks.

Part of this problem in determination of vulcanisate structure forms the subject of this review.

1.6.1 Microphysical network structure

The determination of network chain densities and cross-link concentrations in unfilled elastomers using stress-strain relaxation and swelling methods ignores the contribution of chain ends and entanglements by assuming that the joining polymer molecules have infinite molecular weight. According to the statistical theory of rubber like elasticity,[65-68] an expression of the stress-strain in terms of the Mooney Rivlin equation (1.20) leads to an evaluation of the constant C_1, which is indirectly related to the molecular weight of chain segments between physically effective crosslinks, $\bar{M}c$; this is directly related to the concentration of physically effective crosslinks in the sample.[69-72]

$$F[2Ao(\lambda-\lambda^{-2})] = C_1 + C_2\lambda^{-1} \qquad (1.20)$$

Where F is the force required to maintain the sample at a small extension ratio, λ, Ao is the unstrained cross-sectional area of the sample, C_1 and C_2 are parameters of vulcanisate pertaining to ideal and non ideal elastic behaviour respectively.

Alternatively, $\bar{M}c$ can be related to the volume fraction of crosslinked network in the swollen gel at equilibrium swelling, ν_r, by the Flory-Rehner equation[73-75] (1.21).

$$-[\ell n(1-\nu_r) + \nu_r + \mu\nu_r^2] = \int \nu_o (\bar{M}_c)^{-1} (\nu_r^{1/3} - 2\nu_{r/f}) \quad (1.21$$

Where ν_o is the molar volume of the swelling liquid, f is the functionality of the system, which is in this case four, $\int$ is

the density of the rubber network and μ is the polymer-solvent interaction parameter. The Flory-Rehner equation derived from the statistical theory and the thermodynamic of mixing of liquids with networks requires prior knowledge of the μ, which varies considerably both with the level of curative and with the time of cure.[54,76-80] This procedure, because of its simplicity, has been applied in chapter three for the determination of $\bar{M}_c$.

Mullin[71] has succeeded in evaluating the correction for free chain ends in networks of natural rubber and, Moore and Watson[81] derived the relationship between chemical crosslink concentration in natural rubber, using di-t-butyl peroxide as the crosslinking agent. The relation, based on work with model olefins,[52,57,81] assumed that the rubber radicals undergo mutual combination exclusively. However, the subsequent work[82] indicates that the non-rubber components in the natural rubber compete with the rubber hydrocarbon for alkylperoxy and methyl radicals.

1.6.2 Molecular network structure

Various types of chemical reagents have been used for the determination of crosslink structures, which react and break crosslinks of particular types. The physical assessment before and after treatment with the reagent, then allows the determination of concentration of that type of crosslinks which have been broken. Differences in chemical reactivity allow mono-, di-, and trisulphides to be determined in this way. Sulphur rank equal or greater than three can not be distinguished and, therefore, are treated as polysulphides in

this review. The treatment of elastomers with thiols in piperidine has been discussed extensively in chapter nine.

Chemicals used for the cleavage of both di- and poly-sulphides, are as follows:

(a) Lithium aluminium hydride in tetrahydrofuran[39,83-89]

$$RS_xR' \xrightarrow[(ii)\ H^+]{(i)\ LiAlH_4} RSH + R'SH + (x-2)H_2S \quad (1.22)$$

$$RSSR' \xrightarrow[(ii)\ H^+]{(i)\ LiAlH_4} RSH + R'SH \quad (1.23)$$

(b) Sodium di-n-butyl phosphite in benzene[80,90,91]

$$RS_xR' + (x-1)(Bu^nO)_2P(O)^-Na^+ \longrightarrow RS^-Na^+ + (x-2)(Bu^nO)_2P(O)S^-Na^+ + Bu^n(O)_2P(O)SR \quad (1.24)$$

$$RSSR' + (Bu^nO)_2P(O)^-Na^+ \longrightarrow RS^-Na^+ + (BuO)_2P(O)SR \quad (1.25)$$

(c) Triethyl phosphite in benzene[92,93]

$$RS_xR' + (x-2)(C_2H_5O)_3P \longrightarrow RSSR' + (x-2)(C_2H_5O)_3PS \quad (1.26)$$

$$RSSR' + (C_2H_5O)_3P \longrightarrow RSC_2H_5 + (C_2H_5O)_2P(O)SR' \quad (1.27)$$

When R' is a 2-alkenyl group, the reaction equation competes with reaction (1.27).[94]

$$RSSR' + (C_2H_5O)_3P \longrightarrow RSR' + (C_2H_5O)_3PS \quad (1.28)$$

(d) n-Hexanethiol (1M) in piperidine[91,95]

$$RS_xR' + (2x-3)\text{hexyl-}S^- \longrightarrow RSS\text{-hexyl} + R'S^- + (x-2)(\text{hexyl-}S)_2 + (x-2)S^{2-} \quad (1.29)$$

$$RSSR' + \text{hexyl-}S^- \longrightarrow RSS\text{-hexyl} + R'S^- \quad (1.30).$$

A solution of propane-2-thiol (0.4M) and piperidine (0.4M) in heptane has been reported to cleave polysulphide linkages only, leaving di- and monosulphides crosslinks intact in sulphur vulcanisate in two hours at 20°C.[96,97]

(e) Propane-2-thiol (0.4M) and piperidine in n-heptane

$$RS_xR' + (2x-3)(CH_3)_2CH\bar{S} \longrightarrow RSS(CH_3)_2 + R'S^- + (x-2)(CH_3)_2CHSSCH(CH_3)_2 + (x-2)S^{2-} \quad (1.31)$$

The treatment assumes that the polysulphides are one thousand times more reactive than disulphides and, the concentration of disulphides remains essentially unchanged, under the employed conditions. The use of this reagent in conjunction with treatment (d) allows to estimate the relative proportion of mono-, di- and polysulphides to the total degree of chemical crosslinking.

Other, less popular, methods for the determination of overall numbers of polysulphide sulphur atoms in a vulcanisate network have been used by determining the hydrogen sulphide, formed on treatment with lithium aluminium hydride in ethereal solvent,[39,83-89] by determining the amount of network-combined

sulphur that is exchangeable with radioactive molecular sulphur ($^{35}S_8$) (exchange sulphur in organic accelerator also occurs),[98-100] and by determining the amount of network-combined sulphur, removable by treatment with triphenylphosphine for four days at 80°C.[41,80,90] The successful application of triphenylphosphine demands the elimination of free-sulphur present in vulcanisate prior to the treatment.

The use of methyl iodide is even less favourable, mainly because both di- and polysulphides react to give sulphonium salts and, the allylic iodides formed are highly reactive and may result in carbon-carbon crosslinks in subsequent reactions.[96,101-103]

1.6.3 Main-chain modifications

The background information of types of modifications to the main chains, in the literature, comes almost exclusively from studies of the sulphuration of model olefins.[31] The problem is associated with the identification and estimation of all various types of modifications in actual rubber vulcanisates. Modification of the main chain such as accelerator-pendent groups[90] (Figure 1.7), olefinic modifications[31] and cyclic sulphide groups[31,104,105] have so far been identified by a variety of methods.

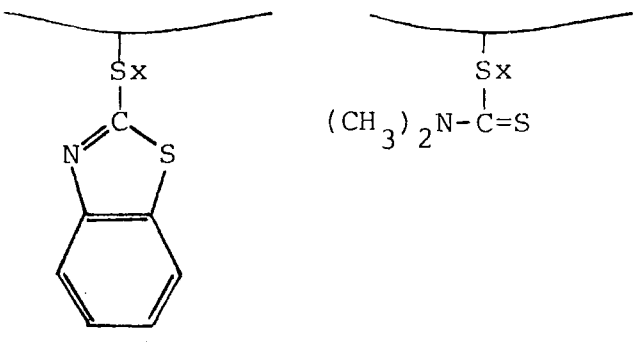

Figure 1.7. Accelerator-terminated pendent groups attached to rubber.

Other physical methods such as infrared and more recently nuclear magnetic resonance spectroscopy have been used to study the structural features.

1.7 Structural Studies

1.7.1 Infrared spectroscopy

Infrared spectroscopy, as a very useful tool in the field of chemistry for analysing and identifying the compounds of similar chemical and physical properties, has been widely applied for characterisation of elastomers and additives and the spectra have been well documented over the years.[106,107] In most cases, the natural elastomers have been studied in microtomed sections, cut in solvent (acetone or toluene), and in cast and hot-pressed films, whereas the spectra of additives in the form of a powder have been obtained by means of the potassium chloride or bromide disc technique.[106,107] The applications of infrared spectroscopy discussed by Clark[108] and the theoretical analysis of some polymers by Krimm[109] lead to the assignment of many of the bands in the spectra of polymers. The absorption bands at 7.27 and 7.22 microns have been used for the determination of relative proportion of cis-1,4 and trans-1,4 units of polyisoprene, respectively.[110] Corish[111,112] determined the amount of cis-1,4 units in a polyisoprene by measuring the intensity of the 2.46 micron band. The bands at 11.25 and 11.9 microns are attributed to 3,4 and 1,4 units, respectively.

It has been shown[113,114] that the 7.64 and 7.4 micron

bands are due to cis- and trans units of butadienes. The absorption band at 11.0 micron is characteristic of 1,2 unit.

The detailed information and the results of this investigation are provided in chapter three.

1.7.2 Nuclear magnetic resonance

The overall contents of the isomeric structural units in elastomers such as polybutadiene and polyisoprene were determined by infrared spectroscopy before 1970, while a method of determining the sequence distribution of these units by nuclear magnetic resonance spectroscopy has been known in the last few years.[115-127] Carbon-13 NMR has been applied to study the sequence distribution of the isomeric structures in polyisoprenes.[116-119] Proton decoupled ^{1}H NMR spectroscopy has applied to the analysis of cis and trans units in butadiene.[123-125] The successful application of these methods required swelling or solution of a polymer in a suitable solvent. In contrast to these methods, natural and synthetic polymers are currently studied extensively with the application of cross polarisation combined with magic angle spinning (CP-MAS),[128] although it is still in its infancy. The detailed results of sulphur vulcanised, Natsyn 2200, elastomers are given in chapter three.

1.8 The Mechanism of Oxidation

Almost, the entire fundamental knowledge of oxidation of rubber has been derived from the oxidation of the natural (cis-1,4-polyisoprene) elastomer, the motivation being the great technological importance of rubbers. At present, the

widely accepted mechanism of oxidation is based on work at the Natural Rubber Producers' Research Association.[275,285,301]

General Mechanism of Oxidation

1.8.1 The initiation reaction

A rapid oxidation of elastomers results from the breakdown of a hydrocarbon molecule into two radicals:

$$RH \longrightarrow R^{\circ} + H^{\circ} \qquad (1.32)$$

where RH is the polymer and R° is the polymer radical. The initiation reaction may be induced by physical factors (UV radiations, ionising radiation, temperature, ultrasonics and mechanical shearing) and chemical agents (catalyst, direct activity of oxygen, singlet oxygen and ozone).

(a) Physical factors

The chemical structure of the polymer has a great influence on the type of macro-radicals formation. The dissociation energies of particular bonds between the atoms of the polymer will, thus, dictate the direction of fragmentation that is likely to occur in relation to the amount of energy being fed to the system. This is particularly important for the mastication of raw elastomers, carried out in internal mixers or on roll mill at an elevated temperature. The mastication in the presence of oxygen is accompanied by a marked decrease in the molecular weight and increased oxidative degradation of the elastomer.

Figure 1.8 shows the relationship between the bond energy and the energy available from sunlight to cause the photo-

oxidative degradation of the elastomer.

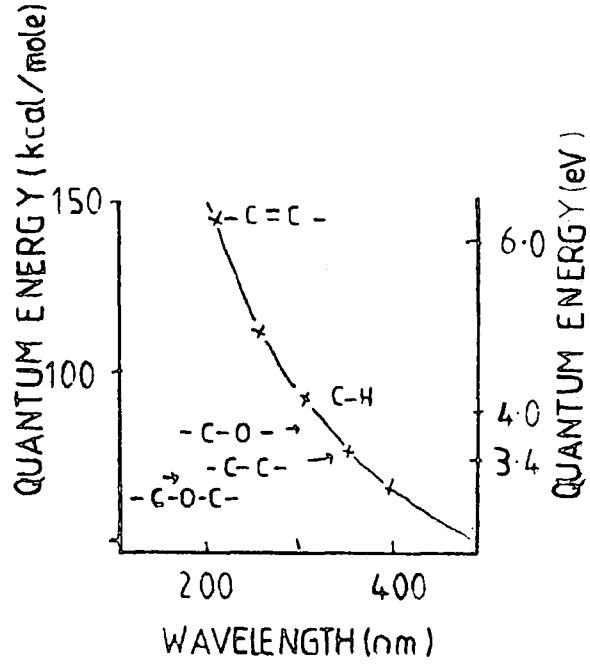

Figure 1.8. Bond strength in relation to light energy.

(b) Chemical agents

(i) Initiation induced by molecular oxygen

A molecule of oxygen ($^3\Sigma$state), electronic configuration [$KK(\sigma g2S)^2(\sigma u2S)^2(\sigma g2P)^2(\pi u2P)^4(\pi g2P)^2$], has a biradical nature and can rapidly combine with radicals by addition to form peroxy radicals. The direct reaction of molecular

$$R^\circ + O_2 \longrightarrow ROO^\circ \qquad (1.33)$$

$$RH + O_2 \xrightarrow{X} ROOH \qquad (1.34)$$

oxygen with a polymer is not favoured, due to the endothermic nature of the process (30 - 45 kcal).[129]

(ii) Initiation by external initiators

External initiators present as impurities in the form of catalysts, peroxides, hydroperoxides, inhibitors, solvents and other materials incorporated in the synthesis of polymers may induce the oxidation process by decomposing into free radicals, which are then able to react with the polymer.

(iii) Initiation induced by ozone

Traces of ozone present in the atmosphere (a few parts per hundred million) are sufficient to cause severe cracking in elastomers, within a few weeks to months. The mechanism of ozonolysis proposed initially by Criegee[130] and amplified by Baily[131] can explain the initial attack of the ozone, particularly with respect to the orientation of addition to an unsymmetrical carbon-carbon double bond. The primary step

Scheme 1.8

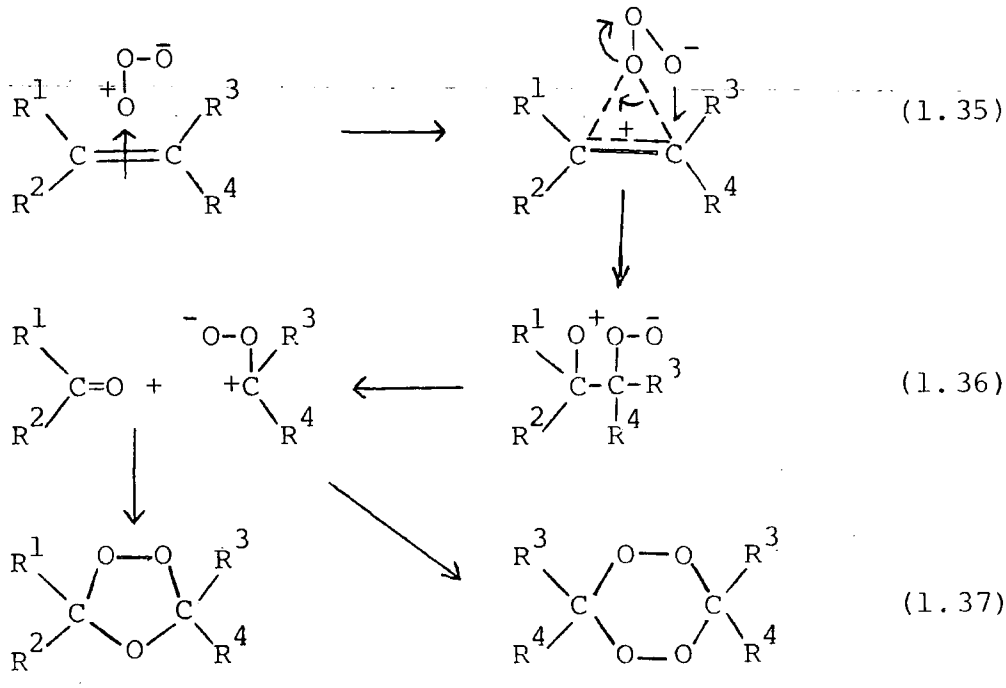

(1.35)

(1.36)

(1.37)

in the reaction sequence involves complex formation between the electron-deficient terminal oxygen atom of the ozone molecule and the π electrons of the double bond. A rapid rearrangement of this π complex, directed by the electronic character of the neighbouring groups, yields an aldehyde or ketone (ozonolysis of polyisoprene gives water, formic acid, acetic, levalinaldehyde, 2,5-hexanedione and propionic acid).

1.8.2 The propagation reaction

Peroxy radical ($ROO^{\bullet}$) produced by a rapid combination of hydrocarbon radicals (R°) with oxygen in equation (1.33) reacts with hydrocarbon via hydrogen abstraction, resulting in the formation of a hydroperoxide.

$$ROO^{\circ} + RH \longrightarrow ROOH + R^{\circ} \qquad (1.38)$$

In general, peroxy radicals abstract tertiary bonded hydrogen in preference to secondary and primary hydrogen.

1.8.3 Decomposition of polymer hydroperoxides

Whilst the radical (R°) again participates in reaction (1.33), the hydroperoxide may decompose by the following mechanisms:

$$ROOH \longrightarrow RO^{\circ} + {}^{\circ}OH \qquad (1.39)$$

$$2ROOH \longrightarrow RO^{\circ} + ROO^{\bullet} + H_2O \qquad (1.40)$$

or react as follows:

$$ROOH + RH \longrightarrow RO^{\bullet} + R^{\circ} + H_2O \qquad (1.41)$$

Elevated temperatures,[132,133] metal catalysts[134,135] and

sunlight can also enhance the rate of hydroperoxide decomposition.

1.8.4 Formation of hydroxyl groups

Hydroxyl groups are formed from the reaction of alkoxy polymer radicals with hydrocarbon molecules. These groups may

$$RO^{\circ} + RH \longrightarrow ROH + R^{\circ} \qquad (1.42)$$

occur along the hydrocarbon chain or on its end groups, the latter being relatively rare.[136]

1.8.5 Formation of carbonyl groups

Carbonyl groups may result in the following ways:[136]

(a) β-Scission of alkoxy radicals[137,138]

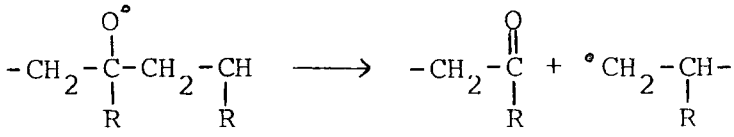

(1.43)

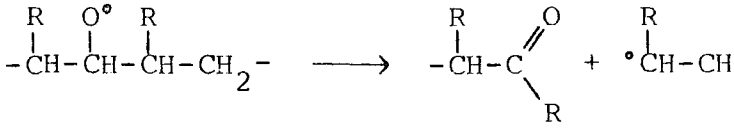

(1.44)

These reactions participate in the backbone scission of hydrocarbon chains and in the formation of alkyl radical at chain ends.

(b) An intermediate formed from abstraction of a labile hydrogen via a cage effect by a hydroxy radical subsequently undergoes rearrangement to give a carbonyl group.

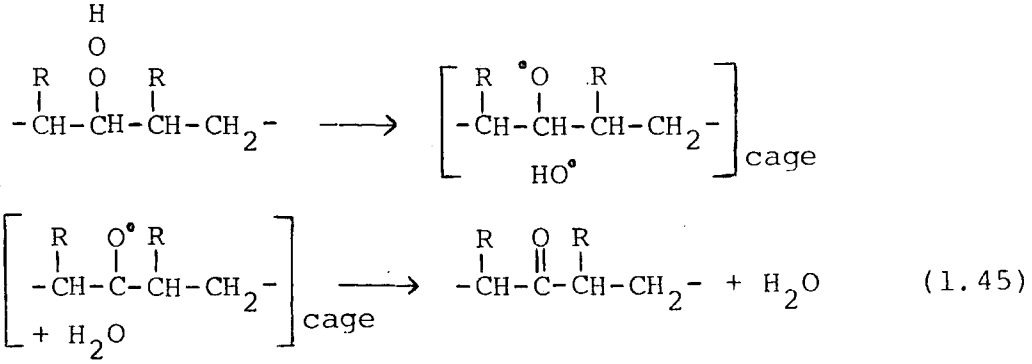

(1.45)

(c) A biradical resulting from the decomposition of a hydroperoxide, subsequently yields ketone.

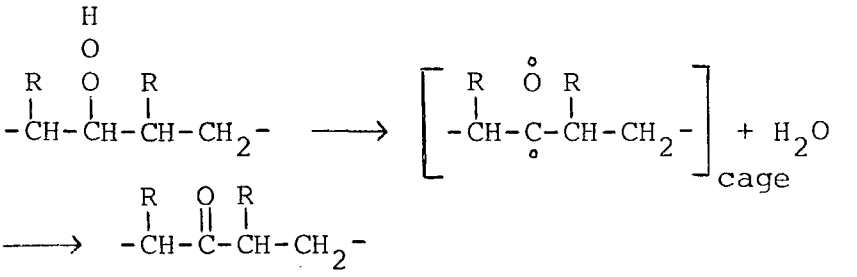

(1.46)

(d) A reaction between two polymer alkoxy radicals, via disproportionation, produces simultaneously ketone and alcohol.

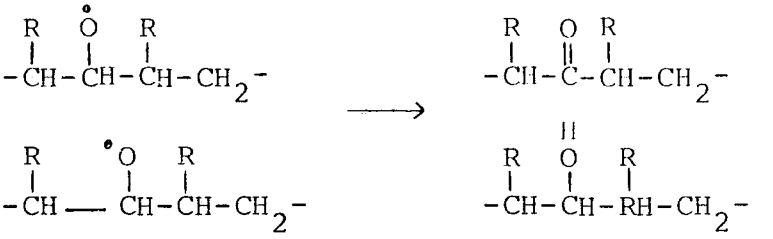

(1.47)

1.8.6 The termination reaction[275,285,301]

The chain reaction terminates by the reactions:

$$ROO^{\circ} + ROO^{\circ} \longrightarrow \text{Non-radical products} \quad (1.44)$$

$$ROO^{\circ} + R^{\circ} \longrightarrow ROOR \quad (1.45)$$

$$R^{\circ} + R \longrightarrow R\text{-}R \quad (1.46)$$

} inactive products

etc.

Reaction (1.44) predominates in high partial pressure of oxygen.

1.8.7 Plasma and thermal treatments

The surface reactions with active species in oxygen and hydrogen plasmas, and with air at 100°C are discussed extensively in chapters six, seven and eight respectively.

1.8.8 Areas of interest

It is evident from the necessarily brief survey of the literature that the techniques employed for studying the chemistry of elastomers have been the subject of bulk investigations. Since, the solids communicate with the surrounding environment by way of their surfaces, a knowledge of the changes in surface chemistry is of fundamental importance for any detailed discussion at the molecular level of the way in which the materials interact with the environment. The use of multiple attenuated total reflectance infrared spectroscopy (MATR-IR)[139] provides only limited information of the surface changes but, a sampling depth of 1000Å, does not necessarily reflect the changes occurring in a surface layer of thickness ~ 50Å. Over the past few years, Clark and co-workers have shown in an extensive series of publications, how a most powerful surface sensitive technique, Electron Spectroscopy for Chemical Applications (ESCA), can be applied to study the polymer surfaces.[229-235]

In view of the complexities associated with the chemistry of vulcanisation and of unexplored area of the chemical changes at the surface of elastomers, the aim of this thesis has been initially to establish the generality of the technique applied to the rubbers by conducting a systematic study of models and elastomers and then to subject the selected elastomers to plasmas, thermal oxidation and chemical treatments. The flow-chart in Figure 1.9 summarises the areas of interest studies in this thesis.

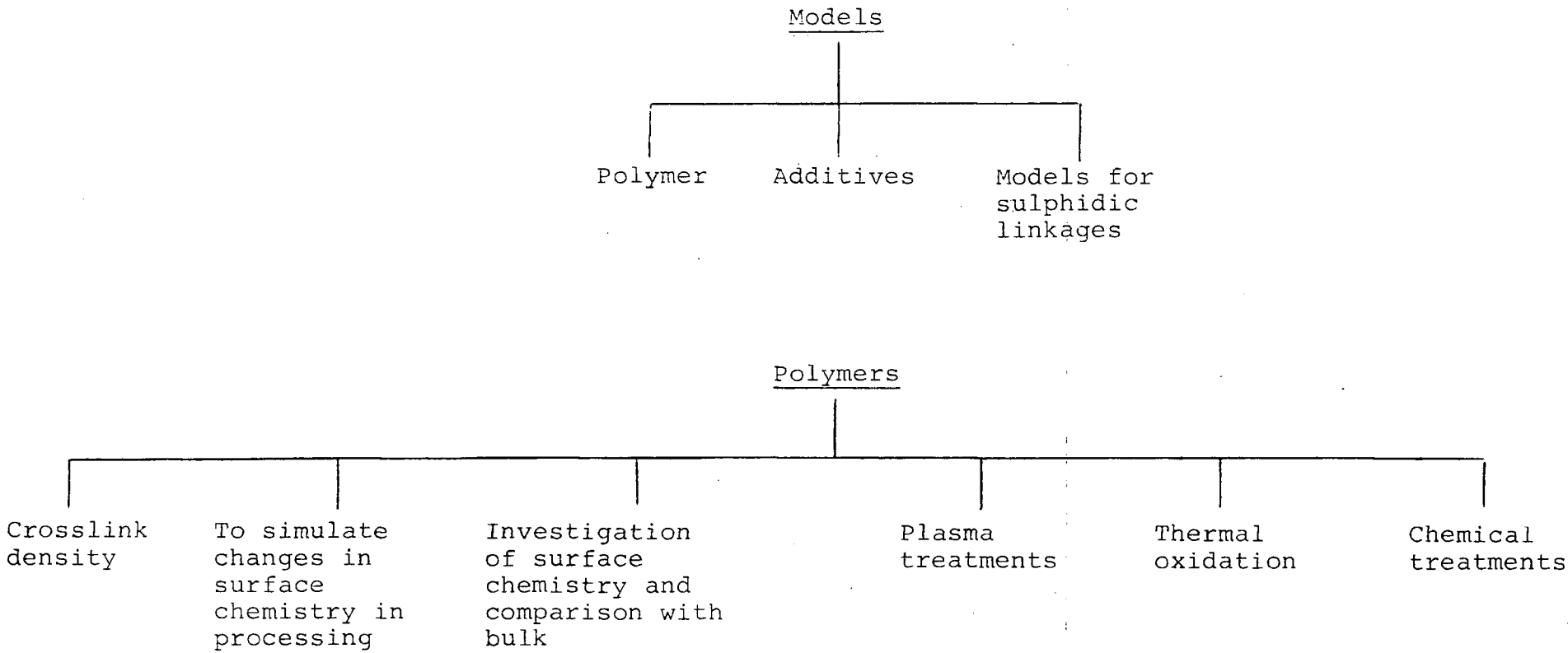

Figure 1.9. Flow-chart.

CHAPTER TWO

ELECTRON SPECTROSCOPY FOR CHEMICAL APPLICATIONS (ESCA)

2.1 Introduction

The ESCA experiment involves the measurement of binding energies of electrons, ejected by interactions of a monochromatic beam of soft X-rays with an atom in a molecule. In common with most other spectroscopic techniques, X-ray photoelectron spectroscopy was originally developed by physicists and, is now extensively utilised by chemists, as a tool for investigating the structure, bonding and reactivity.[140]

As early as 1888, Hallwachs,[141] working in Germany, observed the effect of ultra-violet light on electrically charged sheets of zinc that the electric discharge between two electrodes occurred more readily, when one of the plates was irradiated with ultra-violet light. It was further shown in 1900 by Lenard[142] that the irradiation of metal resulted in emission of electrons from the metal. This phenomena, unexplainable by the classical wave theory, was followed by Einstein in 1905, who introduced the light quantum concept to explain the photoelectric effects.[143] He suggested that the light consists of a stream of particles, (photons), each possessing energy $h\nu$, where h is the Plank constant and ν is the frequency of light; and, each of these photons imparts its energy to an electron in the metal. Part of the photon energy is used in just removing the electron from the metal surface and, the remaining energy appears as the kinetic energy (KE) of the photoelectron, given by the equation:

$$h\nu = KE + W \qquad (2.1)$$

where W is the 'work function', the minimum energy required to remove the electron from the surface of metal. However, it was not until much later, that Robison[144] and De Broglie[145] investigated the energy distribution of electrons from various elements by the X-ray irradiation of thin foils. The distribution of electron energies for the transmitted photo-electrons was recorded photographically and, analysed using a homogeneous magnetic field. Since, the radiation source consisted of a continuous spectrum (Bremsstrahlung) with the characteristic line spectrum of the anode material superimposed, the electron distributions obtained were characterised by long tails with distinct edges at the high energy end. Measurement of these edge positions gave a determination of the energy levels of the different atomic levels and, with a knowledge of the exciting X-ray line, binding energies were calculated. It was not until the 1950's, however, that Siegbahn[146] revived the principle of X-ray photoelectron spectroscopy and, developed an iron-free magnetic double focussing electron analyser for the high resolution studies of β-ray energies. In 1954, attempts were made to record high resolution photoelectron spectra, excited by soft X-rays. The observation of sharp lines, which could be resolved from each electron veil, changed the course of the future development of the technique. The photoelectrons, to which such lines corresponded, had the important property that they did not suffer energy losses and, therefore, possessed the binding energy of the atomic level from which, they were ejected; and, could be measured to a precision of a

few tenths of an electron volt.[147] The realisation of chemical shifts for copper and its oxides[148] was a great step forward in relation to the environment of the core levels, but the general utility of the technique was appreciated only in 1964.[149,150]

Much of the early work of Siegbahn and co-workers was extensively documented in 1968 in 'ESCA', Atomic, Molecular and Solid State Structure Studied by Means of Electron Spectroscopy.[151] Later work was published in 1968 in the standard text of 'ESCA Applied to Free Molecules'.[152]

In addition, the technique of ESCA is also known as:

(1) X-ray Photoelectron Spectroscopy (XPS)

(2) High Energy Photoelectron Spectroscopy (HEPS)

(3) Induced Electron Emission Spectroscopy (IEES)

(4) Photoelectron Spectroscopy of the Inner Shell (PESIS).

There are several techniques available, which may be classified under the generic term 'Electron Spectroscopy'. Table 2.1 shows various types of electron spectroscopy, whose detailed features are well documented.[153,154] An enormous amount of research activity has been directed, in the last decade, at all aspects of instrumentation and, the application of ESCA to a variety of industrial and academic circles has made the technique the most important and adaptable means of analysing surface characteristics. Since much of the work described in this thesis is related to ESCA, it is, therefore, convenient to provide a brief explanation of the principles involved and the application of X-ray photoelectron spectroscopy.

Table 2.1

Types of Electron Spectroscopy

Name of Technique	Basis of Technique
Photoelectron spectroscopy UPS or (Ultra-violet excitation) PES	Electrons ejected from materials by monoenergetic ultra-violet photons are energy analysed.
Photoelectron spectroscopy ESCA or (X-ray excitation) XPS	Electrons ejected from materials by monoenergetic X-ray photons are energy analysed.
Auger electron spectroscopy AES	Auger electrons ejected from materials following initial ionisation by electrons or photons (not necessarily monoenergetic) are energy analysed.
Ion neutralisation spectroscopy INS	Auger electrons ejected from surfaces following impact of a noble gas ion are energy analysed.
Penning ionisation spectroscopy PIS	Metastable atoms are used to eject electrons from materials. The electrons are energy analysed.
Autoionisation electron spectroscopy	Similar to Auger electron spectroscopy. Electrons ejected in an autoionising decay of super-excited states are measured. Electron or photon impact can be used to produce the super-excited states.
Resonance electron capture electron transmission spectroscopy	The elastic scattering cross-section for electrons is measured as a function of the energy of the electron beam and scattering angle.

2.2 Processes Involved in ESCA

2.2.1 Photoionisation

The interaction of a monoenergetic beam of X-ray with an atom in a molecule results in the photoemission of electrons with specific kinetic energies, related to the nature of atom.[151] The most commonly employed X-ray sources are $Mg_{k\alpha_{1,2}}$ and $Al_{k\alpha_{1,2}}$ with photon energies of 1253.7 eV and 1486.6 eV respectively. The advent of electronically operated dual anodes has led to use the harder sources such as Ti with photon energy of 4510 eV for analytical depth profiles. The photoejected electrons may be either core or valence electrons, the latter are usually studied, using ultra-violet photoelectron spectroscopy (UPS)[152] with He(I) (21.22 eV) or He(II) (40.8 eV) radiation. The lifetimes of the core hole states are typically 10^{-13} - 10^{-15} seconds,[155] emphasizing the extremely short time scales involved in ESCA, compared with most other spectroscopic techniques.

The total kinetic energy of an emitted photoelectron, including contributions from the vibrationals, rotational and translational motions, as well as electronic is given by equation (2.2):

$$KE = h\nu - BE - Er \qquad (2.2)$$

where $h\nu$ is the energy of the incident photon (ν is the frequency of the X-ray radiation and h is Planck's constant); BE is the binding energy of the photoejected electron - defined as the energy required to remove an electron to infinity with zero kinetic energy and, Er is the recoil energy

of the atom, which decreases with increasing atomic number and, in fact, it is only significant for the first few members of the periodic table that a recoil energy greater than 0.1 eV has been computed (H = 0.9 eV, Li = 0.1 eV, Na = 0.04 eV and K = 0.02 eV).[151] With the present resolution of typical ESCA spectra of solid systems, contributions from translational, vibrational and rotational motions are seldom observed and, thus, the equation (2.2) for a free molecule reduces to:

$$KE = h\nu - BE \qquad (2.3)$$

An important relationship exists between the binding energies observed experimentally by ESCA for solids versus free molecules, when compared with the values calculated theoretically by 'ab initio' and semi-empirical LCAO-MO-SCF treatments.

The most convenient reference level for a conducting sample is the Fermi level[156] or electron chemical potential, which is generally defined as the highest occupied level at absolute zero.

The work function, ϕ_s, for a solid is given by the energy difference between the free electron (vacuum) level and the Fermi level in a solid; and is represented schematically in Figure 2.1. The vacuum levels for the solid sample and the spectrometer may, however, be different and the emitted electron will experience either a retarding or accelerating potential equal to $\phi_s - \phi_{spec.}$, where $\phi_{spec.}$ is the work function of the spectrometer.[151] In ESCA, it is the kinetic

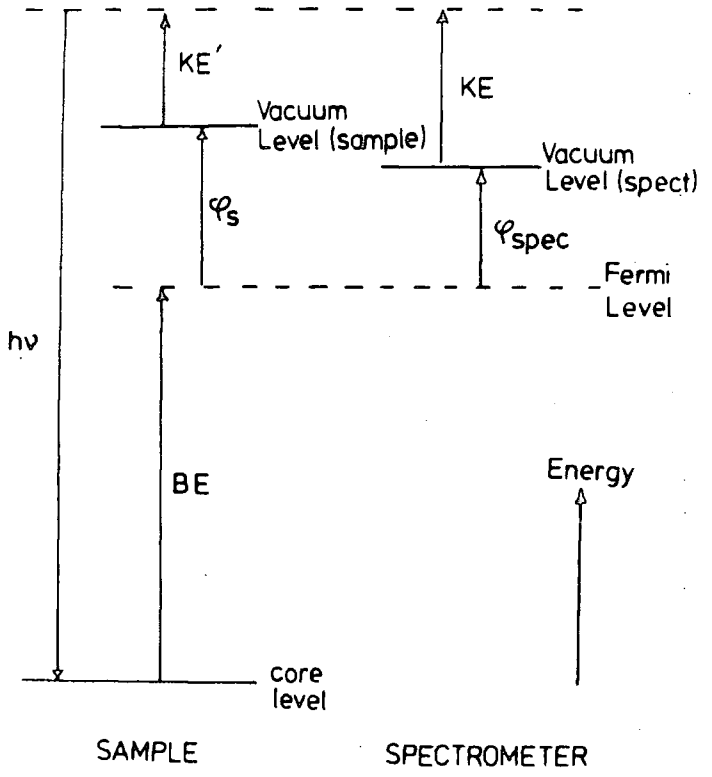

Figure 2.1. Relationship between vacuum level and Fermi level for a sample, isolated from the spectrometer.

energy of the electron that is measured as it enters the analyser and, taking zero binding energy to be the Fermi level of the sample. The following equation results:

$$BE = h\nu - KE - \phi_{spec.} \qquad (2.4)$$

The binding energy, referred to the Fermi level, does not depend on the work function of the sample but on that of the spectrometer and this represents a constant correction to all binding energies. Energy referencing and sample charging effects are discussed in section 2.5.

2.2.2 Processes accompanying photoionisation

Several processes accompany photoionisation and, these may be classed into two main groups depending upon whether they are slow compared to the original photoionisation, or occur within a similar time span. Electronic relaxation processes such as shake-up and shake-off are rapid processes and, occur within a similar time span, resulting in a measurable change of the kinetic energy of the photoemitted electrons. Auger and X-ray fluorescence, on the other hand, are relatively slow processes and, have little effect on the kinetic energy of the photoelectron. The basic processes involved in Auger and X-ray fluorescence are illustrated diagrammetically in Figure 2.2.

2.2.3 Electronic relaxation

The photoionisation of core electrons is accompanied by a substantial electronic relaxation of the valence electrons,[157-15] and this process is complete within a time scale of approximately 10^{-17} seconds. Experimental and theoretical studies have shown that for a given core level, the magnitude of relaxation energy (RE) is a sensitive function of the electronic environment of a molecule.[160-164] It is, therefore, of considerable importance in determining the absolute binding energy and the lineshapes of observed peaks by means of

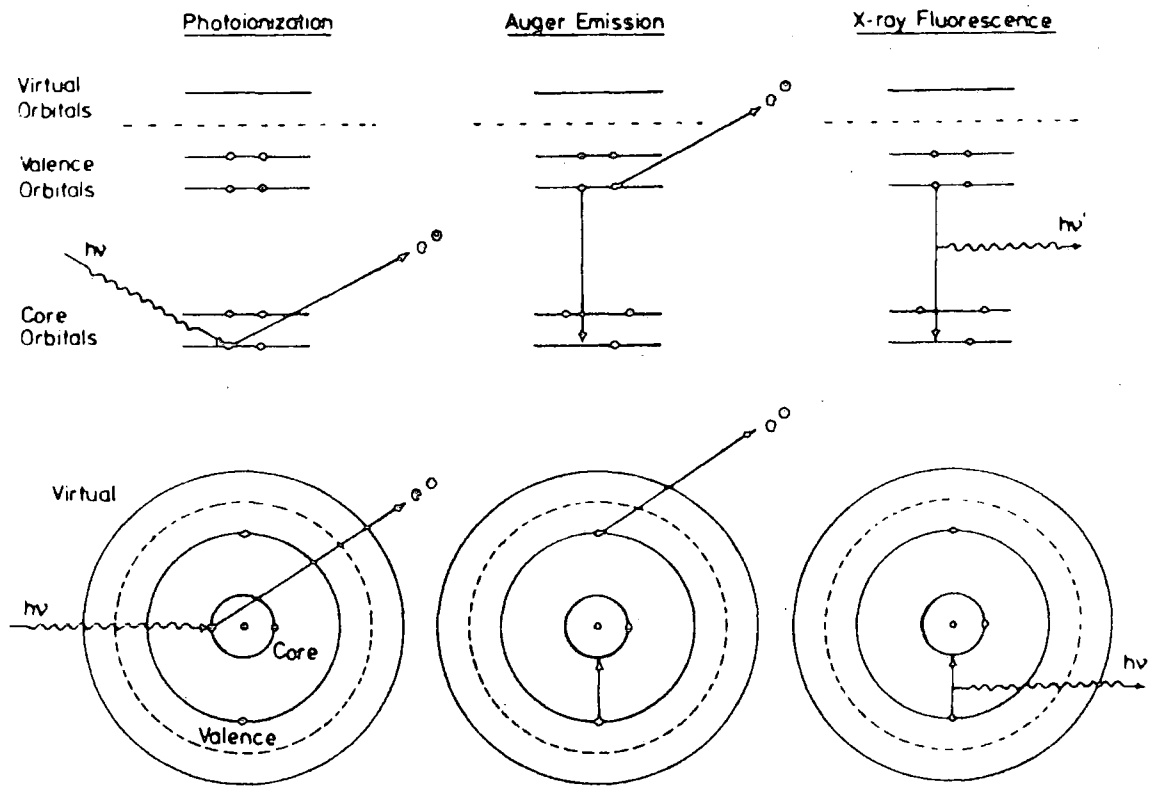

Figure 2.2. Schematic representation of direct photoionisation, Auger and X-ray fluorescence processes.

vibrational fine structure. Relaxation energies associated with the core ionisations of first row elements are considerable[165] and, are caused by the reorganisation of the valence electrons in response to the decreased shielding of the nuclear charge, whilst the relaxation of the core levels themselves contribute very little to the total reorganisation. The reorganisation changes the spatial distribution of the remaining electrons. The differences in relaxation energies for closely related molecules are small and, therefore, result

in minor shifts of binding energies. This is consistent with the tendency of Koopmans' theorem and self-consistent field (ΔSCF) calculations to give the same estimates of shifts despite the fact that Koopmans' theorem ignores the effect of electronic relaxation.[164] This provides a method for investigating the relaxation energies.

$$RE = BE\ (Koopmans) - BE\ (\Delta SCF) \qquad (2.5)$$

2.2.4 Shake-up and shake-off phenomena

The removal of a tightly bound core electron, which is almost completely screening as far as the valence electrons are concerned, is followed by substantial electronic reorganisation (relaxation) of the valence electrons in response to the effective increase in nuclear charge; and, this is sufficient perturbation such that the direct photo-ionisation leading to the ground state of a core ionised species is accompanied by simultaneous excitation of an electron from a higher occupied to lower unoccupied valence level (shake-up) and, in the limit, leads to a doubly ionised state (shake-off). Shake-up and shake-off processes, therefore, give rise to satellite peaks to the low kinetic energy side of the direct photoionisation peak, as shown in Figure 2.3. Since the energy for both these processes is derived from the original photoionisation, an equation (2.3) is adjusted to account for these multielectron processes:

$$KE = h\nu - BE + \bar{E} \qquad (2.6)$$

where $\bar{E}$ is the energy of the multielectron process.

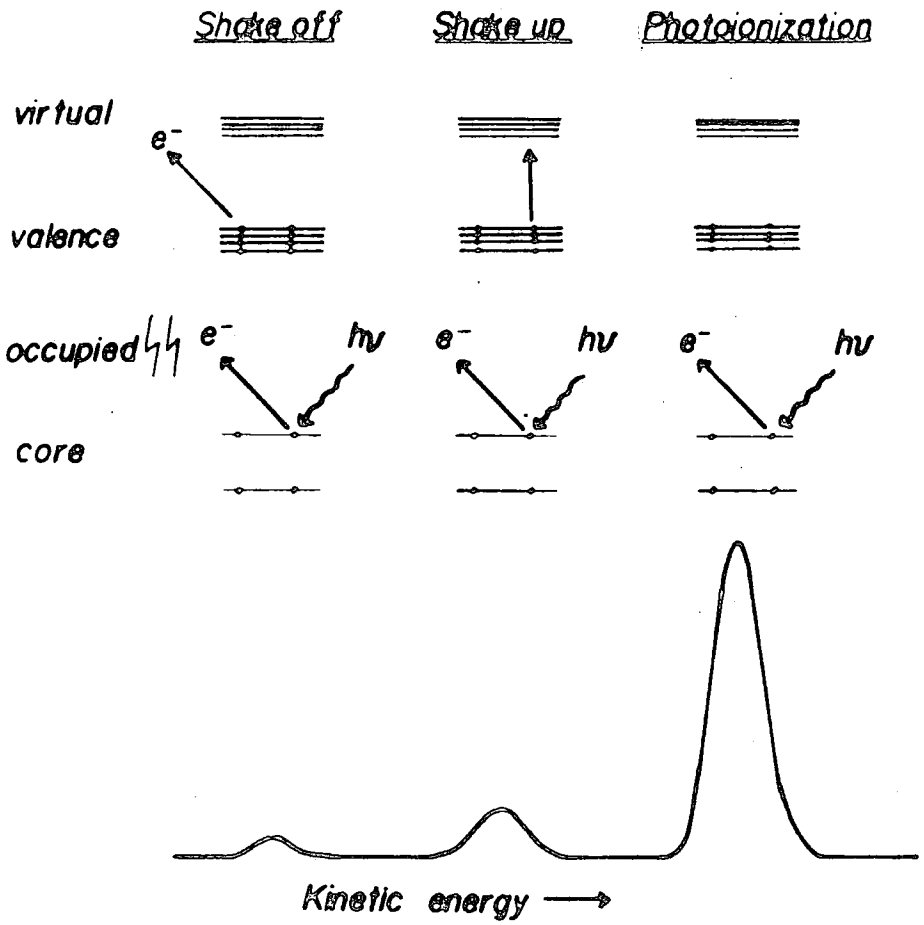

Figure 2.3. Schematic representation of photoionisation, shake-up and shake-off processes.

These excitations follow the monopole selection rules ($\Delta J = \Delta L = \Delta S = \Delta M_J = \Delta M_L = \Delta M_S = 0$), as indicated in equations (2.7) to (2.9).

$$\psi_i = \sum_{u=1}^{n} Cui\,\phi u \qquad (2.7)$$

$$\psi'_f = \sum_{v=1}^{n} kvf\,\phi' v \qquad (2.8)$$

$$P_{f \leftarrow i} = N \left| \sum_{u=1}^{n} kufc\mu i \; < \phi' u | \phi u > \right|^2 \qquad (2.9)$$

where, ψ_i is the initial state wave function and ψ_f is the final state wave function.

In the sudden approximation, transitions are directly related to the sums of one centre overlap terms involving the occupied orbitals of the initial system and the unoccupied (relaxed orbitals) of the final state.[166] These monopole excited states are analogues of the more familiar dipole, allowed excited states of the neutral molecule studied in conventional electronic spectroscopy.

The situation of shake-up transitions can be further visualised by considering excitations involving a core hole state in the doublet manifold, as depicted in Figure 2.4. There are two possibilities for a given excitation configuration, a singlet and triplet state can be generated in a simple orbital model. It is apparent that either unpaired electron in the valence orbital and that excited to the virtual orbital have opposite spins (singlet origin), or both may possess the same spin (triplet origin). The triplet state is lower in energy than that of singlet origin. Since both represent doublet states, transitions from the ground state of the core hole state may be viewed as both being allowed. In principle, one can expect experimentally to observe the energy separation and intensities for the components of the shake-up states of a given excitation configuration.

The direct relationship between shake-up and shake-off processes and relaxation energies was established by Manne

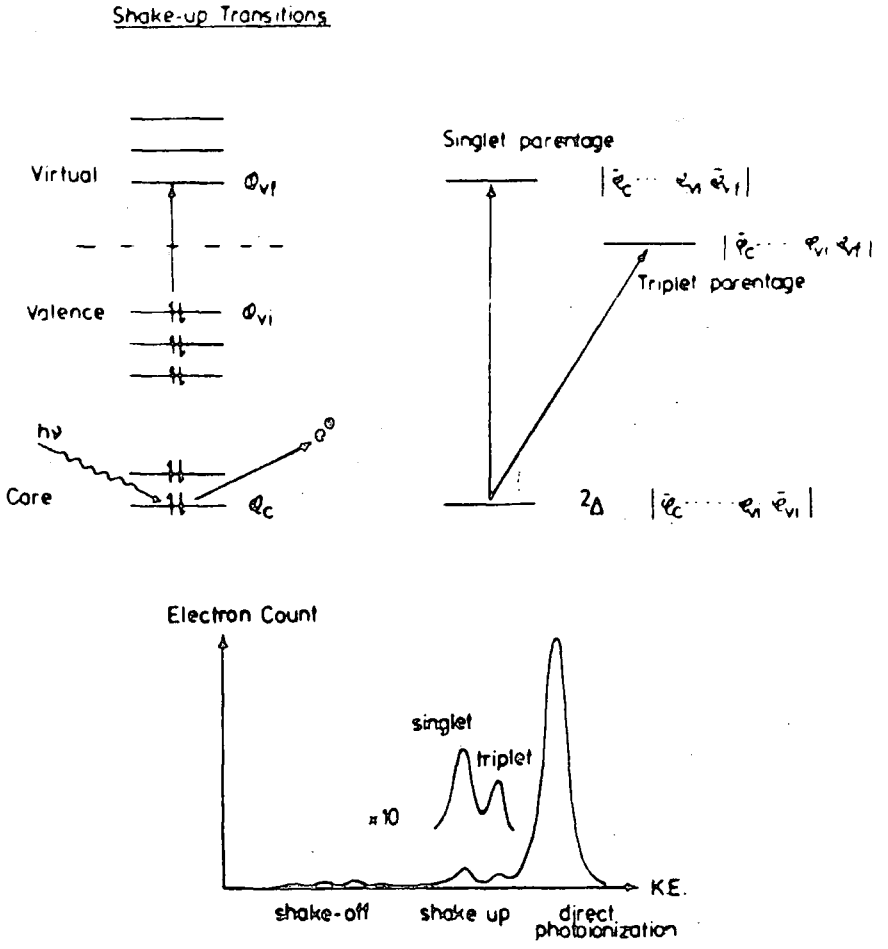

Figure 2.4. Schematic representation of singlet-triplet shake-up.

and Aberg.[167] They showed that the weighted average over the direct photoionisation, shake-up and shake-off peaks corresponds to the binding energy of the unrelaxed system (given by Koopmans' theorem). This is shown schematically in Figure 2.5.

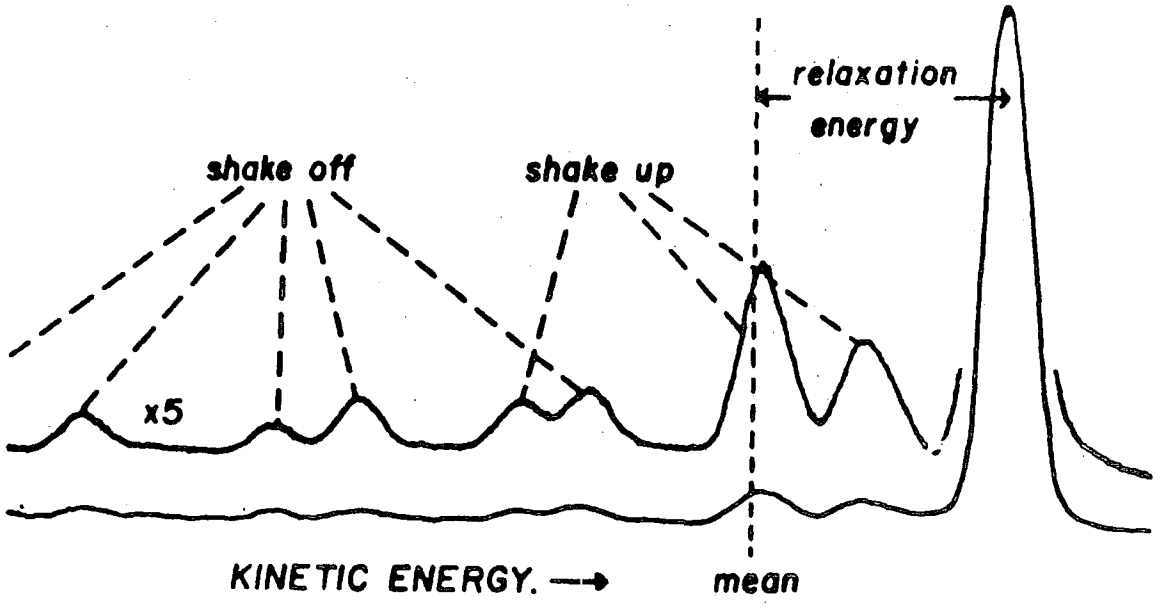

Figure 2.5. Relationship between relaxation energies, Koopmans' theorem (mean) and the relative intensities of direct photoionisation and shake-up and shake-off transitions.

The transition probabilities for high energy shake-off processes are relatively small, compared to the shake-up processes (which are of lower energy) and, these transitions of higher probability fall reasonably close to the weighted mean. In principle, the relaxation energy should be available from experimental measurements but, in practice, this is not generally feasible since the smaller shake-off peaks are often complicated by the presence of the general inelastic

tail (arising from photoemission from a given core level, followed by energy loss by a variety of scattering processes), which provides a broad energy distribution usually peaking for organic systems at approximately 20 eV below the direct photoionisation peak.

Shake-up and shake-off structures have been studied in organic and inorganic materials with particular attention to the transition elements. The shake-up phenomenon has proved to be valuable in elucidating the detailed structure and bonding in polymer systems, which are not directly attainable from the primary information levels in ESCA.[168-170]

2.2.5 Auger emission and X-ray fluorescence

De-excitation of the hole state, produced in a core sub-shell by X-ray radiation, can occur by X-ray fluorescence and Auger emission, the latter being most probable for elements of low atomic number, while the former becomes important for heavy elements (Figure 2.7). These fundamental processes are illustrated diagrammetically in Figure 2.6, which are comparatively slow compared to photoionisation; and, therefore, do not have much effect on the kinetic energy of the original photoelectron.

Auger emission may be viewed as a two step process, involving the ejection of an electron from an inner shell by a photon, followed by an electron dropping down from a higher orbital level to the vacancy in the inner shell with the simultaneous emission of a second electron.[171-176] When the electron drops from a valence shell to fill the inner shell vacancy, the Auger spectrum is related to the energies of both the valence and core orbitals.

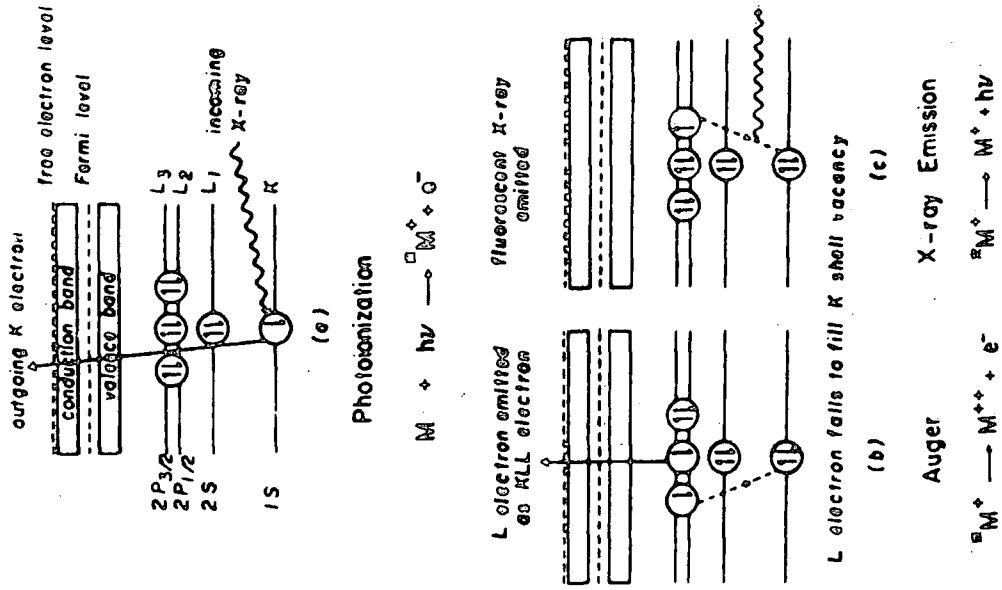

Figure 2.6. Photoionisation, Auger emission and X-ray Fluorescence.

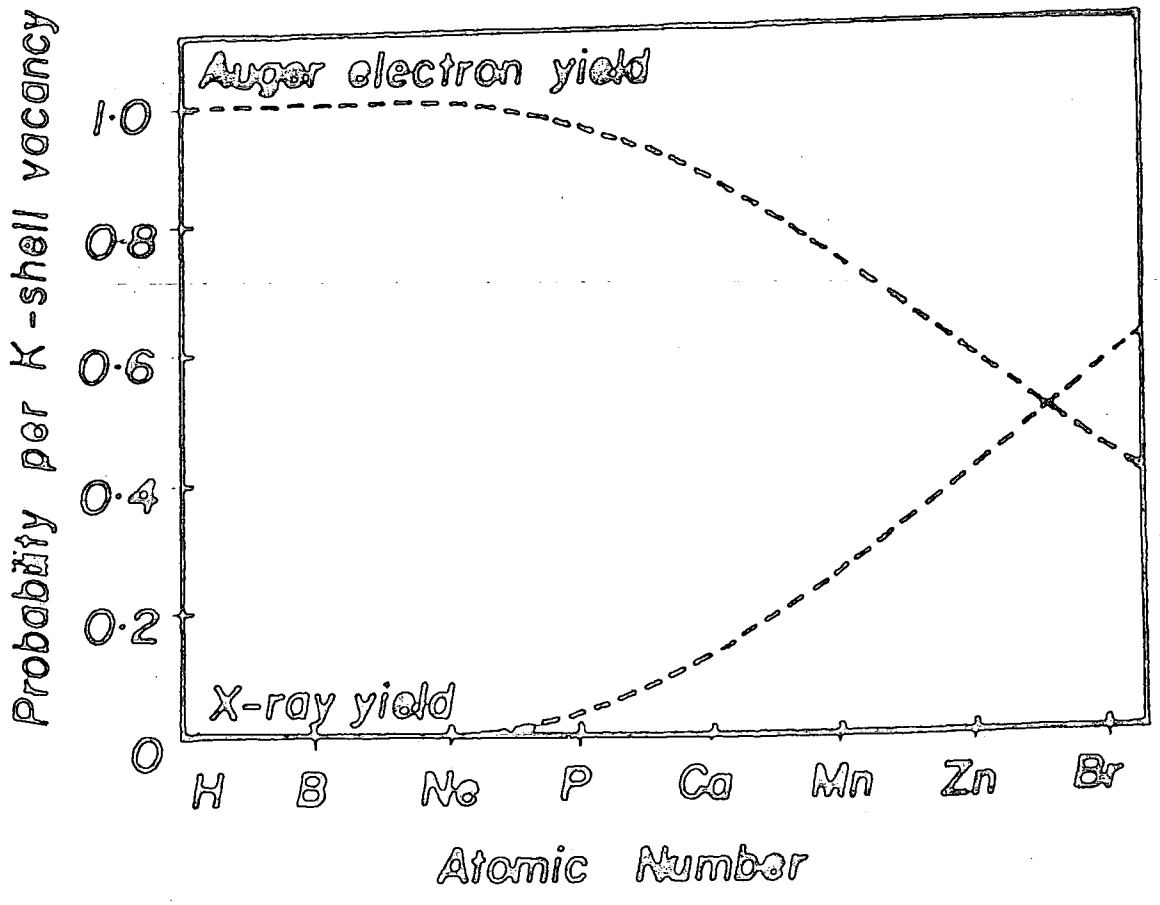

Figure 2.7. Efficiency of Auger and X-ray Fluorescence processes as a function of atomic number.

When the electronic vacancy in the inner shell is filled by an electron from another inner shell (Coster-Kronig transition),[175] the Auger spectrum is related to the inner orbital transition. Such spectra are often very well resolved but, unfortunately, lead to the broadening of ESCA spectrum as a result of very short lifetime of the process. The energy difference between the orbitals for the Coster-Kronig process to occur must be sufficiently large to eject an electron from an orbital in the higher shell. These processes only occur in elements of atomic number less than forty.[177]

Auger emission spectroscopy (AES) has become an important analytical technique, in particular, for studying the surfaces of metals and semi-conductors. Commercial Auger spectrometers use an electron beam as the source of excitation radiation. The flux of the incident electron is approximately three orders of magnitude larger than typical ESCA photon beam and, the radiation damage to organic materials is, therefore, a severe problem.[178,179]

The complexity of the Auger electron signal, therefore, hinders a straightforward extraction of chemical information as in ESCA. However, in the case of metal oxides, for example, the Auger chemical shift is much larger than the photoelectron chemical shift observed in ESCA because of polarisation screening effects. The direction of the shift is such that the kinetic energy of Auger electrons from polarisable atoms is increased more than the energy of photoelectrons in ESCA. A relationship between the shifts in Auger energy and the shifts in photoionisation has been

established from the studies of copper, zinc, lithium and sodium systems.[180-185]

The concept of the Auger parameter was developed by Wagner[186] by taking as the kinetic energy of the sharpest and most intense Auger line subtracted from the most intense photoelectron peak. This quantity is of considerable importance to analytical chemists since the Auger parameter does not involve sample charging effects. Chemical state scatter plot,[187] on which photoelectron and Auger data representative of a given element are used in conjunction with the ESCA data for the identification of chemical states. The Auger parameters for zinc systems are discussed in chapter three for the identification of ZnO and ZnS states.

X-ray fluorescence (secondary-emission) is an excellent technique for the qualitative analysis of elements with atomic number greater than ten. Concentrations down to 0.1% for light elements and 0.01% for heavy elements (Fe, Co, Ni) have been detected.[188]

2.3 Chemical Shifts

The energies of core electrons are characteristic of a particular element (Table 2.2) and, are sensitive to the electronic environment of that atom (Figure 2.8). The changes in chemical environment of a given atom give rise to measurable changes (chemical shift) in binding energies of photoemitted electrons, often representative of a given structural feature. Figure 2.8 illustrates the C_{1s} spectrum of ethyl trifluoroacetate. The experimental chemical shifts

Table 2.2

Approximate core binding energies (eV)

	Li	Be	B	C	N	O	F	Ne
1s	55	111	188	284	399	532	686	867
	Na	Mg	Al	Si	P	S	Cl	Ar
1s	1072	1305	1560	1839	2149	2472	2823	3203
2s	53	89	118	149	189	229	270	320
$2p_{1/2}$	31	52	74	100	136	165	202	247
$2p_{3/2}$	31	52	73	99	135	164	200	245

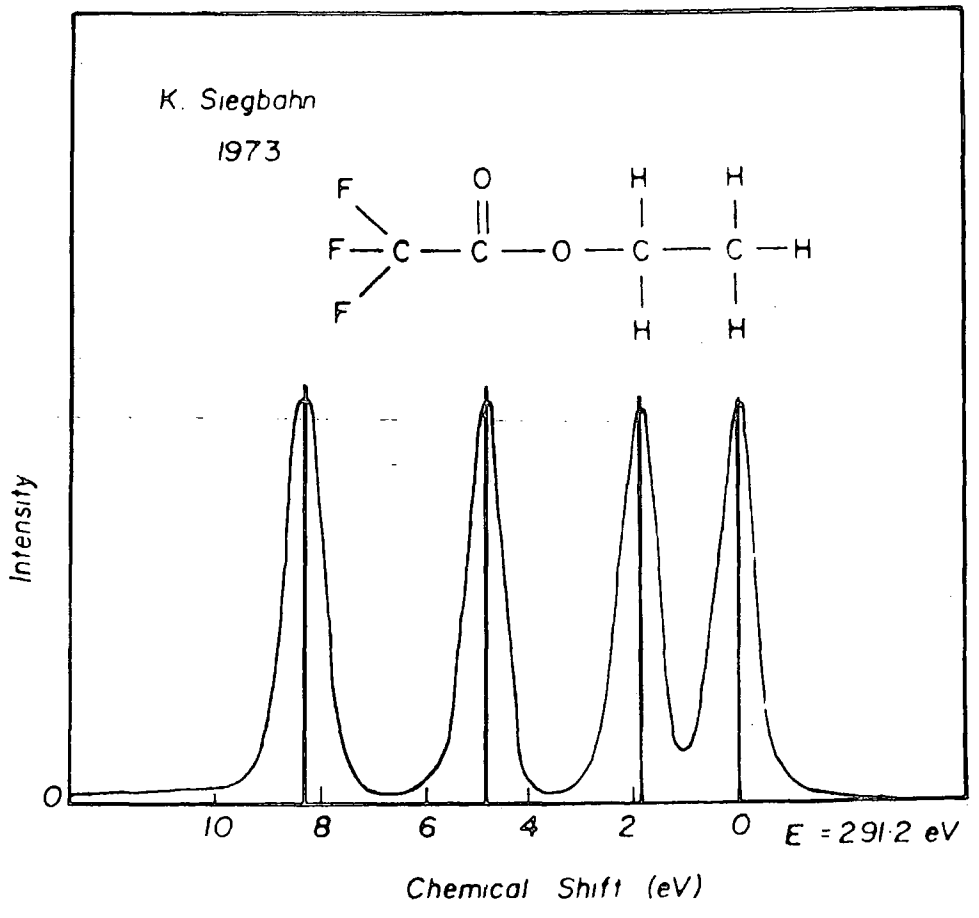

Figure 2.8. C_{1s} spectrum of trifluoroacetate.

have been calculated theoretically by several distinct approaches:

(i) Koopmans' theorem[189]

(ii) Core hole calculations[236,237] - linear combination of atomic orbitals - molecular orbital - self consistent method (LCAO-MO-SCF)

(iii) Equivalent cores model[190]

(iv) Charge potential model[152]

(v) Quantum mechanical potential model[191-193]

(vi) Many body formalism.

An account of the physical processes involved in electron photoemission and their effects from a theoretical standpoint has been provided by Fadley.[115]

2.4 Fine Structure

2.4.1 Multiplet splitting

Multiplet splittings occur in paramagnetic systems from interactions between unpaired electrons present in the system and the unpaired core orbital electrons, remaining after photoionisation. Examples of the core level spectra for transition element compounds are well known.[195,196] The theoretical interpretation of multiple splittings is relatively simple only for S-hole states and, is based on Van Vlecks' vector coupling model.[197] The splitting, ΔE, (the energy difference between the states $S + \frac{1}{2}$ and $S - \frac{1}{2}$) is proportional to the multiplicity of the ground state, given by equation (2.10):

$$\Delta E = (2S + 1)K \qquad (2.10)$$

where K is the exchange integral between the core (c) and the

valence (v) electrons under consideration and, is defined by:

$$K = \langle \phi_r(1)\phi_c(2)\left|\frac{1}{r_{12}}\right|\phi_v(2)\phi_c(1) \rangle \qquad (2.11)$$

The intensities of the peaks are proportional to the degeneracies of the final states:

$$[2(S + \tfrac{1}{2}) + 1]/[2(S - \tfrac{1}{2}) + 1] = (S + 1):S \qquad (2.12)$$

The magnitudes of multiple splittings are independent of sample charging effects and reference level. A detailed review has been provided by Fadley.[198] The magnitude of the splitting for a given ion or atom can provide valuable information, concerning the localisation, or delocalisation of the unpaired valence electrons in compounds,[151,199] since the splitting increases with increasing spin density on an atom. The multiplet splitting ΔE^i on the i^{th} atom can be approximated by assigning a fraction of spin density to the i^{th} atom; and, is given by equation (2.13):

$$\Delta E = f_i(2S + 1)K_i \qquad (2.13)$$

For example, simple molecules N_2, NO and O_2, studied by Siegbahn et al[152] in the gas phase, revealed that the N_2 molecule did not possess core level splitting since the core level (1S) after photoionation was degenerate with respect to spin; whereas, NO and O_2 core levels were split by the presence of unpaired electrons. Figure 2.9 describes the orbital levels in N_2, NO and O_2 and Figure 2.10 the ESCA 1S levels of the molecules. The NO molecule has one unpaired electron in the 2π orbital and, therefore, upon photoemission

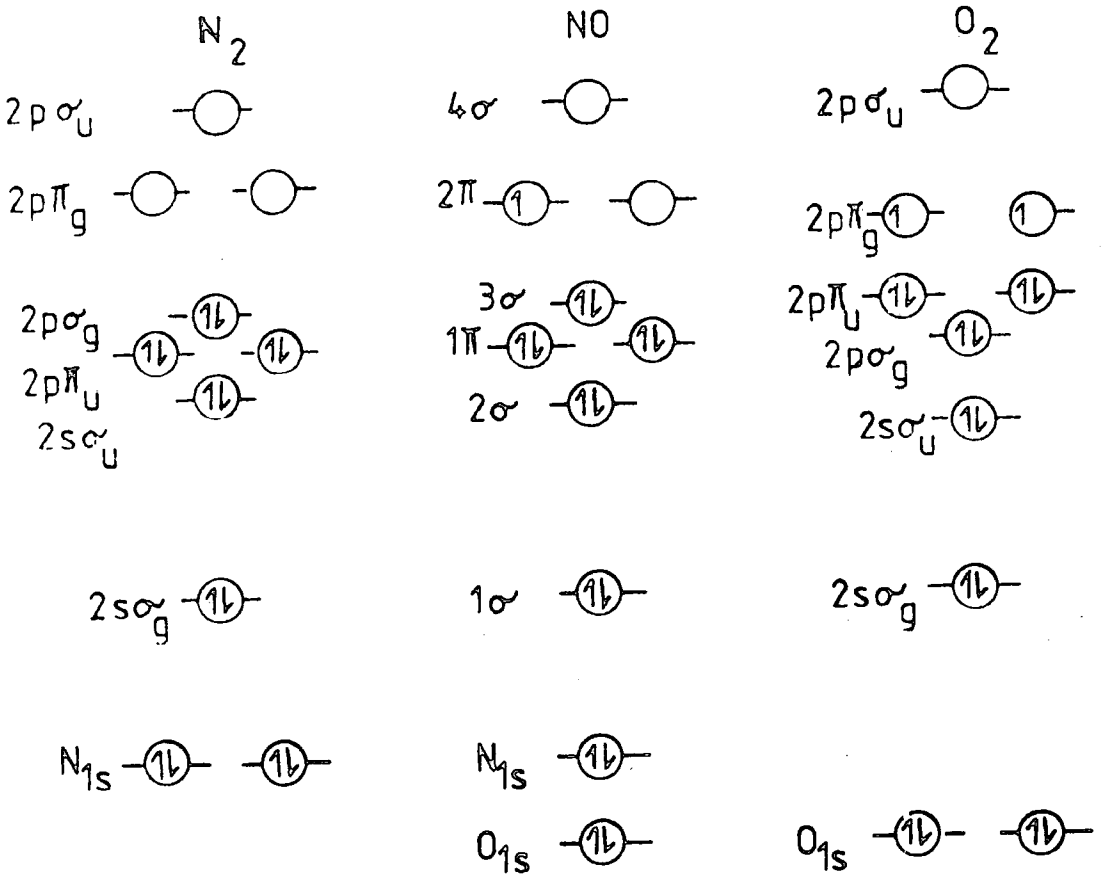

Figure 2.9. Electronic configurations of N_2, NO and O_2.

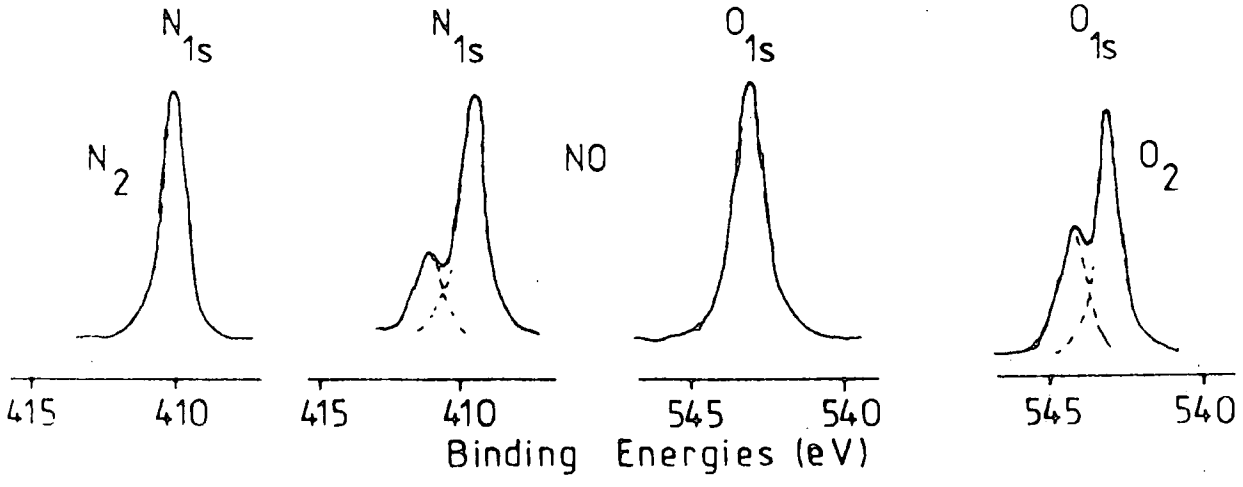

Figure 2.10. ESCA peaks for N_2, NO and O_2, gas phase.

of either an oxygen 1S, or nitrogen 1S, the molecular ion (NO^+) is left in either a triplet, or singlet state respectively. The observed splitting in the 1S spectrum can be attributed to the exchange interaction between the core electrons and the two unpaired electrons having different energies. The O_2 molecule has a similar electron configuration to NO but with two unpaired electrons in its outer πg orbital and, again, splitting of the oxygen peak is observed.

2.4.2 Spin-orbit splitting

Spin-orbit splitting results upon photoionisation of an orbital, which has an orbital quantum number (ℓ) greater than one (i.e. from p, d and f orbitals). The doublet structure occurs from a coupling of the two magnetic moments of the spin (S) and the orbital angular momenta (L) of the electron to yield a total momentum (J):[323,324]

$$J = S + L \qquad (2.14)$$

When the spin-orbit coupling is weak, the orbital angular momenta couple to give a resultant L instead of coupling to the spin angular momenta.

The relative intensities of the component peaks in the doublet structure are proportional to the ratio of the degeneracies of the states, which is quantum mechanically defined by $(2J + 1)$. The relative signal intensities of the J states for the S, p, d and f levels are indicated in Table 2.3 and illustrated in Figure 2.11.

Table 2.3

Intensity ratios for different levels

Orbital	Orbital quantum number	Total quantum number $J = (\ell \pm S)$	Intensity ratio $(2J + 1)/(2J + 1)$
S	0	$^1/_2$	singlet
P	1	$^1/_2$, $^3/_2$	1:2
d	2	$^3/_2$, $^5/_2$	2:3
f	3	$^5/_2$, $^7/_2$	3:4

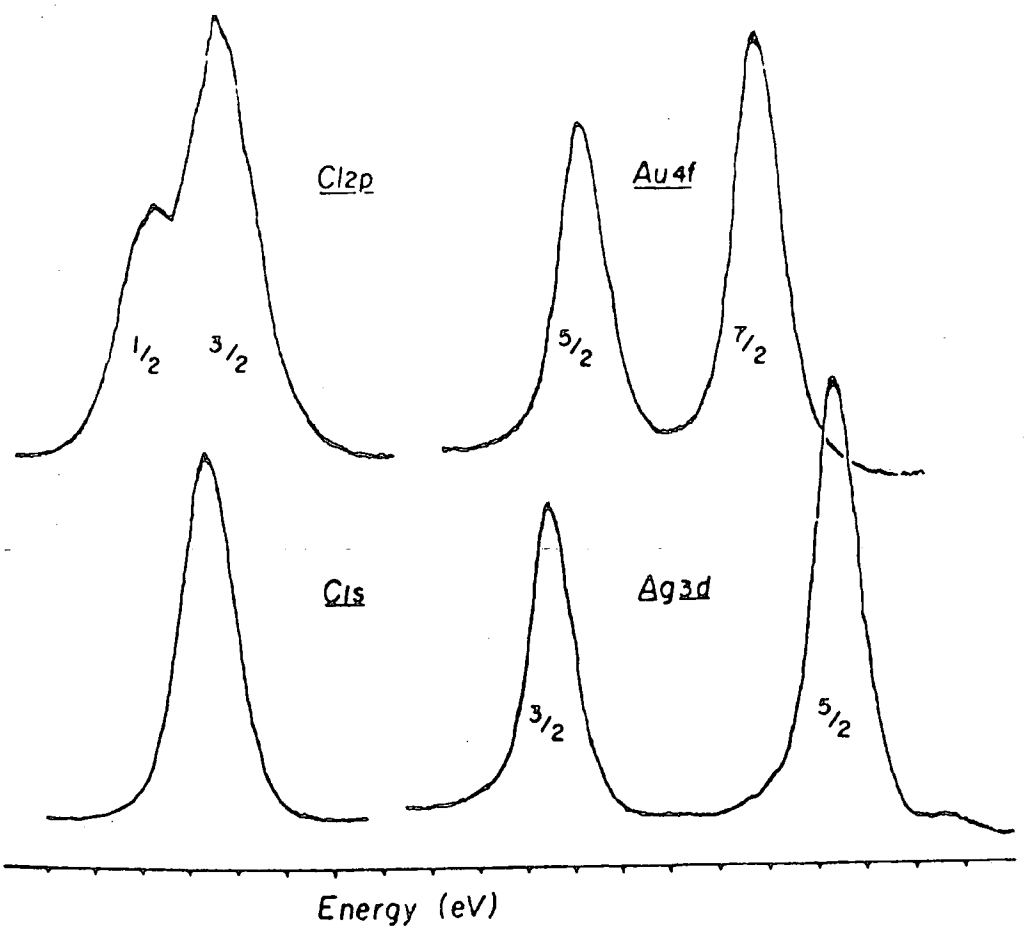

Figure 2.11. Spin-orbit splittings in C_{1s}, Cl_{2p}, Ag_{3d} and Au_{4f} core levels.

2.4.3 Electrostatic splitting

This results from the differential interaction between the external electrostatic field and the spin states of the core level under investigation.[325,326] Electrostatic splittings have been observed for a number of systems, for example, the $5p_{3/2}$ levels of uranium and thorium and in some compounds of gold.[327,328] A definite correlation has been found between electrostatic splitting and the quadrupole splittings obtained from Mössbauer spectroscopy,[329] which arise from the interaction of the nuclear quadrupole moment with an inhomogeneous electric field.

The types of fine structures, which may be encountered in ESCA, are summarised in Figure 2.12.

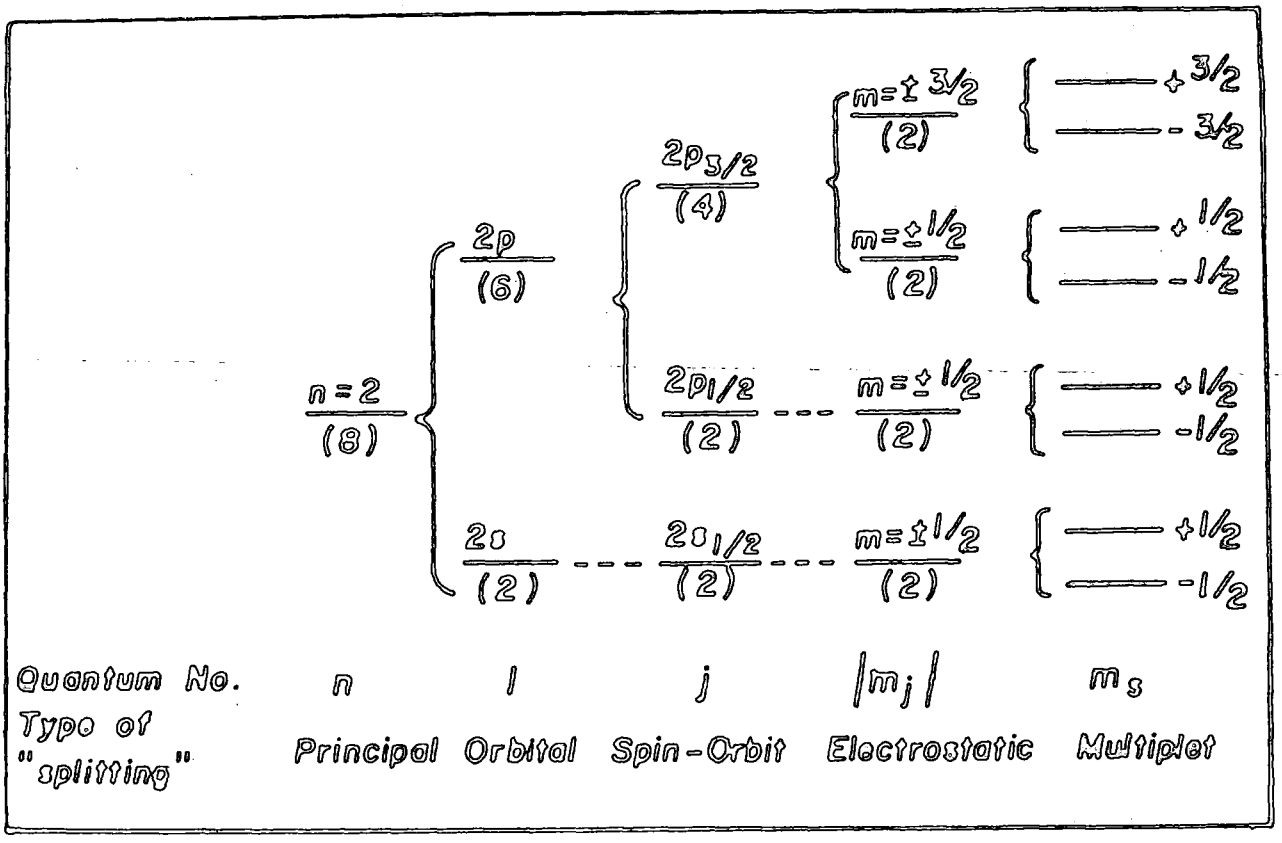

Figure 2.12. Schematic of the types of splitting encountered in ESCA.

2.5 Energy Referencing

As it has been stated in section 2.2.1 that for samples in electrical contact with the spectrometer, the energy levels referenced with respect to the Fermi level of the sample are operationally convenient. However, for insulating samples such as polymers, the Fermi level is not well defined and, it lies somewhere between the predominantly filled valence bands and predominantly empty conduction bands. Consequently, the sample charging must be detected for correction of this phenomenon, if absolute binding energies are required.

Three basic situations may arise for samples studied as solids in the spectrometer. In the first, the sample is in electrical contact with spectrometer. This is usually the case for films deposited in situ on a conducting substrate in the spectrometer source. Since the mean free path for the incident X-ray beam is very large,[151] depending on the conditions, for films of the order of 1000Å to have sufficient charge carriers to remain in electrical contact with the spectrometer. This can most readily be the case by applying a bias voltage to the sample probe.[330] If the sample is in electrical contact, the apparent shift in energy scale will exactly follow the applied bias. It is, therefore, possible to study the secondary electron distribution by shifting the position of the true zero of the kinetic energy scale and, this provides a direct energy reference. If the sample has been deposited on a substrate such as gold, it is possible to measure the core levels of the sample whilst monitoring the

$Au_{4f_{7/2}}$ core level[155] and, this provides a convenient means of energy referencing.

The second situation arises for thick insulating samples. It is often convenient to study samples mounted on double sided Scotch tape either as powder, or as discrete films. In this circumstance, there is only a fortuitous possibility that the samples will be in electrical contact with the spectrometer and, in general, it will be floating at some potential, due to surface charging; and, indeed, this charging process may be time dependent. If care is taken in the measurements, the charge built up on a sample and its time dependence may be used to investigate the electrical and chemical characteristics of samples.[331,332] The most reliable method of energy referencing is to follow the slow build up of hydrocarbon contamination at the surface. With a base pressure of $\sim 10^{-8}$ torr, the partial pressure of extraneous hydrocarbon material is such that taken in conjunction with the low sticking coefficient for most organic and polymeric systems, it normally takes several hours before any signal arising from hydrocarbon is apparent (binding energy 285 eV for hydrocarbon must be independently established for a given spectrometer. It almost certainly arises from long chain hydrocarbon material). It is, of course, possible to deliberately leak in straight hydrocarbon material to follow the build up at the surface. Such material almost always goes down in uniform coverage and, at submonolayer coverage acquires the same surface potential as the sample. This is not necessarily the situation with regard to metals deposited

on the surface since there is a marked tendency to 'island' and as such, differential charging may occur. In addition, since gold is normally evaporated from a filament, the possibility of surface damage, reaction or evaporation of substrate during deposition cannot be discounted. The use of the so-called 'gold decoration' technique[333] is, therefore, not recommended for organic and polymeric materials. The insulating samples provide the motivation for the use of electron 'flood guns'[334] in spectrometers employing monochromatic X-ray sources. The removal of Bremsstrahlung as a source of secondary electrons can lead to shifts in the kinetic energy scale in the hundred electron volt range and, can be compensated by flooding the sample with low energy electrons. However, the samples can become negatively charged and the method needs great care to achieve an accuracy comparable with that for the other methods. An alternative source of low energy electrons is to illuminate the sample region with ultra-violet radiation from a low pressure, low power mercury lamp via a quartz viewing port in the source region of the spectrometer. Sufficient secondary electrons are generated from photoemission, from the metal surfaces that sample charging is reduced to a low level.

The third situation can arise for films of thickness greater than one micron, which have been built up by deposition on a conducting substrate. Such films behave as 'leaky' capacitors in that they exhibit rather striking time dependent charging and discharging characteristics and, follow an applied bias potential in a particular manner. Since the dynamic

equilibrium, which is established under X-ray irradiation, invariably, produces an overall positive charge on the sample, the application of a positive bias voltage causes a smaller shift in the kinetic energy scale than the applied voltage, whereas a negative bias voltage produces a larger shift in the kinetic energy scale than the applied voltage. From a study of these effects and from the secondary electron distribution, the energy reference may readily be established. The investigation of such effects as a function of film thickness in the range 1 - 100 micron provides an interesting insight into the electrical characteristics of polymer samples[331,332] and, the typical behaviour, which is observed is shown in Figure 2.13.

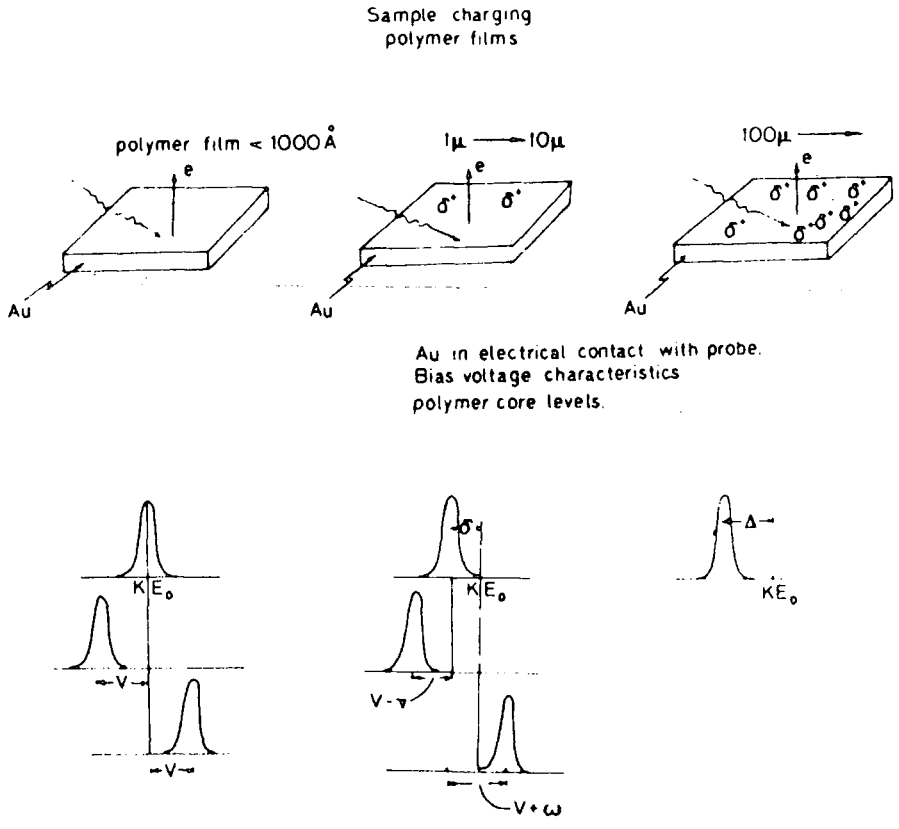

Figure 2.13. Typical sample charging characteristics for polymer films.

The energy reference in each case for the measurements described above is the Fermi level. Although the exact location of this level in relation to the valence and conduction bands is generally unknown for polymers, it is possible for an 'insulator' to be in electrical contact with the spectrometer (i.e. their Fermi levels are the same). Despite the difficulties associated with defining an analytical expression for the Fermi level of an insulator, the use of the Fermi level as an energy reference is operationally convenient. If the work function of the insulator is known, one can calculate the binding energy with respect to the vacuum level.

Although sample charging has been regarded as somewhat of a nuisance, which must be circumvented, recent work has shown[335,336] that sample charging is an interesting phenomenom in its own right and in appropriate cases provides an important means of studying photoconductivity in polymer films.

2.6 Signal Intensities

Figure 2.14 illustrates a schematic representation of the general geometry of the ESCA experiment, employing a fixed arrangement of analyser and X-ray source. $h\nu$ represents the incident X-rays and $\bar{e}$ the fraction of the photoelectrons entering the analyser. ϕ is the angle between the X-ray source and the analyser entrance slit and, θ describes the angle of the sample in relation to the analyser (low values of θ approximately equal to zero correspond to grazing incidence of the X-rays and, high values of θ approximately

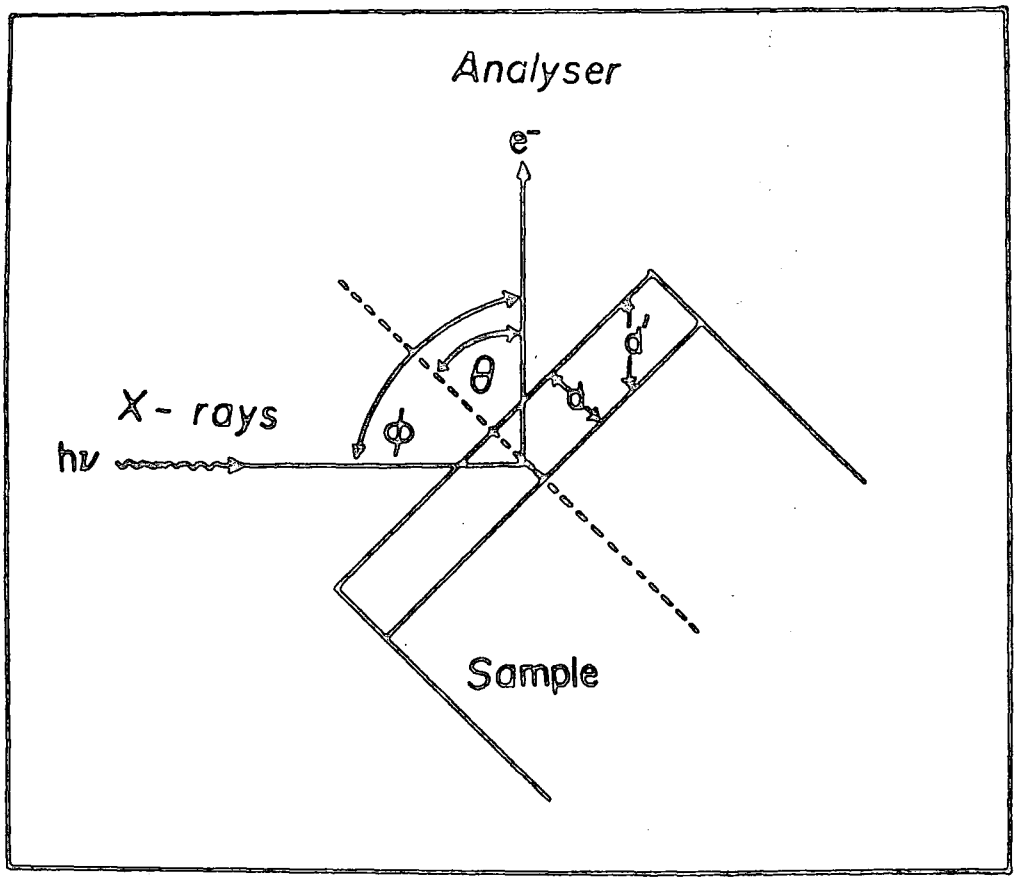

Figure 2.14. Schematic representation of the sample geometry relative to the X-ray gun and analyser.

equal to 90° correspond to grazing exit from the sample of the photoemitted electrons, which are analysed). The parameters affecting the signal intensities are discussed in the proceeding sections.

2.6.1 Fixed angle studies

For an 'infinitely thick' homogeneous sample, the intensity (I) of the elastic (no energy loss) photoionisation peak from a core level (i) is expressed as:[337,338]

$$dI_i = F\alpha_i N_i K_i e^{-x/\lambda_i} dx \qquad (2.15)$$

where I_i is the intensity arising from the core level i,

F is the exciting photon flux,

d_i is the number of atoms per unit volume, on which the core level is localised,

k_i is the spectrometer factor, and

λ_i is the electron mean free path.

Integration of equation (2.15) gives:

$$I_i = \int_0^{\alpha} F\alpha_i N_i K_i e^{-x/\lambda_i} dx \qquad (2.16)$$

$$I_i = F\alpha_i N_i K_i \lambda_i \qquad (2.17)$$

The various factors and parameters governing the intensity of a given signal in ESCA are discussed individually in the ensuing discussion.

The X-ray flux (F) is primarily dependent on the power applied to and the efficiency of the X-ray gun. However, the angle of incidence ϕ of the X-rays and the analyser and θ do have an effect on the intensity of the photoionisation peak.

The cross-section (α_i) for photoionisation of core level (i) is a parameter, which describes the probability of the core level being ionised, when irradiated by a photon of known energy[339] and, includes only the fraction of the total number of electrons photoemitted within the angle of acceptance of the analyser focussing lens. α_i is a function of the core level to which, it relates and of the energy of the incident photon. α_i values can be calculated from the fundamental properties of the atom[340] or determined experimentally from gas phase ESCA experiments.[152] The geometry of the X-ray

source with respect to the analyser entrance slit affects α_i values but α_i is normally constant for a particular spectrometer with the same X-ray source and a fixed value of ϕ. It has been well established that the cross-section, in the dipole approximation, for randomly oriented polyatomic molecules and unpolarised light is of the form:[341,342]

$$\alpha_i = \alpha_i^{TOT}/4\pi[1 - \frac{1}{4}\beta_i(3\cos^2\phi - 1)] \qquad (2.18)$$

where β_i is the asymmetry parameter[343] of the core level and α_i^{TOT} is the total cross-section of the level. With $Mg_{k\alpha_{1,2}}$ and $Al_{k\alpha_{1,2}}$, the cross-sections for photoionisation of core levels of most elements in the periodic table are within two orders of magnitude of that for the C_{ls} levels; and, therefore, the ESCA has a convenient sensitivity range for all elements. The cross-sections for core levels are generally considerably higher than for valence levels.

The spectrometer factor (K_i), which varies from one instrument to another, depends on the detector efficiency, transmission characteristics of the analyser - which are both dependent on the kinetic energy of the core electrons being analysed, and geometric arrangement of the sample chamber (i.e. angle of acceptance by solid) to the analyser.

The electron mean free path (λ_i) of photoemitted electrons (alternatively referred to as the escape depth) is the distance in the solid through which the electrons will travel before $^1/_e$ of them have not suffered energy loss through inelastic collisions. The values of electron mean free path have calculated theoretically[344] and determined

experimentally.[345,346] The mean free path is a function of kinetic energy of the photoemitted electrons and ranges from $\sim$ 4Å for electrons of approximately 80 eV kinetic energy to $\sim$ 30Å for electrons of approximately 1500 eV.

The sampling depth is defined as the depth from which 95% of the signal comes from a given core level and is related to λ by:

$$\text{Sampling depth} = -\lambda \ell n 0.05 \simeq 3\lambda \qquad (2.19)$$

If the photoelectrons are emitted from a depth (d) of the sample, their true path length (d') will be:

$$d' = d\cos\theta \qquad (2.20)$$

(see Figure 2.14).

As an example, for the carbon 1s level investigated by a $Mg_{k\alpha_{1,2}}$ X-ray source, the kinetic energy of the photoelectrons is $\sim$ 960 eV and the mean free path of the electron is $\sim$ 10Å. 50% of the signal seen by ESCA is derived from the outermost 7Å and 95% from the top 30Å. This, clearly, illustrates the high surface sensitivity of the ESCA.

N_i is the number of atoms per unit volume on which the core level is localised. The most significant property of N_i is that the relative signal intensities for core holes in a homogeneous sample are directly related to the overall stoichiometries of the atoms in the sample. This is due to the fact that the peak intensity from a given core level is directly proportional to the number per unit volume of the atom in the sample,[166]

$$\frac{I_i}{I_j} = \frac{F\alpha_i N_i K_i \lambda_i}{F\alpha_j N_j K_j \lambda_j} \qquad (2.21)$$

where I_i and I_j correspond to the core level intensities. If i and j are core levels of the same atom, then the state of equation (2.21) becomes:

$$\frac{I_i}{I_j} = \frac{N_i}{N_j} \qquad (2.22)$$

If i and j are different core levels then $K_i\alpha_i\lambda_i \neq K_j\alpha_j\lambda_j$ and

$$\frac{N_i}{N_j} = \frac{I_i}{I_j}\frac{K_j\alpha_j\lambda_j}{K_i\alpha_i\lambda_i} \qquad (2.23)$$

The ratio $\frac{K_j\alpha_j\lambda_j}{K_i\alpha_i\lambda_i}$ is known as the sensitivity factor, which can be determined from known samples of simple stoichiometry. These ratios vary from one spectrometer to another and, therefore, must be determined for the particular spectrometer.

2.6.2 Analytical depth profiling

It is often important to investigate samples for which the surface is not representative of the bulk that a single homogeneous component of thickness (d) is present on a homogeneous base, as is illustrated in Figure 2.15. The intensity of the signal arising solely from the overlayer can be expressed by integrating equation (2.16) between x = 0 and x = d.

$$I_i^{over.} = F\alpha_i N_i \lambda_i (1 - e^{d/\lambda_i}) \qquad (2.24)$$

Similarly, a solution for the signal intensity arising from the substrate is obtained.

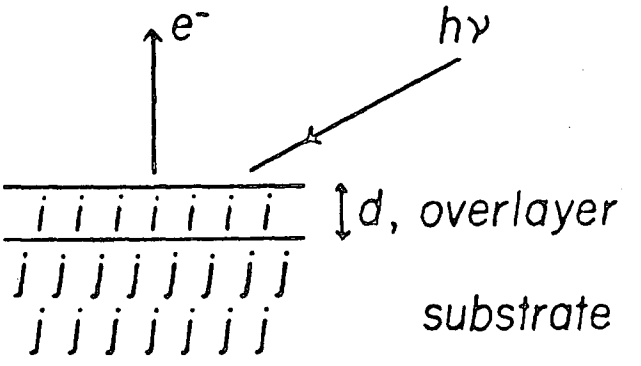

Figure 2.15. Substrate/overlayer model.

$$I_j^{subs.} = F\alpha_j N_j K_j \lambda_j e^{-d/\lambda_j} \qquad (2.25)$$

Figure 2.16 illustrates a general correlation between the electron mean free path and its kinetic energy. In the energy range of interest to ESCA (greater than 300 eV), the mean free path increases with increasing kinetic energy. As a consequence of this increase in mean free path and, hence, the effect of λ_j on the intensity (I_j) from the substrate, the attenuation of a signal arising from a core level in the substrate by an overlayer is dependent strongly on the kinetic energy of the photoemitted electrons. Thus a non-fluorine containing overlayer on a fluorine containing substrate will result in a decrease of F_{1s}/F_{2s} ratio since the kinetic energy and mean free path of the F_{2s} photoemitted electrons are greater than those for the F_{1s} photoelectrons.

In order to analytically depth profile a sample, it is,

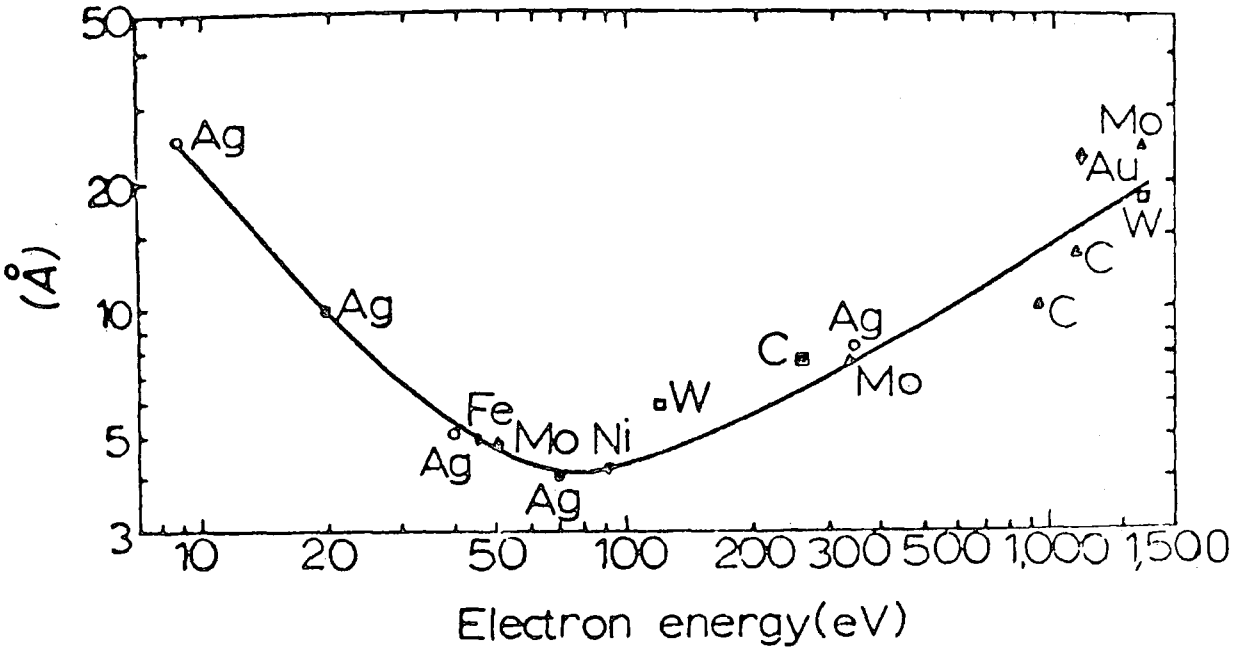

Figure 2.16. Mean free paths of photoemitted electrons.

therefore, necessary to obtain accurately the electron mean paths at the kinetic energies of interest, in the materials being investigated.

2.6.3 Angular dependence of signal intensities

The use of angular studies to delineate the surface and subsurface is a well established technique, and is used extensively in this laboratory.[347] The Figure 2.17 draws a comparison between a narrow X-ray beam and a beam, which is broader than the width of the sample (ω). For a narrow beam, the total flux hitting the sample is not affected by varying θ. However, with a broader beam, the total flux hitting the sample varies $\omega\sin\theta$; and, therefore, this effect tends to increase the signal intensity as the θ is increased. For a given value of θ, the entrance slit of the analyser allows the photoemitted

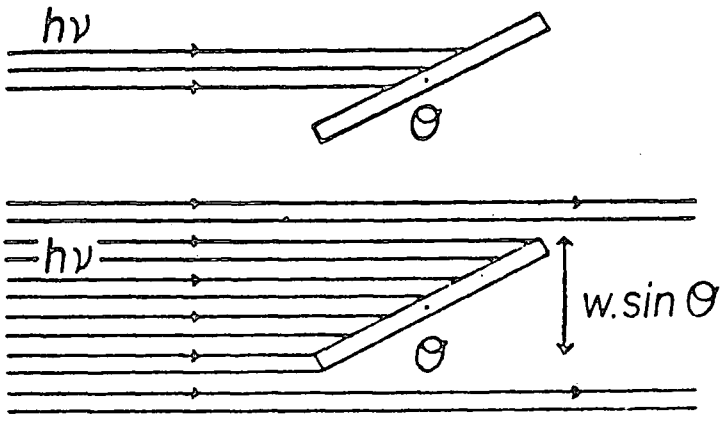

Figure 2.17. Narrow and wide X-ray beam.

electrons from a sample area proportional to $w\cos\theta$. As θ is increased, this effect tends to decrease the signal intensity. The convolution of these two opposing effects produces an overall function of θ ($f_i(\theta)$ for a core level (i)), which exhibits a maximum value. Equation (2.17), therefore, takes the form of:

$$I_i = f_i(\theta) F \alpha_i N_i K_i \lambda_i \tag{2.26}$$

where $f_i(\theta)$ can be determined empirically. The addition of angular effects into equations (2.24) and (2.25) gives:

$$I_i^{over.} = f_i(\theta) F \alpha_i N_i K_i \lambda_i (1 - e^{-d/\lambda_i \cos\theta}) \tag{2.27}$$

$$I_j^{subs.} = f_j(\theta) F \alpha_j N_j K_j \lambda_j e^{-d/\lambda_i \cos\theta} \tag{2.28}$$

Further detailed information of these angular phenomena can be found elsewhere.[331,347]

2.7 Line Shape Analysis

The larger inherent width of the core level than the chemical shift of that level arising in ESCA measurements, has led to the need for an accurate line shape analysis for delineation of core environments within a given envelope.[155] The major contribution to broadening line-widths arises from the less efficient monochromatisation of the X-ray photon source, although, with efficient monochromation of X-ray radiation, the need for such analysis may well disappear. However, a precise method of analysis remains a necessity with present instrumentation to make full use of the available information levels from ESCA.

The measured line-widths for core levels (after taking into account spin orbit splittings, if these are not resolved) may be expressed as:

$$(\Delta Em)^2 = (\Delta Ex)^2 + (\Delta Es)^2 + (\Delta Ecl)^2 \qquad (2.29)$$

where, ΔEm is the measured width at half height, so-called full width at half maximum (FWHM).

ΔEx is the FWHM of the X-ray photon source

ΔEs is the contribution to the FWHM due to the spectrometer (i.e. analyser), and

ΔEcl is the natural width of the core level under investigation (for solids, this includes solid state effects not directly associated with the lifetime of the core hole state, but rather with slightly differing binding energy, due to differences in lattice environment)

$Mg_{k\alpha_{1,2}}$ and $Al_{k\alpha_{1,2}}$ are the most useful photon sources from the standpoint of keeping the contribution of Ex to the total line-width small. With well-designed magnetic or electrostatic analysers, the contribution ΔEs can be reduced to negligible proportions so that the major limiting factors in terms of resolution are photon line-width (which may be reduced by monochromatisation of X-ray radiation) and the inherent width of the level itself. For solids in which longer range interactions are important (e.g. ionic lattices or hydrogen bonded covalent solids), solid state effects can contribute to the overall line-widths. Some examples of natural line-widths (ΔEcl), derived from X-ray spectroscopic studies are given in Table 2.4. The uncertainty principle in the form $\Delta E\ \Delta t > \frac{h}{4\pi}$ shows that for a core hole state with lifetime of $\sim 6.6 \times 10^{-16}$ seconds,[348] the line-width (uncertainty in the energy of the state) is $\sim$ 1 eV.

It is clearly evident from Table 2.4 that there are large variations in natural line-widths both for different levels of the same element and for the same levels of different elements. These reflect differences in lifetimes of the hole state, the lifetime being a composite of radiative (fluorescence) and non-radiative (Auger) contributions, the importance of the former increasing with atomic number. This emphasises the fact that there is no particular virtue in studying the innermost core level. For gold, as an example, the FWHM of 54 for the 1s would swamp any chemical shift.

It has been well substantiated that the contributions to the ΔEm from ΔEs are essentially Gaussian line shapes and are

Table 2.4

Approximate natural widths of some core levels (eV)

Level		Atom							
		S	Ar	Ti	Mn	Cu	Mo	Ag	Au
	1s	0.35	0.5	0.8	1.05	1.5	5.0	7.5	54
	$^{2}p_{3/2}$	0.10	-	0.25	0.35	0.5	1.7	2.2	4.4
Radiative width	1s	0.04	0.07	0.2	0.33	0.65	3.6	6.0	50
Fluorescence yields	1s	0.1	0.14	0.22	0.31	0.43	0.72	0.8	0.93

primarily due to analyser, focussing and detector imperfections; whereas for the Ecl, the contributions are considered to be Lorentzian, being dependent upon the Auger and X-ray fluorescence processes, upon photoionisation of a core level. The convolution of these shapes produces a general line-shape with Gaussian characteristics[152] and the Lorentzian character in the tails. It is believed that the use of pure Gaussian shapes introduce only small errors and, therefore, this forms the basis of most analogue techniques.

Deconvolution procedures may be classed into two main categories:

(i) Deconvolutions by mathematical enhancement;[349]

(ii) Curve fitting by simulation, either in analogue or digital fashion.

The curve fitting procedure demands a close control over a number of variables such as binding energy, line-width and peak height. These parameters are most conveniently controlled in the analogue mode; and, the work in this thesis is predominantly based on this method, using a DuPont Curve Resolver (Model 310). The basic approach to curve simulation is outlined in Table 2.5.

Caution is required, when using either form of deconvolution method, as it is often possible to obtain more than one solution. When dealing with complex line-shapes, a knowledge of prototype systems is imperative such that the solution is one, based on the chemical uniqueness.

Table 2.5

Line shape analysis by curve fitting; schematic of logic procedure

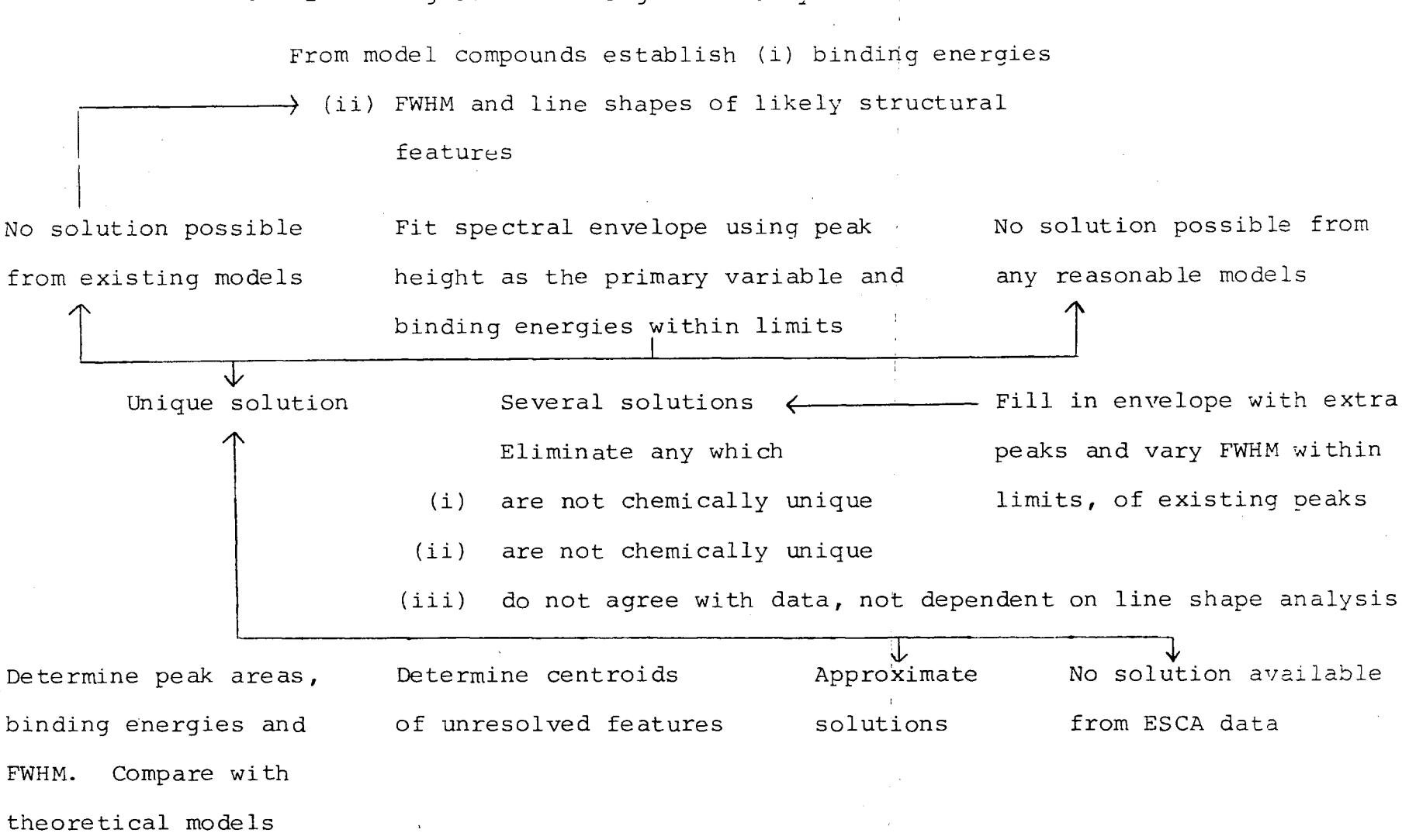

2.8 ESCA Instrumentation

The ESCA instrument, essentially, consists of an excitation source, an electron energy analyser, and an ultra-high vacuum system. A schematic representation of the essential components is given in Figure 2.18. In addition to these basic requirements, most spectrometers also possess ancillary experimental facilities, which enhance their analytical capabilities, as well as an array of sophisticated

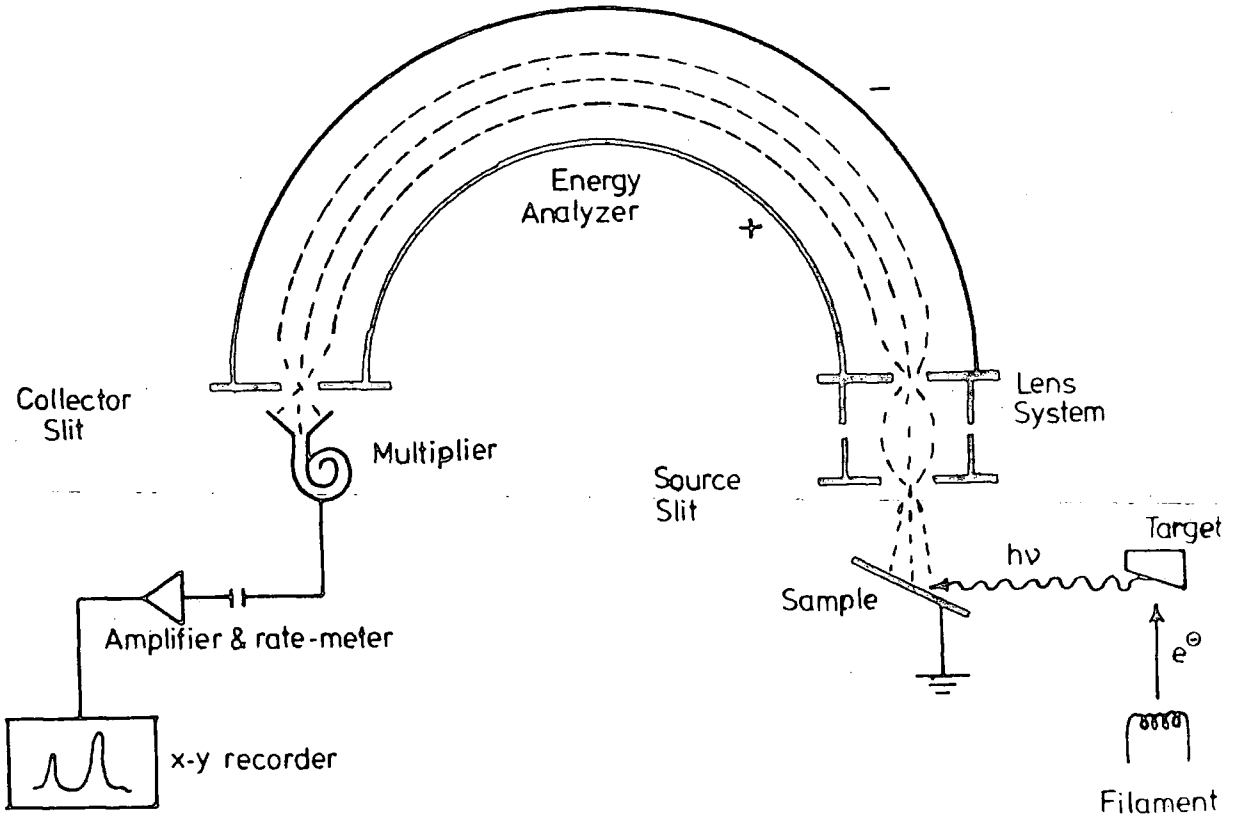

Figure 2.18. Schematic representation of the ESCA instrumentation.

electronics to aid data acquisition, processing and display. The work in this thesis was carried out on an A.E.I. ES200 AA/B spectrometer, although a custom-designed Kratos ES300 spectrometer, fitted with a Mg/Ti dual anode was also used for preliminary examinations.

The description of the spectrometer can be divided under four headings:

(i) X-ray source;

(ii) Sample chamber;

(iii) Electron energy analyser;

(iv) Electron detection.

2.8.1 X-ray source

Conventional X-ray sources operate on the principle of X-ray emission. Electrons from a hot cathode (usually a tungsten filament, resistively heated to $\sim$ 2500°K) are made to impinge upon a water-cooled solid anode, de-excitation of which produces X-rays of characteristic energies. A typical non-monochromatic X-ray spectrum is shown in Figure 2.19. The spectrum consists of characteristic lines of the anode material, superimposed on a continuous spectrum (Bremsstrahlung),[350] the shape of which depends only on the energy of the incident electrons striking on the anode, and not on the anode material. The cutoff frequency (ν_o) is proportional to the electron kinetic energy (E) in equation (2.30):

$$h\nu = E \qquad (2.30)$$

where h is Planck's constant. The total X-ray energy per

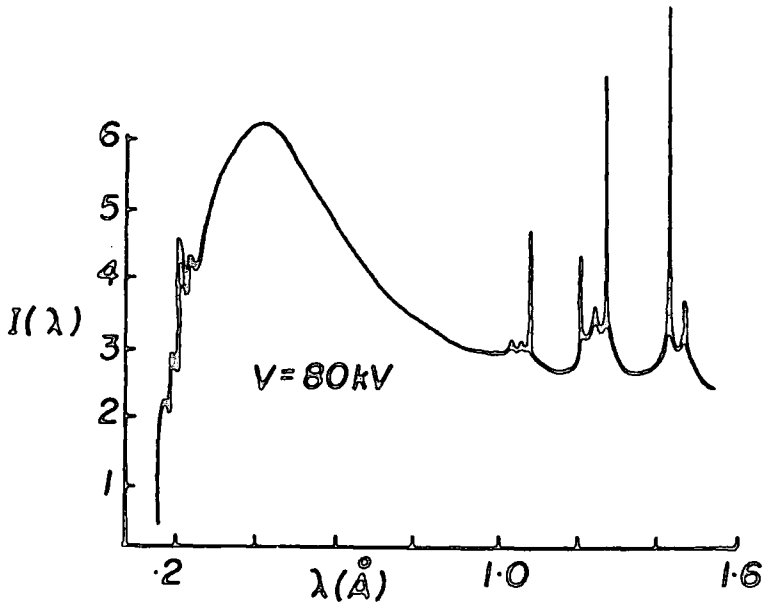

Figure 2.19. X-ray spectrum of a tungsten anode.

electron (E_T) is related to the integral over all of the continuum and is given by:

$$E_T = KZE^2 \tag{2.31}$$

where $K \simeq 0.7 \times 10^{-4}$, when E and E_T are in MeV, and Z is the atomic number of the anode. The fraction of the electron kinetic energy converted into X-ray energy is:

$$E_{T/E} = KZE \tag{2.32}$$

For a magnesium anode and voltage of 12 kV, $E_{T/E}$ is only 10^{-3}%.

The most commonly used targets are magnesium (characteristic $k\alpha_{1,2}$ X-ray energy of 1253.7 eV) and aluminium (characteristic $k\alpha_{1,2}$ X-ray energy of 1486.6 eV), which produce X-ray line-widths of 0.7 eV and 0.85 eV respectively. It is often desirable to use the harder X-rays such as $Cu_{k\alpha}$ ($h\nu$ = 8048 eV) and an intermediate energy source, $Ti_{k\alpha}$ ($h\nu$ = 4510 eV) for some applications.

The ES200 instrument employs a Marconi-Elliot type GXS high voltage generator with integrally variable voltage (0 - 60 kV) and current output (0 - 80 mA). The X-ray source consists of an unmonochromatised magnesium anode of the Henke hidden filament design,[351] which reduces the risk of contamination of the target by material, evaporated from the electron gun filament. The X-ray flux is of the order of 0.1 millirad/sec., which is essentially non-destructive for most polymeric systems. A thin aluminium window isolating the target from the sample prevents the interference of electrons from the filament. The risk of scattered electrons exciting X-ray radiation from the aluminium window is reduced by operating the filament at slightly positve potential (+10 V) and the anode at very high positive voltage.

The ES300 has a smaller solid state high voltage generator with variable voltage and current output; and, is fitted with magnesium and titanium dual anode targets and a monochromatised $Al_{k\alpha_{1,2}}$ X-ray source. The monochromator for the $Al_{k\alpha_{1,2}}$ uses slit filtering and diffraction technique from the (10$\bar{1}$0) plane of quartz at the Bragg angle of 78.3° to eliminate the satellites and the continuum for the production of pure $k\alpha_{1,2}$

radiation.

The difficulties in finding a suitable crystal with the appropriate lattice spacing for monochromatisation of $Mg_{k\alpha}$ radiation have prevented a more widespread use of monochromatised X-ray radiation.

Figure 2.20, however, illustrates three techniques available for $Al_{k\alpha}$ monochromatisation. These are (a) slit filtering; (b) dispersion compensation, and (c) fine focussing, all using crystal diffraction of the X-ray radiation

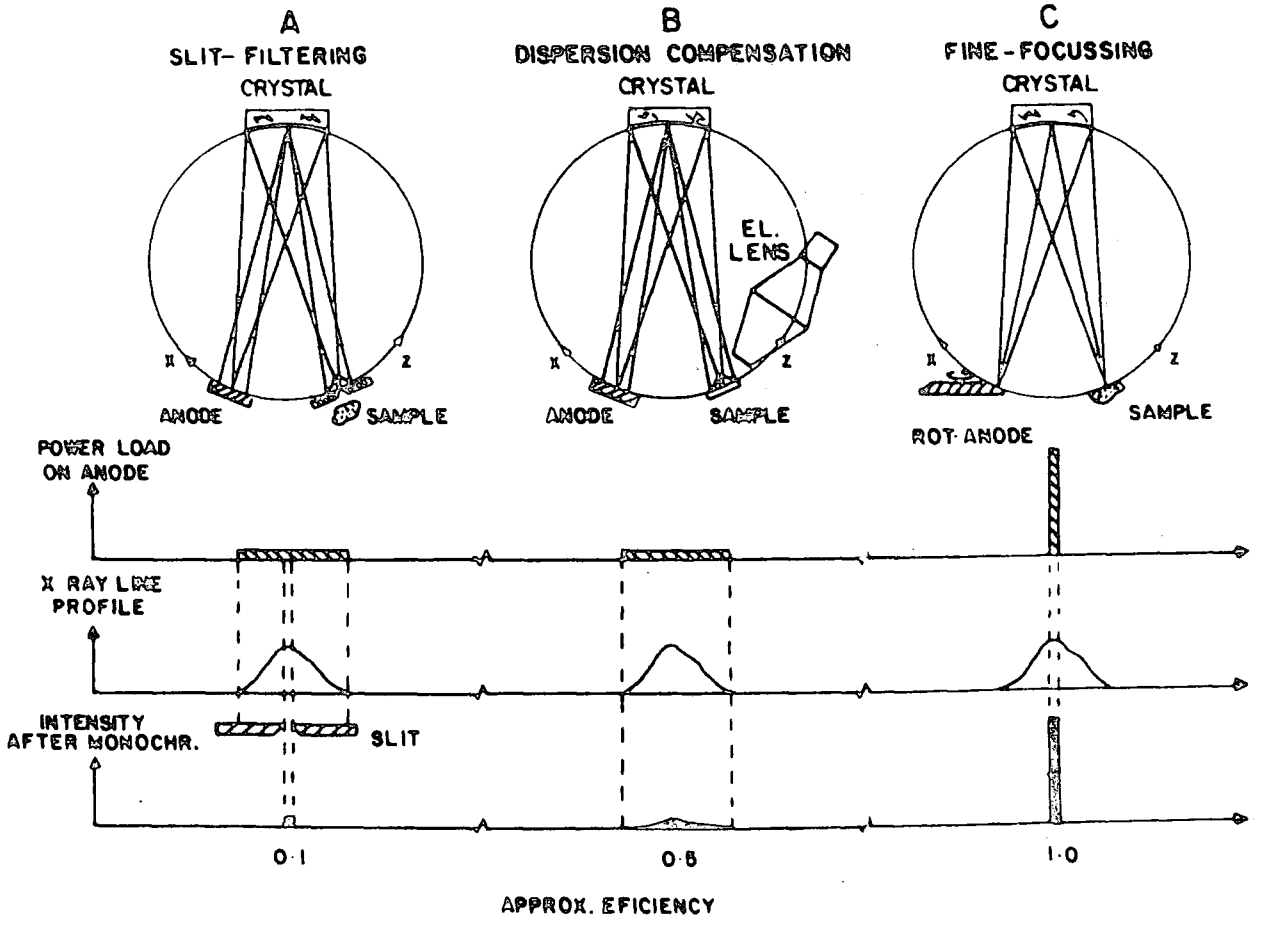

Figure 2.20. Monochromator designs for $Al_{k\alpha}$ monochromatisation.

and, these techniques can, in principle, attain ultimate line-widths of 0.2 eV. The fine-focussing technique uses a high power electron gun and requires a rotating anode (5 - 10,000 revolutions per minute).

2.8.2 Sample chamber

Figure 2.21 is the general format of an ES200B spectrometer, showing the relative positions of the sample, analyser and X-ray sources equipped with monochromator.

The chamber is accessed by several ports for sample introduction and treatments. Fast-entry insertion locks allow rapid sample entry into the sample chamber. The sample mounted on a probe tip (typically 18 mm x 5 mm), using double sided Scotch tape, is pushed through the insertion lock to the high vacuum chamber for analysis. Purpose-built reaction chambers may be attached to the source chambers via an insertion lock and, this provides facilities for 'in situ' treatment of samples.

The ES200B has a base pressure in the range 10^{-8} torr, achieved using cold-trapped diffusion pumps backed by rotary pumps. Whereas, the ES300, possesses a permanently mounted preparation sample chamber, pumped by a diffusion pump, the source and analyser regions are independently pumped by an Alcatel electric turbomolecular pump with pumping capacity of 350 litres per second. The base pressure is typically of the order of 10^{-9} torr.

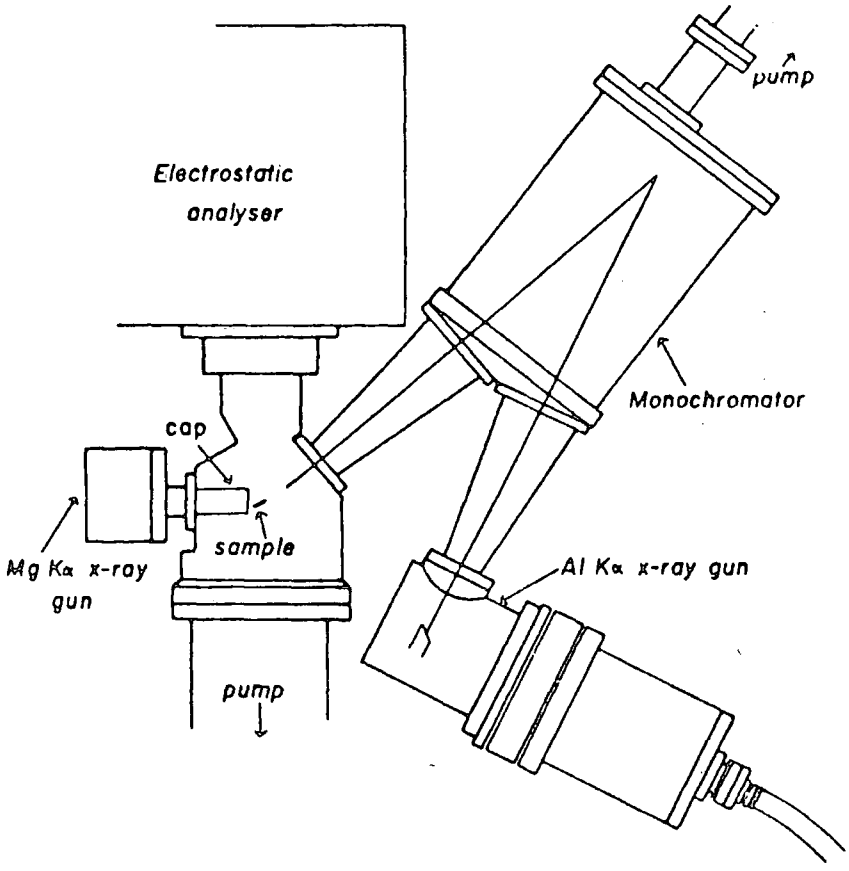

Figure 2.21. General layout of the AEI ES200B spectrometer.

2.8.3 Electron energy analyser

The analyser on the ES200B is a hemispherical double focussing electrostatic analyser, which was originally described by Purcell,[352] enclosed within two mu-metal shields for protection from external magnetic interference. The resolution of the hemispherical analyser depends on the:

(i) mean radius of the hemisphere (R)

(ii) width of the entrance slit, and

(iii) width of the exit slit.

The resolution ($\Delta E_{/E}$), where E is the energy of the electrons is $\Delta E_{/E} = R_{/W}$, where W is the combined width of the entrance and exit slits. It is, therefore, quite clear that the resolution can be improved by:

(i) reducing the slit width, which decreases the signal intensity

(ii) increasing the hemispherical radius, which, in turn, increases the engineering cost and pumping requirements, and

(iii) retarding the electrons before entry into the analyser.

A reasonable compromise is made on the slit widths to obtain sufficient signal intensity and on the size of the hemisphere to prevent mechanical distortions and to minimise the engineering costs. A retarding lens assembly slows the electrons down before entering into the analyser thus allowing more flexibility on the resolution, and allows the analyser to be situated at convenient distance physically from the source chamber, which permits a maximum flexibility in sample handling.[353]

The electrons passing through the analyser with the required kinetic energy can be focussed at the collector by either of two methods:

(i) Scanning the retarding potential applied to the lens while keeping the potential constant between

the two hemispheres, or

(ii) Simultaneously scanning the retarding potential applied to the lens and the hemispherical potential, and keeping a constant ratio between the two.

The first method of fixed analyser transmission (FAT) has a greater sensitivity at low kinetic energies (less than 500 eV), whereas the second, fixed retardation ratio (FRR) possesses a greater sensitivity at higher electron kinetic energies. The FRR mode employed on ES200B is used in this thesis.

2.8.4 Electron detection and data acquisition

The electrons of pre-selected kinetic energy pass through the exit slit of the analyser into an electron multiplier. The output pulses from the channel multiplier are amplified and processed in a data handling system. The spectra can be generated by one of two methods:

(i) The continuous scan, where the electrostatic field is increased from the present starting kinetic energy continuously while the signals from the multiplier are monitored by a rate meter. A graph of the electron counts per second versus the kinetic energy of the electrons is plotted directly onto an X-Y recorder.

(ii) The step scan, where the field is increased by preset increments (typically 0.1 eV) and at each increment, (a) the counts may be measured for a fixed length of time, or (b) a fixed number of counts may be timed.

The data obtained from the step scans is accumulated in a multichannel analyser or by the use of a mini computer (floppy disc). Many scans can be accumulated in this manner to average random fluctuations in background, thereby, enhancing the signal to noise ratios.

In both continuous and step scan modes, where the data acquisition is a relatively long process (e.g. an hour), care must be taken to avoid long term sample changes. For example, time dependent sampling charging and hydrocarbon contamination (which the latter may alter the peak ratios) may produce erroneous results.

2.9 Sample Handling

2.9.1 Solid samples

Solids, available as a powder, are often convenient to study them as such by applying the powder to double sided Scotch tape, mounted on the sample probe. Care is taken in this approach that the extraneous signals are not observed from the sample backing and, also, that no chemical reaction occurs between the sample and substrate. The incomplete coverage and uneven surface topography of samples prepared in this way, generally, lead to lower signal/noise ratios than samples studied directly as films. A more satisfactory method involves deposition of a thin layer of the sample onto a gold substrate (for instance, from a suitable solvent or through sublimation). Small strips or wires may be held in a chuck and, powdered samples may be directly mounted by pressing into a

metal gauge or piece of soft metal foil such as lead or indium. The volatile solids are usually sublimed from a capillary tube (which may be heated) onto a cooled probe tip.

2.9.2 Liquids

In principle, solids, liquids and gases can be studied by ESCA, but the limitations of instrument design, usually, restricts the range to low vapour pressure solid samples. Although the development of liquid studies is still in its infancy,[354] the only technique presently viable on commercially available instruments involves the injection of the liquid into a heatable (25 - 150^{o}C) evacuated reservoir shaft, followed by diffusion of the vapour through a metrosil leak and subsequent condensation onto a cooled gold strip. Since the sample surface is continually renewed, the contamination and radiation damage effects are, therefore, further minimised.

Siegbahn has developed two techniques, where liquids and solutions may be studied as sublimeter beams,[355] or as a film on a wire loop passing through the X-ray beam parallel to the analyser entrance slit.[350]

A typical ESCA probe, on the AEI ES200B and Kratos ES300 spectrometers, has the facility for heating or cooling the sample. The samples of low vapour pressure are heated by means of conduction from a thermostatically controlled heater; whereas, cooling is carried out by pumping liquid nitrogen through the probe, thus enabling the study of samples, which are volatile in ultra-high vacuum chamber.

2.9.3 Gases

Gases may be studied either by condensing onto the cooled probe, or in the gaseous phase for which special gas cells have been developed. Studies of molecules in the gas phase have the following advantages:[160]

(1) No inherent broadening of the levels due to solid state effects,

(2) Sample charging problems are removed,

(3) Increased signal to noise ratio,

(4) Radiation damage, if it occurs, is of no importance unless the sample is recirculated,

(5) By mixing with standard gases, peaks may be readily calibrated,

(6) Inelastic losses and shake-up and shake-off processes may be distinguished by varying the sample pressure,

(7) Direct comparison with theoretical calculations is simplified.

2.10 General Aspects of ESCA

ESCA is an extremely powerful tool with wide ranging applicability. The principal advantages of the technique may be summarised as follows:

(1) The sample may be solid, liquid or gas and sample sizes are small, e.g. in solids, 10^{-3} g, 0.1 ml liquid and 0.5 cm^3 of a gas at STP;

(2) The technique is essentially non-destructive since the X-ray flux is small (0.1 millirad $sec.^{-1}$);

(3) The technique is independent of the spin properties of

the nucleus and can be used to study any element of the periodic table with the exception of hydrogen and helium. These are the only elements for which the core levels are also the valence levels;

(4) Materials may be studied 'in situ' with a minimum of preparation;

(5) The technique provides a large number of information levels from a single experiment as displayed in Table 2.6;

(6) ESCA has a higher sensitivity than many other analytical techniques as shown in Table 2.7;

(7) The data is often complementary to that obtained by other techniques;

(8) For solids, ESCA has the capability of differentiating the surface from subsurface and bulk phenomena, allowing analytical depth profiling;

(9) The information relates directly to bonding and molecular structure and applies to both inner and valence orbitals of the molecule. This allows a thorough analysis of electronic structure of the system to be made;

(10) The information levels are such that 'ab initio' investigations are possible and the theoretical basis is well understood.

The disadvantages of ESCA are surprisingly few:

(1) The overall costs are quite high;

(2) While the technique has superior depth resolution, $\sim$ 200Å, the spatial resolution is poor and an area of

0.3 cm^2 is normally sampled;

(3) If the surface differs from the bulk, then it is not possible to say anything about the bulk structure by means of ESCA without sectioning the sample.

Table 2.6

The hierarchy of information of levels available in ESCA

(1) Absolute binding energies, relative peak intensities, shifts in binding energies. Elemental mapping of solids, analytical depth profiling, identification of structural features, etc. Short-range effects, longer-range effects indirectly.

(2) Shake-up/shake-off satellites. Monopole excited states; energy separation with respect to direct photoionisation and relative intensities of components of 'singlet and triplet' origin. Short and longer range effects directly. (Analogue of uv.)

(3) Multiplet effects. For paramagnetic systems, spin state, distribution of unpaired electrons.

(4) Valence energy levels, longer range effects directly.

(5) Angular dependent studies. For solids with fixed arrangement of analyser and X-ray source, varying take-off angle between sample and analyser provides means of distinguishing surface from subsurface and bulk effects. For gases with variable angle between analyser and X-ray source, angular dependence of cross-sections, asymmetry parameter β,[343] symmetries of levels.

Table 2.7

Sensitivities of various analytical techniques

Bulk Techniques	Minimum Detectable Quantity (g)
Infrared absorption	10^{-6}
Atomic absorption	10^{-9} - 10^{-2}
Vapour phase chromatography	10^{-3} - 10^{-7}
High pressure liquid chromatography	10^{-6} - 10^{-9}
Mass spectroscopy	10^{-9} - 10^{-15}
Surface Techniques	
ESCA	10^{-10}
Neutron activation analysis	10^{-12}
X-ray fluorescence	10^{-7}
Ion scattering spectrometry	10^{-15}
Auger emission spectroscopy	10^{-14}
Secondary ion mass spectrometry	10^{-13}

CHAPTER THREE

AN ESCA INVESTIGATION OF A SERIES OF NATSYN 2200 CURED ELASTOMERS

PART I

3.1 Introduction

The long history of successive improvements and developments in the properties of natural rubber (NR) brought about by vulcanisation with sulphur have led the basic process of vulcanisation to a high degree of refinement and versatility, whereby natural rubber and other synthetic rubbers can be vulcanised in various forms at temperatures ranging from ambient to 200°C.[1,2,10,31,63] A conventional high sulphur-low accelerator system produces a high percentage of poly-sulphide crosslinks, which impart excellent strength and fatigue properties at the expense of resistance to compression set, cure reversion, and thermal and oxidative aging; whereas, high accelerator-low sulphur systems producing mainly mono- or disulphide crosslinks possess a greater resistance to reversion and aging, but inferior mechanical properties.[1,2,47,48,301] Vulcanisation is usually affected industrially by heating the mechanically plasticised rubber with sulphur and auxillary vulcanising agents (organic accelerators and metal oxides - preferably zinc oxide) and by long chain fatty acids (stearic or lauric acid), or the zinc soaps of these acids. (It is worthwhile noting that the elastomeric samples kindly provided by Dunlop were vulcanised by heating the premixed ingredients on a calendering system at 150°C in air, with a 2 mm nip setting to draw into sheets.)

Despite the scientific and technological importance of elastomers and the numerous investigations, which have been conducted in a wide variety of areas, such as the effect of sulphur vulcanisate structures on the mechanical[1,46-48,63]

properties, and characterisation of 'sulphur-vulcanisates', using chemical reagents (chapters one and nine),[91,95-97] and physio-chemical techniques (infrared and NMR spectroscopies - the latter employed only in the last few years),[107,115-127] the fact is that there are a number of fundamental questions, which remain unanswered with regard to both the surface and bulk chemistry of sulphur-vulcanised systems. The predominant emphasis in the literature has been bulk analysis by the usual chemical and physical methods,[106] however, there has been very little or no work on surface analysis of industrially important elastomers;[284] and, therefore ESCA offers the excellent possibility of undertaking such surface studies. Although, it may be anticipated that the very complex nature of elastomers, due to the presence of various additives in the system, may lead to difficulties or ambiguities of interpretation. The large volume of ESCA background information available at Durham make an investigation of the changes in surface chemistry, as a function of cure worthwhile at this time, if only from an empirical basis because of the paucity of alternative data in the literature.

Since the environmental modification of the elastomers is of considerable industrial and technological importance and since all solids communicate with the rest of the universe primarily by means of their surfaces, the detailed knowledge of surface structure is of paramount importance in any detailed discussion at the molecular level of many important phenomena such as delineating the aspects of structure and bonding, which are of crucial importance in determining many of the physical,

chemical, mechanical and electrical properties. A recent example of this genre is the important work of Van Ooij[362] on the interface of vulcanised rubbers with brass coated steel cords, which circumscribes adhesion problems encountered in the production of steel belted radial tyres.

Clark and coworkers have shown in an extensive series of publications, how ESCA may be applied to investigate the structure, bonding and reactivity at polymer surfaces.[229-235] The strong dependence of mean free path on the kinetic energy of the photoemitted electrons enables differentiation of the surface, subsurface and bulk. This and the subsequent chapters (four and five) are exclusively concerned with an ESCA investigation of the as received elastomers, as a function of cure time, as a preliminary to applying plasma techniques (chapters six and seven) to the elaboration of crosslink functionality.

3.2 Experimental

(i) Samples of raw Natsyn 2200, and the Natsyn partially and fully cured systems shown in Table 3.1 were prepared by Dr. M. Kirkham, and were received in Durham with protective sheets of either pigmented polyethylene, (cured samples) or polyethylene-terephthalate (uncured Natsyn 2200).

(ii) The samples have been studied by ESCA over a period of time, however, preliminary experiments revealed that the dissolved air in the uncured system rapidly exploded the samples on introduction to the high

Table 3.1

(a) Natsyn 2200 Sample Formulations

	1	2	3	4
Natsyn 2200 (cis-polyisoprene)	✓	✓	✓	✓
Zinc oxide	✓	✓	✓	–
Stearic acid	✓	✓	✓	–
CBS	✓	–	✓	–
Sulphur	✓	–	✓	–
Permanax B	✓	✓	✓	✓
TMTD	–	✓	✓	–
Dicup R	–	–	–	✓
Cures at 150°C				
50% (partial) minutes	15	5½	8½	
100% (optimum) minutes	25	25	20	120

CBS Cyclohexylbenzthiazyl sulphenamide

Permanax B Acetone/diphenylamine condensate antioxidant

TMTD Tetramethylthiuram disulphide

Dicup R Dicumyl peroxide

(b) Raw polymer

Cis-polyisoprene	ZnO	Stearic acid	CBS	Sulphur
–	–	–	–	–

Permanax B	TMTD	Dicup R
–	–	–

vacuum system of the spectrometer, causing on several occasions contamination of the window. Attempts at cooling the samples, prior to introduction into the spectrometer high vacuum system (to ∿ 170K), did not prove successful, and it is clear that the trapped air bubbles in the samples cannot readily be removed.

(iii) The only spectra, which have been recorded for the uncured system, have been those of a residual film adhering to the PET film since removing this film results in cohesive failure in the rubber layer.

(iv) In all cases, the samples have been handled in air. The cured systems were cut to a size with a pair of scissors, care being taken not to contaminate the surface of the sample, during this procedure. Samples were cut to a size (20 mm x 6 mm x 2.5 mm) appropriate for mounting onto the spectrometer probe tip. In the case of the uncured rubber, the production of samples of the appropriate size presented some difficulties, owing to the tack and high viscoelasticity of the material. Attempts at freeze microtoming were not noticeably successful, and the samples were, therefore, again prepared by cutting samples (with difficulty) of the appropriate size by means of a pair of scissors.

(v) Samples for Multiple Attenuated Infrared spectroscopic examination were also prepared by

cutting from the original sample, a section of the appropriate size to place against either a Ge or KRS5 crystal.

(vi) The IR data and also limited studies, which have been made using solid state ^{13}C NMR spectroscopy, are discussed in detail at a later stage of this chapter.

(vii) The ESCA examinations have been carried out, using either a Kratos ES300, or AEI ES200A/B electron spectrometer in each case with a $Mg_{K\alpha_{1,2}}$ x-ray source. In either case, spectra were recorded in the Fixed Retardation Ratio (FRR) mode, and under the conditions of these experiments, the $Au_{4f_{7/2}}$ level at 84 eV, used for energy calibration had a FWHM of $\sim$ 1.2 eV. For spectra recorded on the Kratos ES300, take-off angles of 30^{o} and 50^{o} were employed, whilst for the ES200A/B, take-off angles of 30^{o} and 70^{o} were used (a take-off angle θ = 0 corresponds to exit normal to the surface, whilst a higher take-off angle emphasises surface features). A comparison of the data at the two different take-off angles provides information, therefore, on the vertical homogeneity of samples.

(viii) Line shape analysis, and area ratio measurements have been obtained, using either a Dupont 310 curve resolver in analogue fashion, or digitally with an Apple II plus microcomputer with the graphics tablet.

(ix) Swelling tests were carried out on the cured samples according to the following procedure. Equal volumes of a range of solvents of known solubility parameters were added into different sets of two bottles, each set containing known masses of cured elastomer (Natsyn 2200, type 1). The stoppered bottles were left for two weeks to establish the equilibrium at ambient temperature. Solvents were poured off, and the remaining swollen elastomer in each bottle was weighed before and after drying, for an estimation of solubility parameter.

(x) Microanalysis

(a) 'Wet-ashing' method

4 cm^3 of concentrated H_2SO_4 was added to a beaker containing an accurately known mass (ca. 0.3 g) of elastomer followed by 1 cm^3 of concentrated HNO_3 acid. The contents were mixed with a glass rod and heated gently on a hot plate until all the organic matter had been destroyed by wet-ashing with H_2SO_4-HNO_3 acids. The pale yellow solution obtained after destroying the organic matter was heated strongly before cooling. 25 cm^3 of water was added and boiled for about two minutes.

The final colourless solution containing the elastomer gradients was further diluted with water for filtration and the filtrate was transferred

to a 50 cm^3 and made up to the mark with water.

The absorption spectra of elements were detected using atomic absorption/atomic emission spectrometry and the concentration of each element was determined from standard elemental absorption spectra.

(b) 'Combustion method' - involves the combustion of an accurately known mass (2 mg) of material in an oxygen atomosphere, using Perkin Elmer Elemental Analyser (Model 240). The concentration of an element is determined from standard elemental spectra.

(xi) ESCA studies of model systems

(a) Powders

The model systems available in the form of a powder, such as accelerators and activators, were examined at approximately 190K, by mounting onto a double sided 'Scotch' tape, and then tapping off the excess powder that has not adhered.

Care was taken to avoid the incomplete coverage of a tape, which would conceivably result in extraneous signals, arising from the tape backing. Spectra obtained in this manner tend to have higher noise/signal ratio than those obtained using the sheet/film, and, therefore, this results in broader photoionisation peaks.

(b) Liquids

Detailed examinations of commercial poly-

sulphides, in the form of a liquid, as a function of times in the plasmas, are provided in chapters six and seven.

(xii) Background information on the samples

The full details of the compound formulations together with curing times for different types of Natsyn 2200 elastomers are shown in Table 3.12.

The premix of ingredients achieved either in a banbury or two roll mill system is fed into 3/ more roll calendering system with a 2 mm nip setting to draw into sheets.

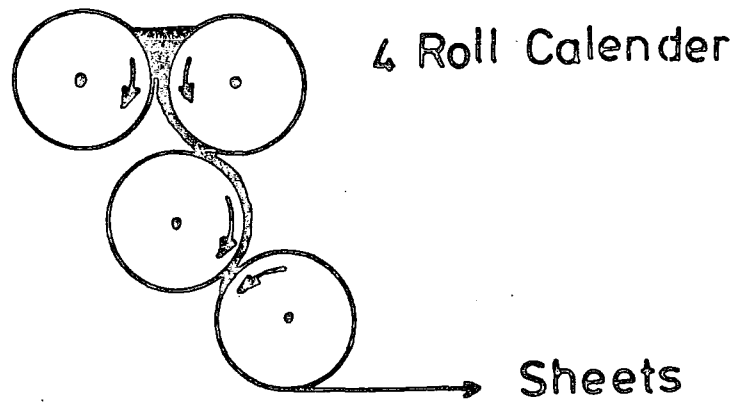

The sheet passes through three successive nips which further mixes and reduces it to a prescribed gauge. The transfer of a sheet from one roll to the next roll is accomplished by various combinations of temperature differential, speed differential and surface-finish differential. The sheet is stripped by a higher-speed roll, which can be also used to stretch the sheet and to give further

reduction in the thickness. The surface finish of the sheet may be controlled by the finish on the rolls. (The plasticised rubber is vulcanised by heating on a calendering system at 150°C in air.)

The cure systems as in Tables 3.1 and 3.12 supplied by Dunlop are as follows:

Types

1 - a conventional standard sulphur system accelerated with a sulphenamide

2 - a sulphurless system in which sulphur is provided by an elimination from a thiuram disulphide

3 - a low sulphur system, which results in a network similar to that obtained from type 2

4 - a peroxide system, which produces a simple network structure of carbon-carbon cross-links.

3.3 Results and Discussion

3.3.1 Swelling behaviour of elastomers

The tendency of a polymer to dissolve in a given solvent depends on the polymer solvent interaction.[64] Solvents of the same solubility parameter as that of solute are most likely to dissolve to give polymer solution. This fact provides a method for determining the solubility parameter, and leads to consideration of molecular weight between cross-linked polymer

chains. Linear polymers dissolve completely in a solvent when the polymer-solvent interactions are greater than the polymer-polymer forces, resulting in the separation and expansion of chains. Maximum swellings of cross-linked polymers occur, when the solubility parameters of polymer and solvent are approximately equal. As the system is swollen by the absorption of solvent molecules, a force of retraction consequently develops in the network in opposition to the swelling process, such that a state of equilibrium is established between these two opposing forces.

The partial molar heat of mixing ΔHm of polymer and solvent, when the dispersion forces are in operation, is given by an equation:[64]

$$\Delta Hm = \nu_o(\delta_s-\delta_p)^2\phi_p^2 \qquad (3.1)$$

where ν_o is the molar volume of solvent and ϕ_p is the volume fraction of polymer. δ_s and δ_p are the solubility parameters of solvent and polymer respectively. It is clearly evident from equation (3.1) that ΔHm is minimal when δ_s and δ_p are equal. When ΔHm is zero ΔGm ($= \Delta Hm-T\Delta\delta_m$) must be negative, since $\Delta\delta m$ is positive. Maximum swelling occurs in this situation.

In the study of polyisoprene elastomers, specimens of accurately known mass (0.2 gram) were cut and placed in a range of solvents for two weeks to establish the equilibrium at ambient temperature. The swelling coefficients were then calculated using an equation:

$$\text{swelling coefficient } Q = \frac{M-Mo}{Mo} \cdot \frac{1}{d} \qquad (3.2)$$

here M and Mo are the masses of swollen and unswollen polyisoprene, and d is the density of solvent.

Table 3.2

	Interaction parameters $(J/cm^3)^{\frac{1}{2}}$	% volume fraction of solvent in swollen gel
n-heptane	15.3	70.71
methylcyclohexane	15.9	80.76
cyclohexane	16.7	80.6
carbon tetrachloride	17.6	84.54
toluene	18.2	81.33
benzene	18.7	79.7
chloroform	19	84.35
di-isopropylketone	16.3	73

Table 3.2 shows the range of solvents used for an estimation of solubility parameter of sulphur vulcanised polyisoprene, and a plot corresponding to this table is shown in Figure 3.1.

The determination of molecular weight between crosslinks makes the use of the Flory-Rehner equation:[73-75]

$$Ve = -\frac{1}{v_o}\ \frac{\ell n(1-v_r) + v_r + \mu v_r^2}{(v_r^{1/3} - 2v_{r/f})} \qquad (3.3)$$

where Ve is the number of polymer chains per unit volume, f is the functionality of the system, which in this case is four and v_r is the volume fraction of polymer in the swollen gel at equilibrium. For an accurate determination of polymer-

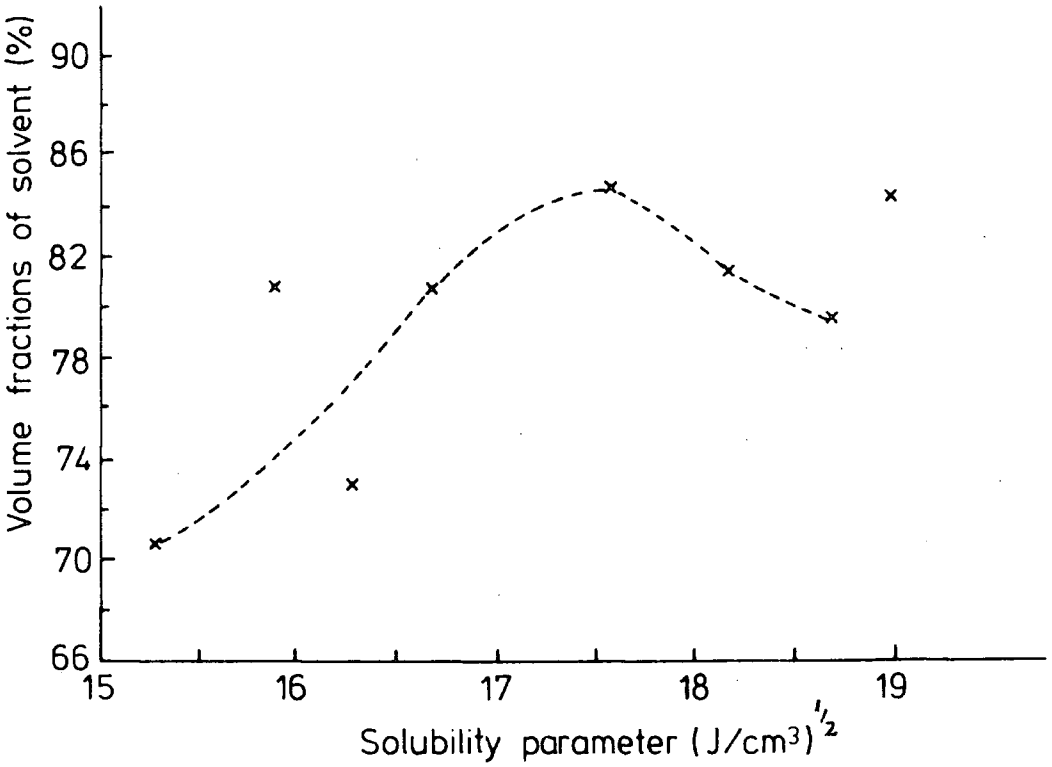

Figure 3.1. Volume fraction of solvent versus solubility parameter for an optimum cured type 1, Natsyn 2200 elastomer at room temperature.

solvent interaction parameter (μ), one can use the semi-empirical equation, proposed by Bristow and Watson:[356]

$$\mu = \beta_1 + \frac{\nu_o}{RT} (\delta_s - \delta_p)^2 \qquad (3.4)$$

where β_1 is the lattice constant approximately equal to 0.34, R is the universal gas constant and T is the absolute temperature.

The number of polymer chains per unit volume and molecular

weight $\bar{M}c$ between crosslinks are related to density ρ of the polymer by:

$$Ve = \rho / \bar{M}c \qquad (3.5)$$

Furthermore, the Young's modulus E at low elongations can be calculated from equation:

$$E = \frac{3RT\rho}{\bar{M}c} \qquad (3.6)$$

The swelling method, leading to values of Ve, hence $\bar{M}c$, was mainly used for calculating the crosslinking density of polyisoprene elastomers (Natsyn 2200 formulation) as a preliminary to elaborate the microstructure. The results are shown in Tables 3.3 and 3.4.

Table 3.3

Optimum cured, Natsyn 2200, elastomers

Type	Crosslinking density Ve (m^{-3})	Average molecular weight between crosslinks $\bar{M}c$	Young's modulus E ($10^5 Nm^{-2}$)
1	135.3	6,725	9.1
2	110	8,272	8.0
3	92.46	9,840	6.7
4	115.7	7,865	8.4

Table 3.4

Partially (50%) cured, Natsyn 2200, elastomer

Type	Crosslinking density Ve (m^{-3})	Average molecular weight between crosslinks $\bar{M}c$	Young's modulus E ($10^5 Nm^{-2}$)
1	136.4	6,670	9.9
2	117.4	7,750	8.5
3	110.9	8,210	8.0

3.3.2 ESCA data on additives

In order to provide a basis for the interpretation on the cured rubber systems, ESCA data has been obtained on each of the materials used in the formulations.

(a) Zinc oxide

The wide scan ESCA spectra of zinc oxide are shown in Figure 3.2a. The photoemission from the Zn_{2p}, O_{1s} and Zn_{3p} levels are as indicated and the spectra also reveal the intense $L_{23}M_{45}M_{45}$ Auger process for Zn, and also that the sample is extensively contaminated with a hydrocarbon overlayer. The relevant binding energies are displayed in Table 3.5, these being derived from the high resolution core level spectra in Figure 3.2b.

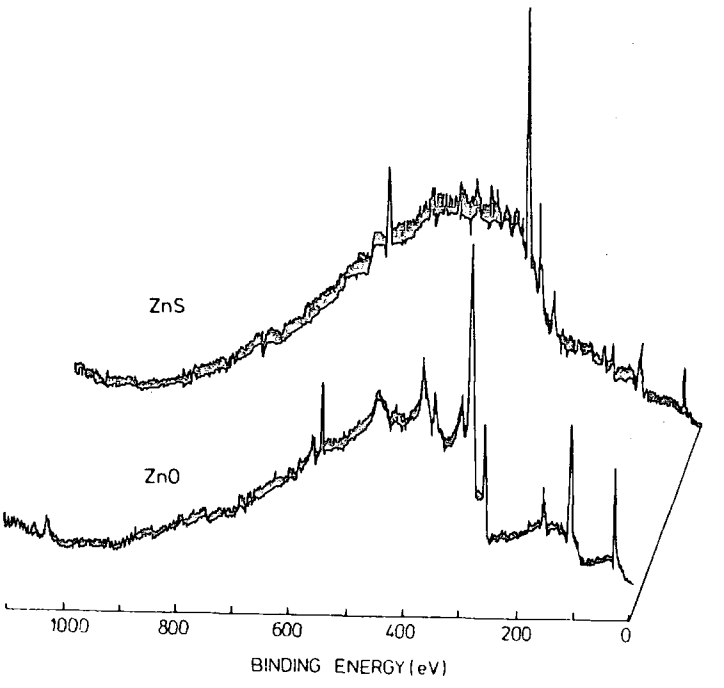

Figure 3.2a. A wide scan of zinc oxide and zinc sulphide.

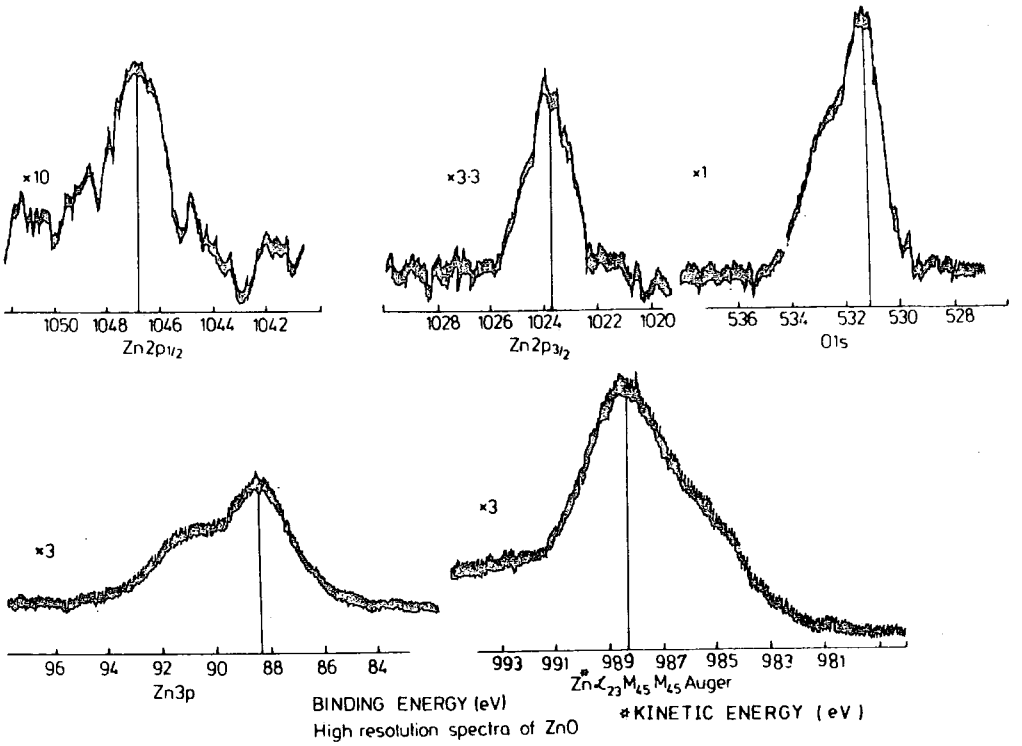

Figure 3.2b. High resolution spectra of ZnO.

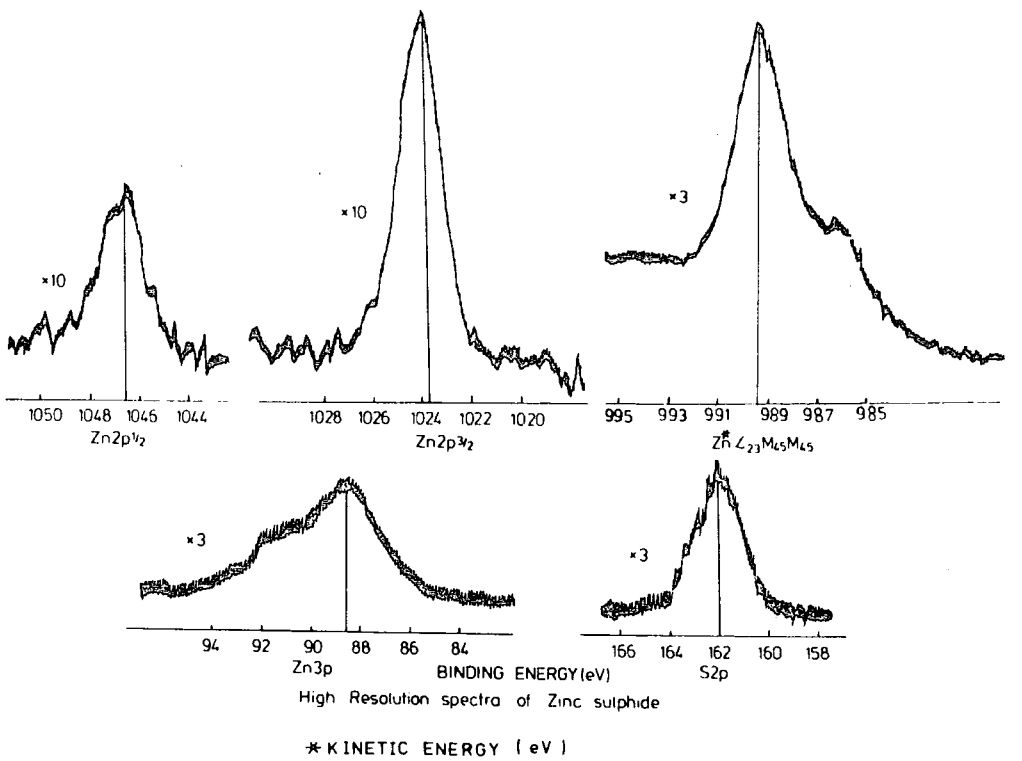

Figure 3.3. High resolution spectra of ZnS.

Table 3.5

Zinc Oxide

	C_{1s}	O_{1s}	$Zn_{2p_{3/2}}$	Zn_{3p}	$Zn^*L_{23}M_{45}M_{45}$
Binding energies (eV)	285	531.1	1023.7	88.4	988.4

	C_{1s}/O_{1s}	Zn_{3p}/O_{1s}	C_{1s}/Zn_{3p}
Intensity Ratio	2.7	2.7	0.3

(* Kinetic energy in eV)

For comparison purposes spectra have also been recorded for zinc sulphide and these are shown in Figure 3.3. The sample is again heavily overcoated with hydrocarbon. The binding energies and relative peak intensity ratios are collected in Table 3.6. A distinctive feature is the very low binding energy for the S_{2p} levels, appropriate to anionic sulphide (162 eV). (It may be added here that the S_{2p} level did not indicate any tendency for oxidation on exposure to an oxygen plasma at a power loading of 10 watts for 10 seconds and a total pressure of 0.2 torr.)

Table 3.6

Zinc Sulphide

	C_{1s}	O_{1s}	$Zn_{2p_{3/2}}$	Zn_{3p}	S_{2p}	$Zn^*L_{23}M_{45}M_{45}$
Binding energies (eV)	285	532.6	1023.7	88.6	162	989.5

	C_{1s}/O_{1s}	C_{1s}/Zn_{3p}	C_{1s}/S_{2p}	Zn_{3p}/S_{2p}
Intensity ratio	3.7	3.7	6.3	1.7

(* Kinetic energy in eV)

(b) Stearic acid

The wide scan ESCA spectrum for the stearic acid is shown in Figure 3.4a. and reveals just carbon and oxygen signals. The high resolution C_{1s} and O_{1s} core level spectra shown in Figure 3.4b are distinctive for a long chain fatty acid. The C_{1s}/O_{1s} intensity ratio of 6.4 with the appropriate sensitivity factors suggests a C/O stoichiometry of 10:1, slightly higher than that required for statistical sampling of the repeat unit; which may suggest partial orientation at the surface (viz. carboxylate groups into the bulk giving rise to a low surface free energy hydrocarbon exterior).

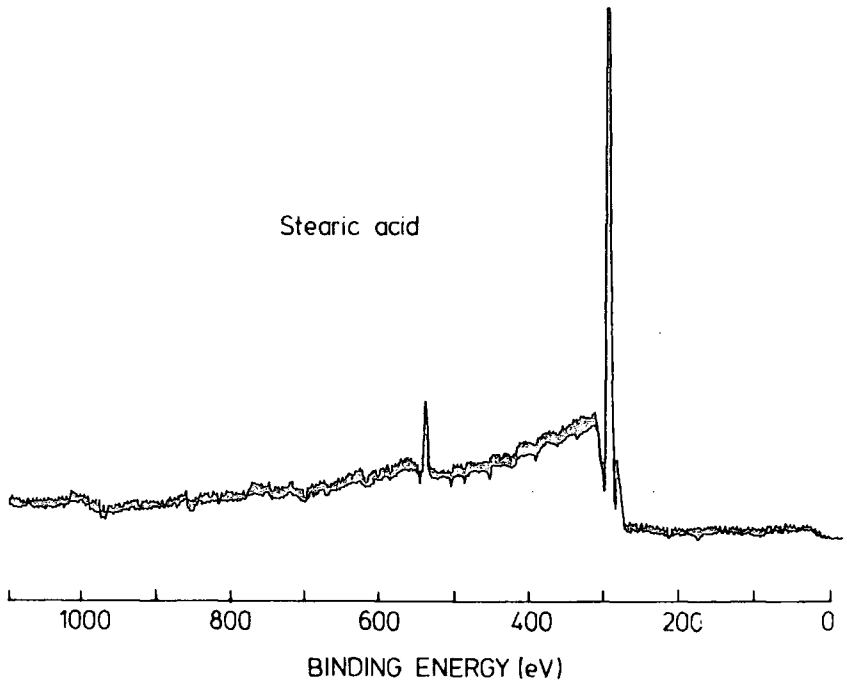

Figure 3.4a. A wide scan of stearic acid.

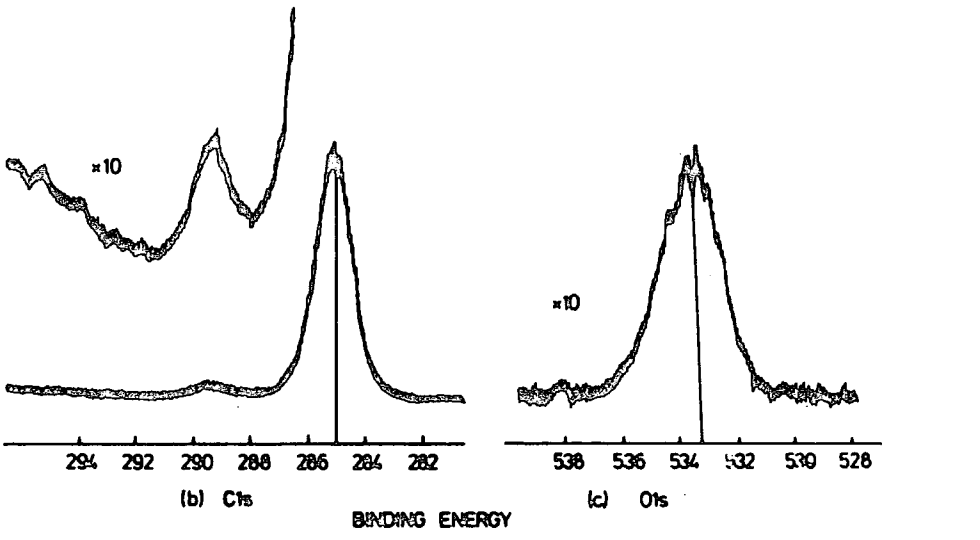

C1s and O1s core levels of stearic acid containing only carbon, hydrogen and oxygen

Figure 3.4b. High resolution spectra of stearic acid.

(c) Cyclohexylbenzthiazyl sulphenamide (CBS)

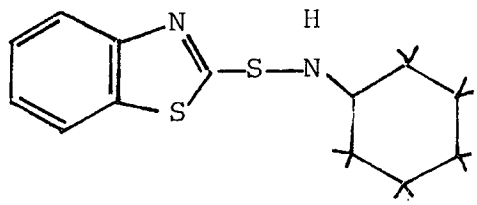

The wide scan ESCA spectrum in Figure 3.5 reveals evidence for the anticipated C_{1s}, N_{1s} and S_{2p} core level spectra, but in addition substantial peaks are observed for O_{1s} and Si_{2s} and Si_{2p} levels. This indicates extensive surface

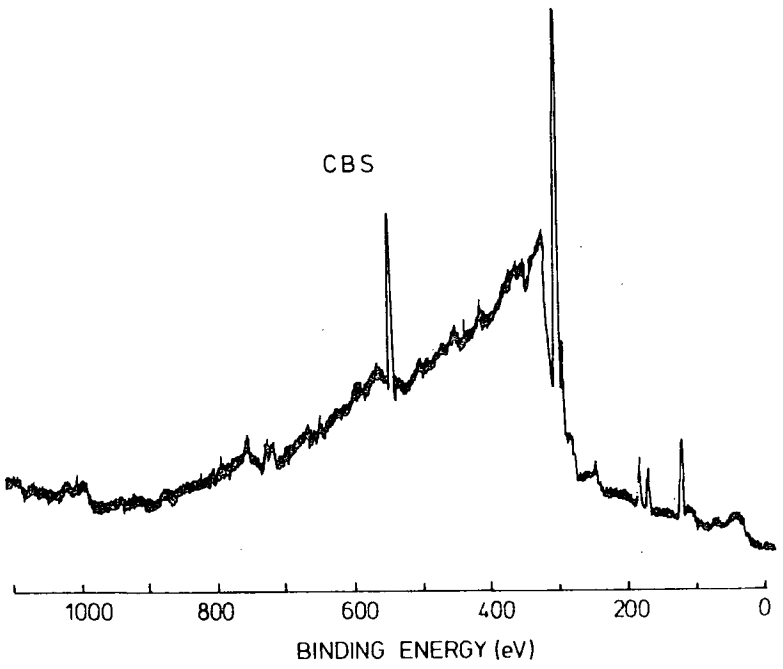

Figure 3.5. A wide scan of cyclohexylbenzthiazyl sulphenamide.

contamination of this material with silicone and this precludes the generation of reliable sensitivity parameters for this sample. The high resolution spectra have, therefore, merely been used to obtain the absolute binding energies for the various structural features and these are displayed in Table 3.7.

Table 3.7

Cyclohexylbenzthiazyl sulphenamide

	C_{1s}	O_{1s}	N_{1s}	S_{2p}	S_{2p} oxidised	Si_{2p}
Binding energies (eV)	285	533	399.7	164	168.4	101

	C_{1s}/O_{1s}	C_{1s}/N_{1s}	C_{1s}/S_{2p}	C_{1s}/Si_{2p}
Intensity ratio	6.0	11	4.0	11.0

(d) Sulphur

Since core level spectra for sulphur have previously been recorded, the data and the binding energies are set out in Table 3.8.

Table 3.8

Sulphur

Compound	Binding energies (eV) of S_{2p}
S_8	163.8
S_n	164.0

(e) Permanax B

Permanax B is a condensate of acetone and diphenylamine, extensively used as an antioxidant additive. The core level spectra for the sample studied in the form of a powder are shown in Figure 3.6b. The wide scan ESCA spectrum in Figure 3.6a shows the intense C_{1s} photoemission, with smaller components arising from the O_{1s} and N_{1s} levels. The high resolution spectra provide the data in Table 3.9. The C/N stoichiometry indicated from this would correspond with a 1:1 condensate. The N_{1s} binding energy is consistent with an amine type environment. The structure of a condensate is

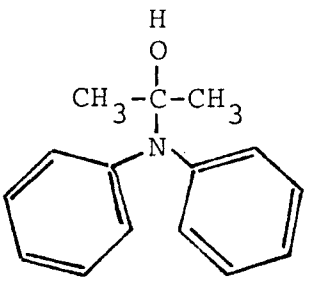

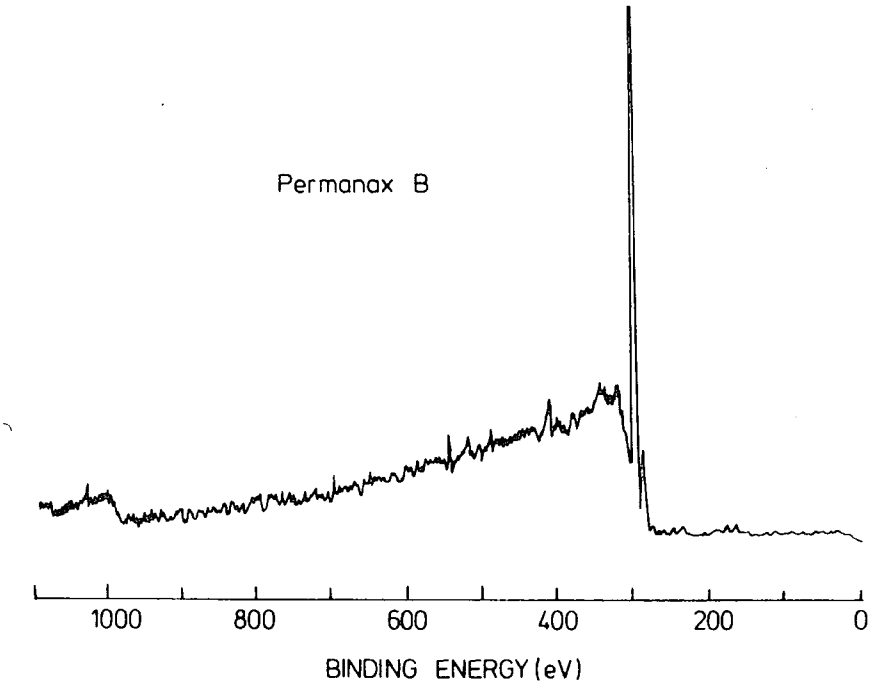

Figure 3.6a. A wide scan of permanax B.

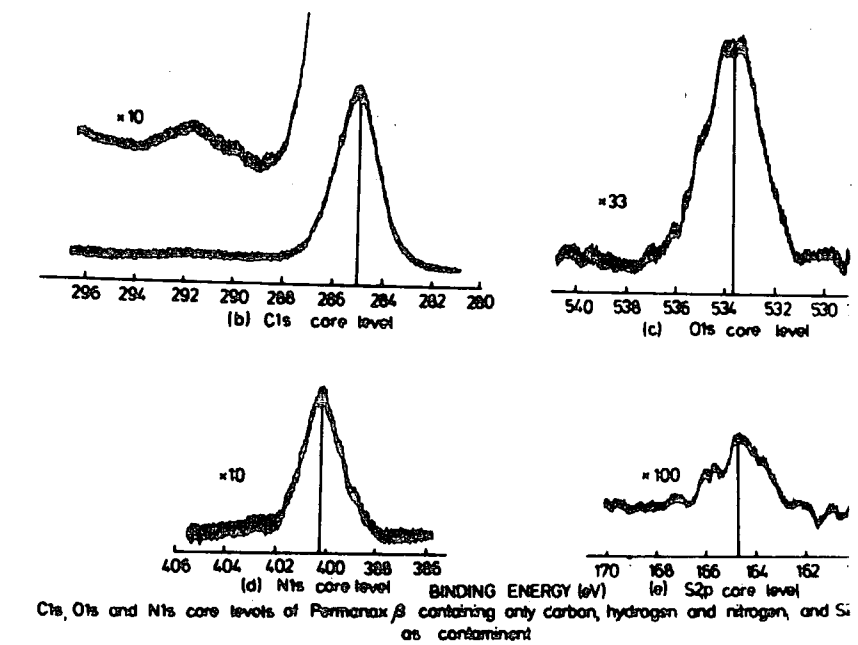

C1s, O1s and N1s core levels of Permanax β containing only carbon, hydrogen and nitrogen, and Si as contaminant

Figure 3.6b. High resolution spectra of permanax B.

Table 3.9

Intensity ratio	C_{1s}/O_{1s}	C_{1s}/N_{1s}
	19.0	14.0

(f) Tetramethylthiuram disulphide (TMD)

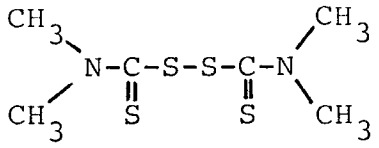

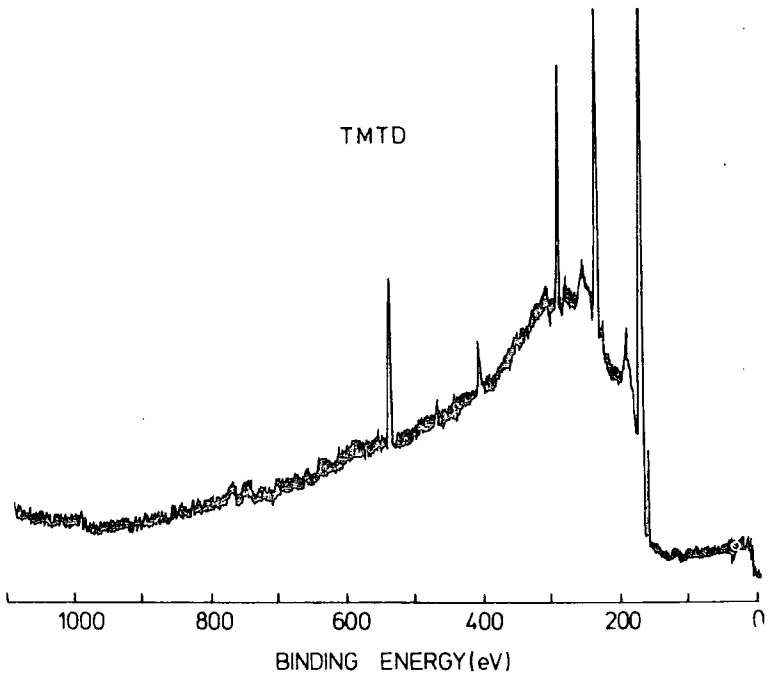

Figure 3.7. A wide scan of TMTD.

The wide scan reveals a substantial signal from extraneous oxygen. The relative intensities of core levels are given in

Table 3.10, together with the binding energies. The S_{2p} levels appear as a slightly broader structure. consistent

Table 3.10

TMTD

Binding energies (eV)	C_{1s}	O_{1s}	N_{1s}	S_{2p}
	285	534.1	401.1	164.4

C_{1s}/O_{1s}	C_{1s}/N_{1s}	C_{1s}/S_{2p}
1.7	10.0	0.31

with a small binding energy difference for the two different types of sulphur (C-S and C=S). The intensity ratio for the $C_{1s/S_{2p}}$ levels is consistent with statistical sampling of the molecular formula indicated above, however, the $S_{2p/N_{1s}}$ intensity ratio indicates a deficit of nitrogen and this coupled with the presence of oxygen indicates an impure sample.

(g) 2(4-Morpholinylmercapto)benthiazole (MBS)

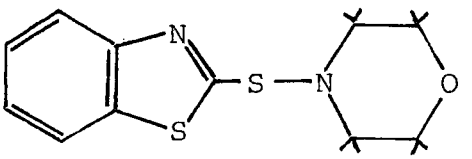

The ESCA spectra for this sample are shown in Figures 3.8a-b and the corresponding intensity ratios are given in Table 3.11. The spectra also reveal evidence of silicone material and the relative intensity ratios do not, therefore, represent statistical sampling of the molecular structure.

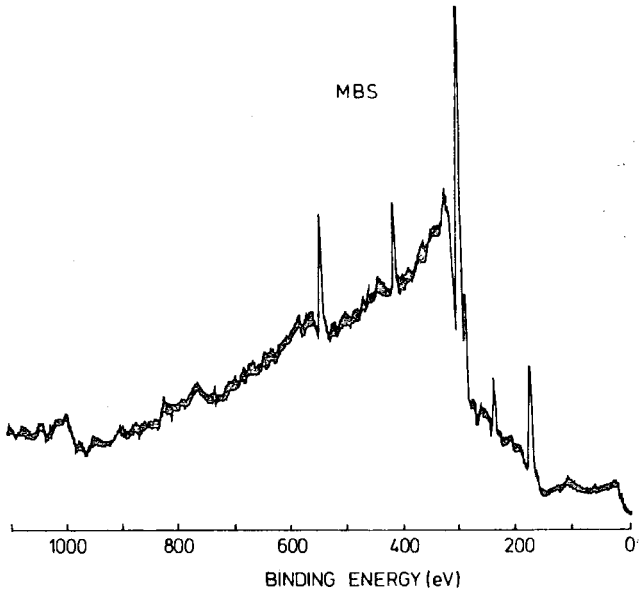

Figure 3.8a. A wide scan of MBS.

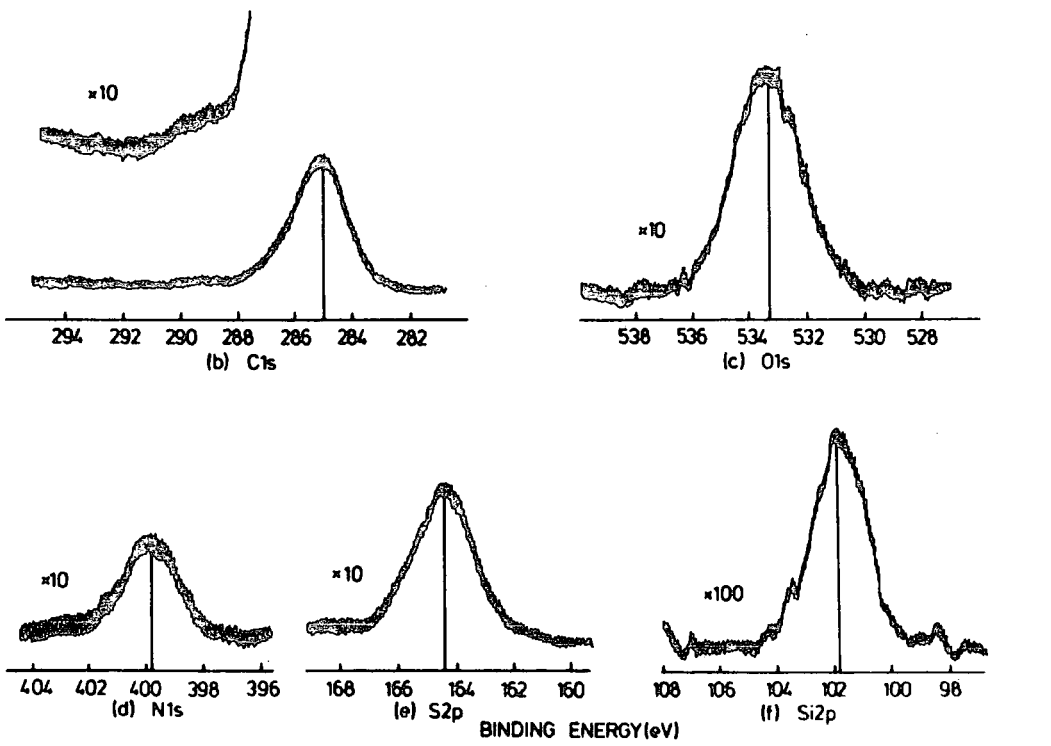

C1s, N1s, O1s and S2p core levels of 2-(4 morpholinyl mercapto) benzthiazole, and Si2p arising from contamination

Figure 3.8b. High resolution spectra of MBS.

Table 3.11

MBS

Intensity ratio	C_{1s}/O_{1s}	C_{1s}/N_{1s}	C_{1s}/S_{2p}	C_{1s}/Si_{2p}
	4.7	13.5	8.2	59.0

Conclusion

The spectra of the additives reveal that in each case to a greater, or lesser degree, there is surface contamination and the samples are clearly of technical grade. The spectra have, therefore, been primarily used to obtain some indication of binding energy as a function of electronic environment. In this connection, one may note the following:

(i) The N_{1s} binding energy for CBS, permanax B and TMTD fall in the range $\sim$ 400 - 401.0 eV;

(ii) The S_{2p} levels for sulphur directly bonded to carbon or to sulphur fall in the narrow binding energy range $\sim$ 164.4 eV, whilst anion, i.e. sulphur (sulphide) is at a much lower binding energy $\sim$ 161.8 eV;

(iii) Oxygen in an anionic environment (e.g. in ZnO) appears at low binding energy $\sim$ 531.0 eV whilst oxygen directly bonded to carbon (e.g. stearate and MBS) is at a substantially higher binding energy.

3.3.3 ESCA analyses of cured samples

(a) Type 1, Natsyn 2200, elastomer

(i) Introduction

It is convenient to consider the ESCA data in detail for one particular case, and then provide a somewhat less detailed analysis for the other systems. The bulk formulation of the Type 1 Natsyn 2200 system is indicated in Table 3.1, and the details of the composition are given in Table 3.12 in terms of weight and normalised mole % terms. On this basis, it is clear that the C_{1s} signal should predominantly derive from the cured Natsyn framework, with small contributions from stearic acid, CBS and permanax B. The N_{1s} signals would be expected from both CBS and permanax B, whilst the sulphur signal should predominantly arise from the added sulphur itself as opposed to the sulphur of CBS. Zinc is added to the formulation as the oxide, and one objective of the ESCA investigation is to effect a chemical speciation, in particular of zinc and sulphur. The O_{1s} signals can conceivably arise from residual metal oxide (low binding energy), from carboxylate and oxygen in stearate and permanax B respectively, and from any oxidative functionalisation arising from sulphur (viz. SO_4^{2-}) or from oxidation of the Natsyn surface during cure. In principle, the ESCA experiment provides five measurable levels to define a C:N:S:Zn:O surface stoichiometry. Apart from any detail of fine structure, which potentially might provide additional information, the measurement of only five levels does not allow an ambiguous assignment of surface composition. Some simplifying

Table 3.12

Natsyn 2200 Sample Formulation

Type	1		2		3		4	
	weight (%)	moles (%)	weight (%)	moles (%)	weight (%)	moles (%)	weight (%)	moles (%)
Natsyn 2200 (cis-polyisoprene)	89.2	90	88.5	94	89.7	93.7	96.9	99.2
Zinc oxide	4.5	4.1	4.4	3.9	4.5	4.0	-	-
Stearic acid	2.7	0.69	2.7	0.72	2.7	0.71	-	-
CBS	0.54	0.14	-	-	1.3	0.36	-	-
Sulphur	2.2	4.8	-	-	0.31	0.71	-	-
Permanax B	0.9	0.27	0.9	0.29	0.9	0.28	0.97	0.28
TMTD	-	-	3.5	1.08	0.6	0.21	-	-
Dicup R	-	-	-	-	-	-	2.1	0.55

(It is worthwhile noting that the microanalysis data were in good agreement with the values of Natsyn formulation.)

assumptions are, therefore, required to enable an analysis to be affected. The first of these is that the ratio of the minor additives CBS and permanax B (or their transformation products) remains the same in the surface as in the bulk.

(ii) Optimum cured type 1, Natsyn 2200, elastomer

The core level spectra for the optimum cured, type 1, sample are shown in Figure 3.9 and the intensity ratios for the components are set out in Table 3.13.

Table 3.13

Optimum cured type 1, Natsyn 2200, elastomer

(a) Intensity ratios Take-off angle	C_{1s}/O_{1s}	C_{1s}/N_{1s}	C_{1s}/S_{2p}	C_{1s}/Zn_{3p}	Zn_{3p}/S_{2p}
30^{o}	16	69	27	24	1.15
70^{o}	14	89	27	27	1.0

The angular dependent data indicate that the samples are reasonably homogeneous, in terms of stoichiometry, as a function of depth into the sample. Before considering a semi-quantitative analysis, one may briefly consider the details of the high resolution core level spectra.

The C_{1s} levels show a broadened signal compared with the uncured system without additives (FWHM 1.7 eV vs. 1.4 eV respectively), and the $\pi \rightarrow \pi^*$ shake-up satellite is of much lower intensity. As far as the ESCA depth sampling scale is concerned, therefore, the unsaturation in the surface regions is lower than for the uncured system.

The high resolution spectra also reveal nitrogen and sulphur, the latter (as the S_{2p} levels) being broadened by the

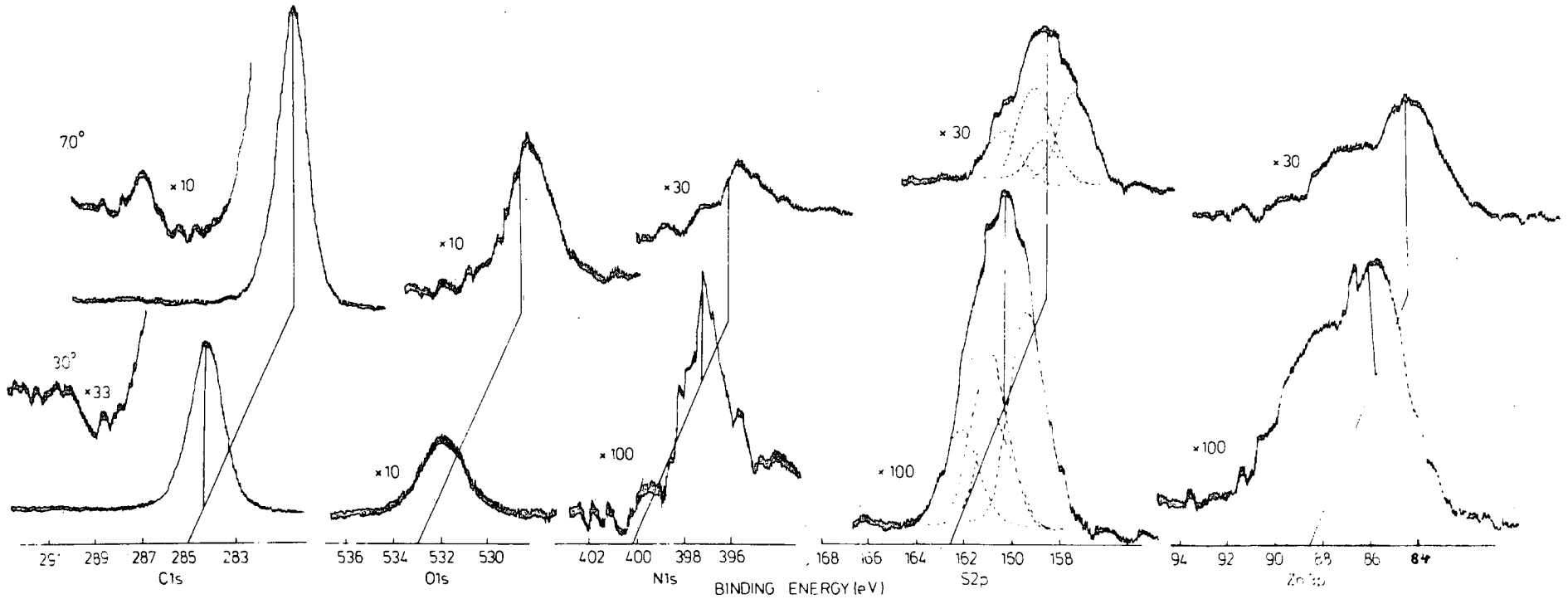

C1s, O1s, N1s, S2p and Zn3p core levels for an optimum cured type 1, Natsyn 2200, elastomer at take off angles of 30° and 70°

Figure 3.9. High resolution spectra of an optimum cured type 1, Natsyn 2200, elastomer.

presence of at least 2 components. Oxygen and zinc are also detected at reasonable levels. The bulk formulation of the type 1 system provides a mole ratio of permanax B to CBS of 2:1. Since these are the only two additives to contribute to the N_{1s} spectrum, one may perform a crude surface analysis as follows:-

The <u>average</u> intensity ratios for the various core levels may be taken as

C_{1s}/N_{1s}	C_{1s}/S_{2p}	C_{1s}/O_{1s}	C_{1s}/Zn_{3p}	Zn_{3p}/S_{2p}
79	27	15	25	1.1

The N_{1s} signal intensity arises from the CBS and permanax B components, whilst the C_{1s} spectrum derives from the Natsyn 2200 (predominantly), and the signal arising from the additives (other than sulphur and zinc oxide for which the initial analysis indicates a small contribution due to the hydrocarbon overlayer). The C_{1s}/N_{1s} intensity ratio corrected for the differences in cross-section provides a means of assessing the C:N stoichiometry in the depth scale monitored by ESCA. Taking the permanax B as a 1:1 adduct provides the following equation

Let y = mole % of Natsyn Let x = mole % of cis

then

permanax = 2x mole %

Total C_{1s} signal = $\underline{5y + 2 \times 15x + 13x + 18 \times 5x}$

Total N_{1s} signal = (2x + 2x)

$$\therefore \quad \frac{5y + 133x}{4x} = 79 \times 1.19 = 94$$

$$5\left(\frac{y}{x}\right) = 243$$

$$\frac{243}{5} = 50$$

(The value of $\left(\frac{y}{x}\right)$ is still the same order of magnitude ($\sim$ 66) regardless of any contribution from stearate.)

Table 3.14

Surface composition (mole %)

Take-off angle	Polyisoprene	Permanax B	CBS	Zn
30^{o}	100	3.5	1.9	1.6
70^{o}	100	2.6	1.4	1.4

The average value of $\frac{y}{x}$ based on 30^{o} and 70^{o} take-off angles in Table 3.14, therefore, gives ratios of 100:3.0:1.6 in moles for Natsyn 2200, permanax B and CBS respectively, indicating higher levels of antioxidant and accelerator by a factor of eight than in the bulk, whilst the level of zinc at the surface is, approximately 1.5 mole %, less compared to that in the bulk ($\sim$ 4.0 mole %).

The 'swelling' data (section 3.3.1) taken in conjunction with the ESCA data (C_{1s}/S_{2p} intensity ratio) provides a basis for the estimation of the average number of sulphur atoms involved in crosslinking two polymer chains, as represented in Figure 3.10. Where $\bar{M}c$ is the number average molecular weight between two crosslinked points and S_x is the average number of sulphur atoms involved in forming a linkage.

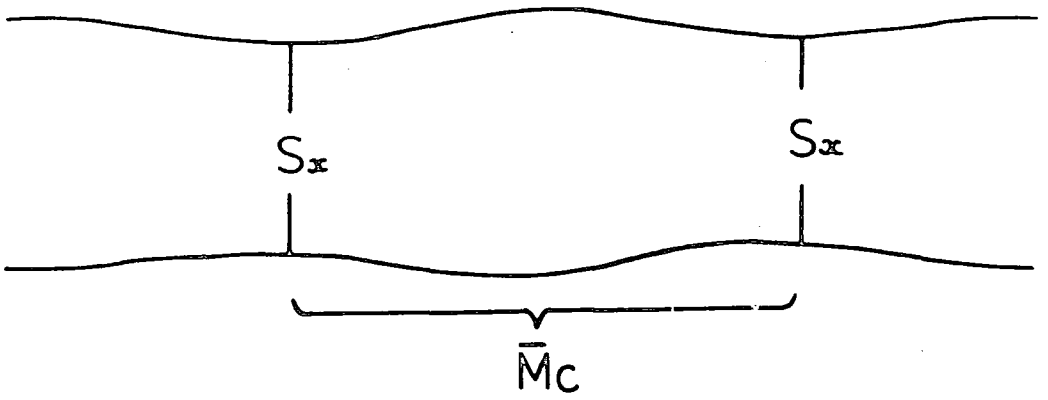

Figure 3.10. Schematic representation of crosslinks of a sulphur vulcanisate.

The S_{2p} peaks are broadened by the presence of at least two components, namely organic and inorganic sulphides, which, in turn, constitute numbers of overlapping peaks, the higher binding energy peaks after deconvolution are attributed to organic sulphide (including polysulphide), and the lower binding energies to zinc sulphide. A unique deconvolution was carried out with a full-width at half maximum of 1.7 $\pm$ 0.1 eV by using an analogue curve fitting procedure, with Gaussian curves positioned approximately at 164.4 eV, 163.1 eV, 162.8 eV and 161.5 eV and treating the height only as a variable to obtain the best fitting curves (chapter six).

As has already been stated, the Flory-Rehner equation[73-79] allows the evaluation of the number average molecular weight between the crosslink points of the polymer chains. The use of this data together with the analysis of the S_{2p} peaks

allow further for an estimate of the average number of sulphur atoms between the crosslink points of two polymer chains; the estimate being made as follows:-

the stoichiometry of cation to sulphur (of higher binding energy approximate to C-S environments)	= 115:1
molecular weight of a repeat unit $(-CH_2-\overset{CH_3}{\overset{\vert}{C}}=CH-CH_2-)$	= 68
number average molecular weight between the crosslinked points	= 6, 725

Since one crosslink per 99 monomer units occurs, the number of carbon atoms between the two crosslink points are 495; and, therefore, the average sulphur functionality is four ($^{495}/_{115}$).

In conclusion, for an optimum cured type 1, Natsyn 2200, elastomer, the surface is rich in permanax B and CBS, by a factor of approximately eight, in contrast to the level of zinc, compared to the bulk composition, and the elastomer possesses on average tetrasulphide linkages; and also the surface is reasonably homogeneous, as far as the ESCA depth profile is concerned.

(iii) 50% cured type 1, Natsyn 2200, elastomer

Figure 3.11 shows the C_{1s}, O, N_{1s}, S_{2p} and Zn_{3p} levels measured at two different take-off angles for a partially cured type 1 sample, whose detailed surface compositions, based on the previous calculation procedure, are considerably different from those of an optimum cured type 1 sample. The

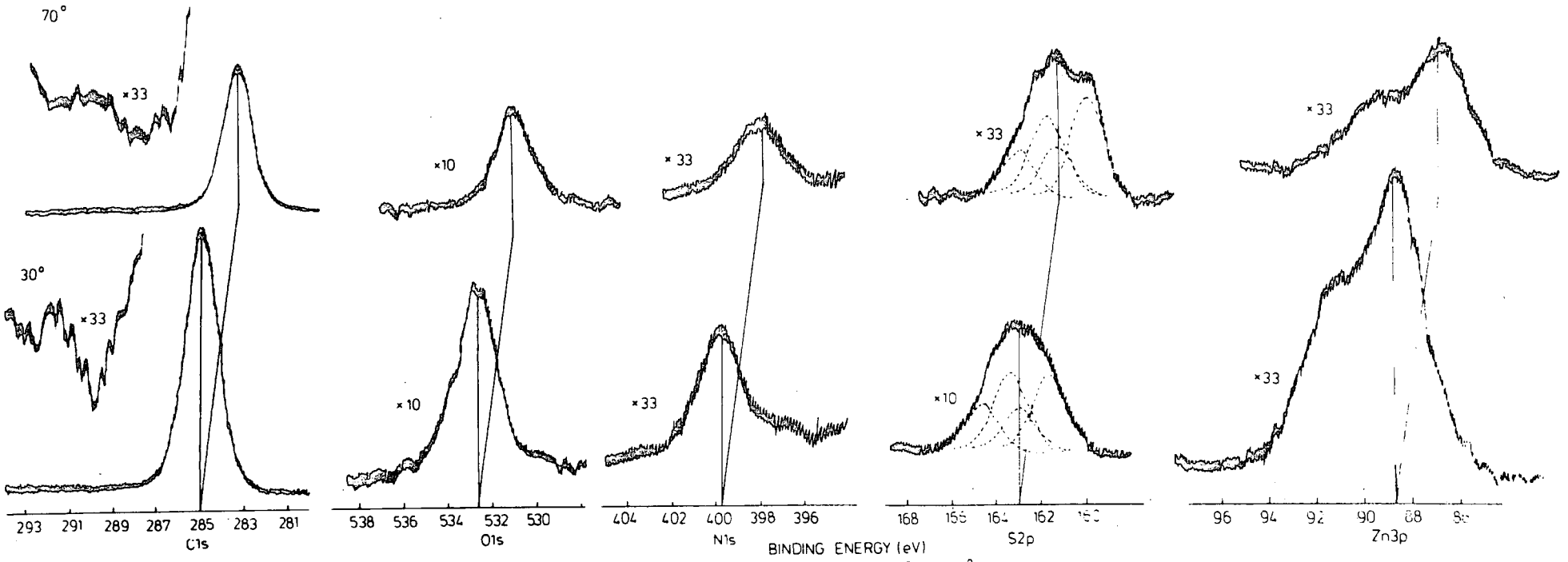

C1s, O1s, N1s, S2p and Zn3p core levels for 50% cured type 1, Natsyn 2200, elastomer at take off angles of 30° and 70°

Figure 3.11. High resolution spectra of a partially cured type 1, Natsyn 2200, elastomer.

intensity ratios and the surface compositions at 30^{o} and 70^{o} take-off angles are set out in Table 3.15.

Table 3.15

50% cured type 1, Natsyn 2200, elastomer

(a) Intensity ratios

Take-off angle	C_{1s}/O_{1s}	C_{1s}/N_{1s}	C_{1s}/S_{2p}	C_{1s}/Zn_{3p}	Zn_{3p}/S_{2p}
30^{o}	13	57	11	11	1.0
70^{o}	11	47	15	15	7.0

(b) Surface composition (mole %)

Take-off angle	Polyisoprene	Permanax B	CBS	Zn
30^{o}	100	4.4	2.3	3.4
70^{o}	100	5.6	2.9	2.5

It is clearly evident that the surface is reasonably homogeneous, in terms of stoichiometry, as a function of vertical depth into the sample. The C_{1s} levels monitored at 30^{o} and 70^{o} take-off angles reveal little evidence for oxidative functionalisation with low intensity of $\pi \rightarrow \pi^{*}$ shake-up transitions, centred approximately at 6.5 eV from the main C_{1s} photoionisation peak, and show broadened signals compared with the uncured system without additives (FWHM 1.8 eV for 30^{o} and 1.7 eV for 70^{o} vs. 1.4 eV of uncured system).

Oxygen, nitrogen, silicon as contaminant, sulphur and zinc signals are also observed at reasonable levels, the S_{2p} peak being broadened (FWHM 4.0 eV of S_{2p} in type 1 system vs. 2.2 eV of S_{2p} in ZnS) by the presence of at least two

components, namely organic and inorganic sulphides.

The evaluation of sulphur functionality, based on the 'swelling' data and area under the higher energies overlapping peaks of S_{2p} again indicates polysulphidic linkages, containing 10 sulphur atoms per bridge in partially cured type 1 sample.

(b) Type 2, Natsyn 2200, elastomer

(i) Introduction

In view of the rather extensive details considered for the type 1 elastomer in the previous sections, it is convenient to provide limited details for the subsequent series of elastomers, and also to present spectra pictorially only for the optimum cured samples, since the results extracted from the raw spectra are tabulated in appropriate sections.

It is clearly evident from the details of the composition in Table 3.12 in terms of weight and normalised mole % that the C_{1s} signals should again predominantly arise from the cured Natsyn framework, with smaller contributions from stearic acid, permanax B and TMTD. The N_{1s} signals would be expected from both permanax B and TMTD, whilst the sulphur intensity should arise from TMTD, since this is the only sulphur containing additive in the system. Zinc is added to the formulation as the oxide to enhance the rate of cure. The O_{1s} signals can conceivably arise from stearate, permanax B and from the oxidation of the Natsyn surface during cure. In principle, the C_{1s}, O_{1s}, N_{1s}, S_{2p} and Zn_{3p} levels monitored at two different take-off angles again allow an unambiguous

assignment of surface composition, on the same assumptions stated for type 1 system.

(ii) Optimum cured type 2, Natsyn 2200, elastomer

The intensity ratios and surface composition of components, extracted from the raw spectra for the optimum cured in Figure 3.12, are set out in Table 3.16.

Table 3.16

Optimum cured type 2, Natsyn 2200, elastomer

(a) Intensity ratios

Take-off angle	C_{1s}/O_{1s}	C_{1s}/N_{1s}	C_{1s}/S_{2p}	C_{1s}/Zn_{3p}	Zn_{3p}/S_{2p}
30^{o}	6	24	12	10	1.2
70^{o}	5	21	10	11	0.9

(b) Surface composition (mole %)

Take-off angle	Polyisoprene	Permanax B	TMT	Zn
30^{o}	100	2.5	9.1	3.7
70^{o}	100	2.9	10.7	3.4

The angular dependent data reveals that the surface is reasonably homogeneous, as a function of depth into the sample. The C_{1s} spectra at both take-off angles indicate an evidence for oxidative functionalisation with the absence of $\pi \rightarrow \pi^*$ shake-up peak, and show broadened signals compared with the uncured system without additives (FWHM 1.9 eV for 30^{o} and 1.7 eV for 70^{o} vs. 1.4 eV of uncured system).

The high resolution spectra also reveal oxygen, nitrogen, silicon as contaminant, zinc and sulphur at reasonable levels,

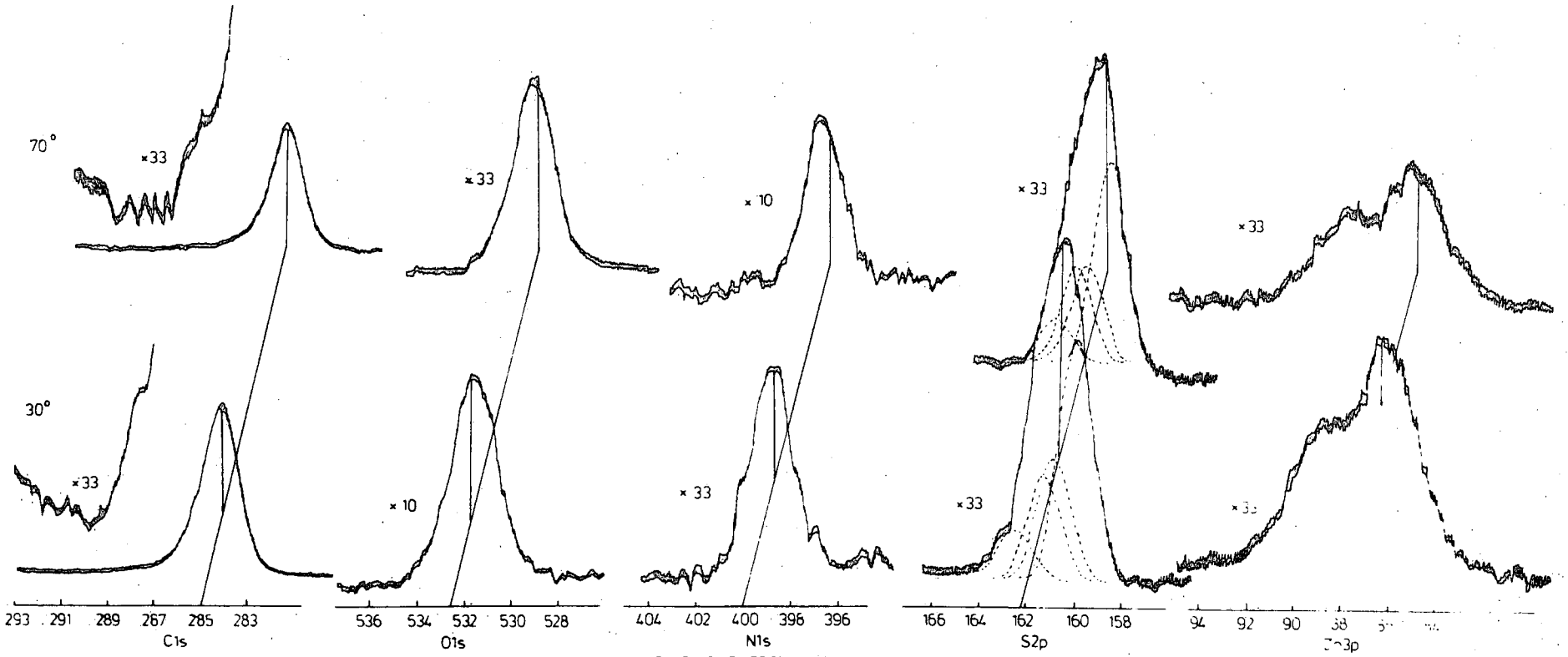

Figure 3.12. High resolution spectra of an optimum cured type 2, Natsyn 2200, elastomer.

the latter being broadened by the presence of at least 2 components (FWHM 2.6 eV for both take-off angles vs. 2.2 eV of ZnS). The composition ratios of Natsyn 2200, permanax B and TMTD, in Table 3.16, calculated in the similar manner as for type 1 sample, indicate higher levels of antioxidant and accelerator by a factor of approximately nine than in the bulk, whilst the level of zinc, less than in the bulk, increases with increasing depth in the surface.

The sulphur functionalities of eight and ten at 30^{o} and 70^{o} take-off angles respectively, suggest that at least nine sulphur atoms are involved in crosslinking two polymer chains.

(iii) 50% cured type 2, Natsyn 2200, elastomer

The C_{1s} spectra at both take-off angles indicated an evidence for oxidative functionalisation, with the complete absence of $\pi \rightarrow \pi^*$ shake-up transitions for 70^{o} take-off angle and with very little shake-up transition for 30^{o} take-off angle, and they also showed broadened C_{1s} signals compared with the uncured Natsyn 2200 without additives (FWHM 1.8 eV for 30^{o} and 1.6 eV for 70^{o} take-off angles vs. 1.4 eV of uncured system). The extent of oxidation in the extreme surface (take-off angle of 70^{o}) was greater than in the sub-surface (take-off angle of 30^{o}).

The high resolution spectra also revealed nitrogen and sulphur, the latter being broadened by the presence of organic and inorganic sulphides (FWHM 3.0 eV for both take-off angles vs. 2.2 eV of ZnS). Oxygen and zinc were also detected at reasonable levels.

The surface composition in Table 3.17 indicates the higher levels of additives at the surface by a factor of approximately two than in the bulk, which is smaller compared to the surface composition for an optimum cured type 2 sample, whilst the level of Zn, less than in the bulk, is nearly the same at both take-off angles.

Table 3.17

Partially (50%) cured type 2, Natsyn 2200, elastomer

(a) Intensity ratios

Take-off angle	C_{1s}/O_{1s}	C_{1s}/N_{1s}	C_{1s}/S_{2p}	C_{1s}/Zn_{2p}	Zn_{3p}/S_{2p}
30°	13	73	33	23	1.4
70°	11	86	46	20	2.3

(b) Surface compositions (mole %)

Take-off angle	Polyisoprene	Permanax B	TMTD	Zn
30°	100	0.7	2.7	1.7
70°	100	0.6	2.3	1.9

The sulphur functionality of three on average reveals trisulphide linkages in the ESCA depth profile.

(c) Type 3, Natsyn 2200, elastomer

(i) Introduction

As expected before, the C_{1s} intensity should predominantly arise from the Natsyn framework, with small contributions arising from stearic acid, CBS, permanax B and TMTD. The N_{1s} signals are expected from CBS, permanax B and TMTD, whilst the sulphur intensity should predominantly arise from the added

sulphur itself, as opposed to the sulphur of CBS and TMTD. The O_{1s} signals can conceivably arise from residual zinc oxide, stearate, permanax B and from oxidation of the Natsyn surface during the process of cure.

The C_{1s}, O_{1s}, N_{1s}, S_{2p} and Zn_{3p} levels again allow the unambiguous assignments of surface composition on the same assumptions stated previously.

(ii) Optimum cured type 3, Natsyn 2200, elastomer

It is clearly evident from the data set out in Table 3.18, extracted from the raw spectra in Figure 3.13 that the surface is reasonably homogeneous, in terms of stoichiometry, as a function of ESCA depth profile into the sample. The C_{1s} levels monitored at 30^{o} and 70^{o} take-off angles show evidence for oxidative functionalisation with components at binding energies of 286.6 eV and 288 eV (corresponding to

Table 3.18

Optimum cured type 3, Natsyn 2200, elastomer

(a) Intensity ratios

Take-off angle	C_{1s}/O_{1s}	C_{1s}/N_{1s}	C_{1s}/S_{2p}	C_{1s}/Zn_{3p}	Zn_{3p}/S_{2p}
30^{o}	8	24	15	17	0.9
70^{o}	8	21	20	20	1.0

(b) Surface composition (mole %)

Take-off angle	Polyisoprene	Permanax B	CBS	TMTD	Sulphur	Zn
30^{o}	100	4.6	6.0	3.4	11.6	2.2
70^{o}	100	5.7	7.3	4.3	11.4	2.0

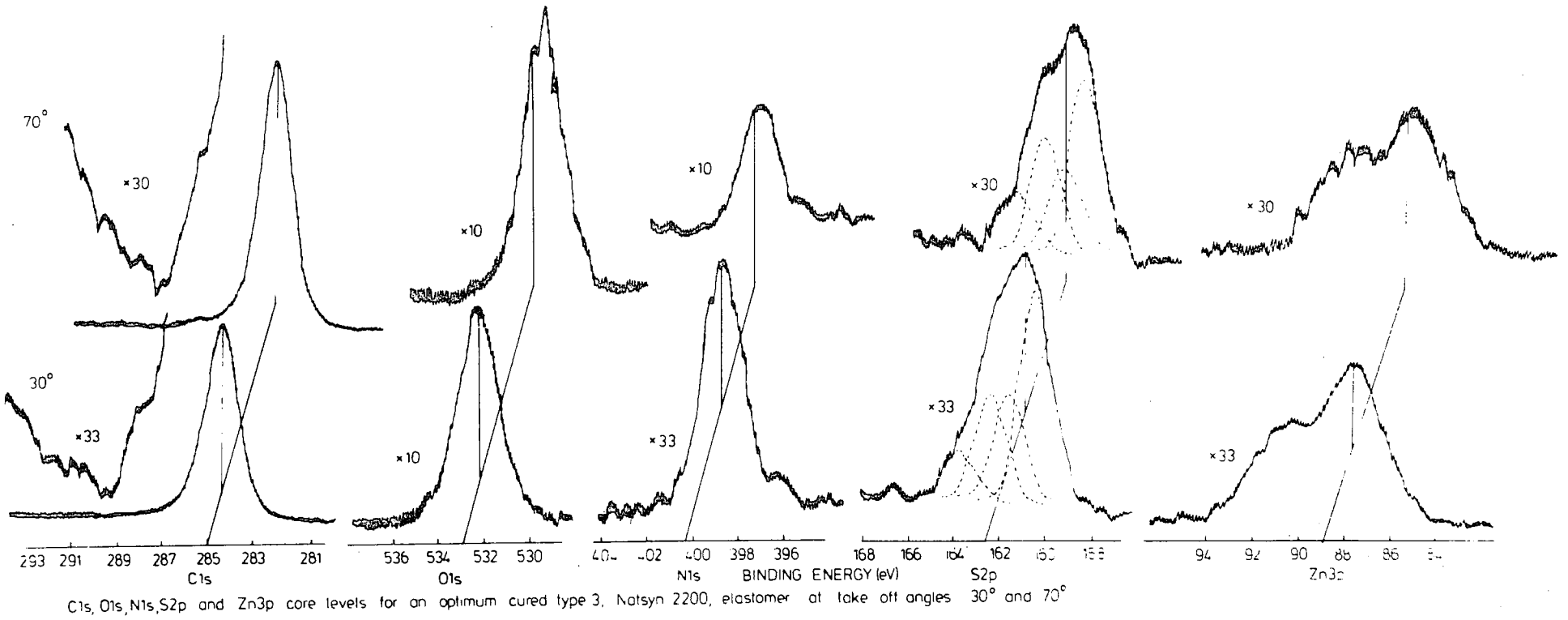

C1s, O1s, N1s, S2p and Zn3p core levels for an optimum cured type 3, Natsyn 2200, elastomer at take off angles 30° and 70°

Figure 3.13. High resolution spectra of an optimum cured type 3, Natsyn 2200, elastomer.

C-O and C=O respectively), with a complete absence of $\pi \rightarrow \pi^*$ shake-up transitions. The signals are broadened, compared with the uncured system without additives (FWHM 1.8 eV for both take-off angles vs. 1.4 eV of uncured system).

The nitrogen and sulphur are also observed at reasonable levels, the latter being broadened by the presence of at least two components (FWHM 3.2 eV for 30° and 3.4 eV for 70° take-off angles vs. 2.2 eV of ZnS). The average number of sulphur atoms between the crosslinked points, based on the 'swelling' data and analysis of the S_{2p} levels, are eight on average, indicating polysulphide linkages.

(iii) 50% cured type 3, Natsyn 2200, elastomer

The data in Table 3.19 are fairly self-explanatory. The surface is reasonably homogeneous as a function of ESCA profile depth into the sample and indicate higher levels of permanax B, CBS, TMTD and sulphur by a factor of approximately six at the surface than in the bulk in contrast to the level of zinc, the latter increases with increasing ESCA depth

Table 3.19

50% cured type 3, Natsyn 2200, elastomer

(a) Intensity ratios

	C_{1s}/O_{1s}	C_{1s}/N_{1s}	C_{1s}/S_{2p}	C_{1s}/Zn_{3p}	Zn_{3p}/S_{2p}
30°	9	49	17	16	1.1
70°	9	54	22	20	1.1

(b) Surface composition (mole %)

Take-off angle	Polyisoprene	Permanax B	CBS	TMTD	Sulphur	Zn
30°	100	1.9	2.5	1.4	5.0	2.4
70°	100	1.8	2.3	1.3	4.5	1.9

profile. The C_{1s} signals at both take-off angles had the same FWHM as those of optimum cured type 3 samples and indicate oxidative functionalities with the complete absence of shake-up peaks. The S_{2p} peaks detected at reasonable levels were also broadened by the presence of organic and inorganic sulphides. The sulphur functionalities estimated at 30^{o} and 70^{o} take-off angles were seven and four on average respectively, indicating polysulphide linkages between the polymer chains.

(d) Type 4, Natsyn 2200, elastomer

(i) Introduction

The detailed composition of the bulk formulation in terms of weight and normalised mole % for type 4 system in Table 3.12 indicates that C_{1s} intensity should predominantly arise from Natsyn framework, with smaller contributions from permanax B and dicumyl peroxide. The N_{1s} signal is expected to arise only from permanax B, since this is the only additive containing nitrogen. The bulk formulation is, therefore, simpler than those of sulphur-vulcanised series. In principle, the ESCA provides C_{1s}, O_{1s} and N_{1s} measurable levels to define the surface stoichiometry on the same assumptions as those have been stated previously.

(ii) Optimum cured type 4, Natsyn 2200, elastomer

The data in Table 3.20 corresponding to Figure 3.14 indicate that the surface is considerably inhomogeneous, in terms of stoichiometry, as far as the ESCA depth profile is concerned. The C_{1s} peaks show broadened signals, compared with the uncured system without additives (FWHM 1.7 eV vs. 1.4 eV respectively), and the $\pi \rightarrow \pi^{*}$ shake-up transitions are of much lower intensity;

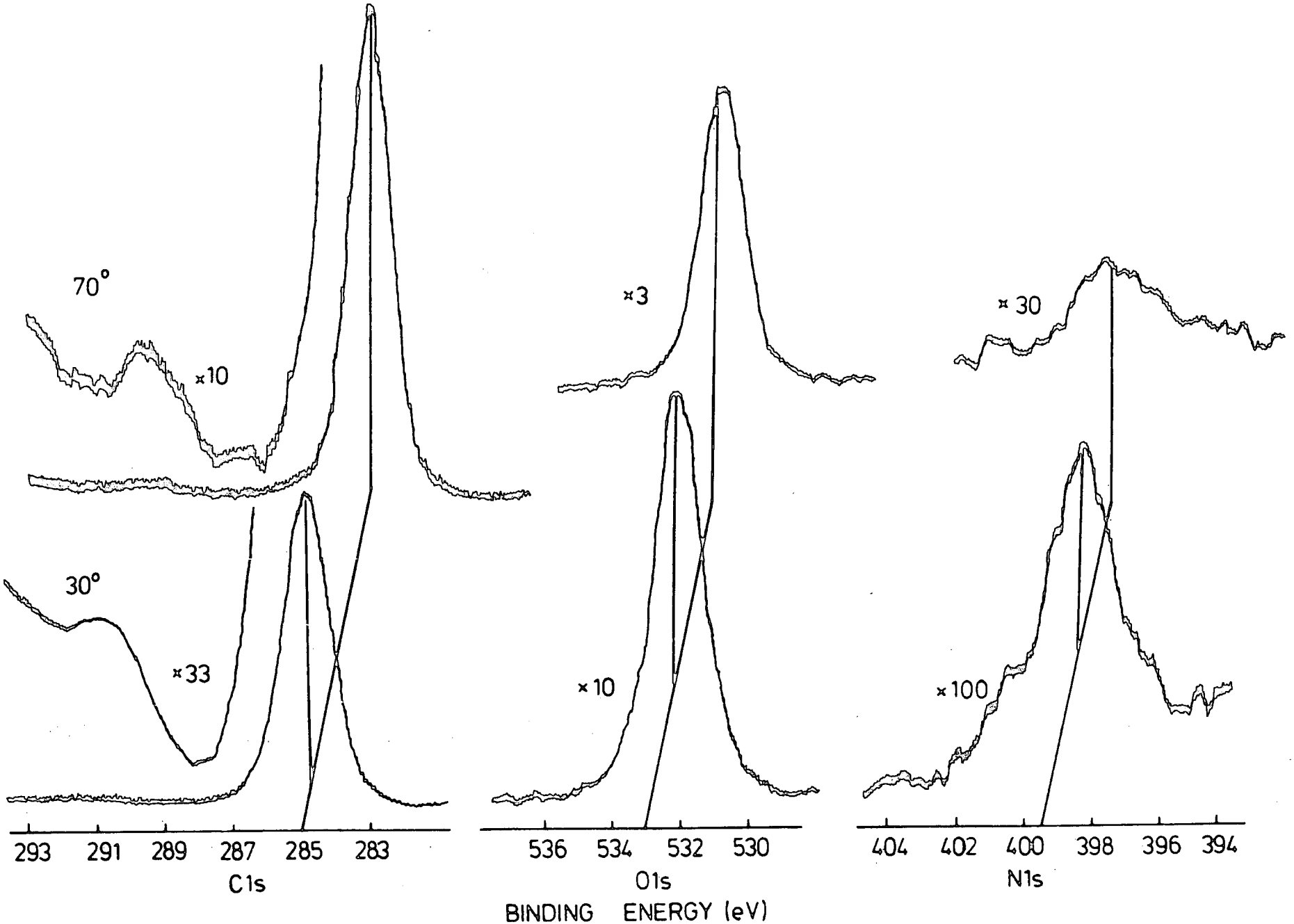

C1s, O1s and N1s core levels for an optimum cored type 4, Natsyn 2200, elastomer at take off angles 30° and 70°

Figure 3.14. High resolution spectra of an optimum cured type 3, Natsyn 2200, elastomer.

and, therefore, the surface unsaturation is lower than the uncured system on the ESCA depth profile. The high resolution spectra also reveal oxygen and nitrogen, the latter being relatively of a low level.

Table 3.20

Optimum cured type 4, Natsyn 2200, elastomer

(a) Intensity ratios

Take-off angle	C_{1s}/O_{1s}	C_{1s}/N_{1s}
30^{o}	7	70
70^{o}	5	113

(b) Surface composition (mole %)

Take-off angle	Polyisoprene	Permanax B	dicumyl peroxide
30^{o}	100	18	37
70^{o}	100	6	12

The surface composition in Table 3.20 reveals higher levels of antioxidant and accelerator than in the bulk.

3.3.4 Uncured Natsyn 2200 samples

(a) Introduction

Three samples of uncured Natsyn 2200 formulation have been received, as follows:

(i) Compressed, emulsion polymerised cis-polyisoprene. Samples have been cut directly for ESCA examination either for the investigation of the as received surfaces or for the fresh surfaces exposed with a scalpel blade.

(ii) Uncured formulations with additives (Table 3.12). As has previously been noted, the large number of voids arising during the mixing process created considerable difficulties for the analysis of these samples and in only one case did it prove possible to obtain partial spectra and, therefore, it was not possible to obtain spectra for uncured systems with additives.

(iii) The spectra for cis-polyisoprene milled for ten minutes and pressed for five minutes at an elevated temperature (140^{o}C) have not been yet obtained.

(b) Emulsion polymerized cis-polyisoprene

(i) As received surface

The wide scan ESCA spectrum for the as received sample revealed little evidence for anything other than the C_{1s} level photoemission. The high resolution scans of the C_{1s} levels in Figure 3.15 indicate a symmetrical peak, due to the carbon framework together with a low intensity ($\sim$ 2%) of $\pi \rightarrow \pi^*$ shake-up structure associated with the π system, separated by $\sim$ 6.5 eV from the direct photoionisation peak. The high resolution spectra also reveal a low level of oxygen, however, this may not be associated with oxidative degradation of the polymer surface since silicon was also detected. The high resolution scans suggest very low levels of nitrogen and zinc, and the overall intensity ratios are collected in Table 3.21.

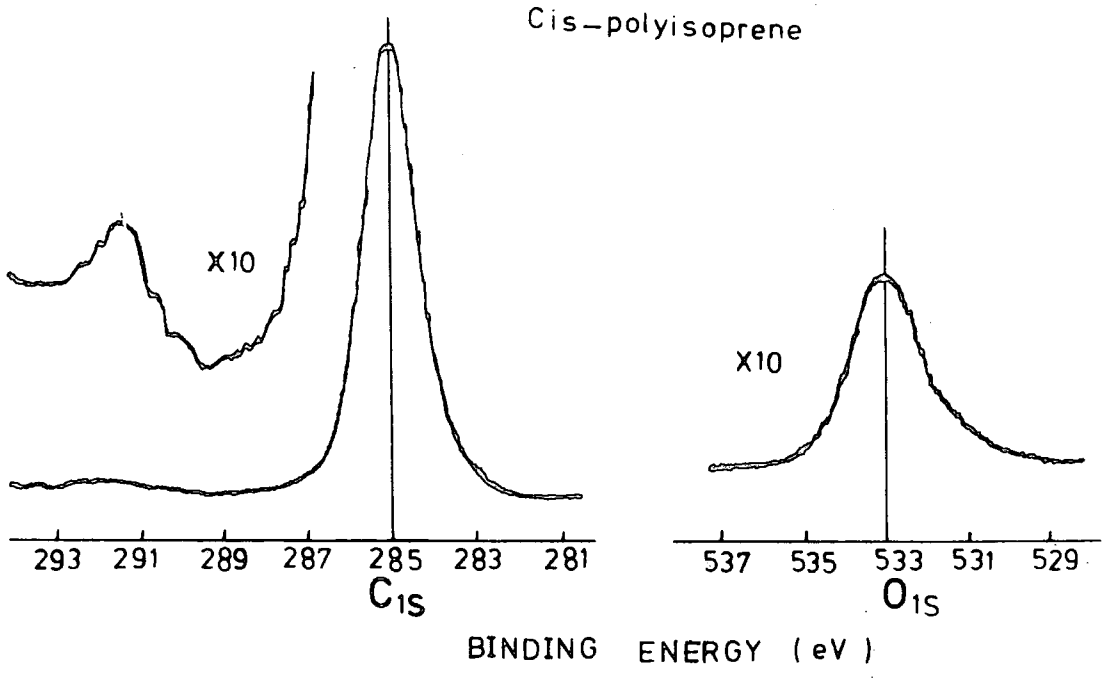

Figure 3.15. C_{1s} and O_{1s} core levels for the as received 97% cis-polyisoprene (emulsion polymerized).

Table 3.21

Intensity ratios for 97% cis-polyisoprene

	C_{1s}/O_{1s}	C_{1s}/Si_{2p}	C_{1s}/N_{1s}	C_{1s}/Zn_{2p}
As received	19	67	400	500
Freshly exposed surface of the as received	29	71	-	-

(ii) Freshly exposed surface

The data for the freshly exposed surface are set out in Table 3.21 for comparison purposes. The level of oxygen is

now somewhat lower, and silicon, and nitrogen are absent at the levels of detection, employed in this work. The C_{1s} spectrum again showed a symmetrical signal, with a low intensity of $\pi \rightarrow \pi^*$ signal arising from the π system of the Natsyn. The relative intensity of the shake-up satellite was higher than for the original surface, and in the light of the oxygen and silicon intensities, the most likely explanation for this is an overlayer of hydrocarbon contamination on the original surface (this would contribute to the direct photoionisation but not to the shake-up peak).

These spectra, therefore, revealed a small degree of surface contamination for the as received samples. (These had been covered with polyethylene terephthalate film for transportation purposes; this being removed prior to sample preparation for the ESCA experiment.)

3.3.5 Covering sheets used for transportation

(a) As received pigmented polyethylene

The wide scan spectra at 30° and 70° take-off angles for the as received pigmented polyethylene indicated very little evidence for anything other than the C_{1s} photoionisation peak. The high resolution scans of the C_{1s} levels in Figure 3.16 reveal a symmetrical peak as a result of the carbon backbone and also indicate a low level of oxygen associated with oxidative degradation of the polymer-surface. The intensity ratios are set out in Table 3.22. The results clearly indicate that the as received polyethylene is free from nitrogen, sulphur and silicon contaminations, and no evidence for pigment in the surface region is derived from the ESCA examination.

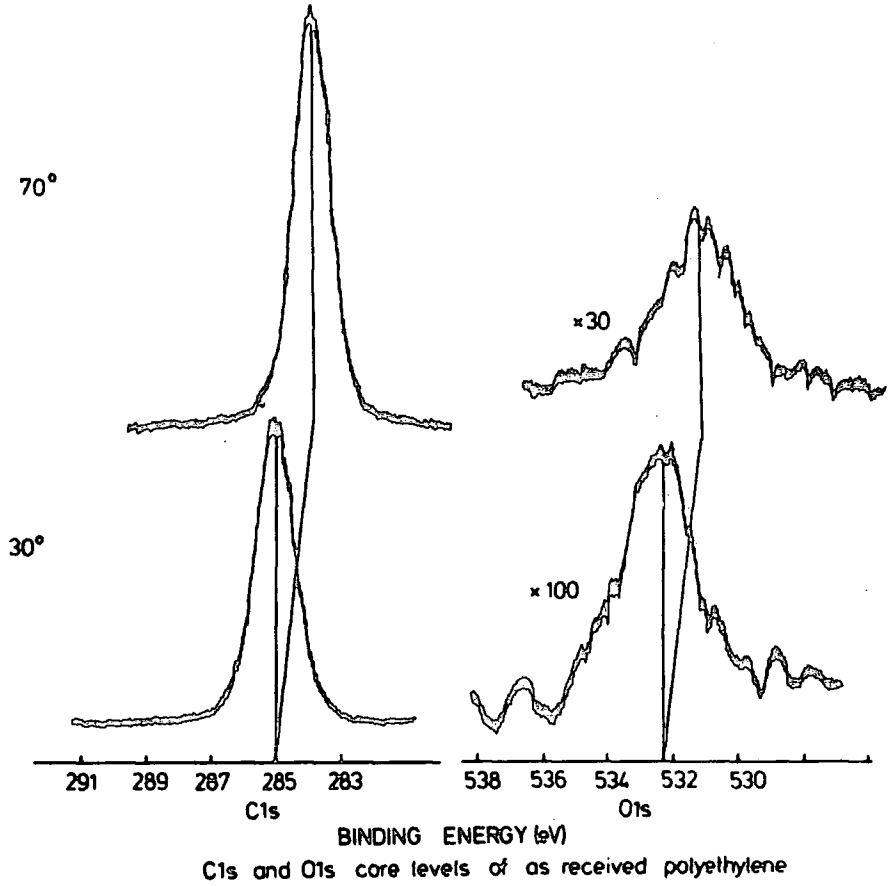

Figure 3.16. High resolution spectra of pigmented polyethylene.

Table 3.22

As received pigmented polyethylene

Intensity ratios	
Take-off angles	C_{1s}/O_{1s}
30^{o}	65
70^{o}	34

(b) Peeled-off pigmented polyethylene from an optimum cured type 1, Natsyn 2200, elastomer

A comparison of the wide scan spectra at 30° and 70° take-off angles for the peeled off polyethylene with those in (a) revealed little evidence for the peeled-off materials other than the C_{1s} photoionization peak. The high resolution scans of C_{1s} levels in Figure 3.17 also reveal a symmetrical peak, arising from the carbon framework.

It was of interest to compare the peeled surface of the polyethylene with that of the as received sample, and also with the exposed surface of the Natsyn 2200 sample (optimum cured type 1).

The relevant area ratios collected in Table 3.23 reveal that there was little mechanical transfer of materials between the surface, since, apart from the C_{1s}/N_{1s} ratios which are essentially the same for both components of the peeled surfaces, the C_{1s}/O_{1s} and C_{1s}/S_{2p} ratios are very substantially different on the Natsyn 2200 and the polyethylene surfaces. This, therefore, provides evidence that the peeling involved essentially adhesive failure at the interface.[357-359]

Table 3.23

(a) Peeled-off pigmented polyethylene

Intensity ratios

Take-off angle	C_{1s}/O_{1s}	C_{1s}/N_{1s}	C_{1s}/S_{2p}	C_{1s}/Si_{2p}
30°	29	85	157	330
70°	30	105	-	-

(b) Optimum cured type 1, Natsyn 2200, elastomer

Intensity ratios

Take-off angle	C_{1s}/O_{1s}	C_{1s}/N_{1s}	C_{1s}/S_{2p}
30°	16	69	27
70°	14	89	27

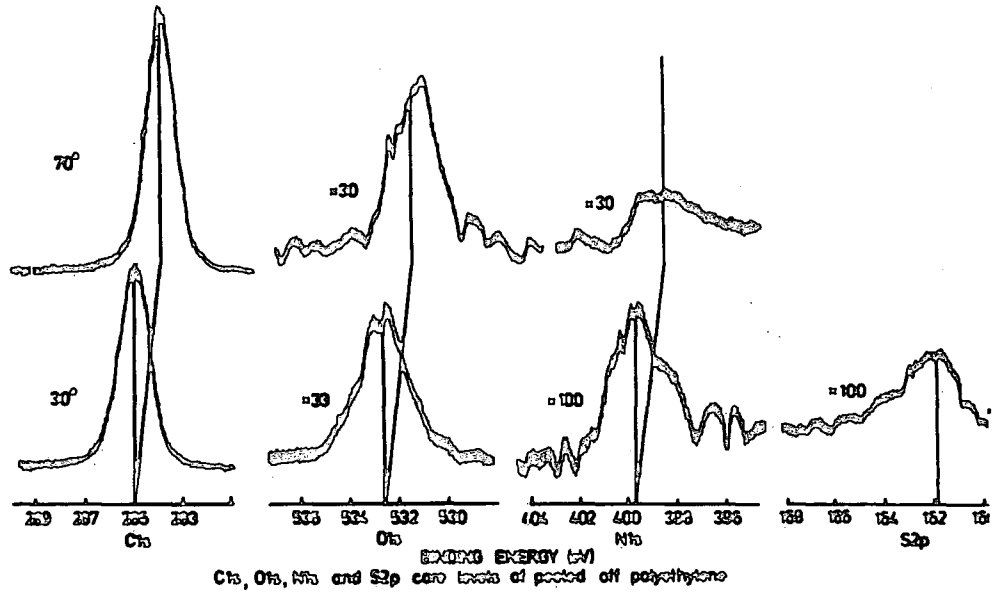

Figure 3.17. High resolution spectra of peeled-off polyethylene.

(c) As received poly(ethylene terephthalate)

The wide scan ESCA spectra at take-off angles of 30° and 70° for the as received PET revealed little evidence for anything other than C_{1s} and O_{1s} photoionization levels. The resolution scans of the C_{1s} levels in Figure 3.18 indicate components, due to C-H, C-O and $\overset{O}{\overset{\|}{C}}$=O, and also show evidence for a low level of $\pi \rightarrow \pi^*$ transitions at approximately 8.0 eV from the main C_{1s} peak. The derived intensity ratios are set out in Table 3.24. The high resolution spectra also reveal a very low level of silicon and a high level of oxygen, the

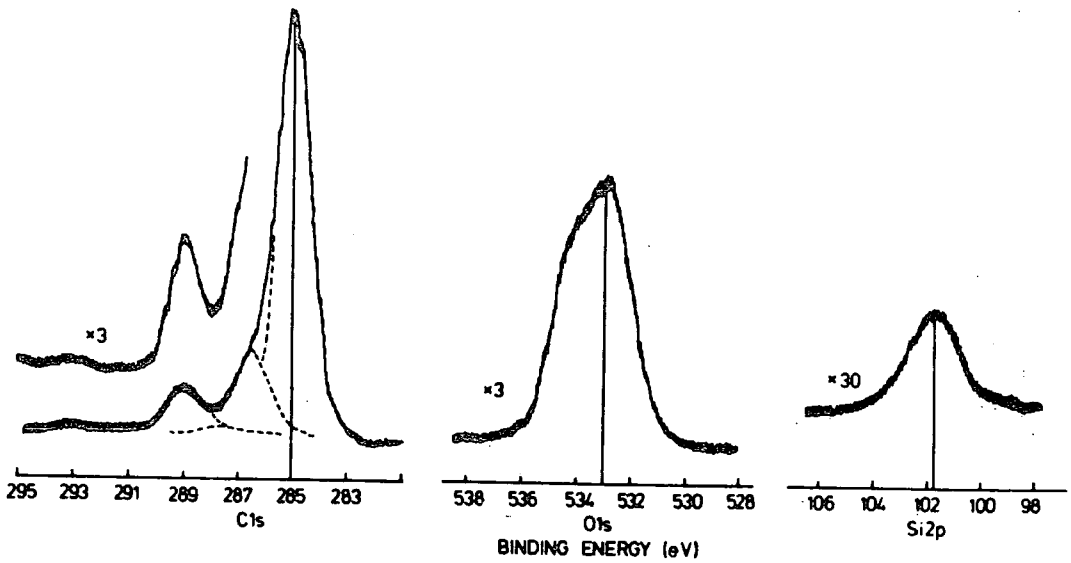

C1s and O1s core levels of as received polyethylene terephthalate, and Si2p core level as contaminant

Figure 3.18. High resolution spectra of the as received PET.

Table 3.24

As received poly(ethylene terephthalate)

Intensity ratios	O ‖ C=O	C-X	C-O	C-H	C-O	C=O	C_{1s}/O_{1s}	C_{1s}/Si_{2p}
Take-off angles								
30°	8	1	15	76	45	55	3	136
70°	5	2	14	79	43	57	4	9

latter being essentially two components, corresponding to $\underline{C}(=O)-\underline{O}$ and $\underline{C}(=\underline{O})-O$ environments, separated by ∿ 1.6 eV. The very different intensity ratios of $\underline{C}=O$, $\underline{C}-O$ and $\underline{C}-H$ components at ∿ 289 eV, ∿ 286.6 eV and 285 eV respectively for 30^{o} and 70^{o} take-off angles, compared to the corresponding theoretical values 1:1:3, may suggest a partial orientation of functional groups; the carboxylic ester groups present at the surface of PET produce a higher energy state, as a result of their greater polar character than hydrocarbon groups, the latter being directed outward, and the build up of an overlayer of hydrocarbon contamination is also indicated.

(d) Peeled-off poly(ethylene terephthalate) from type 1, Natsyn 2200 elastomer at liquid nitrogen temperature

The high resolution scans of peeled-off PET at 77K revealed no evidence for the mechanical transfer of materials from the surface of an elastomer other than C_{1s} and O_{1s} photoionisation levels, suggesting a clean surface of PET after peeling-off at such a low temperature. The data corresponding to Figure 3.19 in Table 3.25 again clearly indicate the difference in intensity ratios of different

Table 3.25

Peeled-off poly(ethylene terephthalate)

Intensity ratios							
Take-off angle	$\underline{C}(=O)$	$\underline{C}-X$	$\underline{C}-O$	$\underline{C}-H$	$C-\underline{O}$	$C=\underline{O}$	C_{1s}/O_{1s}
30^{o}	8	2	19	70	47	53	3.2
70^{o}	5	1	16	78	46	54	4.0

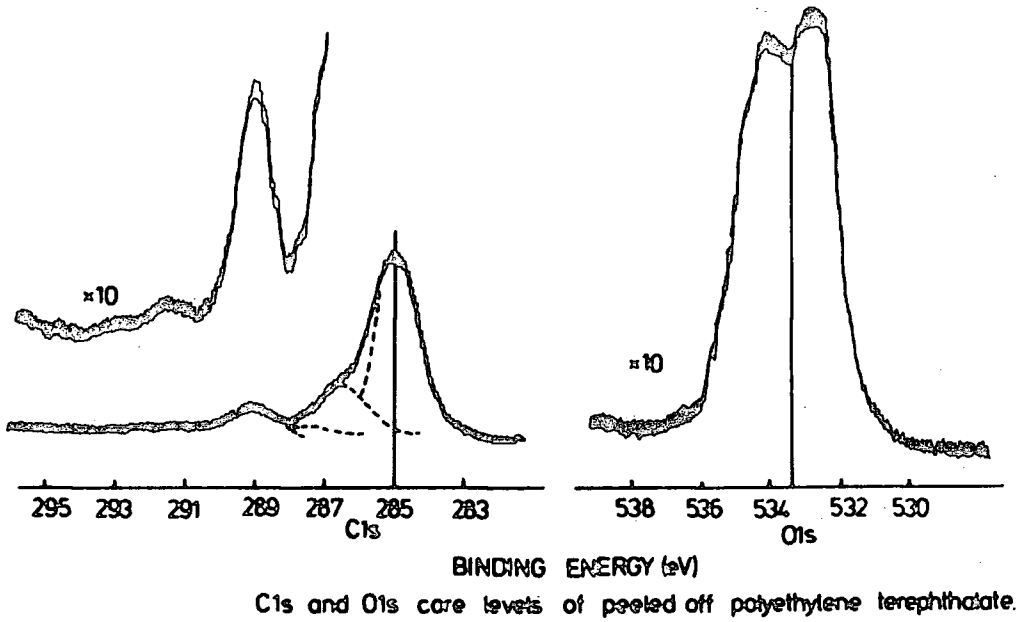

Figure 3.19. High resolution spectra of peeled-off PET.

chemical environments under the C_{1s} envelope at 30^{o} and 70^{o} take-off angles from the theoretical values that the carboxylic ester groups directed 'inward' may be partially responsible for these differences. The cleanness of PET of PET surface is also evident from the distinct separation of O_{1s} components at a high resolution.

3.3.6 Auger parameter

(a) Introduction

It has been already stated in chapter two that irradiation of most atoms[177] with soft x-rays results in emission of at least two energetic electrons:[171-176] the photoelectron from

the core level (ion) and an Auger electron from the decay of original formed ion. As a consequence of the unstable initial ionic state, the inner vacancy (core level) is filled by an electron dropping down from an outer shell and, the energy difference between the initial ion and the final doubly charged ion appears as the kinetic energy of the emitted Auger electron. The probability for such Auger excitation is being higher than for the alternative fluorescent decay for the elements of interest in this work.

The combined use of both photoelectron and x-ray excited Auger lines, therefore, enhances the utility of ESCA for identifying chemical states. The difference in kinetic energies between the photoelectron line and Auger line, called the Auger parameter,[186] provides a unique value for each chemical state; this special property is more accurately determinable than either the photoelectron or Auger electron energy alone because the dynamic charge corrections cancel out. The intensity of the $L_3M_{45}M_{45}$ Auger lines of zinc are the result of decays of ions that are formed with highest probability. The decay scheme for zinc is shown in Figure 3.20. The difference in binding energies between the most intense and sharp $Zn_{2p_{3/2}}$ line and the $L_3M_{45}M_{45}$ Auger line of zinc in Figure 3.21 provides the Auger parameter.

The LMM lines of sulphur observed using the FAT mode in ESCA were broad and diffuse and, therefore, difficult to detect; no attempt was, therefore, made to measure the Auger parameter of sulphur.

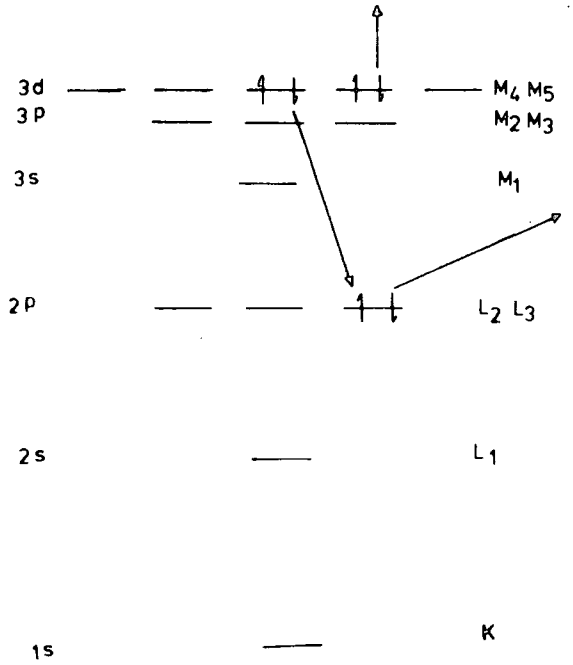

Figure 3.20. The $L_3M_{45}M_{45}$ Auger process for zinc.

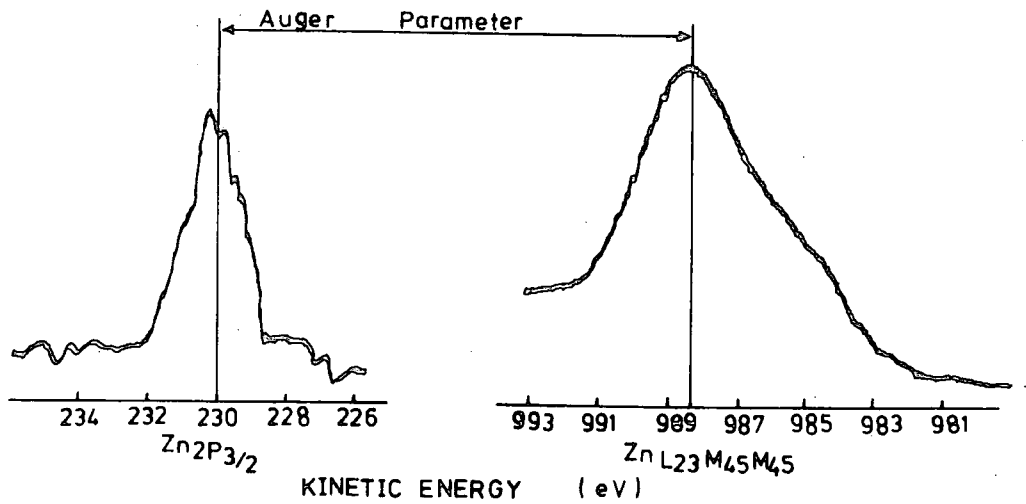

Figure 3.21. $2p_{3/2}$ and $L_3M_{45}M_{45}$ levels of zinc oxide.

The Auger parameter has found particular use for ionic solids, where the convolution of factors contributing to the overall shift in binding energy often imply a negligible small shift for a given core level. For such systems, the shift in Auger energy is often substantial and two-dimensional 'chemical state' plots are, therefore, of particular value. The change in Auger parameter, chemical shift, between two chemical states is related to the difference in extra-atomic relaxation or polarisation energy between the two chemical states.[183]

(b) Data on 'sulphur-vulcanised', Natsyn 2200, elastomers

The Auger parameters for different states of zinc in Table 3.26 reflect the polarisability of the anion.[179]

Table 3.26

Auger energies and the Auger parameters (kinetic energies in eV)

Take-off angle (30^{o})	Auger energy $L_{23}M_{45}M_{45}$	Auger parameter
Optimum cured type 1, Natsyn 2200, elastomer	988.6	494.8
50% cured type 1, Natsyn 2200, elastomer	988.5	494.7
Optimum cured type 2, Natsyn 2200, elastomer	987.7	495.9
50% cured type 2, Natsyn 2200, elastomer	988.1	494.9
Optimum cured type 3, Natsyn 2200 elastomer	987.8	496.1
50% cured type 3, Natsyn 2200, elastomer	988.1	495.9
Zinc oxide	988.4	495.3
Zinc sulphide	989.5	494.2

The tendency for the Auger parameter for zinc in the surface region of type 1 sample is more toward zinc oxide than zinc sulphide. The optimum cured type 2 elastomer tends to have a slightly smaller Auger parameter than type 1, thus indicating more zinc oxide than zinc sulphide, whereas the Auger parameter for 50% cured type 2 is higher than optimum cured type 2 system, revealing a greater tendency towards zinc sulphide environment. The type 3 sample indicates more zinc oxide than zinc sulphide, having essentially the same Auger parameter for both optimum and partially cured samples. The combined use of both photoelectron and x-ray excited Auger lines have, therefore, clearly indicated the presence of more zinc sulphide at the surface of partially cured type 1 and type 2 elastomers than those of optimum cured; and, this is likely to be associated with the amount of zinc complex containing sulphur in the partially cured samples which the prolonged exposure to heat at 150^{o}C for optimum cured samples results in the formation of more zinc oxide than zinc sulphide (chapter three) or least in the surface regions.

In the light of Auger data, the Zn_{3p}/S_{2p} intensity ratios, particularly of low binding energy components of S_{2p}, of a variety of elastomers are set out in Table 3.27 for a comparison with the theoretical value (1.5). It is clear that more sulphur is required in the surface region than is added into the bulk. Conversely, it equally implies that excess zinc is present in the surface regions than is needed for the Natsyn 2200 formulation.

Table 3.27

Ratios of Zn_{3p}/S_{2p} LBE (low binding energy components of S_{2p} levels for a variety of Natsyn 2200 elastomers

	1	2	3	4
Optimum cure	2.0	1.5	1.7	-
50% cure	2.0	2.9	1.7	-

3.3.7 Summary of an ESCA investigation of a series of Natsyn 2200 elastomers

Figure 3.22 summarises the ESCA investigation of a variety of Natsyn 2200 elastomers, cured on a calendering system at 150°C in air with a 2 mm rip setting to draw into sheets. The bulk formulation of Natsyn 2200 elastomers is indicated in Table 3.1, and the details of the composition are given in Table 3.12 in terms of weight and normalised mole % terms.

The ESCA analyses have clearly revealed the surface composition of thickness in the range < 50Å that higher levels of antioxidant and accelerators are present at the surface than in the bulk, whilst the level of zinc increases with increasing ESCA depth profile into the bulk. The optimum cured type 2 and type 3 samples indicate greater sulphur functionality, involved in crosslinking two polymer chains, than the corresponding partially cured systems, whilst the sulphur functionality of four for an optimum cured type 1 sample is much smaller than the functionality (10) for the partially cured elastomer. This suggests that the higher level of sulphur present at the surface of a partially

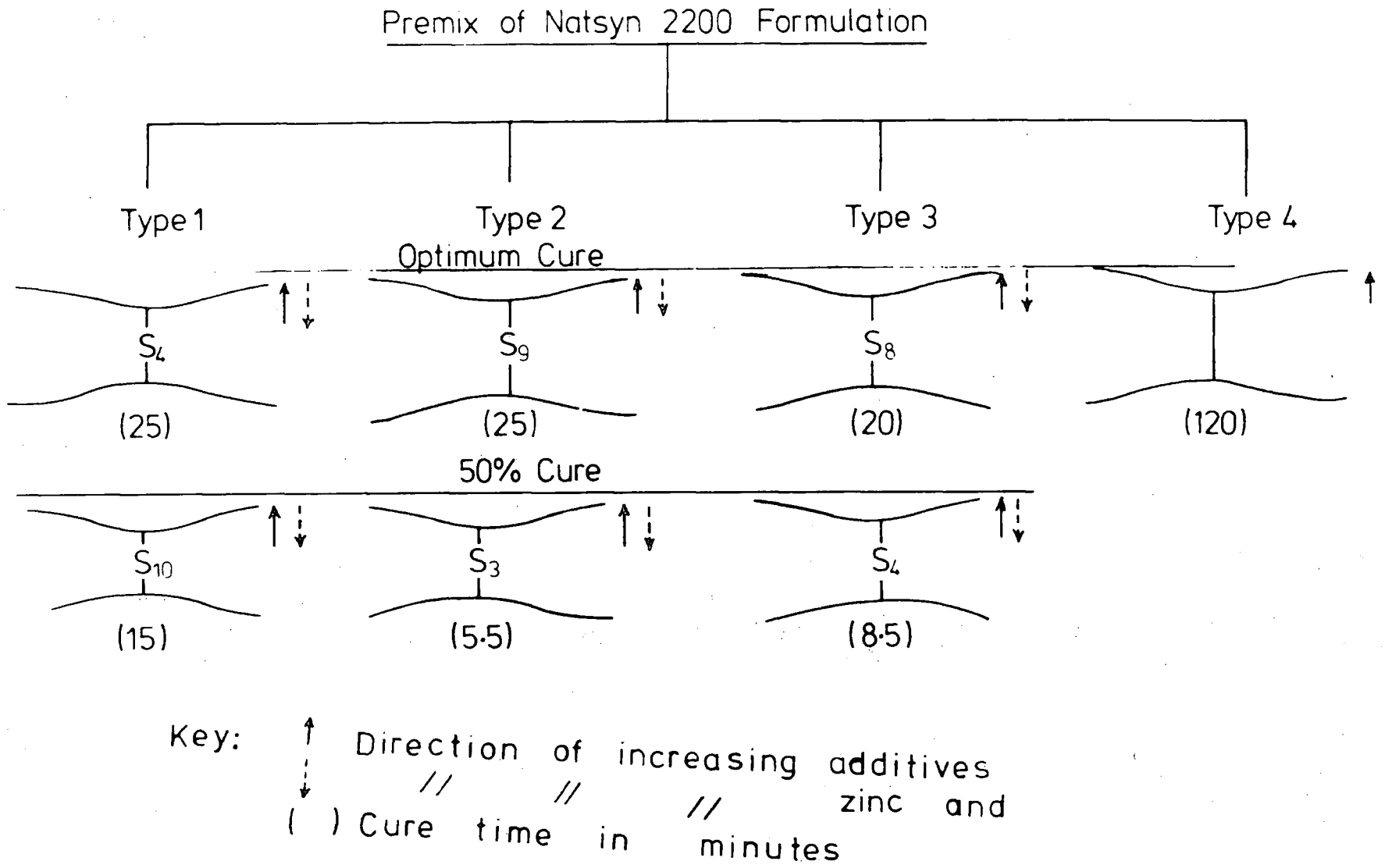

Figure 3.22. Schematic representation of changes in the surface region as in the rubber vulcanisation.

(50%) cured type 1 elastomer is lost either by evaporation or by blooming on a prolonged exposure to heat at 150°C (cure time of a partially cured type 1 sample is fifteen minutes compared to twenty five minutes for the optimum cured elastomer), whereas the increase in sulphur functionality for the optimum cured type 2 and type 3 elastomers, in contrast to the situation for the type 1 sample, is most likely to be associated with the diffusion of sulphur from the bulk to the surface. The loss rate of sulphur is, therefore, determined by the extent of volatilisation, which will cause a concentration gradient near the surface.

The 'swelling' data in section 3.3.1 indicated that the sulphur crosslink occurs on average after 100 repeat (isoprene) units in Natsyn 2200 systems.

3.3.8 Infra-red spectra

(a) Introduction

Organic and inorganic substances exhibit absorption spectra in the electromagnetic infra-red region, extending in the range 50 - 0.025 microns. The section currently of most useful value lies between 10 and 0.625 microns. The infra-red spectra are particularly useful in qualitative analysis of polymer and compositions containing polymers,[106,107] since the characterisation of these materials are often tedious by the more usual chemical analysis[91,95-97] and physical methods.[69-72,76-80]

The infra-red spectroscopy is relatively easier to operate than ESCA, but the sensitivity of this conventional technique becomes almost negligible, when a very thin surface layer of the

material is examined in the usual transmission manner; and, therefore, a technique, multiple attenuated reflection spectroscopy, is preferred, based on internal reflection (Figure 3.23).[139] The incident radiation directed first into a material of high refractive index (n_1) at an angle (θ) greater than the critical angle (θ_c) is reflected from the surface of the sample of refractive index (n_2) lower than n_1. The depth of penetration is given by an equation:

$$dp = \frac{\lambda}{n_1 2\pi(\sin^2\theta - n_{21}^2)^{\frac{1}{2}}} \qquad (3.7)$$

where dp is the penetration depth in medium 2 for the electric field to fall to e^{-1} of its value at the boundary surface medium,

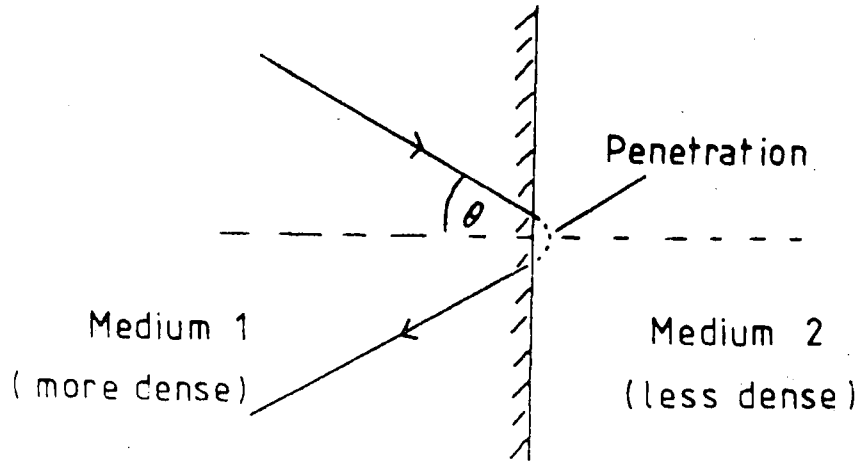

Figure 3.23. Total internal reflection.

λ is the wavelength of the radiation,

n_1 is the refractive index of medium 1,

θ is the angle of reflection, and

$n_{21} = \frac{n_2}{n_1}$, n_2 is the refractive index of the sample.

Equation (3.7) states that the penetration depth depends on the wavelength of radiation and, the refractive indices of medium one and two. It is possible to enhance the amount of absorption by multiplying the number of reflections, as shown in Figure 3.24. An internal reflector plate of thalium bromo-

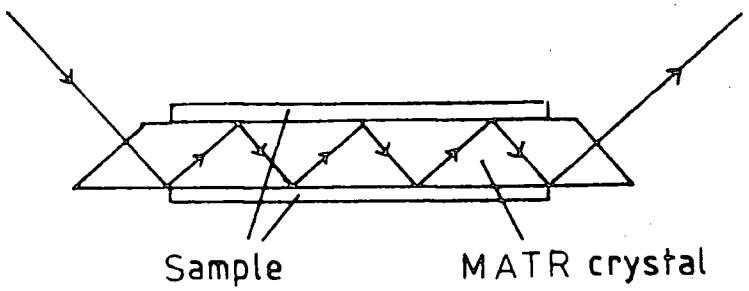

Figure 3.24. MATR crystal and sample.

iodide (KRS5) with refractive index of 2.4, or germanium with refractive index of 4.0, of appropriate size (50 mm x 20 mm x 2 mm) may be used with a 45^{o} angle of incidence (θ), giving approximately 25 reflections; but both crystals were employed in this chapter. The actual MATR unit, made by Specac, was placed in the sampling compartment of an infrared spectrometer (Perkin-Elmer 577). However, there are many

different optical systems available, which may be used in MATR attachments. The use of KRS5 crystal is likely to result in twice the sampling depth compared to that of a germanium crystal. The characteristics of crystals used for internal reflection are given in Table 3.28.

Additives, in the form of a powder, were also studied by dispersing the ground powder in a tablet of potassium bromide. The KBr discs were prepared by grinding the sample (2 mg) with KBr (100 - 200 mg), and then compressing the whole content into a transparent tablet. The spectra were obtained before, and after the oxygen plasma treatment.

(b) Additives

Figure 3.25 represents the spectrum of cyclohexylbenzthiazyl sulphenamide

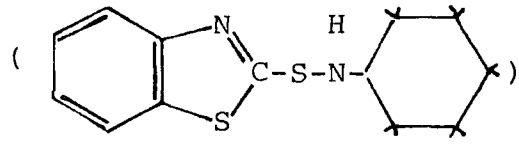

accelerator with prominent features at:

Vibrations	Wavelength (microns)	Remarks
C-H stretching	3.42 asymmetric 3.51 symmetric	Strong, sharp
N-H stretching	3.10	Strong, sharp
C-N	8.08	Strong, sharp
C-S	14.81	Weak, sharp

The O-H stretching approximately at 2.9 microns is likely from the contamination of H_2O in the KBr tablet.

Figure 3.26 is a spectrum of tetramethylthiuram disulphide

Table 3.28

Characteristics of crystals for MATR infrared spectroscopy

Material	Transmission range (microns)	Refractive index at (10 microns)	Critical angle (θ^{o})	Characteristics	
				Desirable	Undesirable
Germanium	2-11.5	4.0	22	High refractive, completely insoluble and does not fracture under high pressure	High toxicity, brittle and fractures easily under high pressure
Thalium-bromide-iodide (KRS-5)	0.5-35	2.37	39		

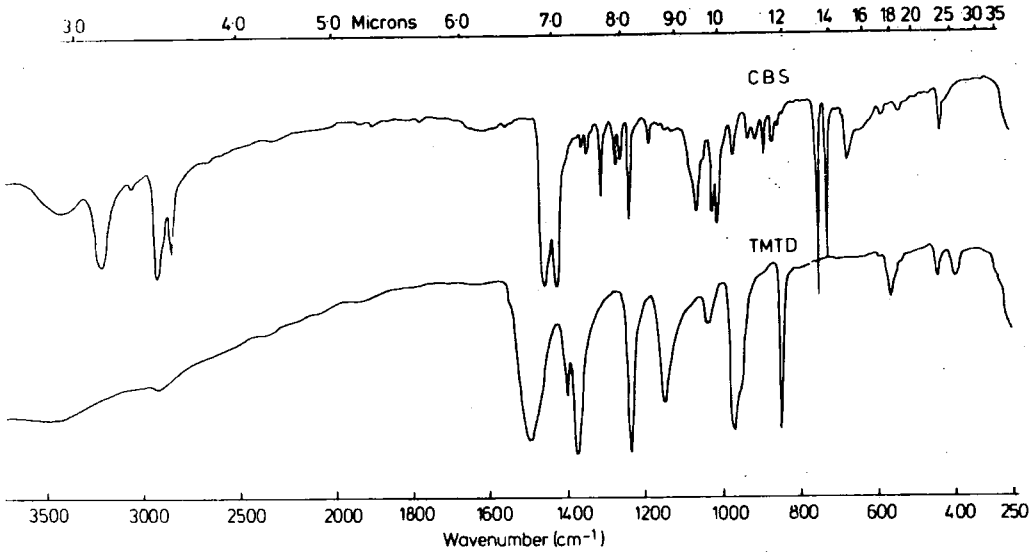

Figure 3.25. Infrared spectrum of cyclohexylbenzthiazyl sulphenamide (CBS).

Figure 3.26. Infrared spectrum of tetramethylthiuram disulphide (TMTD).

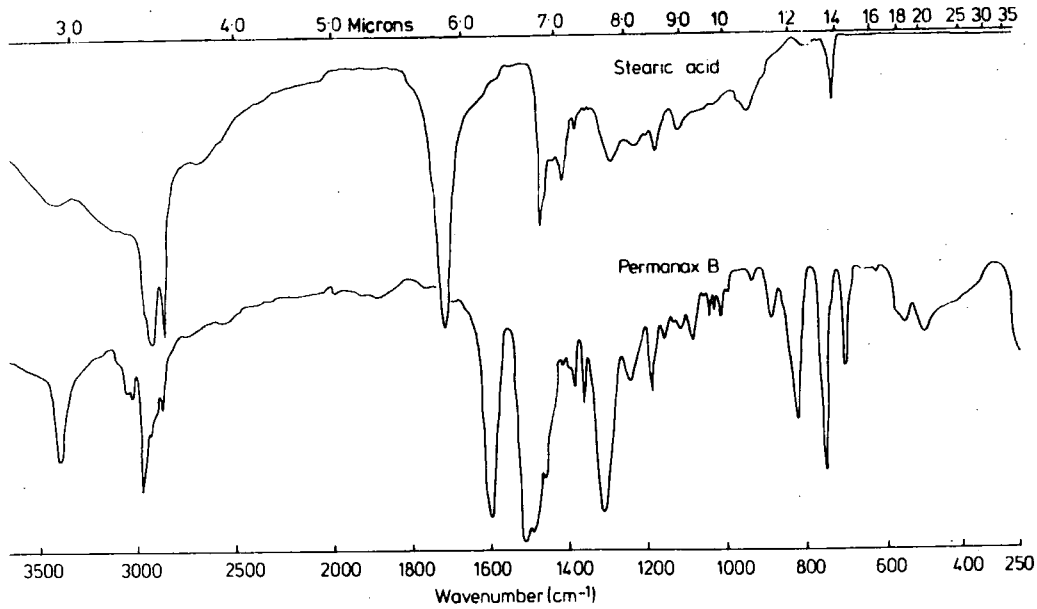

Figure 3.27. Infrared spectrum of stearic acid.

Figure 3.28. Infrared spectrum of permanax B.

accelerator with distinguishable absorptions at:

	Wavelength (microns)	
C-H asymmetrical deformation	6.69	Strong, sharp
C-H symmetrical deformation	7.27	Strong, sharp
C-N	8.10	Strong, sharp
C=S	8.7	Medium, sharp
S-S	22.47	Weak, sharp

The structure is

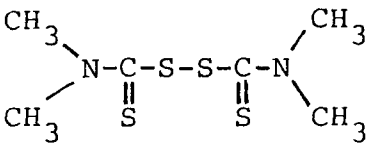

In Figure 3.27, the absorption in the region near 3.45 microns is very strong but the evidence relating to the carbon skeleton of stearic acid can be found elsewhere in the spectrum. Carbonyl absorption is evident as a strong singlet at 5.85 microns and the convincing characteristic absorption of $-\overset{O}{\overset{\|}{C}}O-H$ bonds occurs as a broad peak approximately at 2.94 microns. The substance is stearic acid, employed in elastomers to enhance the rate of cure.

Figure 3.28 shows the spectrum of permanax B, a condensate of acetone and diphenyl amine, with characteristic absorptions at:

Vibrations	Wavelength (microns)	Remarks
N-H stretching		Strong, sharp
C-H stretching		Strong, sharp
C=C		Strong, sharp

The prominent feature in the 'finger-print' region is a characteristic of aromatic absorptions. The structure of permanax B, as it has been supported by ESCA analysis, is

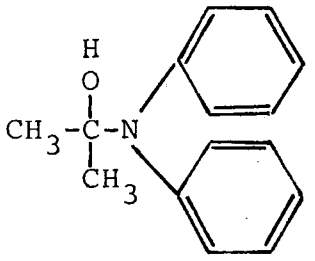

Figure 3.29 is a spectrum of zinc oxide with a strong/ broad absorption band occurring in the region 18.2 - 25 microns, being characteristic of Zn-O bond vibrations. A relatively broad/weak peak approximately at 2.86 microns is from the contamination of H_2O.

Figure 3.30 indicates a spectrum of dicumyl peroxide with characteristic absorptions at:

Vibrations	Wavelength (microns)	Remarks
C-H stretching	3.23-3.45	5 bands, weak, strong and medium
C C stretching (skeletal)	6.25	Weak, sharp
	6.69	Weak, sharp
	6.92	
C-H deformation (in plane)	8.0-10.52	Strong and medium but sharp
C-H deformation (out of plane)		
monosubstitution	13.16	
	14.29	5 adjacent H atoms

Detection of a phenyl ring by infrared spectroscopy usually presents no difficulty, as the C=C stretching vibrations of this structure in Figure 3.30 distinguishes it

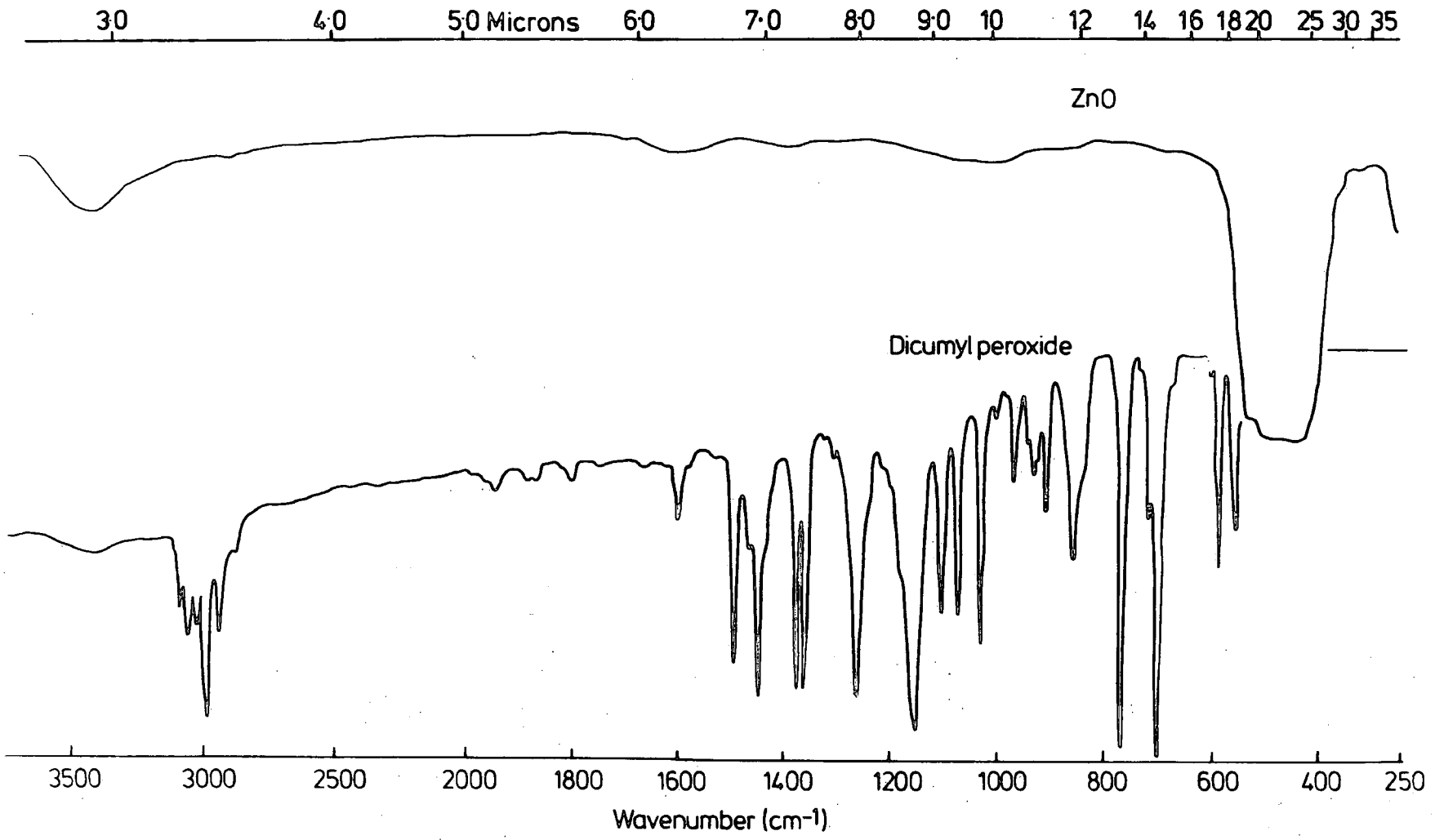

Figure 3.29. Infrared spectrum of zinc oxide.
Figure 3.30. Infrared spectrum of dicumyl peroxide.

from other types of unsaturation. Only two of the four theoretically possible bands in the 6.25 - 6.9 microns region are generally useful, those approximately at 6.25 and 6.67 microns. A third (6.33 microns) is very weak, as is evident from the spectrum, while the fourth at ∿ 6.9 microns may be obscured by alkyl bands. The relative intensities of those bands are variable, but their sharpness is characteristic, and the presence of a needle-like peak approximately at 6.67 microns is particularly indicative of a phenyl ring. Orientation of substituents in a benzene ring

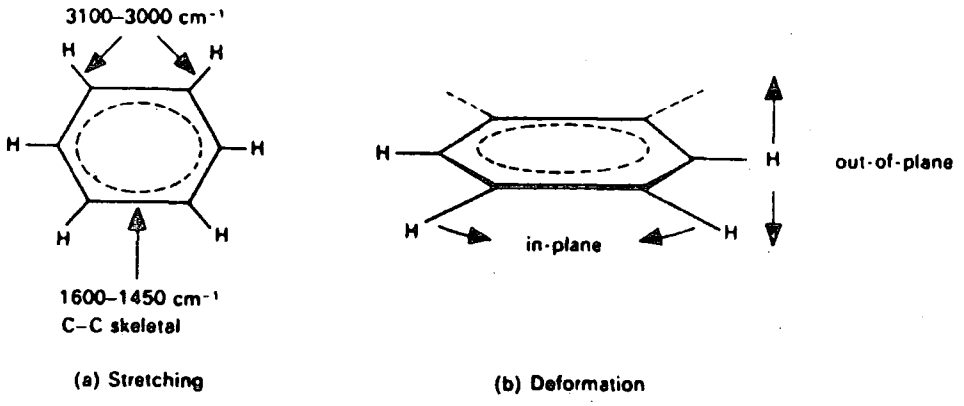

Figure 3.31. Vibrations of benzene ring.

is often clearly indicated by the C-H out-of-plane deformation modes of the remaining hydrogen atoms, which appear in the 'finger-print' region. The structure is:

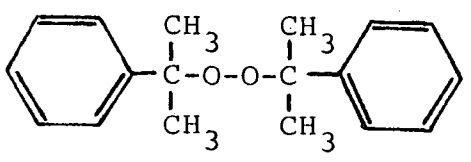

(c) Elastomers

The main objective in this part of the study has been to obtain a qualitative and quantitative analysis for the various types of sulphur-vulcanised systems and also of elastomers vulcanised by dicumyl peroxide, which may lead to a better understanding of the nature of these materials and also may be of help in elucidating the effect of microstructure on rheological properties.

The features arising from various types of Natsyn 2200 elastomers are shown in Figures 3.32 and 3.33. Since the investigation revealed similar spectra forthe various types of elastomers, it is, therefore, convenient to present representative examples. Absorptions occurring below 11.8 microns are omitted, since the germanium crystal absorbs the radiation strongly below this region.

A comparison of spectra of optimum cured with those of partially cured and uncured elastomers in Figures 3.32 and 3.33 revealed the following: (a) the ratio of peak intensities at wavelength (microns) $^{3.38}$/(3.42 and 3.51) corresponding to the total stretching vibrations of $-CH_3$ and $-CH_2-$ groups, remains very nearly constant (1.0), even before and after vulcanisation at 150^{o}C, (b) the ratio of peak intensities at wavelength (microns) $^{6.02}$/(3.42 and 3.51) corresponding to carbon-carbon double bond (C=C) absorbance was almost negligible to account for the rearrangement of cis-1,4 polyisoprene structure, (c) the ratio of peak intensities at wavelength (microns) $^{7.63}$/(3.42 and 3.51) for the uncured, 50% cured and optimum cured samples suggest very

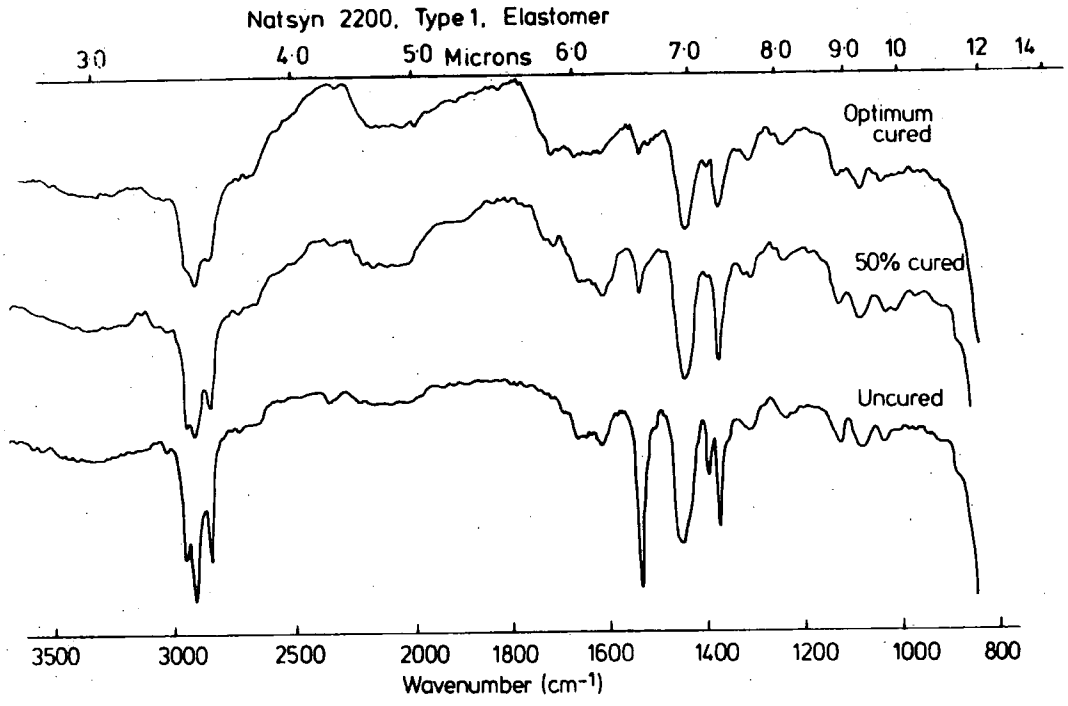

Figure 3.32. Infrared spectra of a type 1, Natsyn 2200, elastomer.

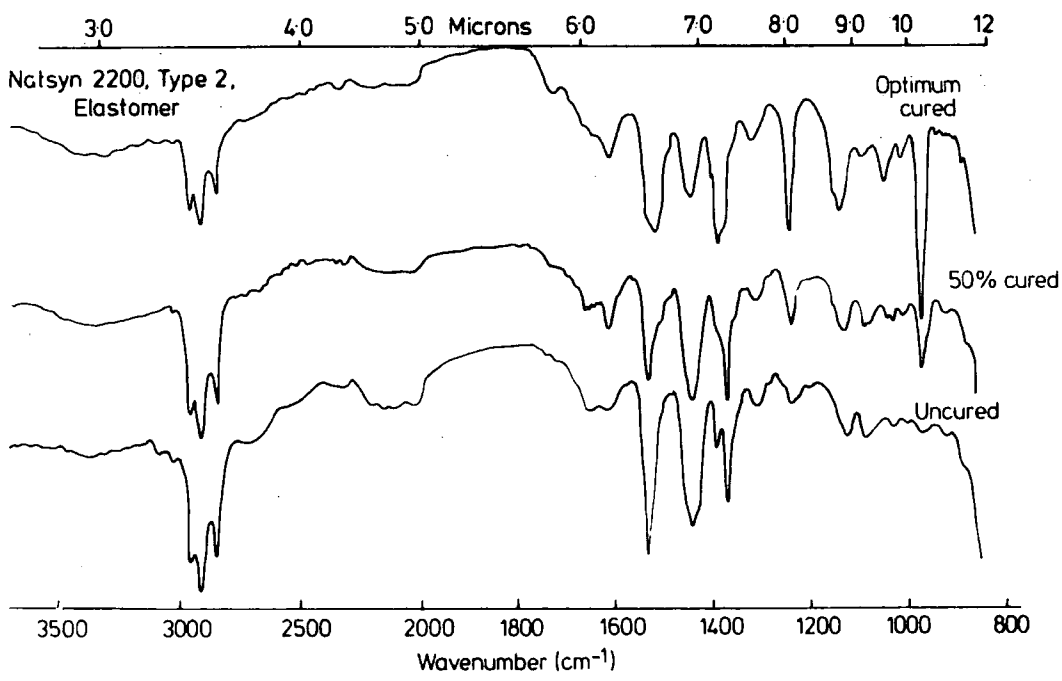

Figure 3.33. Infrared spectra of a type 2, Natsyn 2200, elastomer.

little change in the cis-1,4 polyisoprene structure, and this is also true for the ratio of intensities observed at wavelength (microns) $^{8.85}$/(3.42 and 3.51); and, (d), the occurrence of peaks approximately at wavelengths 8.13, 9.26 and 9.62 microns are, without certainty, attributed to cyclised structures, which further suggests that the cyclised structure would decompose on thermal treatment. The ratio of peak intensity at wavelengths (microns) $^{11.23}$/11.90 was not observed, as a result of strong absorbance below 11.90 microns by the germanium crystal, which probably would have accounted for the transformation of cis-1,4-polyisoprene into structures resembling 3,4-polyisoprene

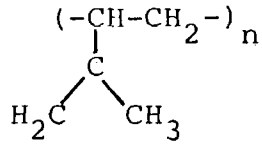

(d) Spectra for the oxygen plasma treated samples

It was of interest to investigate the effect of oxygen plasma on additives and elastomers, using infrared spectroscopy. However, it was observed that the spectra were identical before, and after plasma treatments at different power loadings; and, therefore, it is convenient to present one example of an oxygen plasma treated sample to avoid repetition.

Figure 3.34 shows the spectrum of oxygen plasma treated tetramethylthiram disulphide, dispersed in a KBr tablet, at a power loading of 10 watts for 20 seconds and a total pressure of 0.2 torr. A comparison with the untreated sample in Figure 3.26 reveals spectra, which are indistinguishable. This

emphasises the advantage of the ESCA technique over conventional IR spectroscopy in investigating the very thin modified surface layer arising during plasming processing (chapters six and seven).

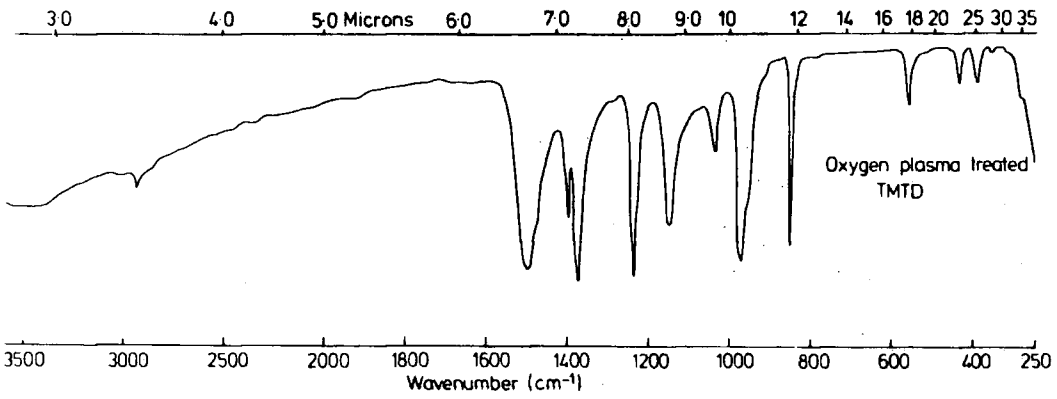

Figure 3.34. Infrared spectrum of tetramethylthiuram disulphide after exposure to an oxygen plasma (10 watts, 20 seconds, 0.2 torr).

The fact that IR spectroscopy fails to reveal the changes in the modified surface layer of a sample, is due to the extent penetration depth of IR radiation in that it samples the surface layer to a depth of the order 10^{4}Å, compared to the modified surface of thickness < 10^{2}Å; and, therefore, the IR spectrum has a very strong absorption from the unmodified substrate. As a result of this penetration depth, the spectrum is essentially the same before, and after plasma treatments.

3.3.9 Solid state magic angle spinning nuclear magnetic resonance

(a) Introduction

The advances in the knowledge of nuclear magnetic resonance (NMR), and its applications to chemical problems,

have been amazingly rapid in the last decade.[115-127] This spectroscopic method operating at the low end of the electromagnetic spectrum allows the measurement of extremely small energy differences (chemical shifts and coupling constants), which, in turn, reflects the small differences in molecular structure and conformation.[116-119,123-125] In high resolution NMR spectra, line separations of less than 0.1 Hz are measured, corresponding to an energy difference of approximately 10^{-12} Joule/mole.[128] In addition to these detailed investigations of molecular structure and conformation, selective measurements of spin lattice relaxation times can provide information on molecular motion and kinetics. Until recently, liquid samples were used in NMR spectroscopy for characterisation of polyisoprene, and, therefore, all solids had to be investigated in suitable solvents (so called high resolution NMR). The requirement of samples being in solution has been a limitation to the application of the NMR technique to polymers, and, this has been due to three main practical reasons in the direct study of solids: (a) the resonance lines are highly broadened by anistropic dipole-dipole (DD) and quadrupole-field gradient (QF) interactions, leading to linewidths in the KHz range, (b) the phenomenon of chemical shift anisotropy leads to broad complex line-shapes for powders, even when the dipolar broadening is absent. These anisotropic interactions are in principle also present in liquids, but fortunately are averaged to zero by the rapid Brownian motion of the molecules, and, (c) ^{13}C nuclei in solids show extremely long spin lattice relaxation times and, therefore,

Fourier transform (FT) experiments demanded long pulse repetition times, resulting in reduced signal accumulation and hence low sensitivity. However, the recent development of sophisticated techniques, called High Power Decoupling, Magic Angle Spin (MAS)[128] and Cross Polarisation (CP), has opened the way to high resolution NMR in solids. In a combination of techniques, homonuclear dipolar interactions, quadrupole field gradient interactions and chemical shift anisotropy effects are, in principle, eliminated by the so-called 'magic angle spinning' (MAS). The principle of MAS operation can be best understood by recalling the three obstacles mentioned earlier.

It is well known that all nuclear with nuclear spin quantum number I≠0 possess a nuclear dipole moment (μ) and the magnetic fields of moments of nuclei in the neighbourhood produce local fields ($h_{loc.}$) at the site of the nucleus, given by:

$$h_{loc.} = \pm \frac{\mu}{\nu_{1,2}^3} (3\cos^2\theta - 1) \qquad (3.8)$$

where $\nu_{1,2}$ is the distance between two nuclei, θ is the angle of rotation about Z-component (see Figure 3.35) and, the sign + and - describe the orientations of neighbour spin to be parallel or antiparallel. The Z-component of the magnetic field of a dipole may be positive or negative depending on the angle θ. The change of spin orientations occur, when the value of θ is $54^{o}44'$ and, at this instance, there is no contribution to the field in Z-direction. Figure 3.36 shows

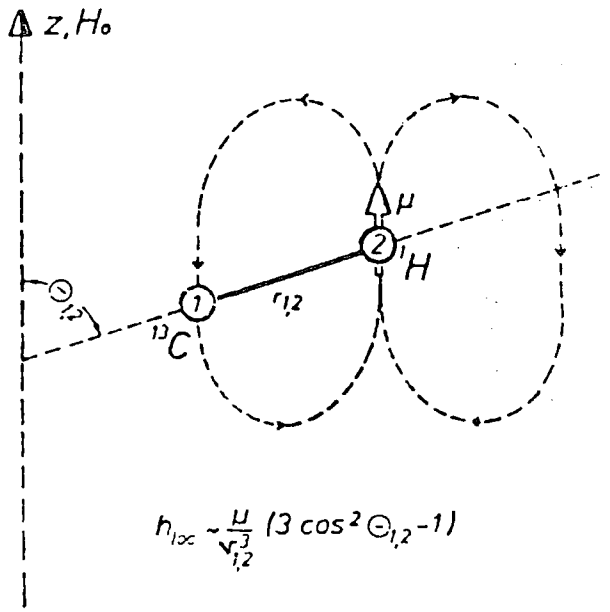

Figure 3.35. Local magnetic field ($h_{loc.}$) at a nucleus 1, produced by a nuclear magnetic dipole moment of a nucleus 2 at a distance $r_{1,2}$.

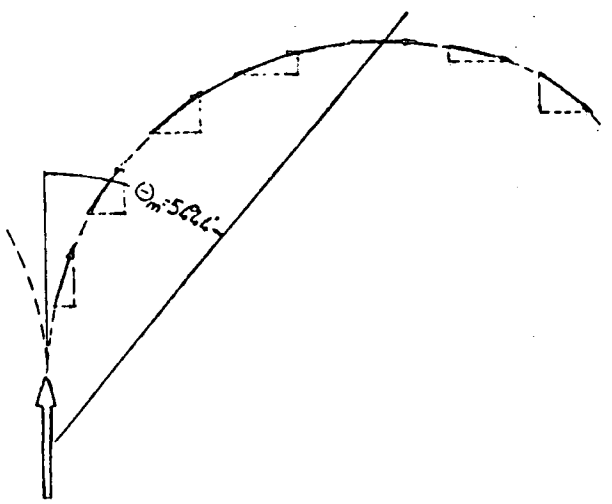

Figure 3.36. Magnetic field line of a magnetic dipole indicating positive and negative Z-components. The Z-component is zero at an angle of 54°44'.

the magnetic field of magnetic dipole at angle of $54^{o}44'$.

In a solid sample, many pairs of spins with difficult ν and θ may be present and, hence, $h_{loc.}$ and the resonance frequency are different for different spins, resulting in a broad resonance line. Similarly, different internal electrical gradients may also broaden the resonance line of the nuclei with a nuclear spin quantum number greater than half, for which a term $(3\cos^2\theta-1)$ again applies. In a powdered or amorphous sample, each molecule or molecular group may be oriented in all possible directions and the spread of chemical shift results in broadening of a resonance line. The external magnetic field induces electronic circulations about a nucleus in a plane perpendicular to the applied field and in a direction such that the associated secondary magnetic field opposes the main field and give rise to chemical shift contributions for nuclei in the molecule. The hindrance of circulations is also dependent upon the orientation of a given bond axis (for example C-C bond) relative to the external field. The chemical shift contribution is again proportional to the term $(3\cos^2\theta-1)$.

It is clearly evident from an equation (3.8) that all the above factors disappear, when the term $(3\cos^2\theta-1)$ becomes zero, and this situation obtains when the value of θ is $54^{o}44'$. The effect of this magic angle spinning can be seen in Figure 3.37. The different connecting vectors with different θ_{ij} are rotated on different cones illustrating that the time averaged direction of all vectors be on the same spinning axis, when the rotation is fast at an angle of $54^{o}44'$. The

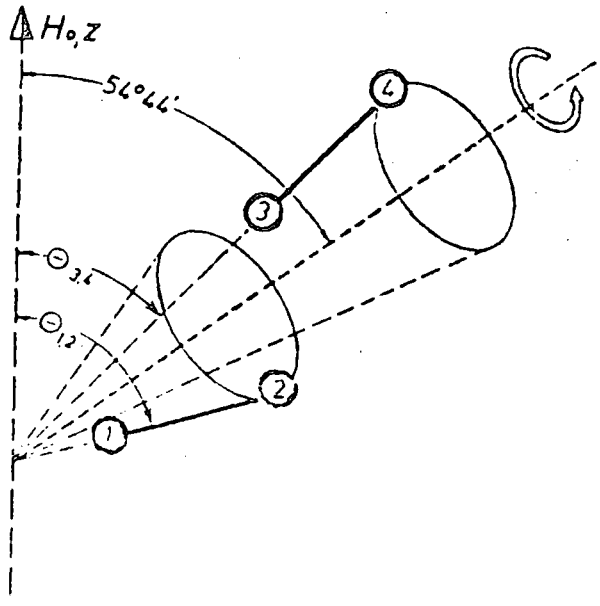

Figure 3.37. Effect of magic angle spinning.

dipolar interactions, quadrupole field gradient interactions and the chemical shift anisotropy effects are, in principle, eliminated when the spinning frequency exceeds the frequency differences present in the sample (the spinning frequency is of the order of a few KHz).

The problems associated with low sensitivity of race spins and their long relaxation time are circumvented by the development of cross polarisation;[360] the method is based on tapping the abundant proton spin system to provide sufficient carbon polarisation, which is more convenient than by thermalisation with the lattice. The result is a higher signal intensity for ^{13}C and, moreover, the relaxation time is dramatically reduced allowing pulse sequences required of

the experiment to be determined by the proton longitudinal relaxation time rather than by that for the carbons. The two main approaches of many variants of cross polarisation experiment are mentioned here.

In spin lock cross polarisation, the protons are first spin locked in a resonant radiofrequency of field strength H_{1H} and, then followed by radiofrequency field, applied near the carbon resonance, such that the condition (Hartmann-Hann)[361] in equation (3.9) is fulfilled. The carbon signal is enhanced

$$\gamma_C H_{1C} = \gamma_H H_{1H} \qquad (3.9)$$

by a factor of four (γ_H/γ_C), compared to the carbon magnetisation which would arise by thermalisation with the lattice.

The second method, initially, brings the system in a state of dipolar order to cross polarise the ^{13}C spins. This is achieved by bringing the ^{13}C system at the 'spin temperature' of ^{13}C in thermal contact with the larger ^{1}H spin system at the spin temperature of ^{1}H. As a result of thermal contact, a large temperature decrease in the ^{13}C system occurs, associated with a marked increase of ^{13}C spins, whereas the temperature of the ^{1}H system, due to the high heat capacity, is only slightly increased resulting very little decrease in polarisation.

Figure 3.38 summarises the experimental details of cross polarisation, performed in four steps: (a) the proton spins are polarised in a high field (H_o) - the population is determined by the energy difference between the two levels in

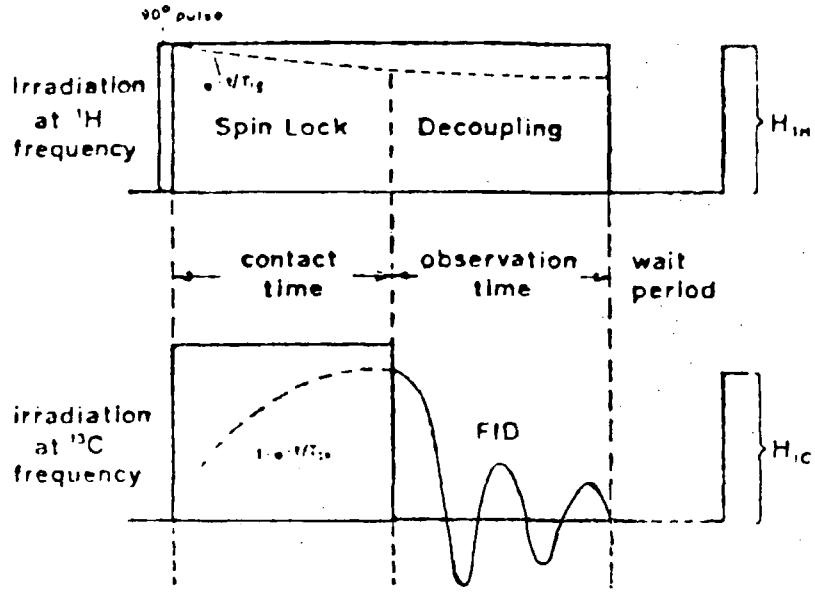

Figure 3.38. Cross polarisation illustrating timing diagram.

the H_o field; (b) the polarised proton spins are then placed in the rotating frame by a 90^o pulse, followed by a 90^o phase shift and continuous application of radiofrequency field H_{1H} - so-called 'spin-locking' field; (c) a thermal contact between the two spin systems (^{13}C-^{1}H) is established for variable time (t) by placing the ^{13}C spins into the rotating frame as well. A Hartmann-Hann condition is fulfilled. The ^{13}C magnetisation increases rapidly, whereas a small decrease in ^{1}H magnetisation occurs; and, (d) the last step involves the sampling of the proton enhanced ^{13}C free induction decay after switching off the ^{13}C radiofrequency field, whilst the ^{1}H radiofrequency is still in operation. The third and fourth

steps are repeated several times for favourable cases during which the ^{1}H polarisation is depleted and the ^{13}C signal is accumulated.

The application of cross polarisation combined with magic angle spinning (CP-MAS) is still in its infancy; nevertheless, natural and synthetic polymers are currently the most investigated materials. In this context, a limited study has been carried out on 'sulphur-vulcanised' Natsyn 2200 elastomers.

(b) ^{13}C-NMR spectra

The spectra of the various cis-1,4-polyisoprene samples, presented in Figures 3.39 and 3.40, reveal five clear distinguishable singlet resonance peaks, which are attributed tp the methyl, two methylene, and two ethylenic carbon atoms of the polymer, all of different intensity. Thus, the spectra of these Natsyn 2200 systems with and without additives (Table 3.12) can be interpreted in terms of a single repeating unit, $(-CH_2-\overset{CH_3}{\overset{|}{C}}=CH-CH_2-)_n$, as is indicated with the structures superimposed on the spectra in Figures 3.39 and 3.40. The structural units are labelled arbitrarily as illustrated in appropriate figures as a matter of convenience for discussing the assignment of resonance peaks.

The resonance peaks of the two ethylenic carbon atoms occur at a low field strength, whereas those of the methyl and methylene carbon atoms occur in the high field region.

Assignment of the resonance peaks to specific carbon atoms was originally made by Duch and Grant,[126] in which they used the technique of selective decoupling. The results of proton

Natsyn 2200, Type 1, Elastomer

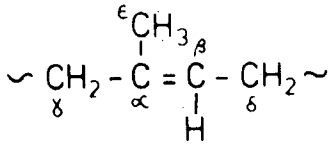

Raw polymer without additives

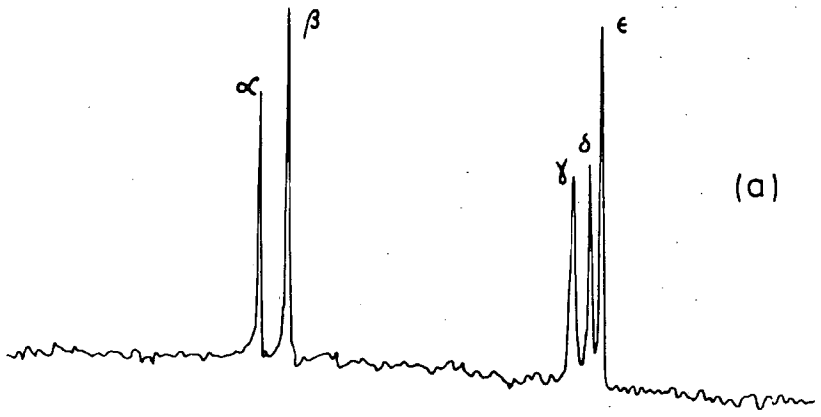

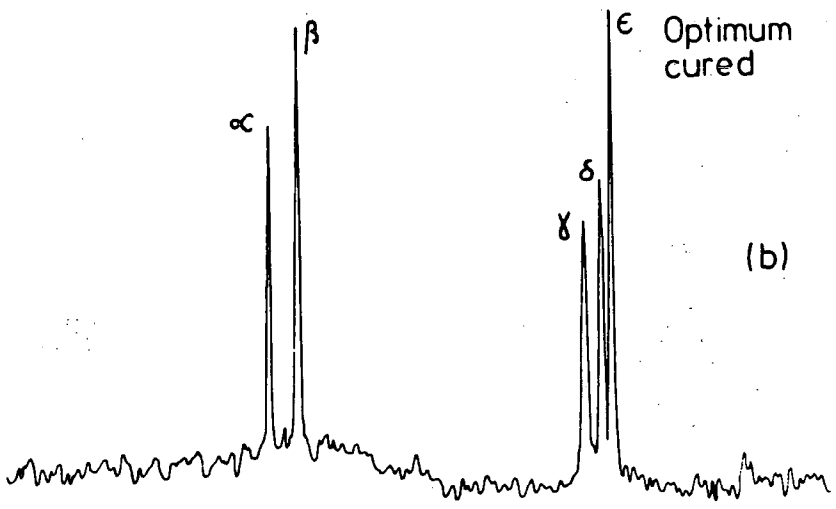

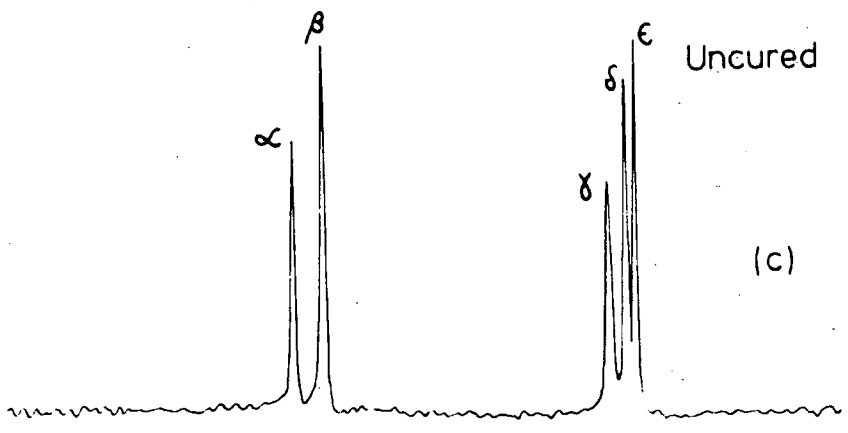

Figure 3.39. ^{13}C NMR spectra of a type 1, Natsyn 2200, elastomer.

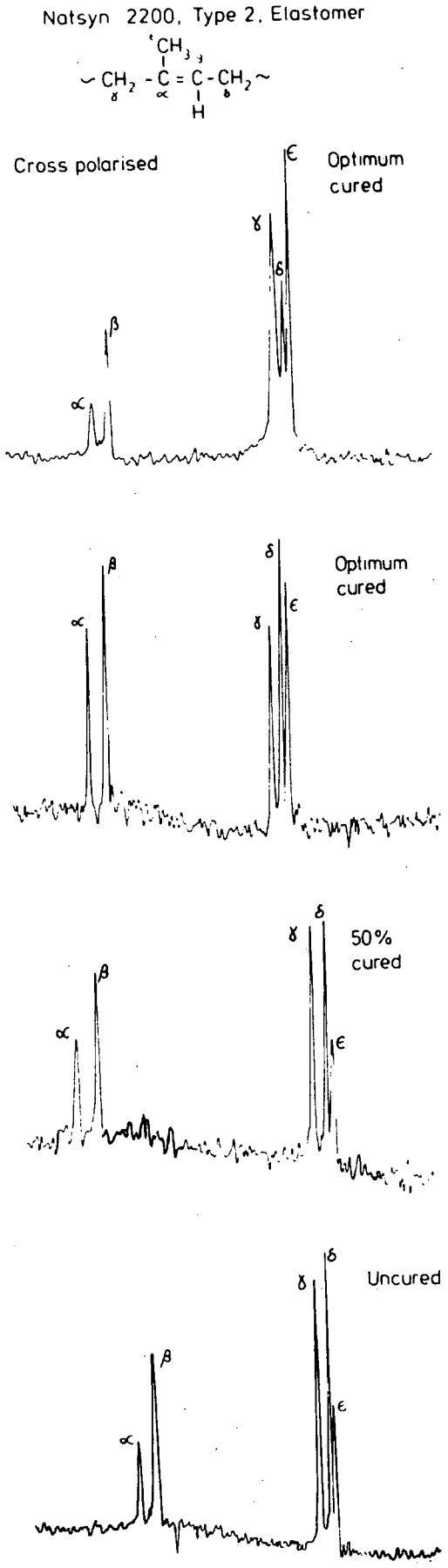

Figure 3.40. ^{13}C NMR spectra of a type 2, Natsyn 2200, elastomer.

nuclear magnetic resonance studies for natural and synthetic cis and trans-1,4-polyisoprenes were particularly useful in this respect.[363-365] The resonance peak of the α-carbon atom, for which the large proton couplings are absent, was assigned to the lowest field peak, because it enhanced to a sharp singlet over a wide range of decoupling frequencies, and, thus, indicated the absence of a directly bonded proton. The resonance of the β-carbon, however, collapsed to a sharp singlet only when the singlet directly bonded ethylenic hydrogen was selectively decoupled. The assignment for the methyl carbon atom was made by Duch and Grant,[126] in a similar procedure involving selective decoupling of the methyl protons. The γ-δ-methylene resonance peaks were not separated from one another in the proton nuclear magnetic resonance spectra, and consequently, their corresponding assignments in the carbon-13 nuclear magnetic resonance were not possible by the selective decoupling technique; and, therefore, Duch and Grant assigned the resonance peaks on an inspection of simple cis- and trans-1,4 polyisoprene models.

It is clearly evident from the indicated spectra that the simplicity of the proton-decoupled carbon-13 nuclear magnetic resonance spectra of a variety of Natsyn 2200 elastomers, run using magic angle spinning and also in one case with cross polarisation, with well separated singlet peaks provides readily interpretation of chemical shifts. However, it is not possible currently to obtain information of minor structures resulting from crosslinking structures or additives, that was originally anticipated for. (It should be noted that one cross-

link occurs on average per 100 isoprene units.) The inherent potentiality of a high resolution solid state NMR spectroscopy may prove useful in future for elucidating the chemistry of 'sulphur-vulcanisation'.

CHAPTER FOUR

AN ESCA INVESTIGATION OF A SERIES OF SOLPRENE 1204 CURED ELASTOMERS

PART II

4.1 Introduction

The investigation in chapter three revealed that, in particular rubber, higher levels of additives are present at the surface than in the bulk in contrast to the level of zinc, where the latter increased with increasing ESCA depth profile into the bulk. The 'swelling' data taken in conjunction with the ESCA data indicated on average one sulphur crosslink after 100 repeat units of isoprene in Natsyn 2200 cured elastomers.

This chapter, as a continuation to the systematic study of elastomers, deals with a variety of Solprene 1204 elastomers, cured on a calendering system at 150^{o}C in air with a 2 mm nip setting to draw into sheets for an ESCA study. The detailed compositions of the bulk formulation are indicated in Table 4.1. The various ingredients in the different types of elastomers are added to obtain the desired mechanical properties.[1,2,47,48,301] A conventional high sulphur-low accelerator system produces a high percentage of polysulphide crosslinks and high accelerator-low sulphur systems produce mainly mono- or disulphide crosslinks with a greater resistance to reversion and aging, but inferior in mechanical properties than the elastomers containing high proportion of polysulphide crosslinks.[1,2]

As noted previously, despite the scientific and technological importance of elastomers and the large number of investigations, which have been made, these primarily pertain to bulk analysis by the usual chemical and physical methods.[95-97,115,123-125] There has been very little or no

Table 4.1

Solprene 1204 Formulation

(a)

Type	1		2		3		4	
	weight %	mole %	weight %	mole %	weight %	mole %	weight %	mole %
Solprene	90.1	94.7	97.8	94.4	90.0	94.7	89.8	94.5
Zinc oxide	4.5	3.9	-	-	4.5	3.9	4.5	3.9
Stearic acid	1.8	0.44	-	-	1.8	0.44	1.8	0.44
CBS	0.9	0.24	-	-	-		-	-
Sulphur	1.8	0.49	-	-	0.63	0.17	-	-
Dicup R	-	-	1.3	0.32	-		-	-
TBTD	-	-	-	-	0.63	0.11	-	-
MBS	-	-	-	-	1.53	0.47	0.9	0.25
DTDM	-	-	-	-	-	-	1.8	0.55
TMTD	-	-	-	-	-	-	0.36	0.11
Permanax B	0.9	0.28	0.98	0.29	0.90	0.28	0.9	0.28

Cure time (minutes) at 150°C

50% (partial)	42	-	22	27
100% (optimum)	60	120	60	60

CBS Cyclohexylbenzthiazyl sulphenamide

Dicup R Dicumyl peroxide

TBTD Tetrabutylthiuram disulphide

MBS 2-(4-morpholinylmercapto)benzthiazole

DTDM Dimorpholine disulphide

TMTD Tetramethylthiuram disulphide

(b)

Raw polymer:	Solprene	ZnO	Stearic acid	CBS	Sulphur
	✓	-	-	-	-

Dicumyl peroxide	TBTD	MBS	DTDM	TMTD
-	-	-	-	-

Permanax B
-

work recorded in the literature on the surface study of industrially important elastomers;[284] and, ESCA offers an excellent possibility for undertaking such study.

The raw Solprene, kindly supplied by Dunlop, is a butadiene-styrene random copolymer (75% butadiene and 25% styrene by weight) polymerised in solution. This chapter is, again, exclusively concerned with the ESCA investigation of the as received elastomers before applying the plasma techniques to elaborate the crosslink functionality.

4.2 Experimental

The experimental procedure is essentially the same as in chapter three and the details are, therefore, not repeated here.

(i) Samples of raw Solprene 1204 and the cured Solprene, partially and fully cured systems in Table 4.1, prepared at Dunlop, were received with protective sheets of either pigmented polyethylene (cured samples) or polyethyleneterephthalate (uncured Solprene 1204).

(ii) The samples have been studied by ESCA over a period of time, however, in the light of difficulties experienced with the uncured Natsyn 2200, the spectra for the uncured Solprene with additives have not yet been obtained. The spectra, which have been recorded of the uncured system, are those of a residual film adhering to the PET film since the removal of this film results in cohesive failure in the rubber layer.

(iii) The samples have been handled in air. The cured elastomers were cut to a size (20 mm x 6 mm x 2.5 mm) appropriate for mounting onto the spectrometer probe tip. In all cases, the samples were cut to a size with a pair of scissors, care being taken not to contaminate the surface of the sample, during this procedure.

(iv) Samples for Multiple Attenuated Infrared spectroscopic examination were also prepared by cutting from the original sample, a section of the appropriate size to place against either a Ge or KRS5 crystal.

(v) The ESCA study has been carried out on an AEI ES200B spectrometer, using $Mg_{K\alpha_{1,2}}$ radiation of energy 1253.7 eV and $Au_{4f_{7/2}}$ level at 84 eV binding energy for calibration purposes, and under these conditions had a full width at half maximum (FWHM) of $\sim$ 1.2 eV.

(vi) In all cases, the deconvolutions of the spectra were carried out on a Dupont (model 310) Curve Resolver with the possible errors of $\pm$ 0.2 eV in binding energies and the area ratios in the range of $\pm$ 5%.

(vii) The 'swelling' procedure was performed in the manner outlined in chapter three. A theoretical interaction parameter (0.360) between the Solprene 1204 and the cyclohexane solvent has been used in the Flory-Rehner equation for the evaluation of

effective crosslinking density and, hence, the average molecular weight between the crosslink points.

(viii) Microanalysis has been carried out as in chapter three.

(ix) Background information on the samples

The detailed bulk composition of Solprene 1204 formulations together with curing times for a variety of elastomers is indicated in Table 4.1.

Vulcanisation is affected by heating the premix of rubber on a calendering system at 150^{o}C in air, with a 2 mm nip setting to draw into sheets (chapter three).

4.3 Results and Discussion

4.3.1 'Swelling' data

The main objective in this part of study has been to use the 'swelling' data in conjunction with the ESCA data for the estimation of the average number of sulphur atoms, involved in crosslinking two polymer chains. The detailed 'swelling' behaviour of elastomers in solvents with different solubility parameters is elaborated in chapter three and, it is convenient to provide only the results for Solprene 1204 systems, immersed in cyclohexane solvent. A theoretical value of Solprene 1204-cyclohexane interaction parameter (0.360) in the Flory-Rehner equation (3.3)[73-75] is used for the determination of average molecular weight between crosslinks. The results are indicated in Tables 4.2 and 4.3. The modulus at low elongations can be calculated from equation (3.6),

Table 4.2

Optimum cured, Solprene 1204, elastomers

Type	Crosslinking density Ve (m^{-3})	Average molecular weight between crosslinks $\bar{M}c$	Young's modulus (10^5 Nm^{-2})
1	198	4,950	14.3
2	548	1,790	39.6
3	193	5,090	14.0
4	229	4,280	16.6

Table 4.3

Partially (50%) cured, Solprene 1204, elastomers

Type 1	Crosslinking density Ve (m^{-3})	Average molecular weight between crosslinks	Young's modulus (10^5 Nm^{-2})
1	214	4,580	15.5
3	210	4,670	15.2
4	186	5,270	13.5

assuming that the density of vulcanised Solprene is 980 kg m^{-3}.

4.3.2 Microanalysis data

It is of interest to compare the experimental results with the bulk values used in the Solprene 1204 formulation before considering the ESCA data in detail.

The results in Tables 4.4 and 4.5, obtained using the 'wet-ashing' and 'combustion' methods (chapter three), indicate that the results for the optimum and uncured samples are, in general, in good agreement with the theoretical values in Table 4.6.

Table 4.4

Optimum cured Solprene 1204 (% by weight)

Type	Carbon	Hydrogen	Nitrogen	Oxygen	Sulphur	Zinc
1	83.4	11.9	-	-	2.0	3.7
2	89.3	11.0	-	-	-	-
3	84.1	11.7	0.9	-	1.3	3.8
4	83.7	11.8	1.2	-	1.0	3.8

Table 4.5

Uncured Solprene 1204 (% by weight)

Type	Carbon	Hydrogen	Nitrogen	Oxygen	Sulphur	Zinc
1	83.7	11.7	0.6	-	1.8	3.8
2	89.2	10.8	-	-		-
3	83.5	10.8	-	-	2.1	3.8
4	83.2	11.2	1.1	-	1.0	3.7

Table 4.6

Theoretical values for Solprene 1204 formulation (% by weight)

Type	Carbon	Hydrogen	Nitrogen	Oxygen	Sulphur	Zinc
1	84	9.2	0.14	1.1	2.0	3.60
2	90	9.8	-	0.2	-	-
3	85	9.2	0.27	1.3	0.64	3.6
4	84.6	9.2	0.37	1.5	0.73	3.6

4.3.3 ESCA analyses of cured samples

(a) Type 1, Solprene 1204, elastomer

(i) Introduction

It is clearly evident from the microanalysis data in Tables 4.4 and 4.5 and the details of the bulk composition given in Table 4.1 and Table 4.6 in terms of weight and normalised mole % terms that the C_{1s} signal should predominantly arise from the Solprene 1204 carbon chains, with smaller contributions from stearic acid, CBS and permanax B. The N_{1s} signals would be expected from both CBS and permanax B, whilst the sulphur signal should predominantly arise from the added sulphur itself as opposed to the sulphur of CBS. Zinc is added to the formulation as the oxide to enhance the rate of cure, and one objective of the ESCA investigation is to affect a chemical speciation, in particular of zinc and sulphur. The O_{1s} signals can conceivably arise from residual metal oxide (low binding energy), from carboxylate and oxygen in stearate and permanax B respectively, and from any oxidative functionalisation from sulphur (viz. SO_4^{2-}) or from oxidation of the Solprene surface during cure on a calendering system at 150°C in air. In principle, the ESCA experiment provides five measurable levels to define the C:N:S:Zn:O surface stoichiometry. Apart from any detail of fine structure such as $\pi \rightarrow \pi^*$ transitions mainly from π system of phenyl and the remaining, if any, from the π bonding in butadiene, which potentially might provide additional information, the measurement of only five levels does not allow an ambiguous assignment of surface composition. The straightforward crude

analysis assumes that the ratio of the minor additives CBS and permanax B (on their transformation products) remain the same in the surface as in the bulk.

It is convenient to present the spectra for the optimum cured elastomers and the relevant data are set out in appropriate tables.

(ii) Optimum cured type 1, Solprene 1204, elastomer

The core level spectra at electron take-off angles of 30^{o} and 70^{o} for the optimum cured type 1, Solprene 1204, elastomer are presented in Figure 4.1 and the relevant intensity ratios for the components are set out in Table 4.7.

Table 4.7

Optimum cured type 1, Solprene 1204, elastomer

Intensity ratios

Take-off angle	C_{1s}/O_{1s}	C_{1s}/N_{1s}	C_{1s}/S_{2p}	C_{1s}/Zn_{3p}	Zn_{3p}/S_{2p}
30^{o}	5	61	25	13	2.0
70^{o}	4.6	96	34	15	2.2

The angular dependent data reveal that the sample is reasonably homogeneous, in terms of stoichiometry, as a function of profile depth into the sample. The C_{1s} levels indicate a broadened signal compared with the raw solprene without additives (FWHM 1.8 eV vs. 1.5 eV respectively), and the anticipated $\pi \rightarrow \pi^{*}$ transitions from the π system of phenyl are absent, compared with the raw solprene, suggesting that the surface covered with a layer of polybutadiene; and the

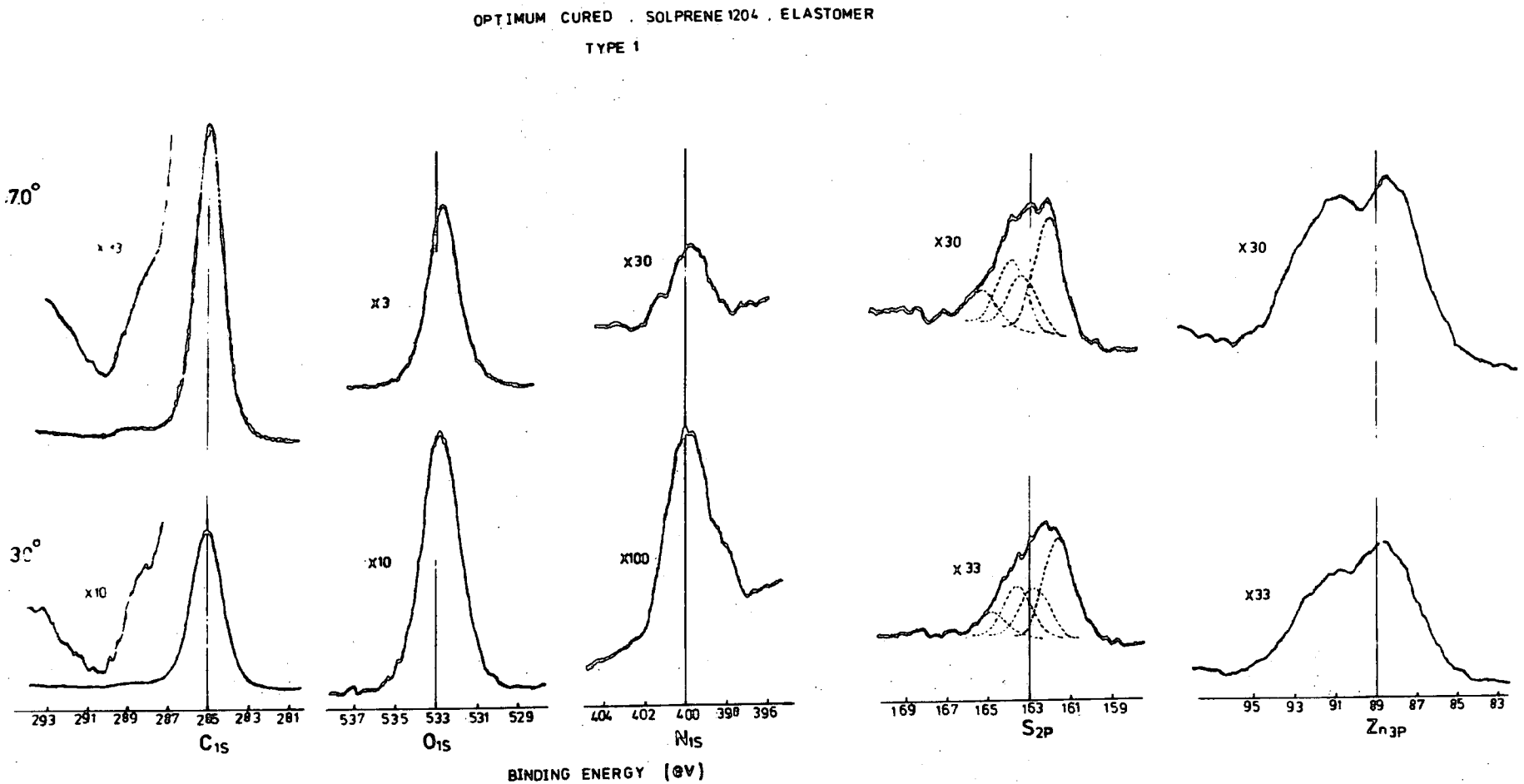

Figure 4.1. High resolution spectra of an optimum cured type 1, Solprene 1204, elastomer.

absence of unsaturation in the surface region, as far as the ESCA depth sampling is concerned, is associated with the oxidative functionalities, as is evidenced by the high binding energy tail of C_{1s} envelope.

The high resolution spectra also reveal nitrogen and sulphur, the latter (S_{2p} levels) being broadened by the presence of at least two components, the higher binding energy peaks after deconvolution are attributed to organic sulphide (including polysulphide), and the lower binding energies to zinc sulphide (FWHM 3.6 eV of S_{2p} for the 'sulphur-vulcanised' Solprene vs. 2.2 eV of S_{2p} for ZnS). Oxygen and zinc are also detected at reasonable levels.

The bulk formulation of the type 1 elastomer gives a mole ratio of permanax B to CBS of 1.2:1. The N_{1s} signal intensity arises from the CBS and permanax B, whilst the C_{1s} spectrum derives predominantly from the Solprene 1204 framework (Solprene 1204 is a butadiene-styrene random polymer of composition, 75% butadiene and 25% styrene by weight, polymerised in solution), and the remaining C_{1s} signal arises from the additives (other than sulphur and zinc oxide for which the analysis in chapter three indicated a small contribution due to the overlayer of hydrocarbon contamination). The C_{1s}/N_{1s} intensity ratio corrected for the differences in cross-section provides a means of assessing the C:N stoichiometry in the profile depth, monitored by ESCA. Since these are the only two additives in the type 1 system to contribute to the N_{1s} signal, one may accomplish a straightforward crude surface analysis, as follows:-

Let x = moles % of Solprene

Let Y = moles of CBS, then permanax B = 1.2Y

Total C_{1s} signal = 5x + 13Y + 1.5 x 1.2Y

Total N_{1s} signal = 2Y + 1.2Y

$$\therefore \quad \frac{5x + 31Y}{3.2Y} = 61 \times 1.19 = 73$$

$$\frac{x}{y} = 40.$$

(If one considers any contribution from stearate, the value of $\frac{x}{y}$ is still the same order of magnitude ($\sim$ 34).)

The results for the optimum cured type 1, Solprene 1204, elastomer at 30° and 70° take-off angles are given in Table 4.8, indicating higher levels of additives by a factor of $\sim$ eight at the surface than in the bulk, and, in contrast, the level of zinc at the surface is less compared to the bulk ($\sim$ 3.8 mole %).

The 'swelling' data (section 4.3.1) taken in conjunction with the ESCA data (C_{1s}/S_{2p} intensity ratio) provides a basis for the estimation of the average number of sulphur atoms, involved in crosslinking two polymer chains.

As has already been reiterated in chapters one and three, the Flory-Rehner equation[73-79] allows the evaluation of the number average molecular weight between the crosslink points of the polymer chains. The use of this data together with the C_{1s}/S_{2p} intensity ratio, particularly of high binding energy components after deconvolution of S_{2p} peak, allow further for an estimate of the average number of sulphur atoms between the crosslink points of two polymer chains; and

the estimate is carried out in the same procedure adopted for the Natsyn 2200 systems in chapter three. The sulphur functionality on average is two, indicating disulphide linkages and the sulphide crosslinkage occurs after ~ 70 Solprene repeat units.

Table 4.8

Optimum cured type 1, Solprene 1204, elastomer

Surface composition (mole %)

Take-off angle	Solprene	CBS	Permanax B	Zn
30°	100	2.5	3	2.9
70°	100	1.5	1.8	2.5

(iii) 50% cured type 1, Solprene 1204, elastomer

The relevant data for a partially cured type 1 sample at 30° and 70° take-off angles are set out in Table 4.9. The angular dependent data reveal that the surface is homogeneous,

Table 4.9

50% cured type 1, Solprene 1204, elastomer

(a) Intensity ratios

Take-off angle	C_{1s}/O_{1s}	C_{1s}/N_{1s}	C_{1s}/S_{2p}	C_{1s}/Zn_{3p}	Zn_{3p}/S_{2p}
30°	6	127	29	19	1.5
70°	5	135	43	19	2.3

(b) Surface composition (mole %)

Take-off angle	Solprene	CBS	Permanax B	Zn
30°	100	1.1	1.3	2.0
70°	100	1.0	1.2	2.0

in terms of stoichiometry, as a function of depth into the sample.

The high resolution C_{1s} spectra at both take-off angles did not reveal any evidence for the $\pi \rightarrow \pi^*$ shake-up transitions and, this is associated with oxidative functionalisation at high binding energy tail of C_{1s} envelope; and, also, showed broadened signals compared with the raw Solprene without additives (FWHM 1.8 eV for both take-off angles vs. 1.5 eV respectively).

The high resolution spectra also revealed nitrogen and sulphur, the latter being broadened by the presence of at least two components, organic sulphide and zinc sulphide (FWHM 3.7 eV for both take-off angles vs. 2.2 eV of S_{2p} in ZnS). Oxygen and zinc were also monitored at reasonable levels.

The surface composition in Table 4.9, based on the previous calculations, indicates higher levels of additives at the surface than in the bulk, being smaller compared to the surface composition for an optimum cured type 1 sample, whilst the level of zinc, being less than in the bulk, is the same at both take-off angles for the partially cured sample.

The partially cured elastomer possesses on average trisulphide linkages.

(b) Type 2, Solprene 1204, elastomer

(i) Introduction

The bulk composition of type 2 system in Table 4.1 suggests that the C_{1s} intensity should predominantly derive

from Solprene framework, with small contributions from permanax B and dicumyl peroxide. The N_{1s} signal would be expected only from permanax B, since this is the only additive containing nitrogen in the system. The bulk formulation is, therefore, simpler than sulphur-vulcanised series. In principle, the ESCA monitors C_{1s}, O_{1s} and N_{1s} levels to define the surface stoichiometry on the same assumptions, which have been stated for type 1 sample.

(ii) Optimum cured type 2, Solprene 1204, elastomer

The C_{1s} levels in Figure 4.2 reveal a broadened signal compared with the raw Solprene without additives (FWHM 1.8 eV vs. 1.5 eV respectively), and the $\pi \rightarrow \pi^*$ transitions are absent as far as the ESCA depth profile is concerned, which, otherwise, would have accounted for the unsaturation in the surface region. The oxidation of the surface during cure on a calendering system at 150°C for 120 minutes in the presence of peroxide as a curing agent accounts for the absence of carbon-carbon double bonds. The relevant data are set out in Table 4.10. The high resolution spectra also showed oxygen and nitrogen, the latter being relatively of low level, and, in addition, zinc and silicon of high intensity are detected as contaminant, which the silicon in the form of silica accounts partly for a high ratio of C_{1s}/O_{1s} in the surface region.

The surface composition indicates higher levels of additives than in the bulk by a factor of twenty five.

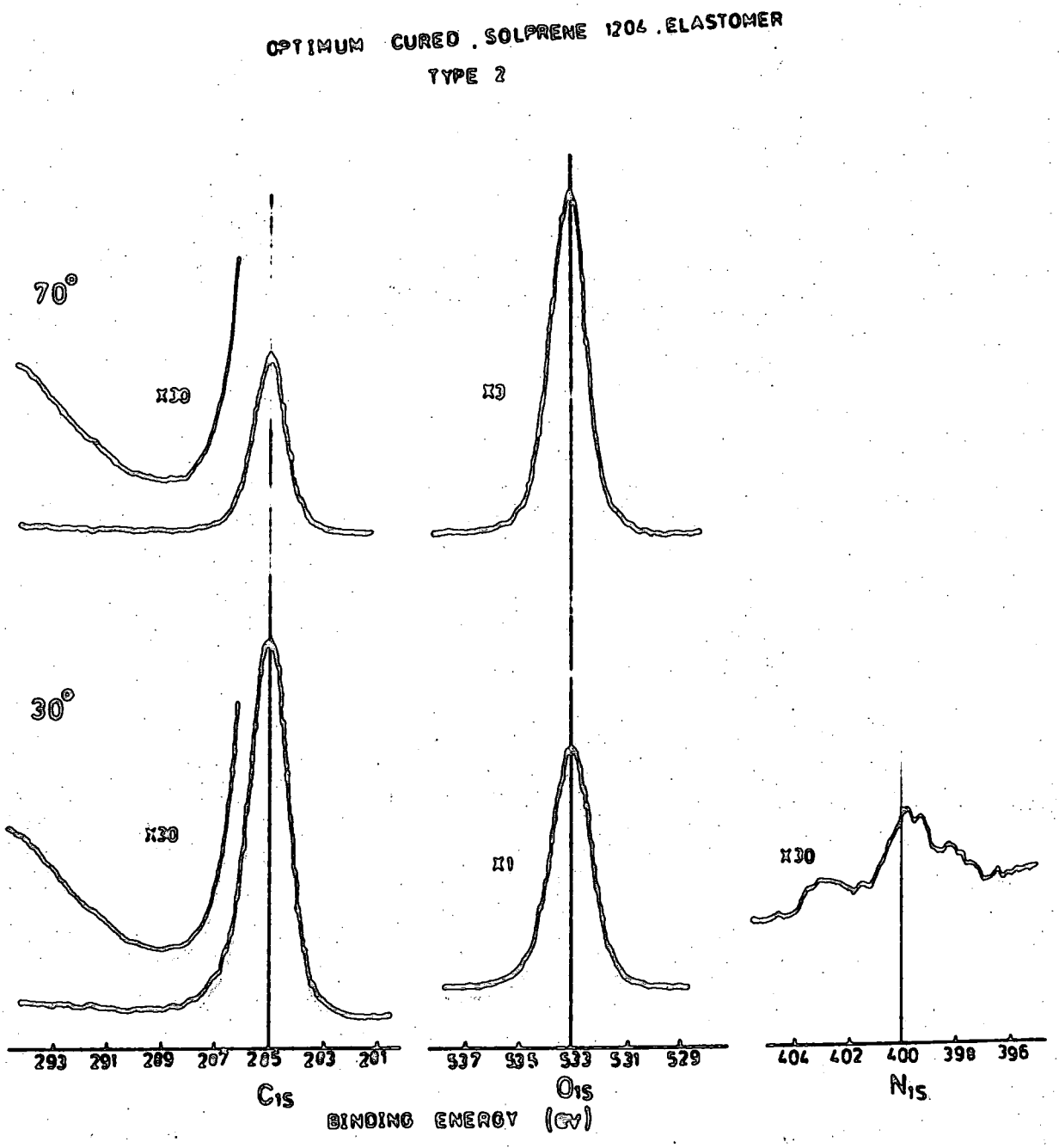

Figure 4.2. High resolution spectra of an optimum cured type 2, Solprene 1204, elastomer.

Table 4.10

Optimum cured type 2, Solprene 1204, elastomer

(a) Intensity ratios

Take-off angle	C_{1s}/O_{1s}	C_{1s}/N_{1s}	C_{1s}/Si_{2p}	C_{1s}/Zn_{3p}
30°	1.6	89	1.9	19
70°	1.4	-	1.7	15

(b) Surface composition (mole %)

Take-off angle	Solprene	Dicumyl peroxide	Permanax B	Zn
30°	100	8.0	7	2.0
70°	-	-	-	2.5

(c) Type 3, Solprene 1204, elastomer

(i) Introduction

The bulk formulation for the type 3 sample in Table 4.1 again indicates that the C_{1s} signals should predominantly derive from the Solprene framework, with small contributions from stearic acid, TBTD, MBS and permanax B. The N_{1s} signals are expected from TBTD, MBS and permanax B, whilst the sulphur intensity should arise by half from the added sulphur itself as opposed to the sulphur of CBS. The O_{1s} signals can conceivably arise from residual metal oxide (low binding energy), from carboxylate and oxygen in stearate, permanax B and MBS respectively, and from the oxidation of the Solprene during cure. In principle, the C_{1s}, O_{1s}, N_{1s}, S_{2p} and Zn_{3p} levels again allow an unambiguous assignment of the surface composition, on the same assumptions stated previously.

(ii) Optimum cured type 3, Solprene 1204, elastomer

The core level spectra at 30° and 70° electron take-off angles are presented in Figure 4.3 and the relevant intensity ratios together with the surface composition are set out in Table 4.11.

Table 4.11

Optimum cured type 3, Solprene 1204, elastomer

(a) Intensity ratios

Take-off angles	C_{1s}/O_{1s}	C_{1s}/N_{1s}	C_{1s}/S_{2p}	C_{1s}/Zn_{3p}	Zn_{3p}/S_{2p}
30°	5	22	7	9	0.8
70°	5	27	8	10.5	0.8

(b) Surface composition (mole %)

Take-off angles	Solprene	TBTD	MBS	Permanax B	Zn
30°	100	0.3	12	0.7	4.0
70°	100	0.2	9	0.6	3.6

The angular dependent data indicate that the surface is homogeneous, as a function of ESCA depth profile into the sample and higher levels of accelerators and antioxidant are present by a factor of approximately two than in the bulk. The C_{1s} spectra at both take-off angles reveal oxidative functionalisation, as is evidenced by the high energy tail of C_{1s} envelope with the absence of $\pi \rightarrow \pi^*$ shake-up transitions, and also show broadened signals compared with raw Solprene without additives (FWHM 1.9 eV for both take-off angles vs. 1.5 eV respectively).

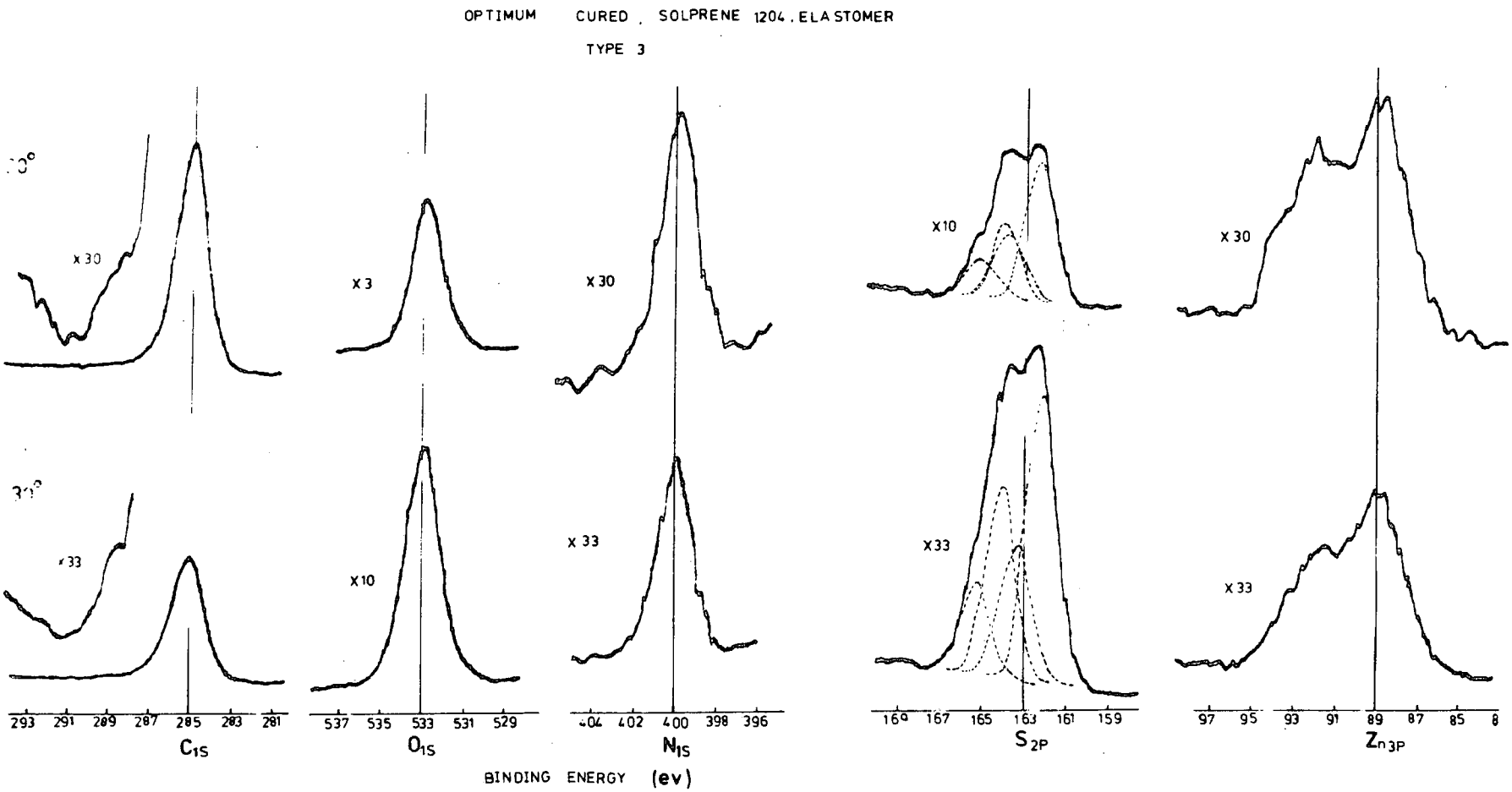

Figure 4.3. High resolution spectra of an optimum cured type 3, Solprene 1204, elastomer.

The high resolution spectra also reveal oxygen, nitrogen, silicon as contaminant, zinc and sulphur at reasonable levels, the latter is broadened by the presence of at least two components (FWHM 3.8 eV for both take-off angles vs. 2.2 eV of S_{2p} in ZnS).

The sulphur functionalities of eleven and eight on average at 30^{o} and 70^{o} take-off angles respectively suggest that at least ten sulphur atoms are involved in crosslinking two polymer chains.

(iii) 50% cured type 3, Solprene, elastomer

The C_{1s} spectra showed oxidative functionalisation at 30^{o} and 70^{o} take-off angles, with the complete absence of $\pi \rightarrow \pi^{*}$ shake-up transitions, and also broadened signals compared with the raw solprene without additives (FWHM 2.0 eV vs. 1.5 eV respectively).

The high resolution also revealed oxygen, nitrogen, zinc and sulphur at reasonable levels, the S_{2p} signal is broadened compared with the ZnS (FWHM 4.0 eV for both take-off angles vs. 2.2 eV respectively). Silicon was also detected as contaminant.

The data in Table 4.12 indicate higher levels of additives at the surface than in the bulk, in contrast to the level of zinc, which increases only slightly on the ESCA depth profile into the sample; and, the surface is inhomogeneous, in terms of stoichiometry, as a function of depth into the sample.

The sulphur functionalities of eight and six on average at 30^{o} and 70^{o} take-off angles respectively indicate at least seven sulphur atoms in the polysulphide linkage.

Table 4.12

50% cured type 3, Solprene 1204, elastomer

(a) Intensity ratios

Take-off angle	C_{1s}/O_{1s}	C_{1s}/N_{1s}	C_{1s}/S_{2p}	C_{1s}/Zn_{3p}	Zn_{3p}/S_{2p}
30^{o}	4	27	12	12	1.0
70^{o}	4	42	16	15	1.1

(b) Surface composition (mole %)

Take-off angle	Solprene	TBTD	MBS	Permanax B	Zn
30^{o}	100	0.2	9	0.6	3.0
70^{o}	100	0.1	5.4	0.3	2.5

(d) Type 4, Solprene 1204, elastomer

(i) Introduction

It is clear from the preceding discussion that the C_{1s} signal arises predominantly from the Solprene, with smaller contributions from the additives. The N_{1s} signals are expected from MBS, DTDM, TMTD and permanax B, whilst the sulphur intensity should arise from the sulphur of MBS, DTDM and TMTD, since the system does not contain free sulphur (Table 4.1). The O_{1s} signals can conceivably arise from oxygen in zinc oxide, stearate, MBS, permanax B and from oxidation of the Solprene during cure on a calendering system at $150^{o}C$ in air.

The C_{1s}, O_{1s}, N_{1s}, S_{2p} and Zn_{3p} levels monitored by ESCA again allow unambiguous assignments of surface composition on the same assumptions stated previously.

(ii) Optimum cured type 4, Solprene, elastomer

The data in Table 4.13, extracted from the raw spectra in Figure 4.4, indicate that the surface is reasonably homogeneous, in terms of stoichiometry, as a function of ESCA depth profile into the sample. The C_{1s} levels at both take-off angles indicate oxidative functionalisation, as is

Table 4.13

Optimum cured type 4, Solprene 1204, elastomer

(a) Intensity ratios

Take-off angle	C_{1s}/O_{1s}	C_{1s}/N_{1s}	C_{1s}/S_{2p}	C_{1s}/Zn_{3p}	Zn_{3p}/S_{2p}
30°	6	26	11	10	1.1
70°	7	31	14	12	1.2

(b) Surface composition (mole %)

Take-off angle	Solprene	TMTD	MBS	Permanax B	DTDM	Zn
30°	100	1.0	2.4	2.5	5.2	3.7
70°	100	0.8	1.9	2.0	4.2	3.1

evidenced by the high energy tail of C_{1s} envelopes, and, also, show broadened signals compared with the raw Solprene without additives (FWHM 1.9 eV for both take-off angles vs. 1.5 eV respectively).

The high resolution spectra also revealed nitrogen, oxygen, silicon (as contaminant), zinc and sulphur, the latter is broadened compared with zinc sulphide (FWHM 3.8 eV vs. 2.2 eV respectively).

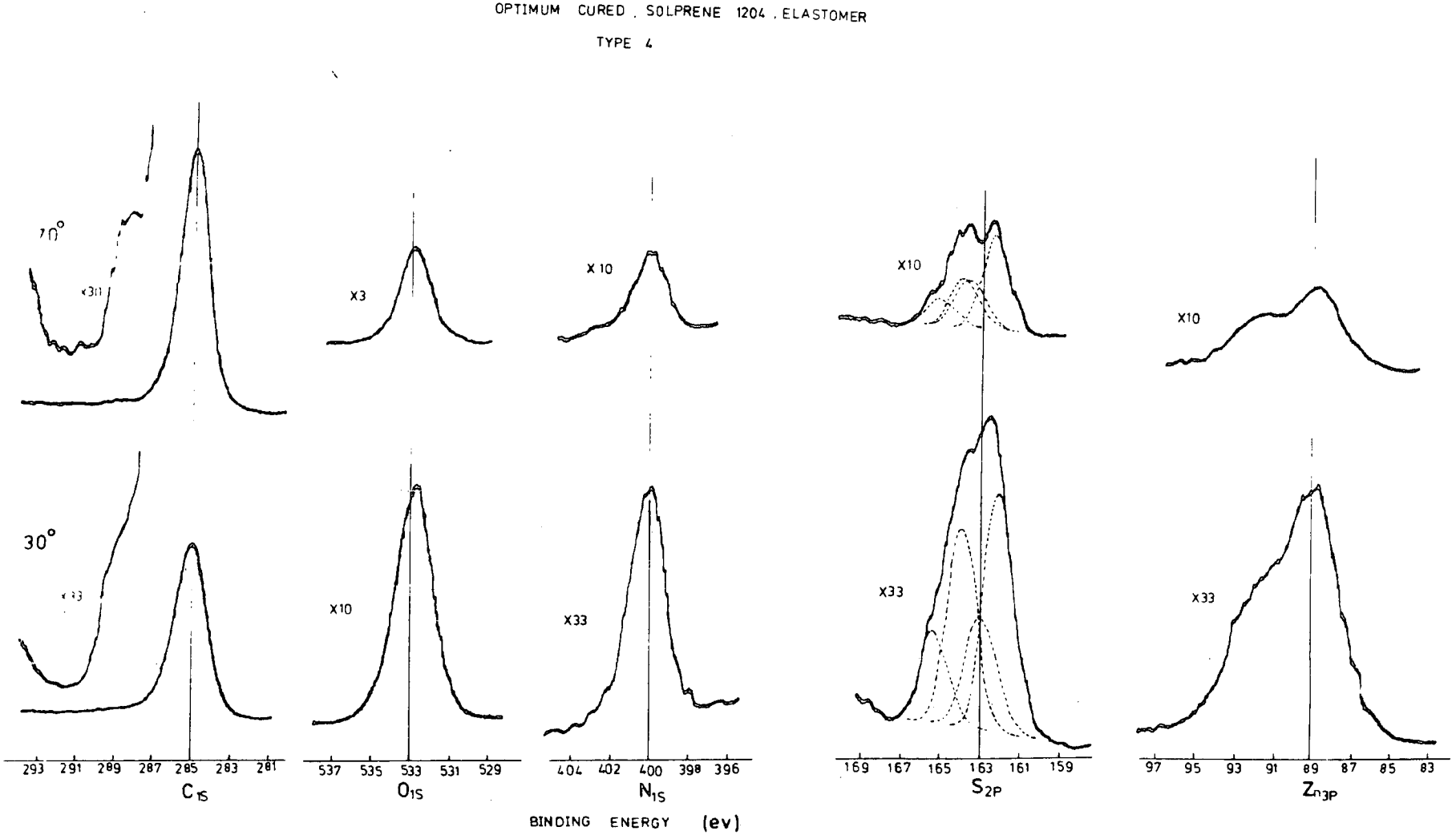

Figure 4.4. High resolution spectra of an optimum cured type 4, Solprene 1204, elastomer.

The sulphur functionalities of seven and four on average at 30° and 70° take-off angles respectively, indicate at least six sulphur atoms in the polysulphide linkage.

(iii) 50% cured type 4, Solprene 1204, elastomer

The data in Table 4.14 are fairly self explanatory. The surface is reasonably homogeneous as a function of ESCA depth profile into the sample and reveal higher levels of antioxidant and accelerators, whereas the level of zinc in the surface region is approximately the same as in the bulk.

Table 4.14

50% cured type 4, Solprene 1204, elastomer

(a) Intensity ratios

Take-off angle	C_{1s}/O_{1s}	C_{1s}/N_{1s}	C_{1s}/S_{2p}	C_{1s}/Zn_{3p}	Zn_{3p}/S_{2p}
30°	4	26	9	10	0.9
70°	4	32	14	14	1.0

(b) Surface composition (mole %)

Take-off angle	Solprene	TMTD	MBS	Permanax B	DTDM	Zn
30°	100	1.0	2.4	2.5	5.2	3.7
70°	100	0.8	1.9	2.0	4.1	2.7

The C_{1s} signals at both take-off angles had the same FWHM as those of optimum cured samples and reveal oxidative functionalities with the complete absence of $\pi \rightarrow \pi^*$ transitions. The S_{2p} signals detected at reasonable levels were also broadened, compared with the zinc sulphide (FWHM 3.8 eV vs.

2.2 eV respectively). The sulphur functionalities at 30° and 70° take-off angles are eight and seven on average respectively, indicating polysulphide linkages.

4.3.4 Uncured Solprene 1204 samples

(a) Introduction

Three samples of uncured Solprene 1204 formulation have been received, are as follows:

(i) Compressed, solution polymerised butadiene-styrene random polymer of composition, 75% butadiene and 25% styrene by weight. Samples have been cut directly for ESCA examination either for the investigation of the as received surfaces or for the fresh surfaces exposed with a scalpel blade.

(ii) Raw Solprene 1204 milled for ten minutes and pressed for five minutes at an elevated temperature (100°C). A sample of appropriate size (20 mm x 7 mm x 3 mm) was prepared by cutting with a pair of scissors from the original sample.

(iii) Uncured Solprene 1204 formulations with additives (Table 4.1). As the difficulties have previously been experienced with the uncured Natsyn 2200 formulation in chapter three, the large number of voids arising during the mixing process exploded the samples on introduction to the high vacuum system of the spectrometer, causing on several occasions contamination of the window; and, therefore, no further attempt has been made to obtain the spectra for the uncured systems with additives.

(b) Solution polymerised butadiene-styrene random polymer

(i) As received surface

The wide scan for the as received Solprene 1204 sample revealed C_{1s} and O_{1s} levels, together little evidence for silicon as contaminant. The high resolution spectra are presented in Figure 4.5 and the relevant data are set out in Table 4.15. The C_{1s} spectrum indicates a symmetrical

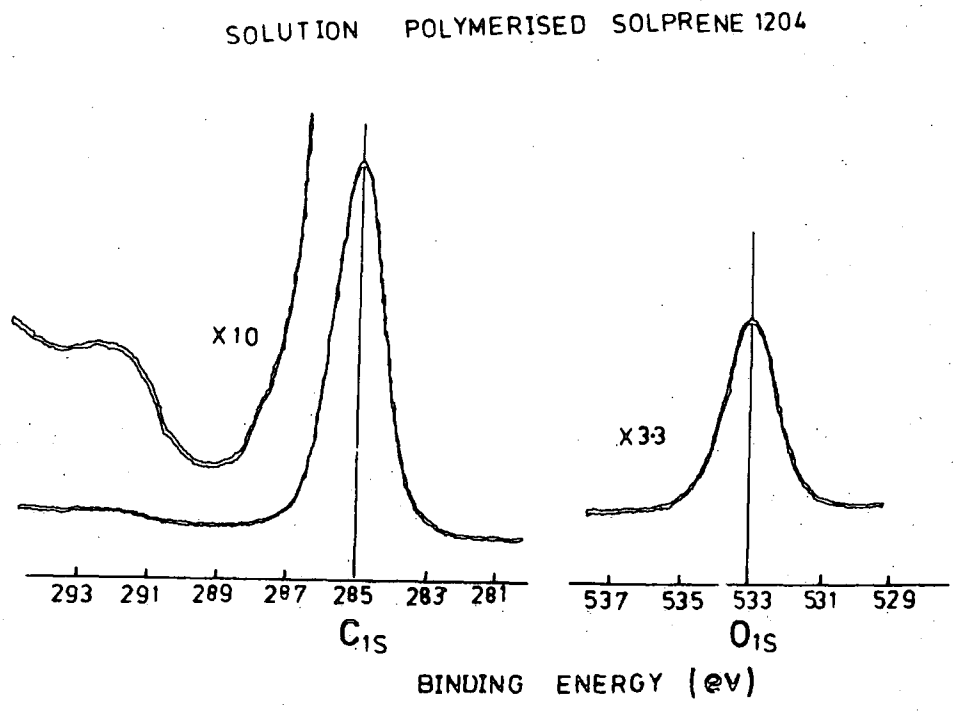

Figure 4.5. C_{1s} and O_{1s} levels for the as received Solprene 1204 (solution polymerised).

peak, with a low intensity (1.9%) of $\pi \rightarrow \pi^*$ transitions, associated with the π system, separated by $\sim$ 7.0 eV from the direct photoionisation peak. The rather high level of oxygen may not, however, be associated with the oxidative degradation of the polymer surface since silicon was also detected at a

Table 4.15

Intensity ratios for the solution polymerised (butadiene-styrene) Solprene 1204

	C_{1s}/O_{1s}	C_{1s}/Si_{2p}
As received	6	13
Freshly exposed surface of the as received	9	14

reasonable level.

(ii) Freshly exposed surface

The data for the freshly exposed surface are set out in Table 4.15 for comparison purposes. The level of oxygen is now somewhat lower than the as received Solprene 1204. The C_{1s} spectrum again indicated a symmetrical peak, with a intensity ($\sim$ 2.4%) of $\pi \rightarrow \pi^*$ transitions arising from the π system of Solprene and, this indicates that the $\pi \rightarrow \pi^*$ signal is entirely from butadiene. The relative intensity of the shake-up peak is higher than for the original surface, and in the light of the oxygen and silicon intensities, the most likely explanation for this is an overlayer of hydrocarbon contamination on the original sample (this would contribute to the direct photoionisation but not to the $\pi \rightarrow \pi^*$ transitions).

(c) Raw Solprene 1204

The wide scans at 30° and 70° take-off angles indicated little evidence for anything other than C_{1s} and O_{1s} levels. The data obtained from high resolution spectra in Figure 4.6 are set out in Table 4.16.

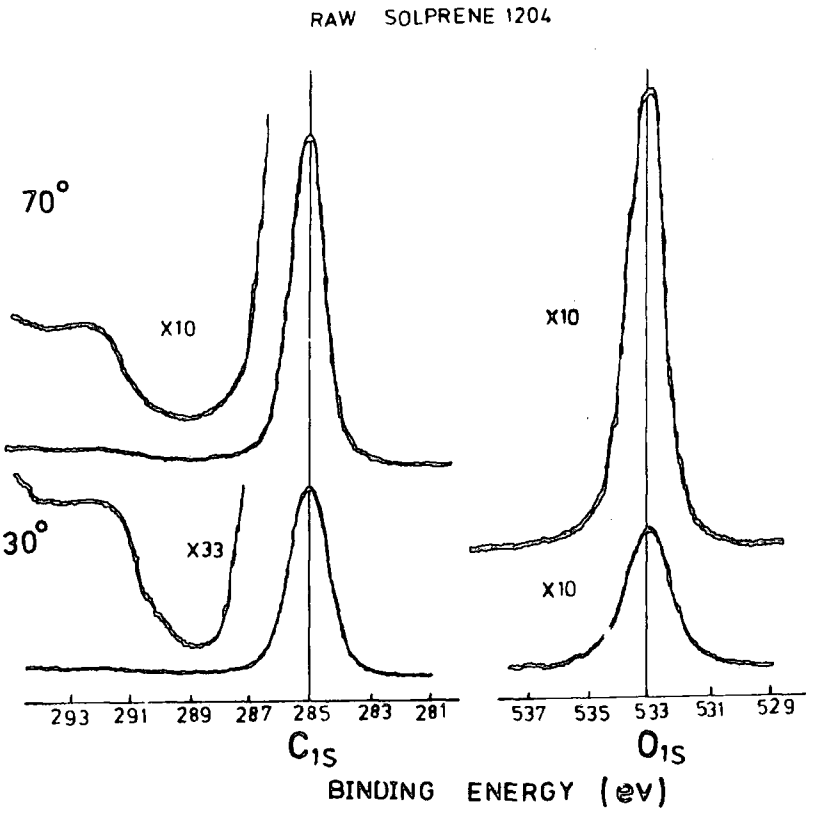

Figure 4.6. C_{1s} and O_{1s} levels for the as received, raw Solprene 1204, milled for 10 minutes and pressed for 5 minutes at 100°C.

Table 4.16

Intensity ratios for raw Solprene, milled for 10 minutes and pressed for 5 minutes at 100°C

Intensity ratios Take-off angle	C_{1s}/O_{1s}	C_{1s}/Si_{2p}
30°	13	25
70°	6	9

The C_{1s} spectrum reveals a symmetrical peak, arising from the carbon framework together with a low intensity ($\sim$ 1.5%) of $\pi \rightarrow \pi^*$ transitions, separated by $\sim$ 7.0 eV from the main photoionisation peak. The relative intensity of the shake-up satellite at 30° take-off angle is slightly higher than for 70° take-off angle; and, therefore, a low level of oxygen may not be associated with oxidative degradation of the Solprene surface since silicon was also detected at a reasonable level. The shake-up intensity for 30° electron take-off angle is slightly lower than that required for statistical sampling of the repeat unit.

4.3.5 Summary of an ESCA investigation of a series of Solprene 1204 elastomers

The schematic representation in Figure 4.7 summarises the ESCA investigation of a variety of Solprene 1204 elastomers (cured on a calendering system at 150°C in air with a 2 mm nip setting to draw into sheets) that the results are complementary to Natsyn 2200 systems in chapter three. The levels of antioxidant and accelerators are higher at the surface than in the bulk, whilst the level of zinc increases with increasing ESCA depth profile into the bulk. The details of the bulk formulation in terms of weight and normalised mole % are indicated in Table 4.1.

The optimum cured type 1 and type 4 elastomers indicate a decrease in the sulphur functionality with increasing cure time than the corresponding partially cured systems, suggesting thatthe higher level of sulphur present at the surface of partially cured type 1 and type 4 is lost either by evaporation or by blooming on a prolonged exposure to heat

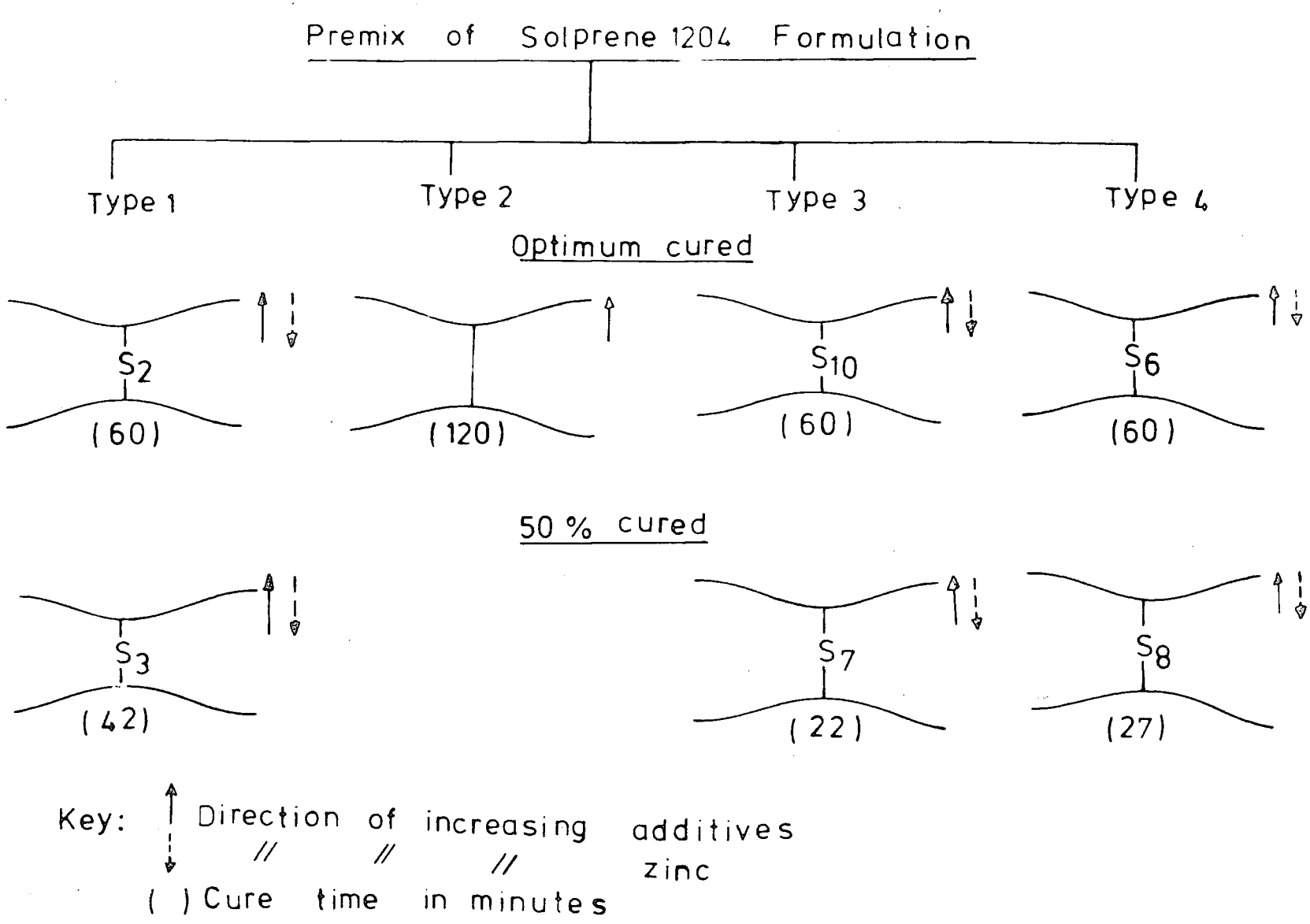

Figure 4.7. Schematic representation of changes in the surface region as in the rubber vulcanisation.

on a calendering system at 150°C, whereas the increase in sulphur functionality for the optimum cured type 3, in contrast to the type 1 and type 4 systems, is most likely to be associated with the diffusion of sulphur from the bulk to the surface. The rate of loss of sulphur is, therefore, manifested by the extent of volatilisation, which causes a concentration gradient near the surface.

It is also of interest to compare the Zn_{3p}/S_{2p} ratios, particularly of low binding energy components of S_{2p}, of a variety of elastomers with the theoretical value (1.5), and the relevant data are indicated in Table 4.17.

Table 4.17

Ratios of Zn_{3p}/S_{2p} LBE (low binding energy components of S_{2p} levels) for a variety of Solprene 1204 elastomers

Type	1	2	3	4
Optimum cure	3.2	-	1.3	1.9
50% cure	3.7	-	2.1	1.6

A comparison of data with the theoretical value (1.5) suggests that more sulphur is needed in the surface region than is added into the bulk. Conversely, it equally implies that excess zinc is present in the surface regions than is required for the Solprene 1204 formulation.

4.3.6 Infrared spectra

The MATR spectra for a variety of Solprene 1204 elastomers have been obtained by placing the samples of appropriate size

against the reflector plate of thalium bromo-iodide (KRS-5) with a refractive index of 2.4 and with a 45° angle of incidence. The details of MATR spectroscopy are provided in chapter three. It is convenient to deal with the representative examples since the MATR spectroscopic examination revealed similar spectra for the various types of elastomers.

Figure 4.8 illustrates the spectra of type 1, Solprene 1204, elastomer as a function of cure time (on a calendering system at 150°C in air), whose detailed bulk composition is indicated in Table 4.1. The IR bands at 11.0, 10.1, 7.1 and

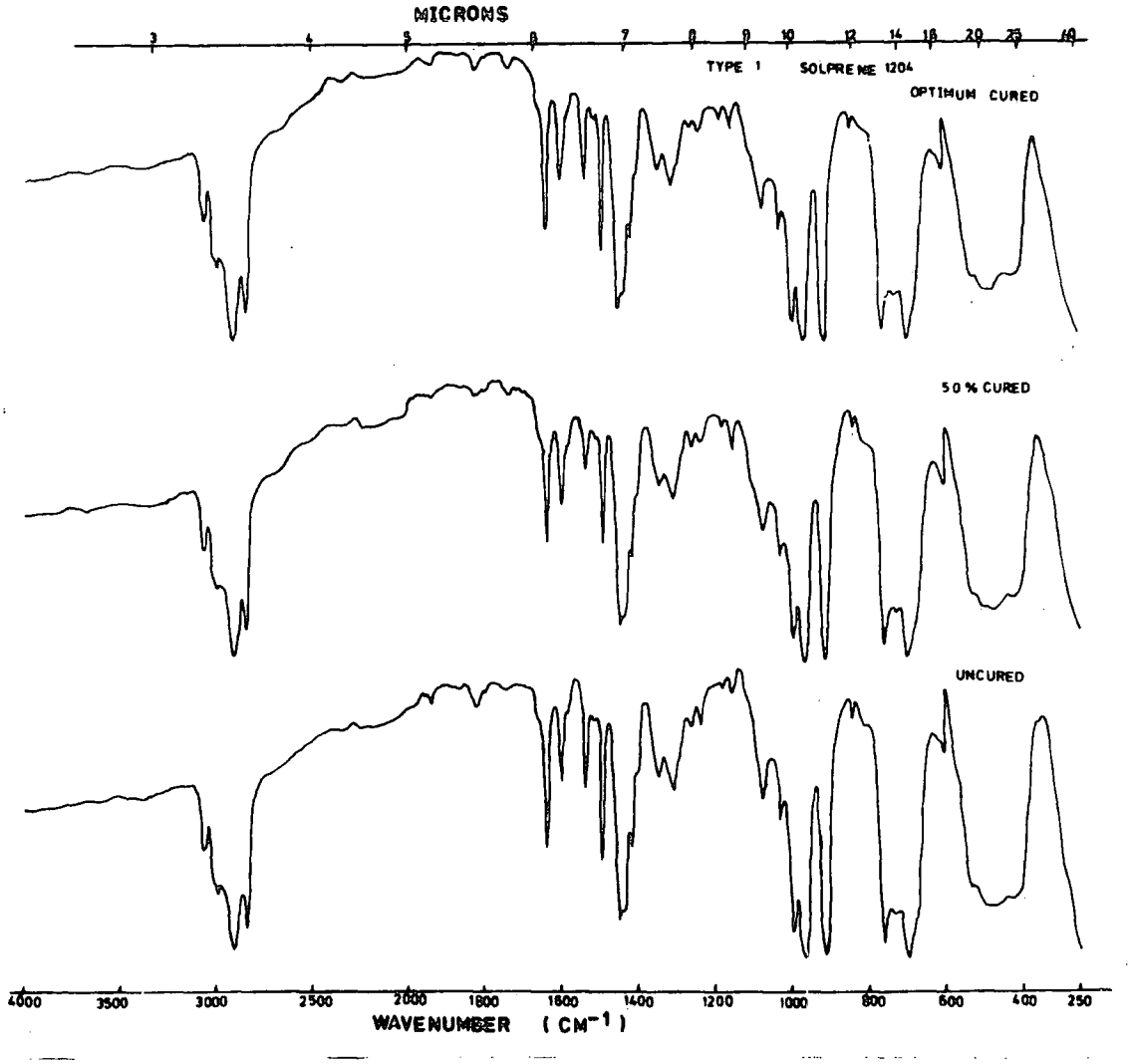

Figure 4.8. Infrared spectra of type 1 Solprene.

6.1 microns are attributed to $-CH=CH_2$ units, while the strong absorption at 6.9 micron signifies the saturation of these vinyl bonds. The very strong appearance of a peak at 10.35 micron can be identified as 1,4-polybutadiene, with cyclised structures and a small amount of trans-CH=CH- units.

The strong absorptions at 13.2 and 14.3 microns are characteristics of pendant monosubstituted benzene rings. A comparison of spectra with the ESCA data clearly reveals that the polystyrene is situated below the ESCA profile depth $< 50\text{Å}$. However, it is not possible to obtain information of minor structures resulting from crosslinking structures or additives. Further details of IR assignments can be found elsewhere.[106,107]

CHAPTER FIVE

AN ESCA INVESTIGATION OF A SERIES OF KRYNAC 34/50 CURED ELASTOMERS

PART III

5.1 Introduction

This last chapter, as a continuation to the systematic study of elastomers, is exclusively concerned with the ESCA investigation of as received nitrile rubbers. The detailed compositions of the bulk formulation for a variety of Krynac (nitrile) 34/54 elastomers are given in Table 5.2. The ingredients are added to obtain the desired properties.[1,2,366-368] The elastomers were cured on a calendering system at 150°C in air with a 2 mm nip setting to draw into sheets for the ESCA study.

The nitrile rubbers are chemically unsaturated copolymers of butadiene and acrylonitrile (66% butadiene and 34% acrylonitrile by weight) that undergo vulcanisation reactions in the presence of sulphur and other vulcanising agents (chapter one); and, the so formed vulcanisates are resistant to a wide variety of liquids, in particular oils.

The nitrile rubbers are prepared in emulsion systems similar to those used for styrene-butadiene (SBR) rubbers. A typical polymerisation recipe is shown in Table 5.1. In general terms, the monomers are emulsified in water and agitated at a constant temperature before a catalyst is added to generate free radicals and, hence, initiation of polymerisation After the desired degree of polymerisation, a short-stop is added to inactivate the catalyst. The residual monomers are removed from the emulsion system by degassing and vacuum distillation and, then, a stabiliser or antioxidant is added to protect the raw polymer during drying and storage periods. The emulsifiers are usually alkali salts of sulphonated alkyl

Table 5.1

Typical polymerisation recipe (parts by weight)

Butadiene	67.0
Acrylonitrile	33.0
Water	200.0
Emulsifier	3.5
Modifier	0.5
Electrolytes	0.3
Catalyst	0.1
Activator	0.05
Short-stop	0.1
Stabiliser	1.25

aryl carboxylic acids, not the fatty acids as employed in the polymerisation of SBR. The 'hot' polymerisation system employs an alkali metal persulphate or an organic peroxide as a catalyst that generates free radicals through thermal decomposition. The 'cold' polymerisation system employs an organic hydroperoxide that requires an activator to initiate the generation of free radicals by reduction of the catalyst. The 'redox' activator contains a chelated ferrous salt and a sulphoxylate reducer, and is used in conjunction with a catalyst such as cumene hydroperoxide. An alkyl mercaptan is employed as a modifier to control the degree of polymerisation and, hence, the Mooney viscosity of the nitrile rubbers. It is anticipated that the use of ingredients containing sulphate groups in the polymerisation recipe and the high sensitivity

of ESCA may lead to ambiguous interpretation on the nature of oxidation of organic sulphides linking the polymer chains.

5.2 Experimental

The experimental procedure has already been described in the preceding chapters.

Samples of raw Krynac 34/50 and the cured Krynac, partially and fully cured systems in Table 5.2, were received with protective sheets of either pigmented polyethylene (cured samples) or polyethyleneterephthalate (uncured Krynac 34/50). In all cases, the samples have been handled in air and cut to a size (20 mm x 6 mm x 2.5 mm), with a pair of scissors, appropriate for mounting onto the spectrometer probe tip. Spectra were recorded with an AEI ES200B spectrometer using $Mg_{K\alpha_{1,2}}$ radiation and $Au_{4f_{7/2}}$ level at 84 eV binding energy for calibration purposes had a FWHM of $\sim$ 1.2 eV. The spectra were resolved and integrated with a DuPont curve resolver.

5.3 Results and Discussion

5.3.1 ESCA analysis of cured samples

(a) Type 1, Krynac 34/50, elastomer

(i) Introduction

The bulk formulation of type 1, Krynac 34/50, elastomer in terms of weight and normalised mole % terms in Table 5.2 suggests that the C_{1s} signal intensity should predominantly be derived from the Krynac framework with small contributions from CBS, stearic acid and permanax B, whilst the N_{1s} signal would be expected predominantly from the Krynac itself as opposed to the nitrogen of CBS and permanax B. The S_{2p} signal

Table 5.2

Krynac 34/50 Formulations

(a) Type	1		2		3		4	
	weight (%)	mole (%)	weight (%)	mole (%)	weight (%)	mole (%)	weight (%)	mole (%)
Krynac 34/50	90.5	95.7	90.7	95.8	85.8	90.7	97.6	99.5
Zinc oxide	4.5	3.2	4.5	3.2	-	-	-	-
Cadmium oxide	-	-	-		4.3	1.9	-	-
Sulphur	1.4	0.31	0.2	0.04	0.4	0.1	-	-
CBS	0.9	0.21	-	-	-	-	-	-
Stearic acid	1.8	0.36	0.9	0.18	1.3	0.26	-	-
Permanax B	0.9	0.23	0.9	0.23	0.9	0.22	1.0	0.24
Dicup R	-	-	-	-	-	-	1.4	0.30
Maglite D	-	-	-	-	4.3	6.1	-	-
Ethyl Cadmate	-	-	-	-	2.1	0.5	-	-
MBT	-	-	-	-	0.9	0.3	-	-
TMTD	-	-	2.7	0.65	-	-	-	-
Cure time (minutes) at 150°C								
50% (partial)	15		14		3		-	
100% (optimum)	45		40		20		120	

Ethyl Cadmade	Cadmium diethyl dithiocarbamate
MBT	Mercapto benzthiazole
Maglite D	Magnesium oxide
CBS	Cyclohexylbenzthiazyl sulphenamide
Permanax B	Acetone/diphenylamine condensate antioxidant
TMTD	Tetramethylthiuram disulphide

(b) Raw polymer:- contains only Krynac 34/50.

should predominantly arise from the added sulphur itself as opposed to the sulphur of CBS. Zinc is added to the formulation as the oxide, which complexes with accelerators to form a sulphurating agent (chapter one), and one objective of the ESCA investigation is to affect a chemical speciation, in particular of zinc and sulphur. The O_{1s} signals can conceivably arise from the residual metal oxide (low binding energy), from carboxylate and oxygen in stearate and permanax B respectively, and from any oxidative functionalisation from sulphur (sulphate additives used in the polymerisation recipe of Krynac 34/50) or from oxidation of the Krynac surface during cure. In principle, the ESCA provides five measurable levels to define a C:O:N:S:Zn surface stoichiometry. Apart from any detail of fine structure, which potentially might provide additional information, the measurement of only five levels does not allow an ambiguous assignment of surface composition. Some simplifying assumptions are, therefore, required to enable an analysis to be affected. The first of these is that the ratios of minor additives are the same at the surface as in the bulk and, secondly, the C:N surface stoichiometry for the cured samples is the same as raw Krynac without additives to enable unambiguous surface analysis. The C_{1s}/N_{1s} intensity ratio of 26 provides 9 moles of butadiene and 1 mole of acrylonitrile at the surface of the as received raw Krynac without additives (section 5.3.2b).

(ii) Optimum cured, type 1, Krynac 34/50 elastomer

The angular dependent data in Table 5.3, extracted from the raw spectra in Figure 5.1, indicate that the optimum cured type 1, Krynac 34/50, sample is inhomogeneous, in terms of stoichiometry, as a function of ESCA profile depth into the sample. The C_{1s} level at 30° electron take-off angle reveals a broadened signal compared with the C_{1s} level at 70° take-off angle (FWHM 2.0 vs. 1.7 eV respectively), and the $\pi \rightarrow \pi^*$ transitions from the π system of butadiene are absent. The surface is considerably oxidised, as is evidenced by the high energy tail of C_{1s} envelope and by the development of a broad band, centred at a binding energy of $\sim$ 168.0 eV in the S_{2p} region.

Table 5.3

Optimum cured type 1, Krynac 34/50, elastomer

Intensity ratios

Take-off angle	C_{1s}/O_{1s}	C_{1s}/N_{1s}	C_{1s}/S_{2p}	C_{1s}/Zn_{3p}	Zn_{3p}/S_{2p}	S_{2p} oxidised %
30°	7	19	22	14	1.6	5
70°	7	111	36	19	1.9	20

The high resolution spectra also reveal zinc nitrogen, a low level of silicon (as contaminant) and sulphur, the latter (S_{2p} levels) being broadened by the presence of at least two components, the higher binding energy peaks after deconvolution are attributed to organic sulphide (including polysulphide), and the lower binding energies to zinc sulphide (FWHM 3.8 eV

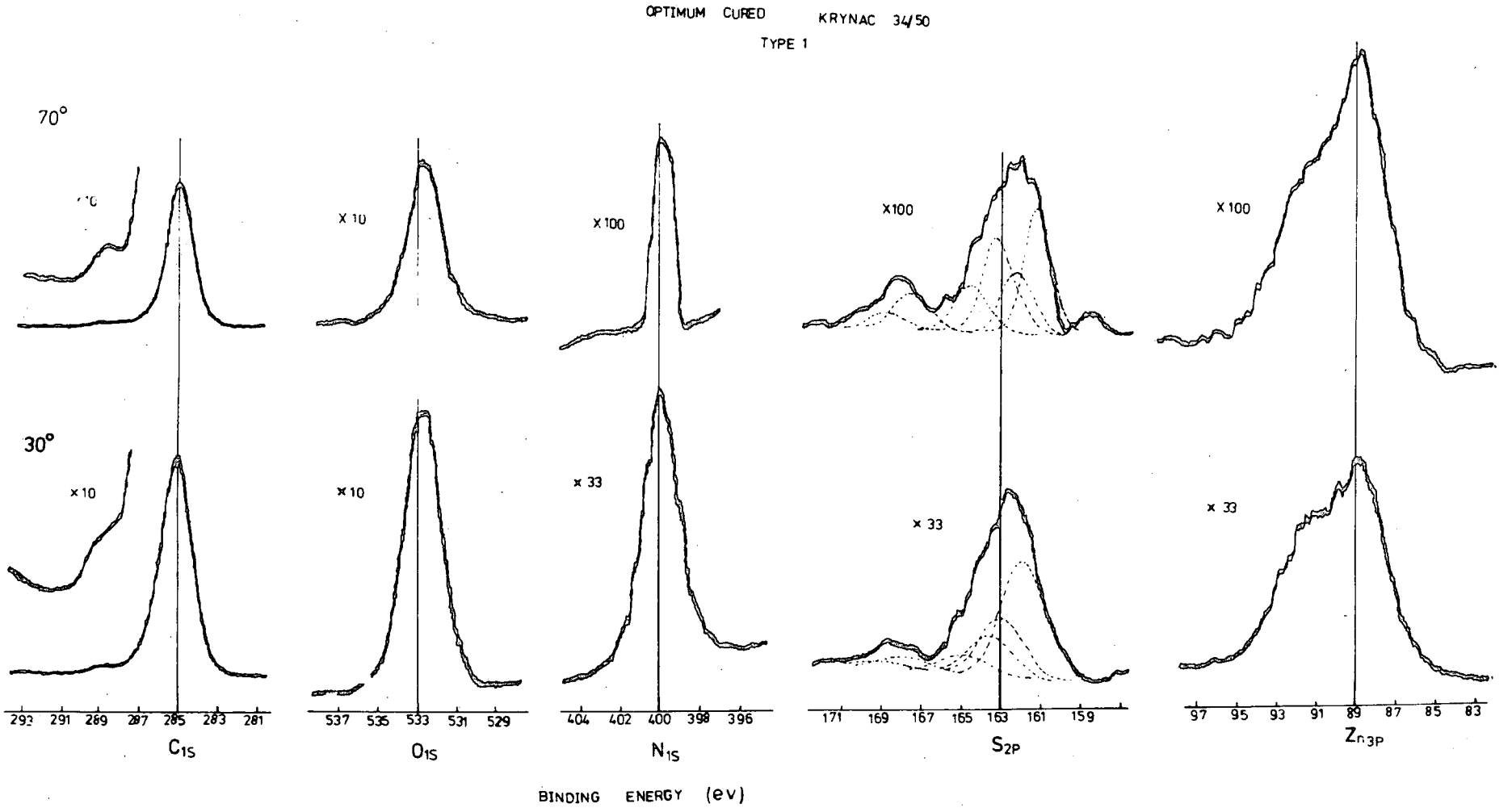

Figure 5.1. High resolution spectra of an optimum cured type 1, Krynac 34/50, elastomer.

of S_{2p} for the 'sulphur-vulcanised' vs. 2.2 eV of S_{2p} for ZnS).

The bulk formulation of the type 1 elastomer in Table 5.2 gives a mole ratio of CBS to permanax B of 1:1.1. The C_{1s} signal intensity derives predominantly from the Krynac 34/50 framework with smaller contributions from CBS, stearic acid and permanax B, whilst the N_{1s} signal arises predominantly from the Krynac itself as opposed to the nitrogen of CBS and permanax B. The bulk composition of butadiene and acrylonitrile in Table 5.2 (66% and 34% by weight respectively) does not allow a straightforward surface analysis. The C_{1s}/N_{1s} intensity ratio of 26 for the as received raw Krynac 34/50 without additives, corrected for the differences in cross-section, gives a mole ratio of butadiene to acrylonitrile of 9:1 at the surface compared to the bulk values (2:1 respectively), and provides a means of assessing the surface stoichiometry unambiguously as a function of depth, monitored by ESCA. A crude surface analysis may be performed, as follows:-

Let x = moles % of Krynac

Let y = moles of CBS, then permanax B = 1.1y

Total C_{1s} signal = 39x + 13y + 15 x 1.1y

Total N_{1s} signal = x + 2y 1.1y

$$\therefore \frac{39x + 29y}{x + 3.1y} = \frac{19}{0.84} = 23$$

$$\frac{x}{y} \simeq 2.6$$

The value of $\frac{x}{y}$ for 30° take-off angle in Table 5.4, therefore gives ratios of 100:3.8:4.2 in moles for Krynac,

Table 5.4

Optimum cured type 1, Krynac 34/50, elastomer

Surface composition

Take-off angle	Krynac	CBS	Permanax B	Zn
30^{o}	100	3.8	4.2	2.7
70^{o}	100	-2.5	-2.7	2.0

CBS and permanax B respectively, indicating higher levels of additives (by a factor of eighteen) than in the bulk, whilst the level of zinc is approximately the same as in the bulk ($\sim$ 3.1 mole %). The data for 70^{o} take-off angle suggest that there is insufficient nitrogen present in the extreme surface region (of thickness < 10Å) for this to be substantiated. However, the C_{1s}/S_{2p} intensity ratio, corrected for the differences in cross-section, suggests higher level of sulphur at the surface than in the bulk and this is predominantly from the added sulphur itself.

(iii) 50% cured type 1, Krynac 34/50, elastomer

The high resolution spectra revealed that the surface of the as received elastomer is considerably oxidised, as is evidenced by the high energy tails of C_{1s} envelopes and by the appearance of broad bands at high binding energies of S_{2p} levels. It is not possible to state with certainty that the appearance of oxidised S_{2p} level is due to the oxidation during cure or arises from the sulphate groups of the ingredients used in the polymerisation recipe of butadiene and acrylonitrile (Table 5.1). This interpretation seems less likely,

however, since it would require considerable retention of the sulphur containing species, added in low amount in the polymerisation process. The C_{1s} levels at 30° take-off angle are broadened, compared with the C_{1s} levels at 70° take-off angle (FWHM 2.1 eV vs. 1.5 eV respectively). The S_{2p} signals show the same extent of broadening at both take-off angles by the presence of at least two components; organic sulphide and zinc sulphide (FWHM 4.0 eV for both take-off angles vs. 2.2 eV of S_{2p} for ZnS).

The angular dependent data in Table 5.5 indicate that the surface is inhomogeneous, in terms of stoichiometry, as a

Table 5.5

50% cured type 1, Krynac 34/50, elastomer

(a) Intensity ratios

Take-off angle	C_{1s}/O_{1s}	C_{1s}/N_{1s}	C_{1s}/S_{2p}	C_{1s}/Zn_{3p}	Zn_{3p}/S_{2p}	S_{2p} oxidised %
30°	6	61	21	15	1.4	26
70°	6	38	49	18	2.7	50

(b) Surface composition (mole %)

Take-off angle	Krynac	CBS	Permanax B	Zn
30°	100	-1.7	-1.9	2.5
70°	100	-0.5	-0.6	2.1

function of depth into the sample and, there is insufficient nitrogen in the surface region for the surface analysis to be true. Alternatively, the surface analysis may be carried out

unambiguously by reconsidering the bulk composition of Krynac 34/50 in Table 5.2 (19 moles of butadiene and 1 mole of acrylonitrile) and the results are given in Table 5.6. This type of analysis again indicates inhomogeneous surface and higher levels of additives are detected at the surface than in the bylk. The level of zinc increases only slightly with increasing ESCA depth into the sample.

Table 5.6

50% cured type 1, Krynac 34/50, elastomer

Surface composition

Take-off angle	Krynac	CBS	Permanax B
30^{o}	100	0.15	0.17
70^{o}	100	1.5	1.7

In addition to the C_{1s}, O_{1s}, S_{2p}, N_{1s} and Zn_{3p} signals, the high resolution spectra also revealed silicon contamination at a reasonable level (C_{1s}/S_{2p} intensity ratio of 25).

(b) Type 2, Krynac 34/50, elastomer

(i) Introduction

The bulk composition of type 2 elastomer in Table 5.2 indicates that the C_{1s} intensity should predominantly derive from the Krynac framework with smaller contributions from additives, whilst the N_{1s} signal is expected predominantly from the Krynac itself as opposed to the nitrogen of permanax B and TMTD. The S_{2p} signal should arise predominantly from the sulphur of TMTD as opposed to the added sulphur. The O_{1s}

signals can conceivably arise from residual zinc oxide, from carboxylate and oxygen in stearate and permanax B respectively, and from the oxidation of Krynac during cure. In principle, the type 2 sample provides C_{1s}, O_{1s}, N_{1s}, S_{2p} and Zn_{3p} levels as a means of assessing the surface composition unambiguously, on the same assumptions stated previously (9 moles of butadiene: 1 mole of acrylonitrile).

(ii) Optimum cured type 2, Krynac 34/50, elastomer

The relevant intensity ratios of core level spectra in Figure 5.2 together with the surface composition are set out in Table 5.7. The angular dependent study reveals that the surface is reasonably homogeneous, as a function of ESCA depth

Table 5.7

Optimum cured type 2, Krynac 34/50 elastomer

(a) Intensity ratios

Take-off angle	C_{1s}/O_{1s}	C_{1s}/N_{1s}	C_{1s}/S_{2p}	C_{1s}/Zn_{3p}	Zn_{3p}/S_{2p}	S_{2p} oxidised %
30°	8	6	2.2	6	0.4	-
70°	7	6.6	2.3	6	0.4	-

(b) Surface composition (mole %)

Take-off angle	Krynac	Permanax B	TMTD	Zn
30°	100	21	60	6.1
70°	100	16	44	6.1

profile into the sample and very high levels of additives are present at the surface compared to the bulk. The increase in

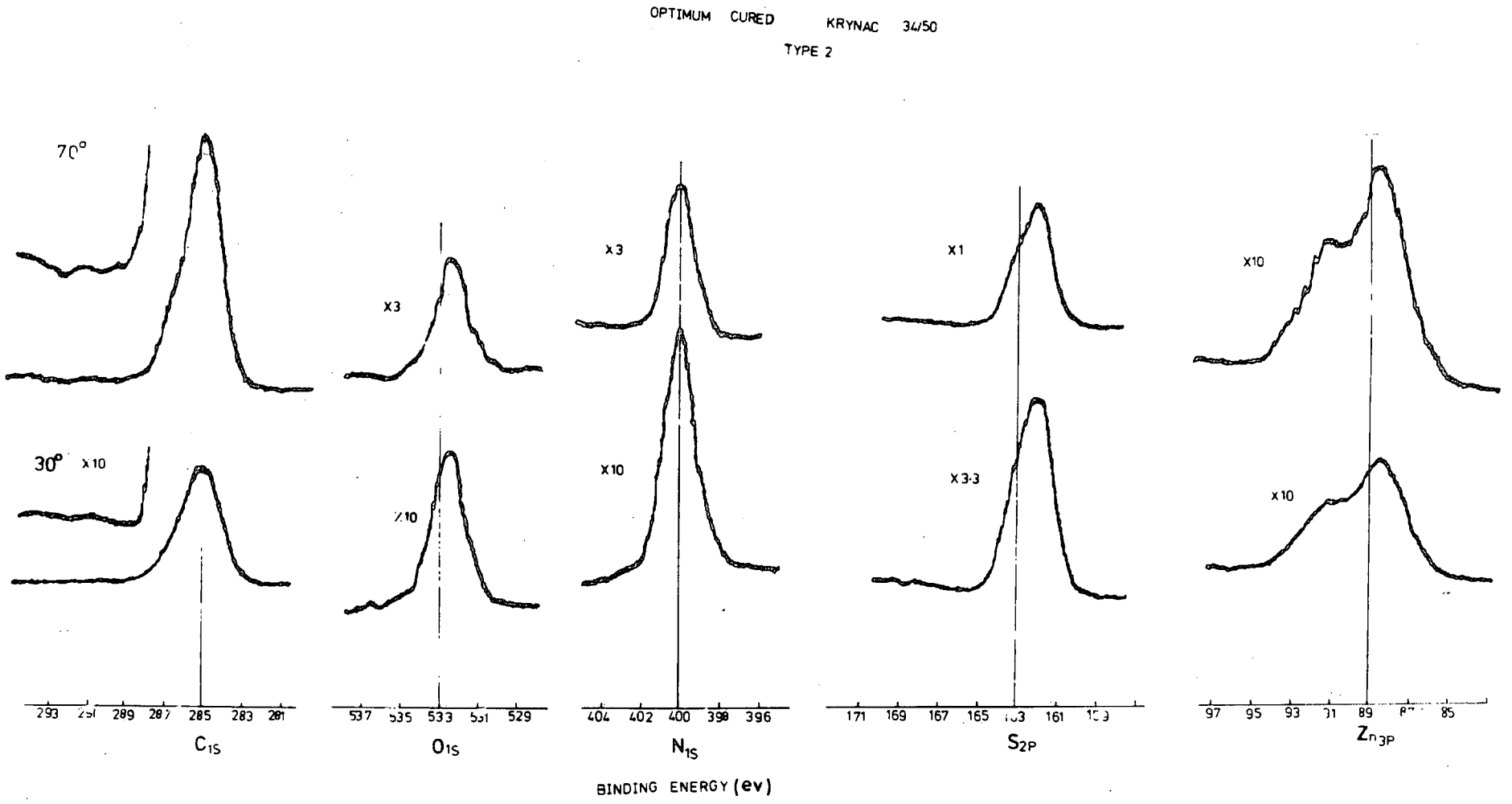

Figure 5.2. High resolution spectra of an optimum cured type 2, Krynac 34/50, elastomer.

the level of zinc by a factor of two at the surface, compared to the bulk, is conceivably associated with the attachment to the polymer or to the TMTD. The types of interaction of the zinc are thought to be:

Krynac (polymer)

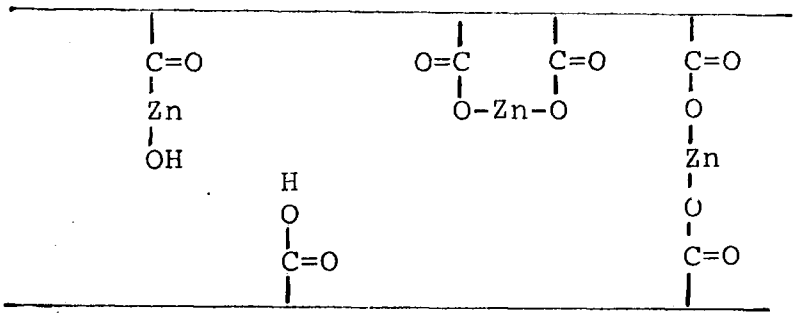

TMTD

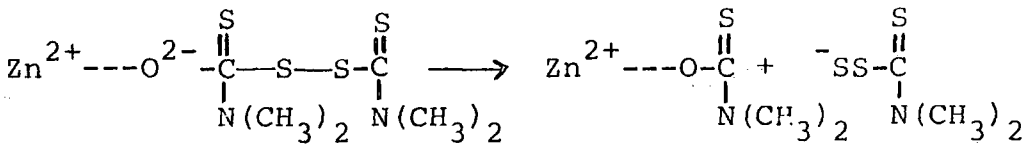

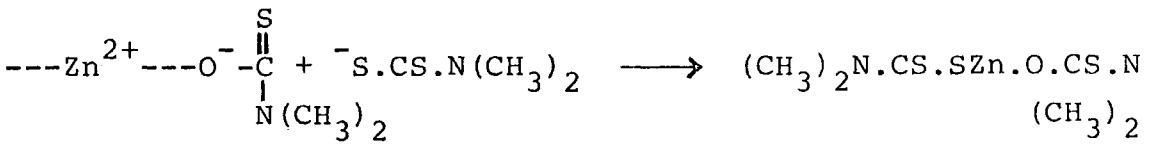

It has been stated in chapter one that, in the TMTD-ZnO system, TMTD reacts exothermically with ZnO at ~ 150°C to form zinc perthiolate complex and this acts as a sulphurating agent. The high level of TMTD at the surface also accounts for the high level of S_{2p} signal intensity.

The effect of the interaction of metal oxide and the polymer is to produce a vulcanisate with unusual characteristics, probably being good heat resistance and high level of abrasion resistance.

The C_{1s} spectra at 30° and 70° take-off angles reveal oxidative functionalisation, as is evidenced by the high energy tail of C_{1s} envelope with FWHM of 2.6 eV and 2.3 eV respectively; whereas the S_{2p} signal did not show any tendency of oxidation at binding energy ∿ 168 and the S_{2p} unoxidised peaks at binding energy ∿ 162.0 with FWHM of 2.4 eV for both take-off angles, compared to the FWHM of S_{2p} for ZnS (2.2 eV), suggests that the sulphur is predominantly in the form of ZnS.

The high resolution spectra also reveal oxygen and zinc at reasonable levels, and a low level of silicon is present as contaminant.

(iii) 50% cured type 2, Krynac 34/50, elastomer

The data in Table 5.8 indicate that the surface of the as received sample is reasonably homogeneous as far as the ESCA depth profile is concerned and higher levels of additives are present at the surface than in the bulk. The increased level

Table 5.8

50% cured type 2, Krynac 34/50, elastomer

(a) Intensity ratios

Take-off angles	C_{1s}/O_{1s}	C_{1s}/N_{1s}	C_{1s}/S_{2p}	C_{1s}/Zn_{3p}	Zn_{3p}/S_{2p}	S_{2p} oxidised %
30°	12	8	2.8	7.4	0.4	-
70°	9	8	3.2	9	0.4	-

(b) Surface composition

Take-off angle	Krynac	Permanax B	TMTD	Zn
30°	100	10	27	5.0
70°	100	10	27	4.1

of zinc at the surface again suggests that zinc is chemically bonded either to the polymer or to the TMTD, but the latter seems more probable as is supported by the appearance of S_{2p} at low binding energy ($\sim$ 162 eV), compared to the binding energy of free sulphur ($\sim$ 164.0 eV). The FWHM of S_{2p} peak is the same order of magnitude for S_{2p} in ZnS (FWHM 2.5 eV for 30^{o} and 2.3 eV for 70^{o} take-off angles vs. 2.2 eV of S_{2p} for ZnS), and the S_{2p} level does not indicate any tendency for oxidative functionalisation, which, in turn, may suggest that the sulphur is predominantly in the form of ZnS.

The surface is considerably oxidised, as is indicated by the development of oxidative functionalisation at high binding energy tail of C_{1s} envelope.

The high resolution spectra also revealed nitrogen, zinc and relatively a low level of silicon as contaminant.

(c) Type 3, Krynac 34/50, elastomer

(i) Introduction

It is clear from the bulk formulation of type 3 elastomer in Table 5.2 that the C_{1s} intensity should predominantly arise from the Krynac system, with smaller contributions from stearic acid, permanax B, ethyl cadmate and MBT, whilst the N_{1s} signal would be expected predominantly from the Krynac itself as opposed to the nitrogen of permanax B and MBT. The S_{2p} signal should predominantly arise from the added sulphur itself and from the sulphur of ethyl cadmate as opposed to the sulphur of MBT. Cadmium is added as cadmium oxide and ethyl cadmate to replace the ZnO as a cure activator. Magnesium oxide is added to the compound as an acid acceptor. Ethyl

cadmate accelerator interacts with the cadmium oxide and other sulphur donating accelerators (MBT); and, one objective of the ESCA investigation is to affect a chemical speciation, in particular of cadmium and sulphur. The O_{1s} signals can conceivably arise from the residual metal oxides (CdO and MgO), from carboxylate and oxygen in stearate and permanax B respectively, and from any oxidative functionalisation from sulphur (sulphate additives used in the polymerisation of Krynac 34/50), or from oxidation of the polymer surface during cure on a calendering system at 150°C in air. In principle, the ESCA provides six measurable levels to define a C:O:N:S:Cd:Mg surface stoichiometry unambiguously, assuming 9 moles of butadiene to 1 mole of acrylonitrile.

(ii) Optimum cured type 3, Krynac 34/50, elastomer

The core level spectra at 30° and 70° electron take-off angles are indicated in Figure 5.3 and the relevant intensity ratios together with the surface composition are set out in Table 5.9. The angular dependent data indicate that the surface is reasonably homogeneous, as far as the ESCA depth profile is concerned, and higher levels of antioxidant and accelerator are present at the surface (by a factor of sixty) than in the bulk in contrast to the level of cadmium (∿ 2.4 mole % in the bulk), which the latter decreases with increasing ESCA depth profile into the sample.

The C_{1s} spectra at both take-off angles reveal oxidative functionalisation, as is evidenced by the high binding energy tail of C_{1s} envelope with FWHM of 2.3 eV and 2.0 eV respectively; whereas the S_{2p} peaks do not indicate any tendency for oxidation

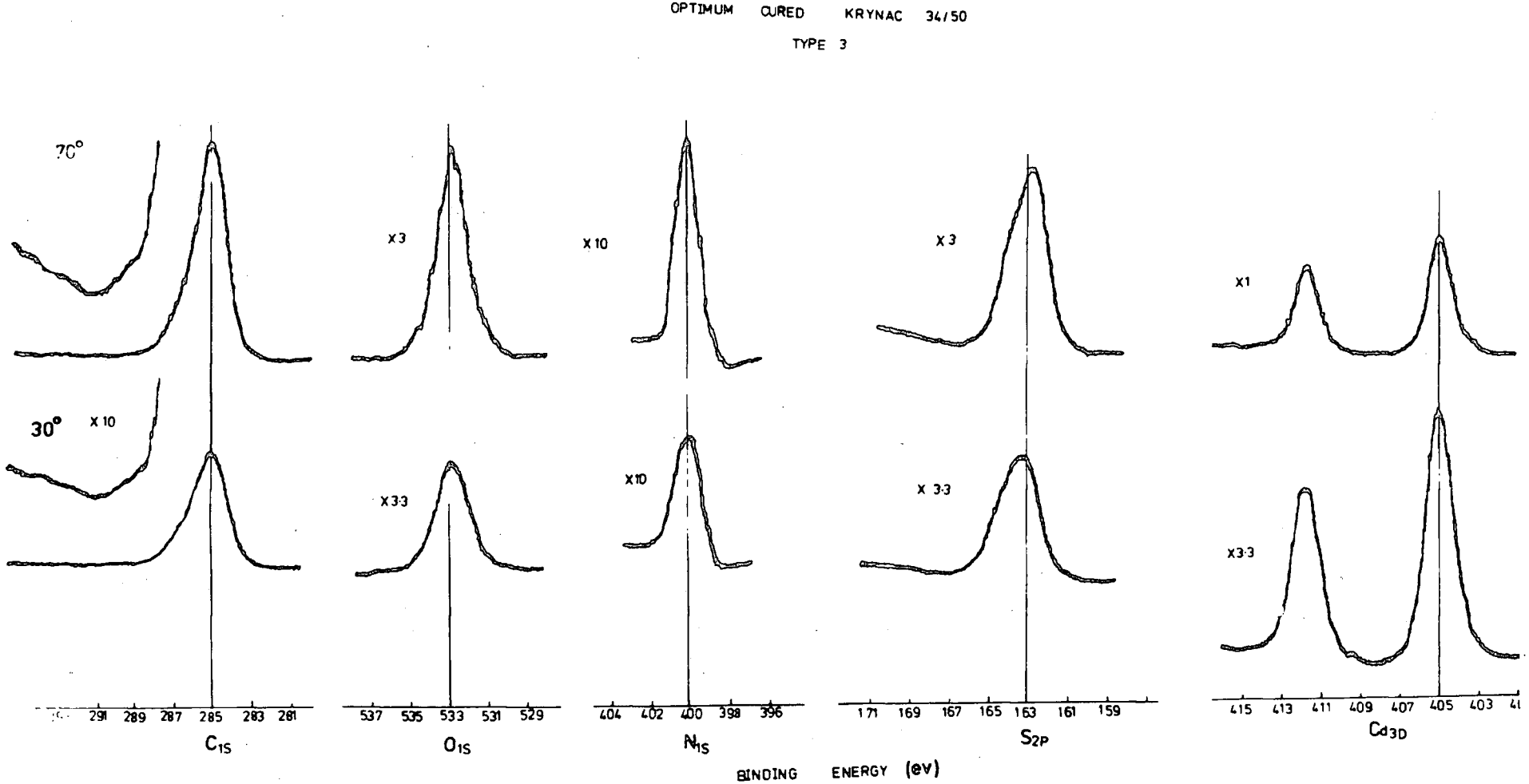

Figure 5.3. High resolution spectra of an optimum cured type 3, Krynac 34/50, elastomer.

Table 5.9

Optimum cured type 3, Krynac 34/50, elastomer

(a) Intensity ratios

Take-off angle	C_{1s}/O_{1s}	C_{1s}/N_{1s}	C_{1s}/S_{2p}	$C_{1s}/Cd_{3D_{5/2}}$	$Cd_{3D_{5/2}}/S_{2p}$	S_{2p} oxidised
30^{o}	3.6	14	3	2.0	1.5	-
70^{o}	3.4	15	3.4	2.7	1.3	-

(b) Surface composition (mole %)

Take-off angle	Krynac	Permanax B	MBT	Cd
30^{o}	100	15	21	4.0
70^{o}	100	12	16	3.0

at binding energy $\sim$ 168.0 eV and the appearance of S_{2p} (unoxidised) peaks at binding energy $\sim$ 162 eV with FWHM of 2.6 eV for 30^{o} and 2.4 eV for 70^{o} take-off angles compared to the FWHM of S_{2p} for ZnS (2.2 eV) suggests that the sulphur is predominantly in the form of CdS.

The high resolution spectra also reveal oxygen and zinc at reasonable levels, and a low level of silicon is present as contaminant.

(iii) 50% cured type 3, Krynac 34/50, elastomer

The data for the partially cured sample at 30^{o} and 70^{o} take-off angles in Table 5.10 indicate that the surface is inhomogeneous in terms of stoichiometry, as a function of ESCA depth profile into the sample; and higher levels of permanax B and MBT are present at the surface than in the bulk. The

Table 5.10

50% cured type 3, Krynac 34/50, elastomer

(a) Intensity ratios

Take-off angle	C_{1s}/O_{1s}	C_{1s}/N_{1s}	C_{1s}/S_{2p}	$C_{1s}/Cd_{3D_{5/2}}$	$Cd_{3D_{5/2}}/S_{2p}$	S_{2p} oxidised %
30^{o}	6.0	13	2.5	1.6	1.6	-
70^{o}	6.0	10	2.4	1.8	1.3	-

(b) Surface composition (mole %)

Take-off angle	Krynac	Permanax B	MBT	Cd
30^{o}	100	20	27	5.0
70^{o}	100	65	91	4.5

level of cadmium is higher at the surface than in the bulk. The FWHM of S_{2p} peak is the same order of magnitude for S_{2p} in ZnS (FWHM 2.4 for 30^{o} and 70^{o} take-off angles vs. 2.2 eV of S_{2p} for ZnS), and the S_{2p} level does not indicate any tendency for oxidative functionalisation, which suggests that the sulphur is again predominantly present as CdS.

The surface is considerably oxidised, as is evidenced by the development of oxidative functionalisation at high binding energy tail of C_{1s} envelope.

The high resolution spectra also revealed a low level of silicon as contaminant.

(d) Type 4, Krynac 34/50, elastomer

(i) Introduction

The detailed composition of the bulk formulation in Table 5.2 suggests that the C_{1s} intensity should predominantly arise

from the Krynac framework, with smaller contributions from permanax B and dicumyl peroxide, whilst the N_{1s} signal would be expected predominantly from the Krynac itself, as opposed to the nitrogen of permanax B. The C_{1s} signal can conceivably arise from permanax B, dicumyl peroxide and from the oxidation of Krynac surface during cure. In principle, the ESCA provides C_{1s}, O_{1s} and N_{1s} measurable levels as a means of assessing the surface stoichiometry unambiguously, on the assumption that the ratio of moles of butadiene to acrylonitrile is 2:1.

(ii) Optimum cured type 4, Krynac 34/50, elastomer

The data in Table 5.11, extracted from the raw spectra in Figure 5.4, indicate that the surface is homogeneous, in terms

Table 5.11

Optimum cured type 4, Krynac 34/50, elastomer

(a) Intensity ratios

Take-off angle	C_{1s}/O_{1s}	C_{1s}/N_{1s}
30°	5	12
70°	4	18

(b) Surface composition (mole %)

Take-off angle	Permanax B	Dicumyl peroxide
30°	4.7	6.5
70°	21	27

of stoichiometry, as a function of ESCA depth profile into the sample and the level of antioxidant increases with decreasing

level of nitrogen in the surface regions (this interpretation is not valid and can be stated unambiguously by considering the C_{1s} signals only from Krynac and antioxidant). The C_{1s} spectra indicate oxidative functionalisation, as is evidenced by the high binding energy tail of C_{1s} envelopes; and the $\pi \rightarrow \pi^*$ transitions, conceivably arising predominantly from the

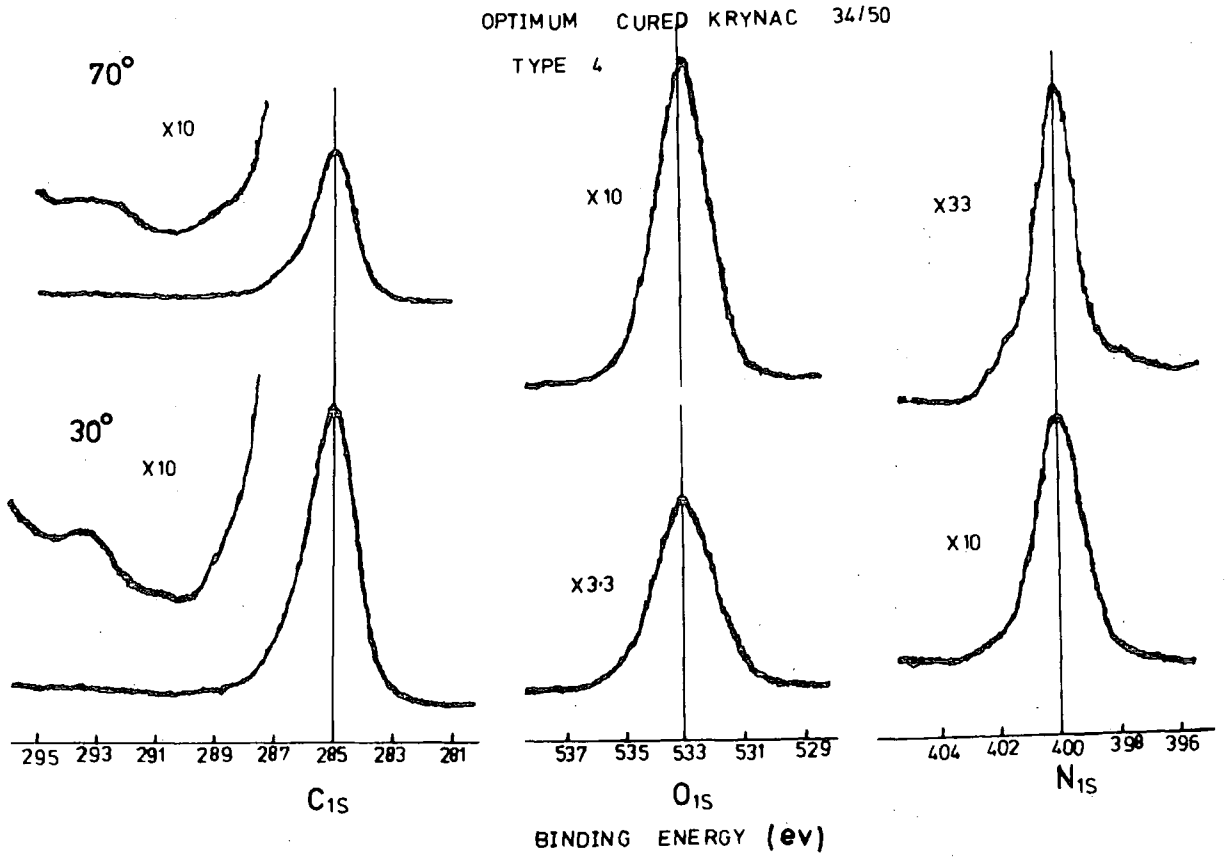

Figure 5.4. High resolution of an optimum cured type 4, Krynac 34/50, elastomer.

aromatic system in antioxidant and dicumyl peroxide, are of a low intensity (< 1%). The high resolution spectra also revealed oxygen and silicon, the latter being relatively of a low level as contaminant.

5.3.2 Uncured Krynac 34/50 samples

(a) Introduction

Two samples of uncured Krynac 34/50 formulation have been received, as follows:

(i) Compressed, emulsion polymerised Krynac 34/50 (66% butadiene and 34% acrylonitrile by weight). Samples have been cut directly for ESCA examination either for the investigation of the as received surfaces or for the fresh surfaces exposed with a scalpel blade.

(ii) Uncured formulation with additives (Table 5.2). As has already been stated in the preceding chapters, the dissolved air in the uncured systems rapidly exploded the samples on introduction to the high vacuum, causing on several occasions contamination of the window. Attempts at cooling the samples, prior to introduction into the spectrometer did not prove successful, and, in only one case, have partial spectra of the uncured type 1, Krynac 34/50, system been obtained.

(b) Emulsion polymerised, Krynac 34/50, sample

(i) As received surface

The wide scan ESCA spectrum for the as received Krynac sample revealed little evidence for anything other than the C_{1s} and O_{1s} photoemission levels. The high resolution spectra are presented in Figure 5.5 and the relevant intensity ratios are set out in Table 5.12.

The C_{1s} levels indicate an asymmetrical peak, associated

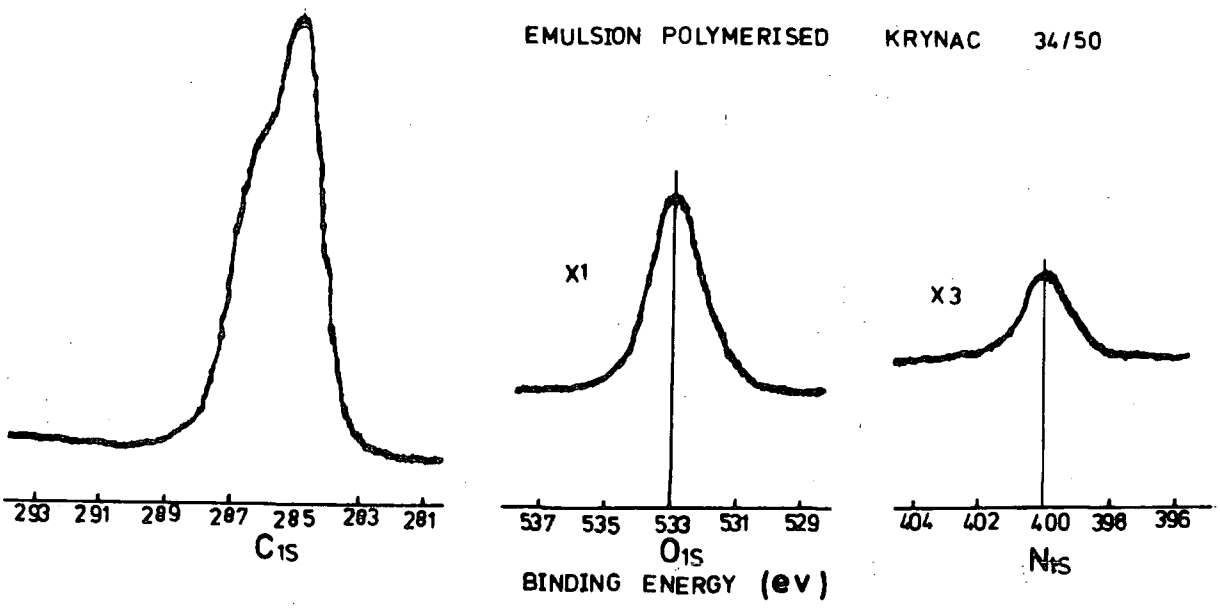

Figure 5.5. High resolution spectra of emulsion polymerised Krynac 34/50.

with oxidative functionalisation at the high binding energy tail of C_{1s} envelope and the surface is extensively oxidised, as is evidenced by the large development of oxidative functionalities at ∿ 286.6 eV and ∿ 288.0 eV binding energies. The high resolution spectra also reveal oxygen and nitrogen at reasonable levels and a very low level of silicon as contaminant. The C_{1s}/N_{1s} intensity ratio after correction for the difference in cross-section gives a mole ratio of butadiene to acrylonitrile of 9:1, compared to the bulk composition (mole ratio of 2:1 respectively). The data

Table 5.12

Intensity ratios for raw Krynac 34/50

	C_{1s}/O_{1s}	C_{1s}/N_{1s}	C_{1s}/Si_{2p}
As received	3.0	26	115
	11	11	100

clearly indicate that the surface is not representative of the bulk.

(ii) Freshly exposed surface

The data for the freshly exposed surface are indicated in Table 5.12 for comparison purposes. The level of oxygen is now substantially lower and the level of nitrogen is considerably higher than the unexposed surface; and, this gives a mole ratio of butadiene to acrylonitrile of 2.5:1 indicating the freshly exposed surface is reasonably representative of the bulk. The slight deviation in the freshly exposed surface composition from the bulk values (2 moles of butadiene and 1 mole of acrylonitrile) may suggest a partial orientation of functional groups; the cyanide groups produce a higher energy state, as a result of their greater polar character than hydrocarbon groups, and the latter is directed outward. The C_{1s} spectrum again indicated an asymmetrical peak, arising from the C-N and C-O and C=O components at binding energies of 285.4 eV, 286.6 eV and 288.0 eV respectively.

(c) Uncured type 1, Krynac 34/50, sample

Figure 5.6 shows the spectra of an uncured Krynac 34/50, sample with additives (whose detailed bulk compositions are

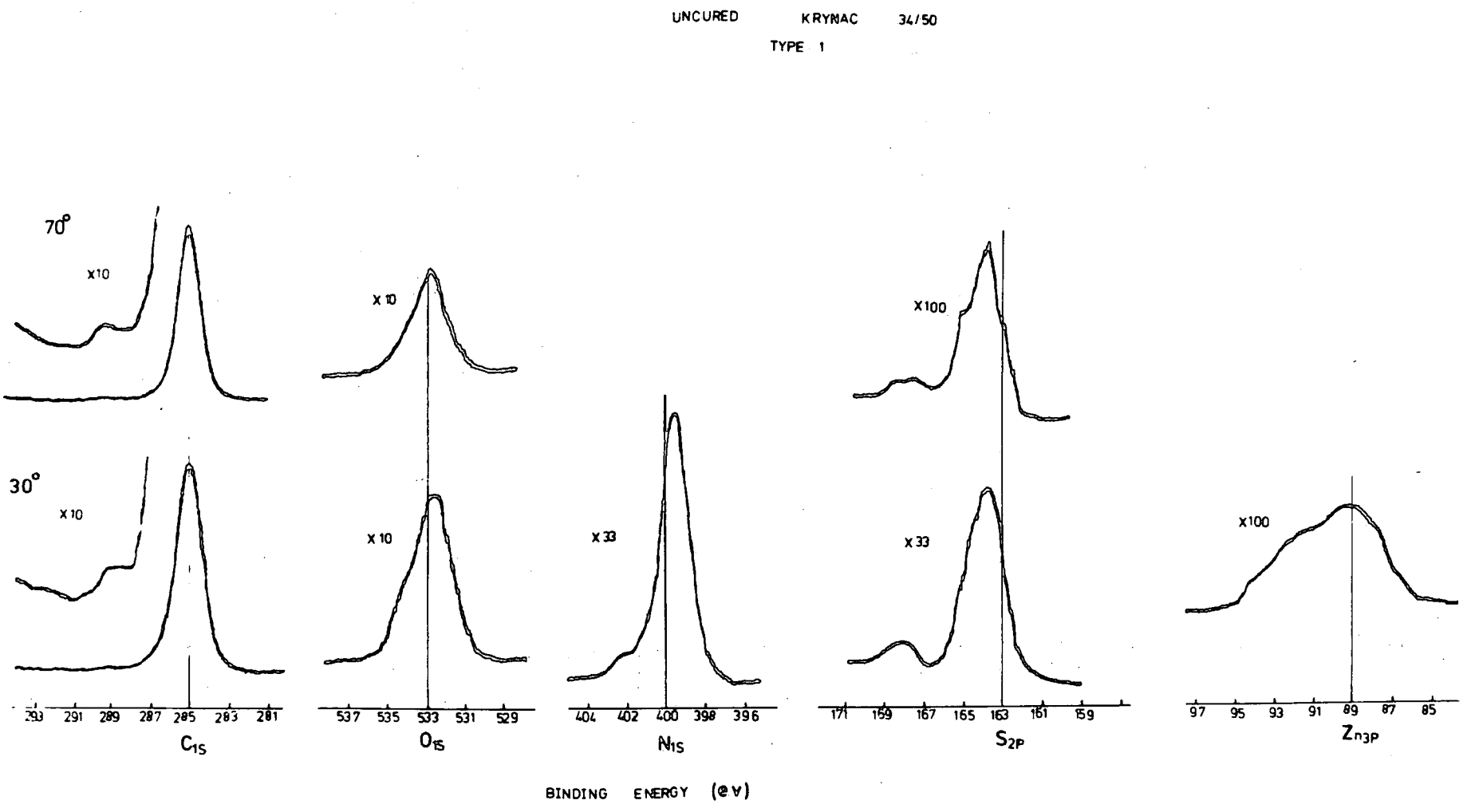

Figure 5.6. High resolution spectra of an uncured type 1, Krynac 34/50, elastomer.

indicated in Table 5.2), and the relevant intensity ratios together with the surface composition are set out in Table 5.13. The data at 30^{o} electron take-off angle indicate that

Table 5.13

Uncured type 1, Krynac 34/50, sample

(a) Intensity ratios

Take-off angle	C_{1s}/O_{1s}	C_{1s}/N_{1s}	C_{1s}/S_{2p}	C_{1s}/Zn_{3p}	Zn_{3p}/S_{2p}	S_{2p} oxidised %
30^{o}	9.0	25	25	66	0.4	14
70^{o}	12	-	29	-	-	12

(b) Surface composition (mole %)

Take-off angle	Krynac	CBS	Permanax B	Zn
	100	1.4	1.5	0.6

higher levels of CBS and permanax B are present at the surface (by a factor of seven) than in the bulk, whilst the level of zinc, less than in the bulk, increases with increasing ESCA depth profile into the sample. (It should be noted that the protective sheets of polyethyleneterephthalate was removed by dipping into liquid nitrogen before examining the sample. The ESCA examination of peeled-off protective sheets in chapter three indicated very little or no mechanical transfer of materials and, therefore, it may be concluded that the curing process results in an increase of zinc level at the surface compared to uncured surface, although, in both uncured and cured systems, the level of zinc is lower at the surface than

in the bulk.)

The C_{1s} levels show very little tendency for oxidation and the high level of oxygen at 30° and 70° take-off angles is from H_2O as contaminant during the cooling process, as is evidenced by the distinct broadening of a shoulder at high binding energy of O_{1s} envelope. The S_{2p} levels reveal very little oxidation at a binding energy ∿ 168.0 eV, and the appearance of S_{2p} peaks at binding energy ∿ 164.0 with FWHM of 2.5 for both take-off angles, compared to the FWHM of free sulphur itself, suggests that the sulphur is present as organic sulphide (S_8 and S-C).

The high resolution spectra also revealed a low level of silicon as contaminant.

5.3.3 Summary of ESCA investigation of a series of Krynac 34/50 elastomers

The ESCA investigation of a variety of Krynac 34/50 elastomers (cured on a calendering system at 150°C in air with a 2 mm nip setting to draw into sheets) revealed that higher levels of antioxidant and accelerators are present at the surface than in the bulk. The type 2 and type 3 samples indicated higher levels of zinc and cadmium in the surface regions, whilst the level of zinc in type 1 system increases only slightly with increasing ESCA depth profile into the sample. Zinc and cadmium in the surface regions are predominantly present as sulphides. The surface compositions of elastomers are assessed unambiguously on preferential segregation of polybutadiene and polyacrylonitrile that the surface is heavily covered with a layer of polybutadiene.

CHAPTER SIX

SURFACE MODIFICATIONS OF MODELS AND ELASTOMERS BY OXYGEN PLASMA

PART I

6.1 Introduction

Chemical reactions, initiated by electrical discharges, have been known for over a hundred years.[200] Areas of considerable technological and academic importance in the surface modification of polymers and solids, in general, have, however, only become the subject of detailed research interest in the last two decades. The primary focus of interest has been in terms of both the improvement of surface free energy or the wettability of materials[201-213] and in the understanding of oxidative degradation, in general. This interest has been motivated partially by the ability of plasmas to produce unique modification and, the ease, by which, the extent of surface modification can be controlled. The plasma treatment technique has many virtues over chemical and physical methods[214] in that the reactions are inherently 'clean', and take only seconds to achieve the desired results, producing profound changes in the surface properties[215] of the material (permeability, bond ability, printability, etc.), whilst the overall bulk properties of the material reamin unchanged (electrical characteristics, tensile strength, etc.). The technique is, therefore, ideally suited to a flow system. However, the surface properties of the material are solely determined by the composition of the outermost few monolayers; and the thickness of the modified layer is typically in the range of 50 - 10^{5}Å,[201,218] depending upon the conditions of the discharges (pressure, power loading, gas, flow rate).

The principal technique employed in this chapter to investigate the surface modification of sulphur-vulcanised

rubbers and model systems affected by oxygen plasma, is that of ESCA, whilst chapter seven is concerned with modifications affected by hydrogen plasmas.

Due to the thinness of such a modified layer, it was not possible to use other conventional techniques to investigate the changes in surface regions. The conventional technique, employed in this field for analysis of the surface, is multiple attenuated total internal reflection (MATR) infrared spectroscopy. This technique like ESCA is non-destructive and, it scans the surface layer to a depth in the order of microns, being much greater than the depth[219] of the plasma modified layer; which, in turn, implies that the infrared spectrum has a very strong absorption from the unmodified substrate and, therefore, the spectrum observed before and after plasma treatment is essentially the same (chapter three).

The term 'cool' plasma, in the field of chemistry, may be defined as a partially ionised gas composed of molecules, atoms, and ions in both ground and excited states and electrons, in which, the numbers of positively and negatively charged species are approximately equal. In a glow discharge, free electrons gain energy from an applied electric field and transfer this energy to molecules through inelastic collisions resulting in the formation of a variety of new species such as metastables, atoms, free radicals, and ions, energetic enough to cause chemical reactions. A wide frequency range of electromagnetic radiation is also produced from the deexcitation of excited states[220] (electronic, vibrational and rotational).

For the ionised gas, produced in a discharge to be properly termed a plasma, it must satisfy the condition of approximate electrical neutrality; a criterion satisfied, when the dimensions of the discharge gas volume are significantly larger than the Debye length (λD), being a function of the square root of the electron energy to density ratio.[221] In (6.1), ε_o is the permittivity of free space, k

$$\lambda D = (\varepsilon_o kTe/ne^2)^{\frac{1}{2}} \qquad (6.1)$$

is the Boltzmann constant, Te is the electron temperature, n is the electron density, and e is the charge on the electron. Figure 6.1 summarises the characteristics of various plasmas occurring naturally and produced in laboratories, defined in terms of their electron density and average electron energy. The region of particular interest to organic chemists is that labelled 'glow-discharges', where the Boltzmann temperature of the massive species is near ambient, whilst the average electron energy is several orders of magnitude greater. These plasmas are termed non-equilibrium, in addition to 'cold plasmas'. By contrast, 'hot plasmas' are very hot ionised gas, in which, the electron and gas temperatures are nearly identical and are usually employed as a high temperature source.

The non-equilibrium plasma may be produced in many ways depending on the cost, ease of construction and convenience. The ease of performance and close control over operating parameters such as the source of electrical power to sustain the plasma, the coupling mechanism and loosely termed plasma environment, has drawn the attention towards the use of

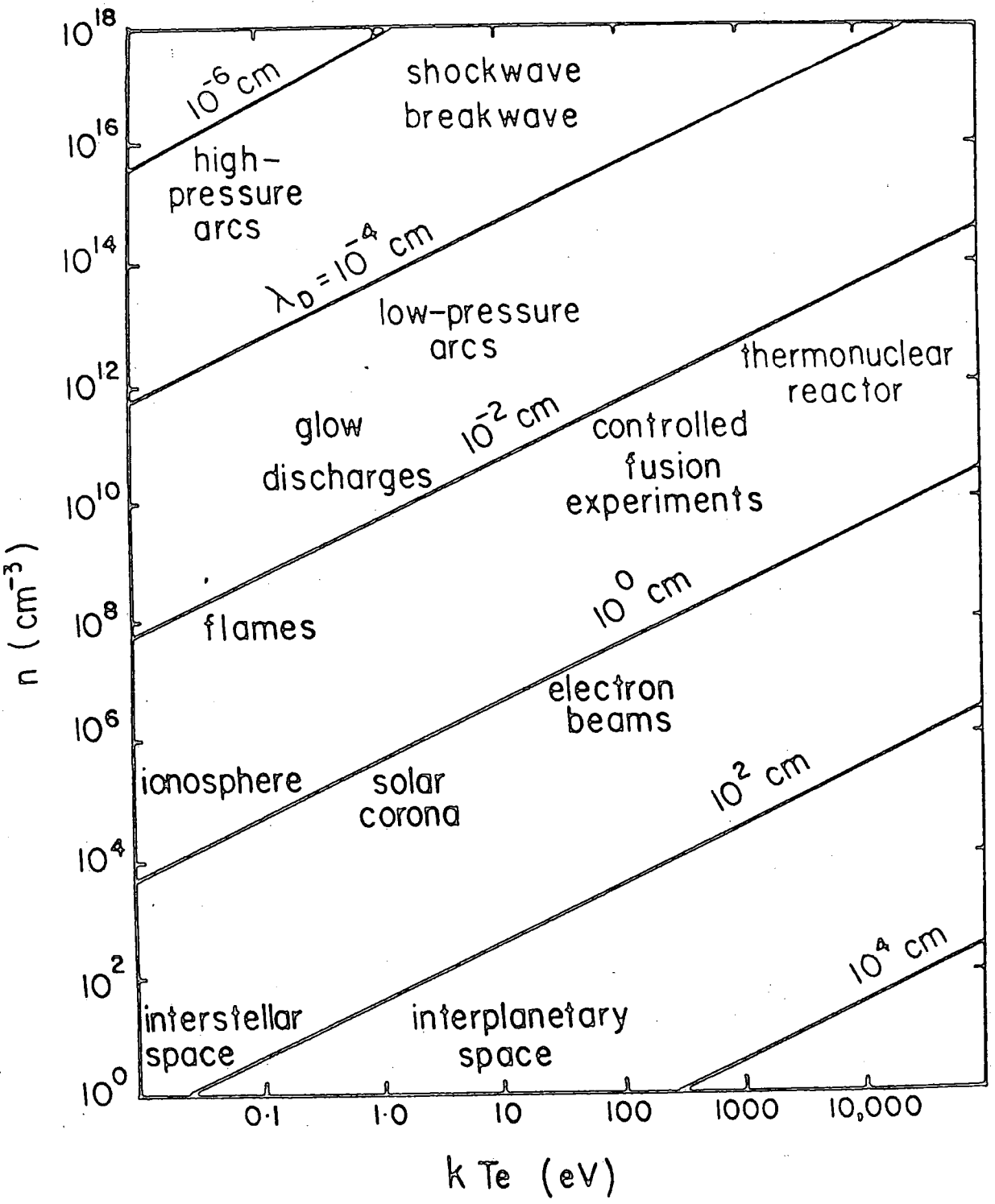

Figure 6.1. Plasmas found in nature and in the laboratory.

inductively coupled radio-frequency and microwave plasmas, whilst most of the early work was based on AC and DC electroded discharges. A good background on radio-frequency discharges is well documented elsewhere.[201,207,222]

The criterion for the selection of electrodeless inductively coupled radio-frequency discharges, excited in pure oxygen for the investigation of surface oxidation of elastomers, in this chapter, enables close examination of all of the variables, which are likely to be encountered and, in addition, allows considerable flexibility in terms of reactor design and configuration for introducing and removing samples. Furthermore, the nature of the technique allows a wide range of pressures and flow rates to be investigated and provides a convenient means of performing kinetic studies as a function of power loading or time. This chapter is exclusively concerned with radio-frequency plasmas excited in pure oxygen.

Although, the plasma treatment of polymers and solids, in general, has been an active area of research interest for some considerable time, in both industrial and academic circles, there is very little information available on the characterisation of plasmas, in terms of the energy distribution of electrons, ions and metastables. Such information is, indeed, only semi-quantitative for very simple systems, despite the fact that the broad theoretical framework has been well documented over the years.[221,223] For an ideal gas, which is not of direct concern here, the solution to the Boltzmann equation leads to a Maxwellian distribution of electron energies. The average electron energies for complex systems

may be analysed by electrical probe measurements[224,225] and direct electron sampling.[226] Figure 6.2 shows the form of the Maxwellian energy distribution for average electron

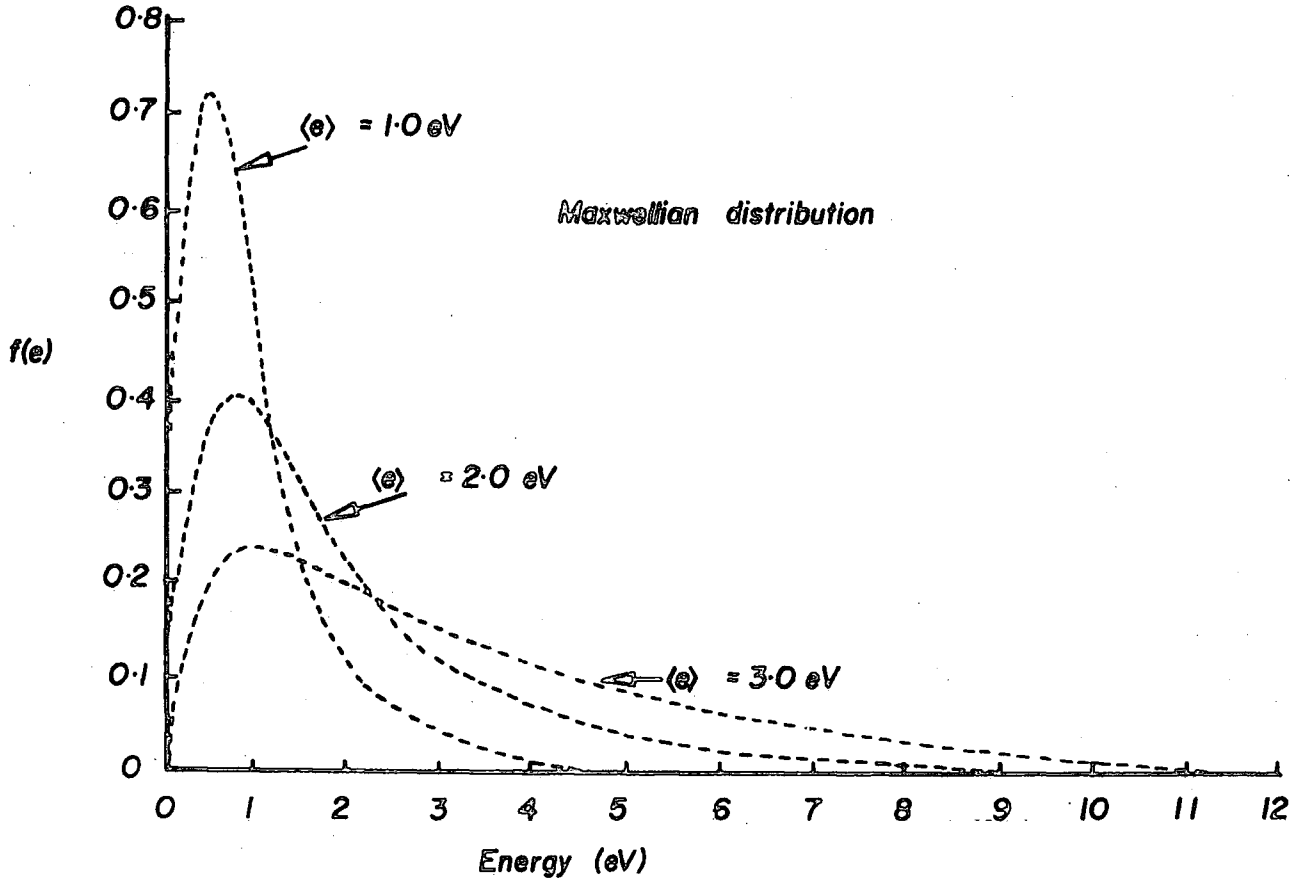

Figure 6.2. Energy distribution of electrons for an ideal gas plasma.

energies of 1.0, 2.0 and 3.0 eV. The average energy expressed in the Boltzmann equation is a function of both the power loading and the pressure. Since, electrons play a dominant

role in the plasma itself, it seems likely that their role is secondary in interactions with polymers.

For plasma excited in oxygen, a very large number of processes appear to take place, the important reactions being between electrons and molecules, ions and molecules, ions and ions, and electrons and ions. Figure 6.3 illustrates the dissociation of some higher energy oxygen states into their

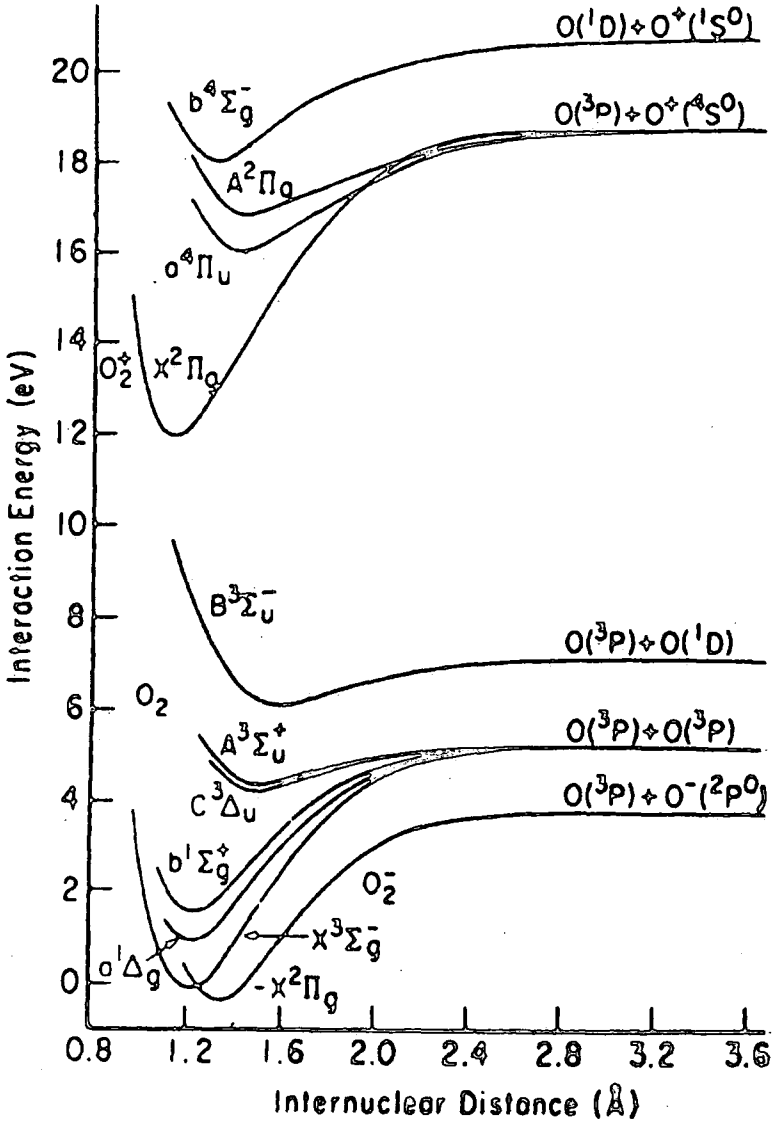

Figure 6.3. Potential energy curves for some states of oxygen.

ground states. The important species capable of undergoing energy transfer to a surface, are the particularly long-lived metastable $a^1\Delta g$ state, which may well further participate in a number of chemical reactions in oxygen discharges. As is clearly evident from the potential energy profile, further excitations of the next higher state leads to the ionisation of the oxygen molecules and the formation of O_2^+ in the $x^2\pi g$ state. In view of the complexities involved in glow discharges, it is not possible to state with certainty, which of the various components are responsible for the surface modification. However, the mean free paths of oxygen ions and metastables in the energy range 0 - 10 eV suggest that they are likely to dominate the direct energy transfer to the outermost surface of few monolayers thickness and, at a greater depth ultra-violet radiation may become a more important factor, in contrast to the situation for electrons.[227,228] The reactions in the outermost few monolayers are primarily due to ion neutral-isation[247] and Penning ionisation[249] of the polymer as the ions and metastables interact with the surface. The possible energy values for these species together with some typical bond energies for organic systems are as follows:

Table 6.1

Plasma	(eV)
electrons	0 - 20
ions	0 - 2
metastable	0 - 20
UV/visible	3 - 40

Chemical bonds	(eV)		(eV)
C-H	4.3	C=C	6.1
C-N	2.9	C=C	8.4
C=O	8.0	C-S	3.2
C-C	3.4	S-S	3.7

Clark and co-workers have shown in an extensive series of publications, how ESCA may be applied to investigate the structure, bonding and reactivity at polymer surfaces.[229-235] The strong dependence of mean free path on the kinetic energy of photoemitted electrons, enables differentiation of the surface, subsurface and bulk. This, and the following chapters are exclusively concerned with the study of plasma treated model compounds (di-, tri-, and tetrasulphides, etc.) and, hence to use this knowledge to elucidate the surface aspects of sulphur-vulcanised elastomers after exposure to plasmas.

6.2 Experimental

6.2.1 Samples

The main emphasis in this chapter has been to investigate the reactions at the solid/plasma interface of model compounds and of some industrially important elastomers, with particular reference to sulphur vulcanised systems. The model compounds (dinonyl trisulphide and ditertiododecyl tetrasulphide etc.) in the form of liquids have been cooled to $\sim$ 200K in the plasma reactor A in Figure 6.4, directly attached to the spectrometer, to avoid the diffusion of oxidised functionalities into the bulk of the compound under investigation after treatment. To facilitate these studies, the liquid samples were spread over a gold strip substrate, cut to a size of a sample probe tip and fixed by small screws, using a clean small spatula.

Model compounds including L. cystine, in the form of a powder, and Natsyn 2200 elastomers, were also mounted on a probe

tip (size of 20 mm x 6 mm and 2.5 mm), and were studied by ESCA, without any pretreatment. Direct handling of the actual samples was avoided to prevent contamination, which could conceivably give rise to extraneous signals.

Oxygen (commercial-grade cylinder gas) was used without further purification.

6.2.2 Instrumentation

The spectra of plasma treated samples were obtained on AEI ES200B spectrometer, using $Mg_{K\alpha_{1,2}}$ radiation of energy 1253.7 eV and $Au_{4f_{7/2}}$ level at 84 eV binding energy for calibration purposes, and under these conditions had a full width at half maximum (FWHM) of 1.15 eV. In all cases, the deconvolution of the spectra were carried out on a Dupont (model 310) Curve Resolver with the possible errors of $\pm$ 0.2 eV in binding energies and the area ratios in the range of $\pm$ 5%.

A Tegal Corporation Radio-frequency Generator, capable of producing a power of up to 100 watts at a frequency of 13.56 MHz was operated in both a continuous and pulse mode, as a matter of convenience, although, depending on the average power loading required. The system, which includes a pulsing facility on a microsecond timescale gives a greater stability to the plasma at low power loadings. A radio-frequency impendence matching network consisting of a vacuum pump with a capacity of 50 litres per minute, and appropriate meters and gauges for monitoring power output and gas flows at the required pressure complete the system.

6.2.3 Plasma configurations

Figure 6.4 shows a schematic representation of reactors A and B, used for the surface modification of model systems and Natsyn 2200 elastomers and, mounted in a greaseless vacuum system, were pumped by a rotary pump at rate of 50 ℓ min.$^{-1}$. Pressures were monitored using Pirani gauges and the oxygen was introduced into the system via a leak value at the required pressure (0.2 torr). Reactor A, particularly designed for studying the model systems, consisted of a pyrex tube 16 cm long and 5 cm in diameter, sandwiched between stainless steel flanges by viton 'O' rings, and was enclosed in a copper cage screen to prevent radio-frequency interference with the electronics of the spectrometer. Reactor A directly coupled to a spectrometer enables considerable flexibility in terms of dealing with liquid samples and the investigations of pressure and power dependence of the surface modifications, without exposure to atmosphere. A sample probe, 60 cm long and ½" in diameter, capable of passing through the reactor, on viton 'O' ring seals and into the spectrometer was used to obtain the spectra of samples without exposing to the atmosphere.

Reactor B is an inverted 'T' shaped configuration with dimensions of 40 cm long, 35 cm high, 6 cm in diameter and, an inlet and outlet diameter of ½". The oxygen discharges are excited in the vertical limb by a copper coil, wound 20 cm from the inlet tube.

The single inlet to the reactors A and B permits an introduction of gas downstream from the external coil. The

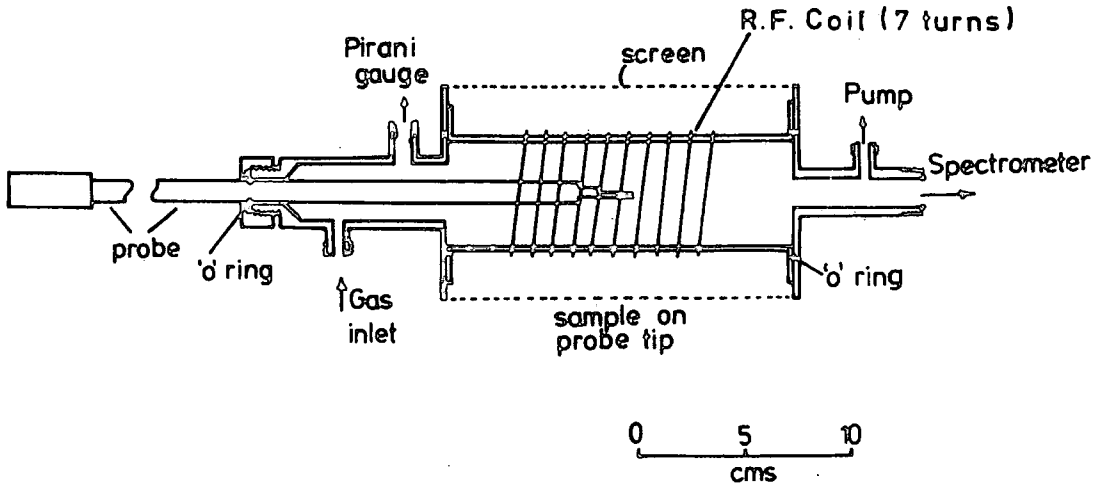

Reactor A

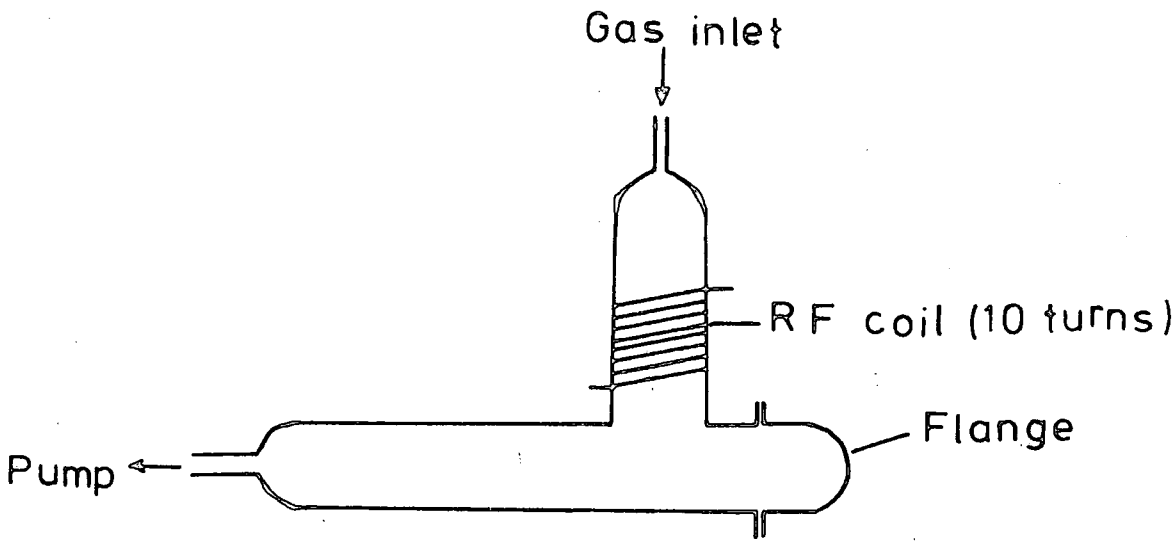

Reactor B

Figure 6.4. Reactor designs A and B.

typical procedure for plasma treatment consisted of initially evacuating the whole system for 20 minutes, followed by leaking the gas into the system at a required pressure for a further 20 minutes before the radiofrequency generator was set for a known power loading prior to the introduction of the sample in the reactor. After the pre-setting of conditions, the pressure in the system was brought to atmosphere for placing the sample in the reactor.

The system with a centrally located sample in the reactor was again evacuated to approximately 4×10^{-2} torr, before the selected gas (oxygen) allowed to flow at a pressure of 0.2 torr to purge the whole system for 20 minutes and then the radio-frequency generator was switched on to the pre-set conditions.

6.2.4 Plasma oxidation of model systems as a function of time

The effects of oxygen glow discharge on the functionalities of model compounds were investigated by monitoring the C_{1s}, O_{1s} and S_{2p} levels, as a function of plasma exposure time.

The procedure for kinetic studies consisted of first inserting the probe into the reactor without a sample such that the probe tip was at a fixed geometry with respect to the reactor. The whole system was purged with oxygen for approximately 20 minutes at the required pressure (0.2 torr) before setting the radio-frequency generator to a known power loading. The probe was then withdrawn and the liquid sample was spread over the gold strip substrate, fixed on the probe tip using small screws, by means of a small spatula ensuring

that the gold surface was completely covered. (This could be readily checked by monitoring the 4f level of the gold substrate, whilst the sample was under investigation.) The system was evacuated on replacing the probe with a mounted sample and, then the pressure was readjusted to flush the reactor for 20 minutes before cooling the probe tip to approximately 200K and, then striking the glow-discharge. The probe tip was further cooled to 160K in the insertion lock of the spectrometer before advancing into the sample chamber, via the 'O' ring seals and a gate valve, for measurement of core level spectra at an electron take-off angle of 30^{o}. The spectra were recorded as rapidly as possible to minimise the hydrocarbon contamination and, a check on this was made by running the C_{1s} level at the start and the finish of the experiment over a period of approximately 1.5 hours.

The cycle of each kinetic run was the same, and, therefore, the investigations were carried out in the usual manner. The choice of time intervals of plasma treatment, increased in the order of 5 secs., 10 secs., 20 secs., gave a convenient spacing of points on the graph.

L.cystine, in the form of a powder, was mounted on a probe tip by means of Scotch tape, ensuring complete coverage of tape surface. The probe tip centrally located in the reactor B was subjected to oxygen plasma treatment at room temperature, before recording the spectra at approximately 200K.

6.3 Results and Discussion

6.3.1 Introduction

The main emphasis of this chapter, with the application of ESCA, has been to determine the nature and extent of functional groups, as a function of oxygen plasma treatment time, developed in the surface regions of models and Natsyn 2200 elastomers, using low temperature oxygen plasma technique.

The backgfound information, in the literature, pertains primarily to the oxidation of organic monosulphides, and to a lesser extent disulphides with relatively few studies on polysulphides. This information arises predominantly from studies of reactions of a variety of reagents in a solution phase, in which, different intermediates, as illustrated in scheme 1, are obtained depending upon the reaction conditions.[242-245] Most intermediates in a solution phase

Scheme 1

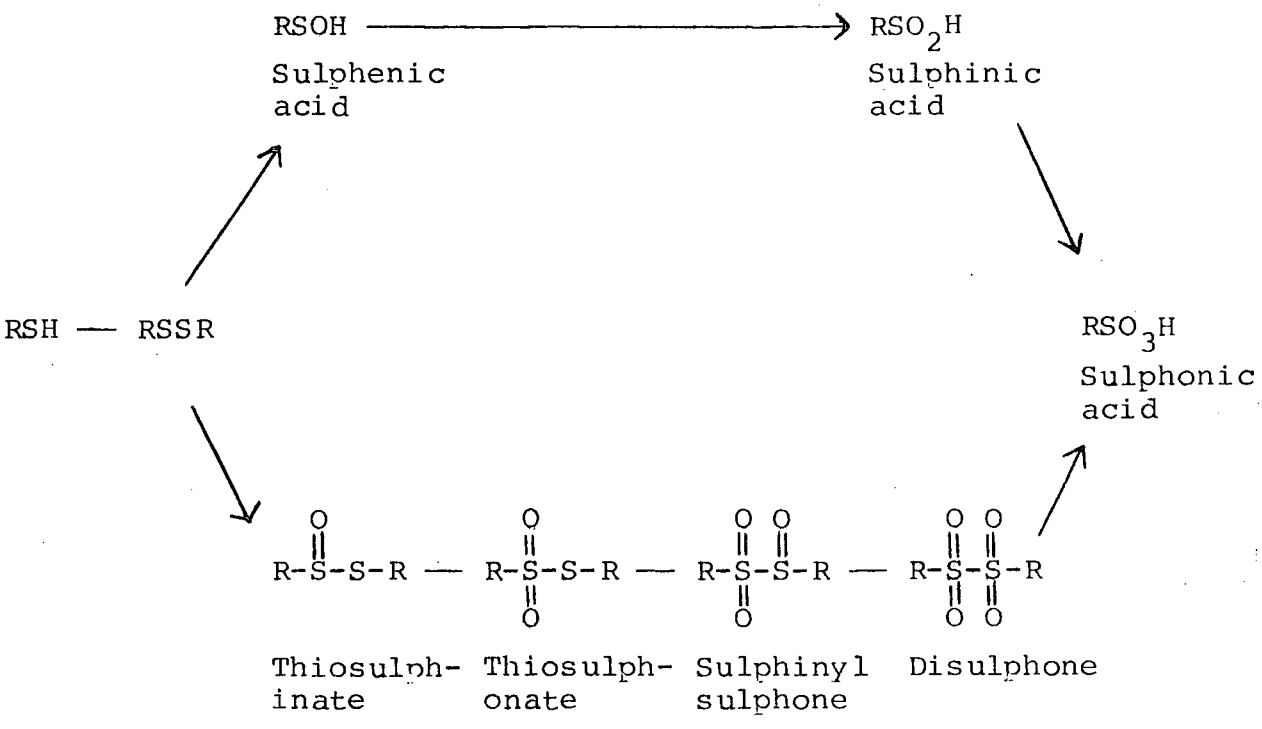

are reversible through appropriate derivatives; however, their true equilibria are quite rare.

The lack of information on the oxidation of higher sulphides in solution and, virtually none on the use of plasma, has been mainly due to the thermal instability, associated with the preparation of derivatives; and, therefore, it is to this problem that ESCA work, coupled with oxygen plasma is addressed. In discussing these results, it is convenient to consider the model investigations first and then to compare these data with those of the elastomers.

The important structural features of carbon (C_{1s}) and sulphur (S_{2p}) in the present study are given in Table 6.2.

Table 6.2

Binding energies for different carbon and sulphur structural features

Structure	Binding energies (eV)
$\underline{C}$-H	285
$\underline{C}$-S	285.4
$\underline{C}$-O	286.6
$\underline{C}$=O	287.9
O-$\underline{C}$=O	289.1
$O_2\underline{C}{=}O$	290.4
$\underline{S}_2$	161.5
C-$\underline{S}$ / S_8	∿ 164.0
$\underline{S}$=O	165.8
O=$\underline{S}$=O	168
$\underline{SO}_3^-$	168.4
$\underline{SO}_4^{2-}$	169.2

For the carbon (C_{1s}) spectrum, a unique deconvolution was performed with a full-width at half maximum of 1.7 $\pm$ 0.1 eV by using an analogue curve fitting procedure, with Gaussian curves positioned at 285, 286.6, 287.9, and 290.4 eV, and treating the height only as a variable. This curve fitting procedure also adapted for the deconvolution of sulphur (S_{2p}) spectra with Gaussian curves positioned approximately at 163.8, 164, 165.8 and 168 eV (taken with the corresponding $2p_{1/2}$, $_{3/2}$ spin orbit split component) produces a unique deconvolution for the S_{2p} spectra.

The allowances for C-ONO_2 and C-NH_2 were not made during the course of deconvolution, which would appear approximately at 287.1 eV and 285.4 eV respectively. The oxygen spectra consisted of a number of closely overlapping peaks, but the attempts were not made to deconvolute them by the method adopted for the C_{1s} spectrum. However, in some spectra, reasonable deconvolutions were achieved for the doubly and singly bonded oxygen. The peroxy structural features, possibly arising in glow-discharge, may then subsequently undergo transformation to other functionalities.

A cursory examination of the various results obtained for model systems and Natsyn 2200 elastomers reveals that the glow-discharge is a very rapid process, resulting in an increase of functionalities, even for a very short period of treatment.

6.3.2 Reactions of models in oxygen plasma

(a) L.cystine in an oxygen plasma as a function of time

Figure 6.5 reveals four distinct readily detectable carbon, nitrogen, oxygen and sulphur levels, whose stoichiometries

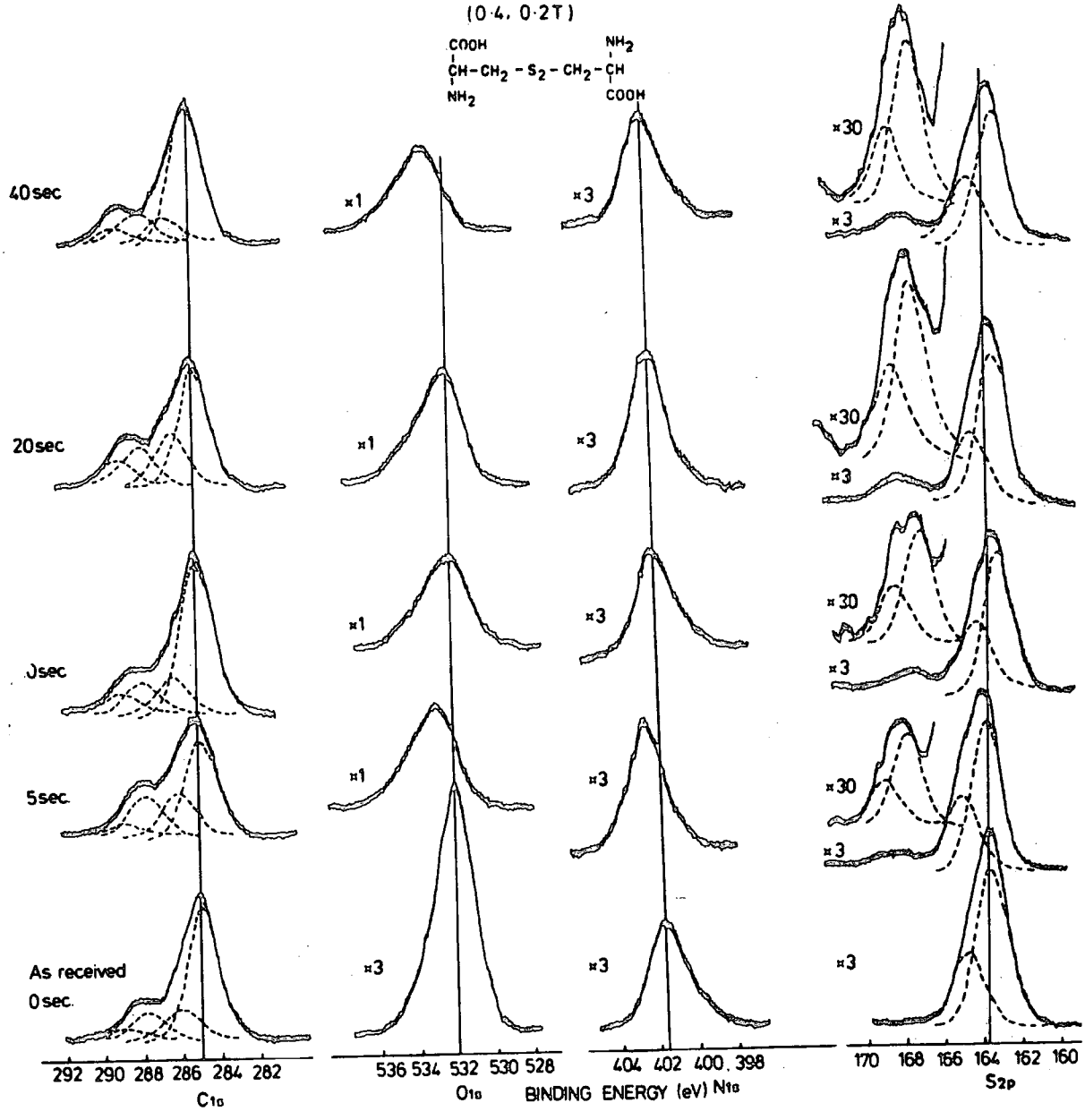

Figure 6.5. C_{1s}, O_{1s}, N_{1s} and S_{2p} spectra of L. cystine vs. time of exposure to an oxygen plasma (0.4 torr, 0.2 torr).

for an untreated sample, derived from the relevant intensity ratios in Figure 6.6a, are not comparable to those of L.cystine itself, indicating that the surface is not entirely representative of the bulk. The derived C:O:N:S stoichiometries of 6:2:1:1 compared to the theoretical values of 3:2:1:1 suggest that the powdered sample must have a surface layer of hydrocarbon contamination and, indeed, the components of the C_{1s} spectra confirm this, the intensity ratios for the components being (C-H) 65 to higher binding energy components (C-N, C(=O)-O etc.) 35 versus the theoretical ratio of 33.3:66.6. Since the sample is typical of that which have been routinely handled in the laboratory, an investigation of the plasma oxidation perhaps mirrors the comparable processing of the sulphur-vulcanised rubbers to be described in section 6.3.5.

The oxygen level for the untreated sample is associated with a singly bonded C-O group, C_{1s} binding energy 286.1 eV, a doubly bonded C=O carbonyl group, C_{1s} binding energy 288 eV and a carboxyl group appearing at 289.2 eV. The presence of a singly bonded C-O group at a rather low binding energy 286.1 eV compared to 286.6 eV of C-O bond suggests that a significant contribution at this position is made from $C-NH_2$ group during the course of deconvolution of C_{1s} peak into C-O, C=O and O-C=O components. The presence of a high concentration of $C-NH_2$ components adds more complications into the method of C_{1s} deconvolution, since the binding energies of C-O and $C-NH_2$ groups are approximately at the same position under the C_{1s} envelope; and, therefore, an attempt was not made to add this particular component. The method of

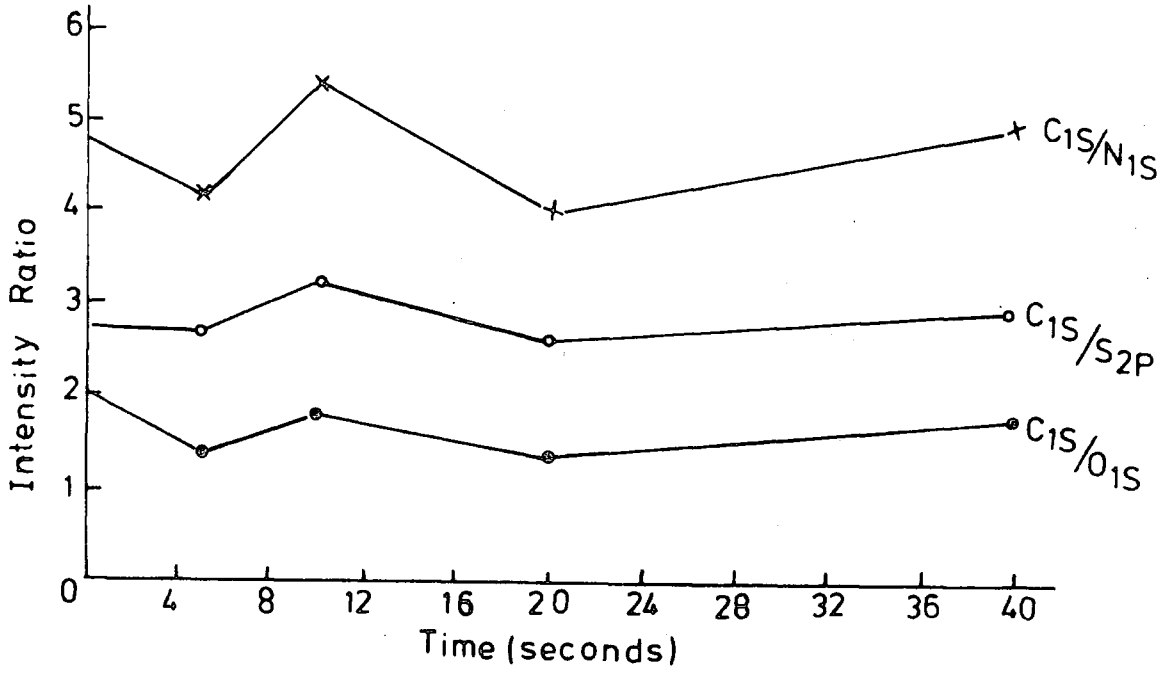

Figure 6.6a. Intensity ratios of the C_{1s}, O_{1s}, N_{1s} and S_{2p} levels in the ESCA spectra of L. cystine vs. time of exposure to the oxygen plasma (0.4 watt and 0.2 torr).

deconvolution was performed, as previously stated, for all the C_{1s} spectra by setting the curve resolver with a number of curves at the required binding energies and fixed full widths at half maxima; and then beginning at the highest binding energy, the curves were added to obtain the best fit for the C_{1s} peak. The total area of the C_{1s} spectrum is taken

as 100 percent. It is clearly apparent that oxygen substituent effects can be treated in terms of an additive model.[236,237] Conceivably, some information can be deduced as to how the carbon and oxygen are bonded in different chemical environments, provided that the area ratios of carbon and oxygen, and their stoichiometries are known in the different chemical environments. For instance, the oxygen singly bonded with carbon, C_{1s} binding energy 286.6 eV, for Natsyn 2200 elastomer, could be a hydroxyl group, either ether C-O-C, peroxide C-O-O-C or a contribution from all of these groups. The hydroxyl and peroxide groups are expected to give the same carbon to oxygen ratio, in contrast to ether linkage C-O-C, the latter being lower than the former; and, therefore, it should, theoretically, be possible to differentiate them. Owing to the difficulties, associated with deconvoluting the O_{1s} spectra into their individual components, it is not always feasible, but one can draw general conclusions as to how the component for C-O bond approximately at 286.6 eV is behaving. Nevertheless, the C_{1s} component at 289.2 eV, corresponding to carboxyl functions and the deconvoluted O_{1s} peak approximately at 534.0 eV can provide limited information on the existence of hydroperoxides. However, it has been shown that direct information for peroxides can be attained by selective chemical transformation to alkyl hydrogen sulphate ($ROSO_2H$) by reaction with SO_2.[238] An examination of the O_{1s} spectra at $\sim$ 534 eV in Figure 6.5 suggests that a significant amount of hydroperoxide is formed after plasma treatment.

The nitrogen N_{1s} peaks suggest more than one type of environment, as is evidenced by the slightly broadened shoulder at a higher binding energy of approximately 402.0 eV. The components at high and low binding energies are attributed to protonated amine and amine C-NH_2 functionalities respectively.

The disulphide linkage in L.cystine shows a tendency for an increase of oxygen functionality at one of its sulphur atoms, whilst the other remains essentially unchanged in the oxygen plasma, even for prolonged treatment, levelling off at 20 seconds as in Figure 6.6b, under a power loading of 0.4 watt and a total pressure of 0.2 torr. The sequence of reactions in the oxygen plasma inferred from this data is as follows:

Scheme 2

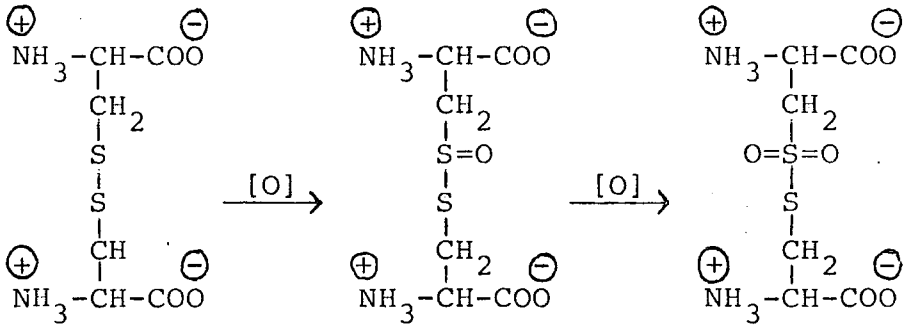

The major product, oxidised 2p level at binding energy approximately 168.3 eV, is (C) compared to (B), which the latter occurring at binding energy 166.5 eV is not observed.

The developments of various carbon-oxygen, carbon-sulphur and sulphur-oxygen features as a function of time are shown in Figures 6.6a-c. The data were accumulated at an electron take-off angle of 30^{o} with samples being cooled to approximately 210K, after having been treated in the oxygen plasma with a total

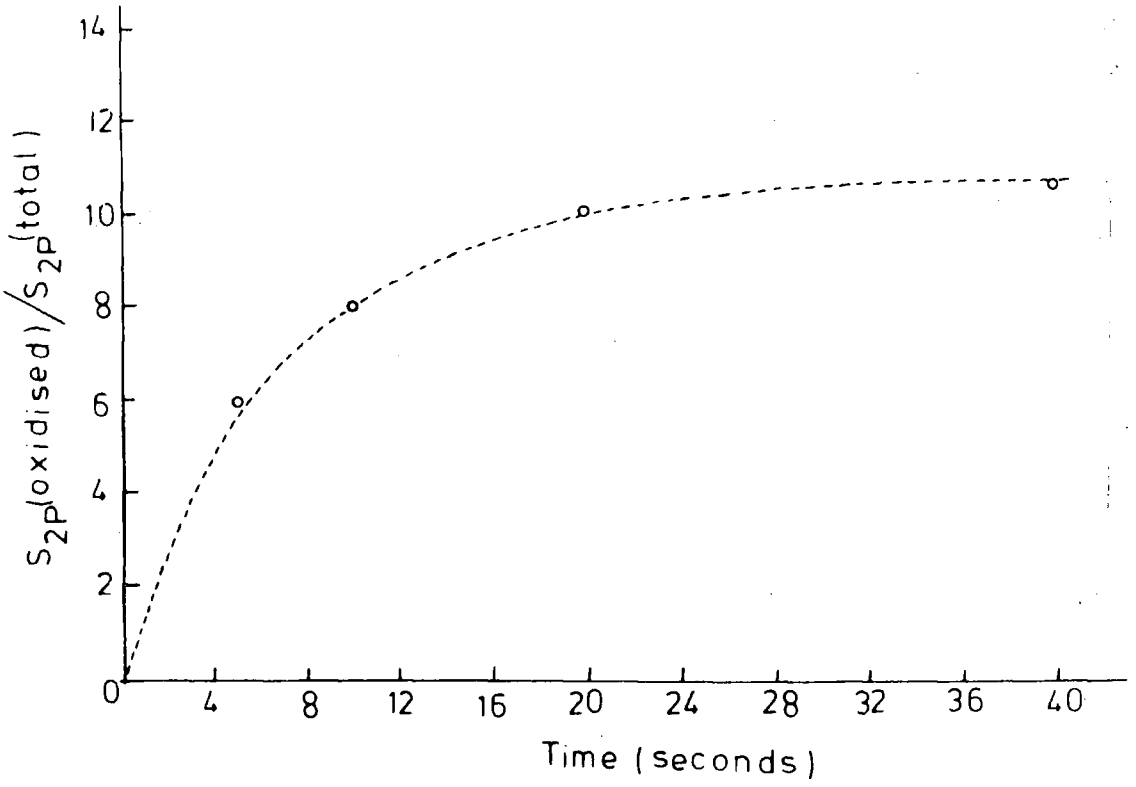

Figure 6.6b. Intensity of the S_{2p} (oxidised) component of the S_{2p} spectrum of L. cystine relative to S_{2p} (total) vs. time of exposure to the oxygen plasma (0.4 watt, 0.2 torr).

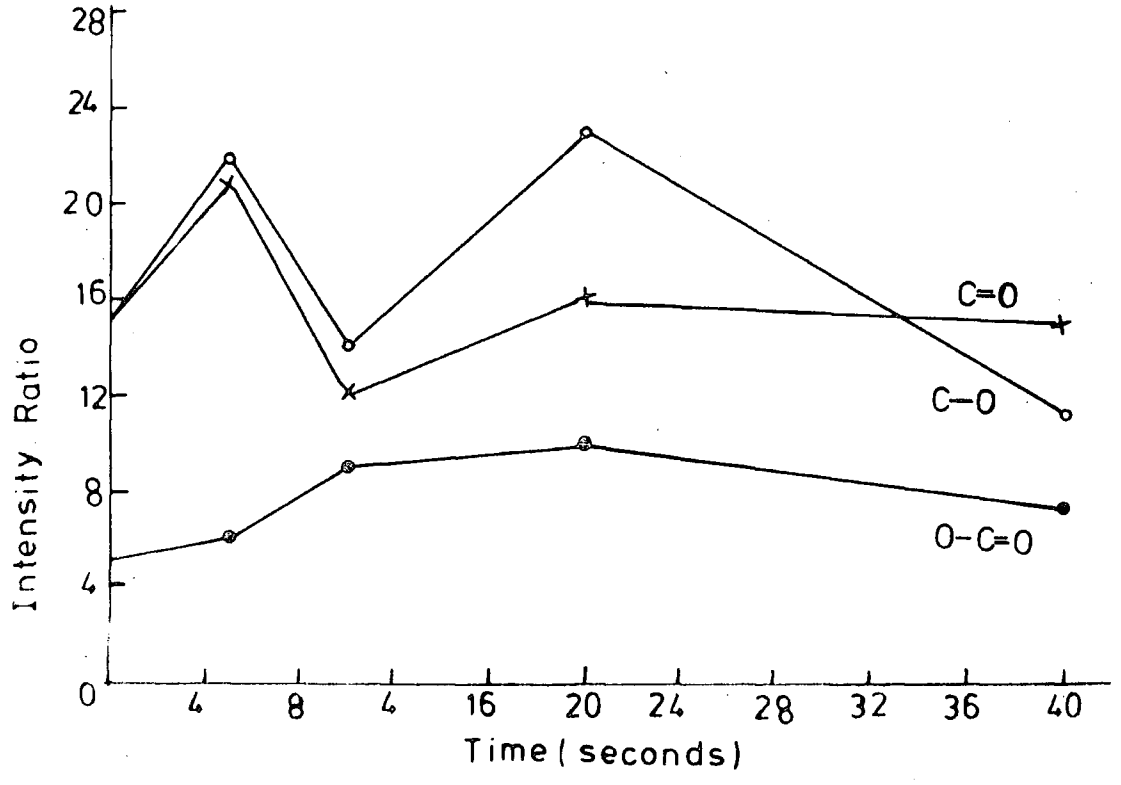

Figure 6.6c. Intensity of the various components of the C_{1s} spectrum of L. cystine relative to the C_{1s} (total) vs. time of exposure to the oxygen plasma (0.4 watt, 0.2 torr).

pressure of 0.2 torr and power loading of 0.4 watt at room temperature. The structural features associated with O-C=O and $\overset{O}{\overset{\|}{S}}\overset{}{\overset{\|}{O}}$ show a clear tendency for reaching a maximum soon after the start of the reaction and then decrease or level off to a constant value, whereas, the general trend for C_{1s}/N_{1s}, C_{1s}/S_{2p} and C_{1s}/O_{1s} intensity ratios indicates that the C/N and C/S stoichiometries remain essentially the same as a function of reaction time. This suggests that oxidation of the sulphur functionalities occurs substantially faster than for the hydrocarbon overlayer.

An important conclusion after the treatment of L-cystine with oxygen plasma under the stated conditions follows that the level of sulphur is essentially the same and the sulphur oxidises without involving the cleavage of the disulphide linkage.

(b) Dinonyl trisulphide in an oxygen plasma as a function of time

The main emphasis in this and proceeding studies of models as a function of exposure time to plasma, excited in pure oxygen is to gain an overall gross picture of the chemistry of oxidation of polysulphide linkages rather than to make a detailed study of the oxidation of the alkyl chains.

Figure 6.7 reveals the three readily detectable C_{1s}, O_{1s} and S_{2p} levels, monitored at an electron take-off angle of 30^{o} and the corresponding plots of C_{1s}/O_{1s} and C_{1s}/S_{2p} ratios are indicated in Figure 6.8a. Also shown in Figure 6.8b are the oxidised S_{2p} levels expressed as a percent of the total

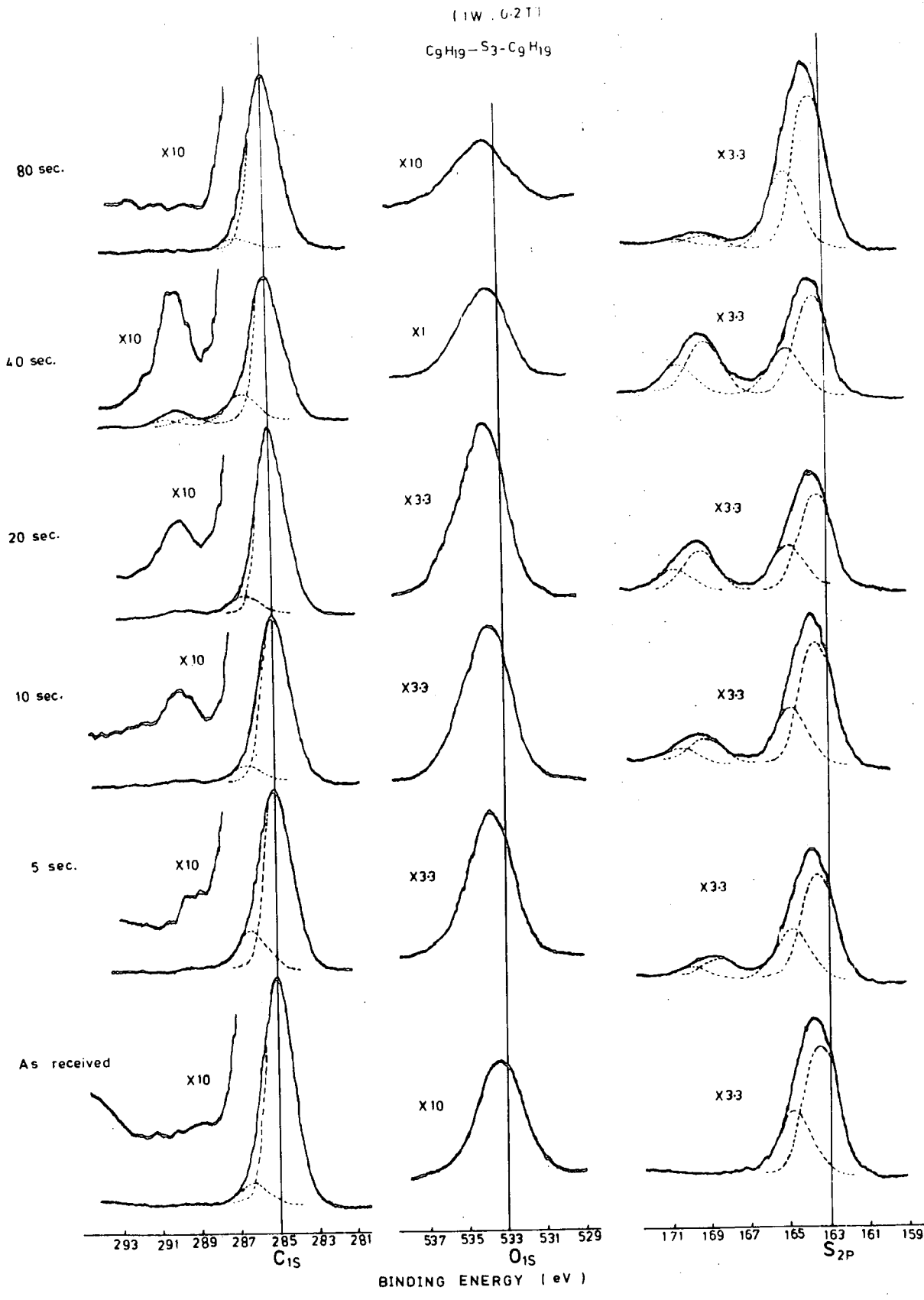

Figure 6.7. C_{1s}, O_{1s} and S_{2p} spectra of dinonyl trisulphide versus time of exposure to an oxygen plasma (1 watt, 0.2 torr).

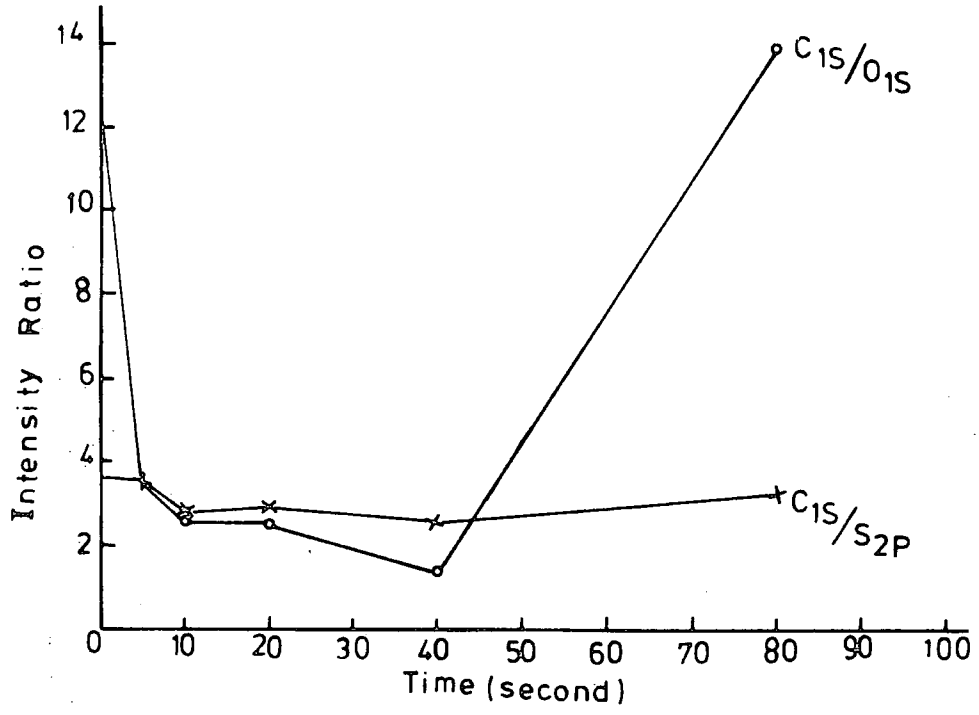

Figure 6.8a. Intensity ratios of the C_{1s}, O_{1s} and S_{2p} levels in the ESCA spectra of dinonyl trisulphide vs. time of exposure to the oxygen plasma (1 watt, 0.2 torr).

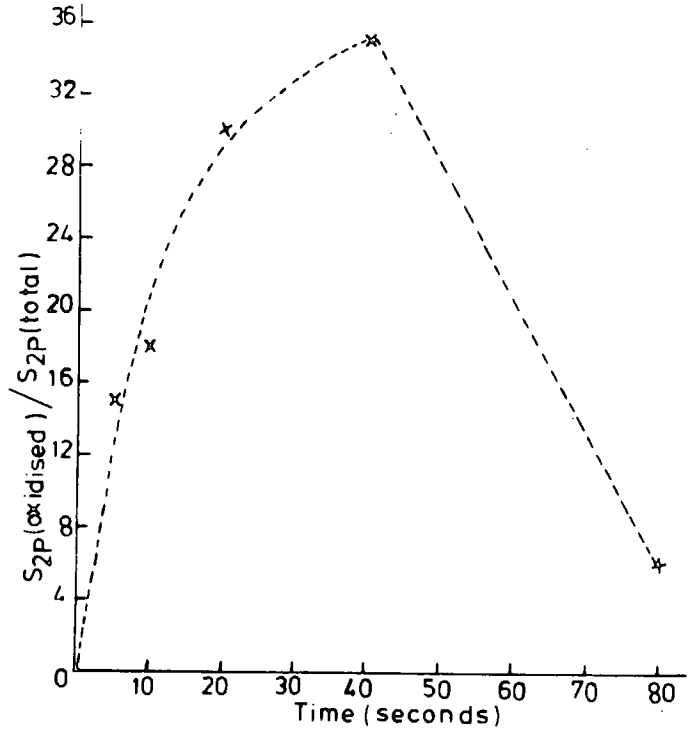

Figure 6.8b. Intensity of the S_{2p} (oxidised) component of the S_{2p} spectrum of dinonyl trisulphide relative to S_{2p} (total) vs. time of exposure to the oxygen plasma (1 watt, 0.2 torr).

S_{2p} band intensity. The data clearly illustrate that the initial rate of oxidation is very fast indeed, with a tendency to level off after 20 seconds in particular for the S_{2p} signal.

Before examining these data in greater detail, it is convenient to estimate the extent of the S_{2p} signal derived from oxidised and unoxidised sulphur under the conditions used in this investigation. The essential features contributing to signal intensity are embodied in equation (6.2):

$$I = f(\theta)F\alpha NK\lambda(1-\bar{e}^{d/\lambda\cos\theta}) \qquad (6.2)$$

where F is the x-ray flux, α is the cross-section for photo-ionisation, N is the number of atoms (on which the core level is localised) per unit volume, K is a spectrometer dependent factor, λ is the mean free path of the photoemitted electrons $\sim 15\text{Å}$ for S_{2p} level using $Mg_{k\alpha_{1,2}}$ radiation, d is the thickness of the surface layer, and $f(\theta)$ is a function of θ that describes the angular dependence of a signal arising from a homogeneous sample. A more detailed description of equation (6.2) can be found elsewhere.[227]

With a knowledge of the mean free path for S_{2p}, an electron take-off angle of 30° and the thickness of the modified layer, which is in the range 5 - 10Å after prolonged exposure to plasma, it follows that approximately 40% of signal intensity is derived from the oxidised surface and the remaining from bulk, as far as the ESCA depth profile is concerned. In comparison of these estimated values with those of an extent of S_{2p} oxidation in Figure 6.8b, it is clearly evident that the S_{2p} oxidised peak, separated by approximately 5.6 eV from the main S_{2p} photo-

ionisation peak, is much smaller than one would anticipate without the knowledge of an equation (6.2). This type of analysis made on sulphur allows with certainty that the trisulphidic bridge in dinonyl trisulphide is in the form of

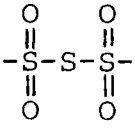

, and, therefore, the overall oxidative reaction in the oxygen plasma can be written as:

Scheme 3

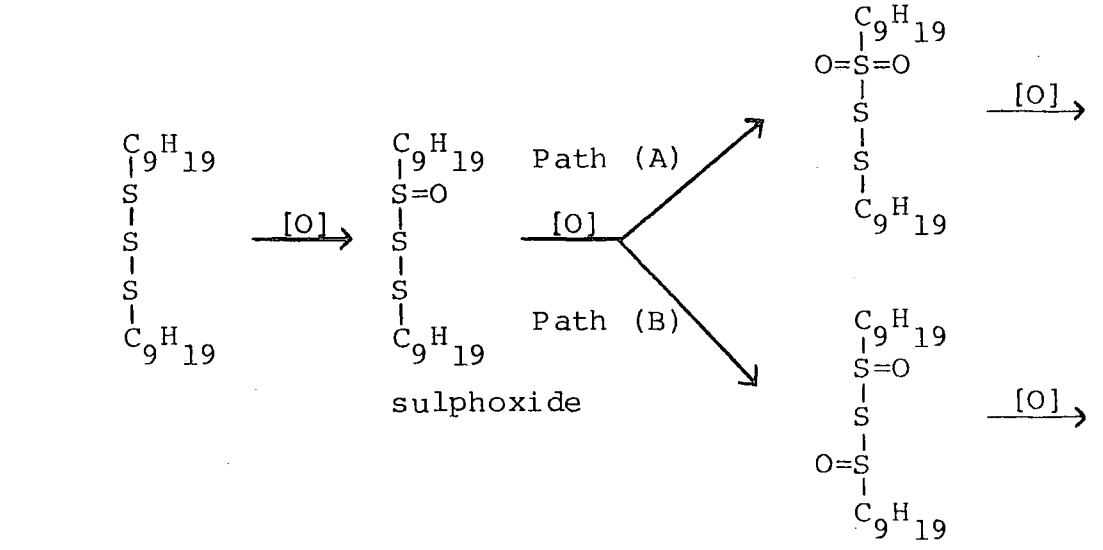

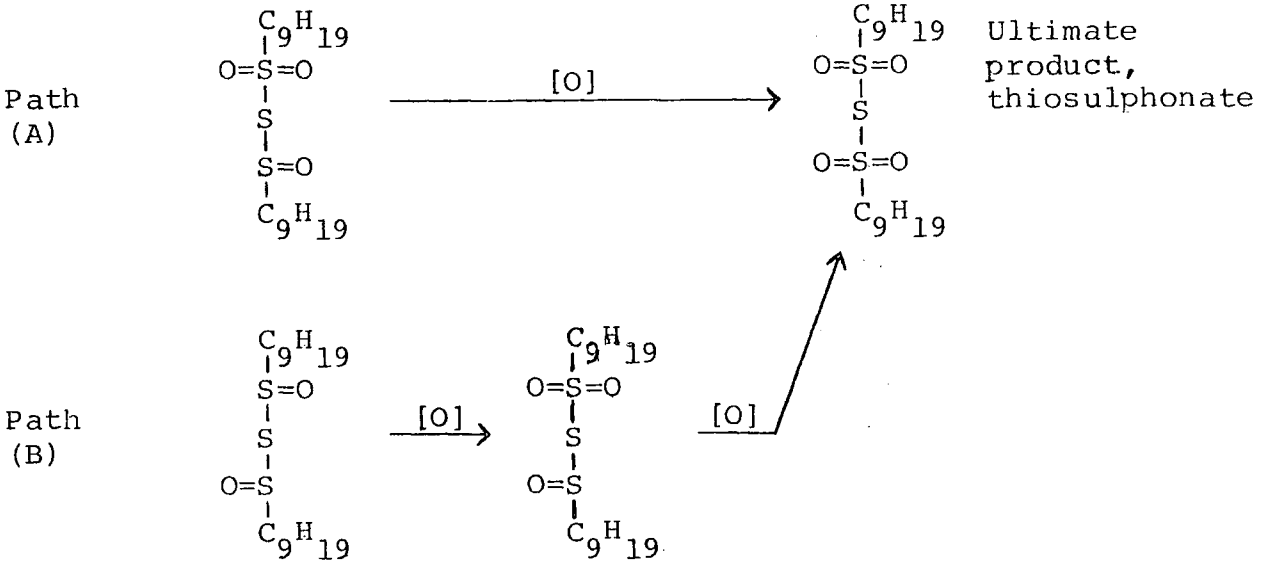

Sulphoxide intermediates shown in the reaction sequences leading ultimately to thiosulphonate were not observed under the conditions employed in this investigation, and, if present, represent less than 1%, immediately reacted with oxygen plasma species, as a result of their high reactivity. The sulphur separating the two sulphate groups was not cleaved, as it is clearly evident from the C_{1s}/S_{2p} ratio versus as a function of time in Figure 6.8a. The data in Table 6.3, obtained by exposing to drastic oxygen plasma conditions (10 watts, 0.2T) for 10 seconds in 'situ' also clearly reveal that sulphur is not lost within the range of employed conditions; and the oxidation stops at thiolsulphonate.

The experimental stoichiometry ratio of atoms, derived from the intensity ratio for an untreated sample, were in good agreement with the theoretical values revealing that the surface is representative of the bulk.

Table 6.3

The ratio of intensities of the C_{1s}, O_{1s} and S_{2p} bands in the ESCA spectra of as received and plasma oxidised dinonyl trisulphide ($C_9H_{19}-S_3-C_9H_{19}$)

Conditions: time = 10 seconds, pressure = 0.2 torr and temperature of a sample = 200K. After plasma treatment, the sample was further cooled to 170K before introducing into the spectrometer for an analysis at an electron take-off angle of 30^{o}.

	Power (watts)	C_{1s}/O_{1s}	C_{1s}/S_{2p}
As received	0	12.3	3.6
	1	2.6	2.7
	10	2.5	2.8

(c) Bis-n-propyl-γ-triethoxysilyl tetrasulphide in an oxygen plasma as a function of time

The main objective in this phase of the work has been to investigate the oxidation of sulphur in bis-n-propyl-γ-triethoxysilyl tetrasulphide, as a function of plasma treatment time under the same conditions as those employed for dinonyl trisulphide.

The results for the untreated bis-n-propyl-γ-triethoxysilyl tetrasulphide with four distinct measurable C_{1s}, O_{1s}, S_{2p} and Si_{2p} levels in Figure 6.9, and the corresponding intensity ratios in Figure 6.10 reveal experimental stoichiometry of atoms, in good agreement with the theoretical values, indicating a very pure sample. The distinctive differences in relative intensities of the spectra at an electron take-off angle of 30^{o} in Figure 6.9 clearly demonstrates by the dramatic change in C_{1s} component at 286.6 eV that the reactive entities in the oxygen plasma are selectively reacting initially with the triethoxy functional groups, attached directly to silicon and, reach a limiting reaction after a relatively short period (5 seconds) of exposure to the oxygen plasma, before the oxidation commences at the tetrasulphide bridge. Whereas, the oxidation of sulphur proceeding after 5 seconds of plasma exposure time, as is most readily appreciated from Figure 6.10b, establishes a maximum change in surface chemistry at ∿ 20 seconds reaction time, before levelling off, under the conditions employed in this work. The C_{1s}/S_{2p} intensity ratio as a function of time in Figure 6.10a clearly indicate that the oxidation of tetrasulphide

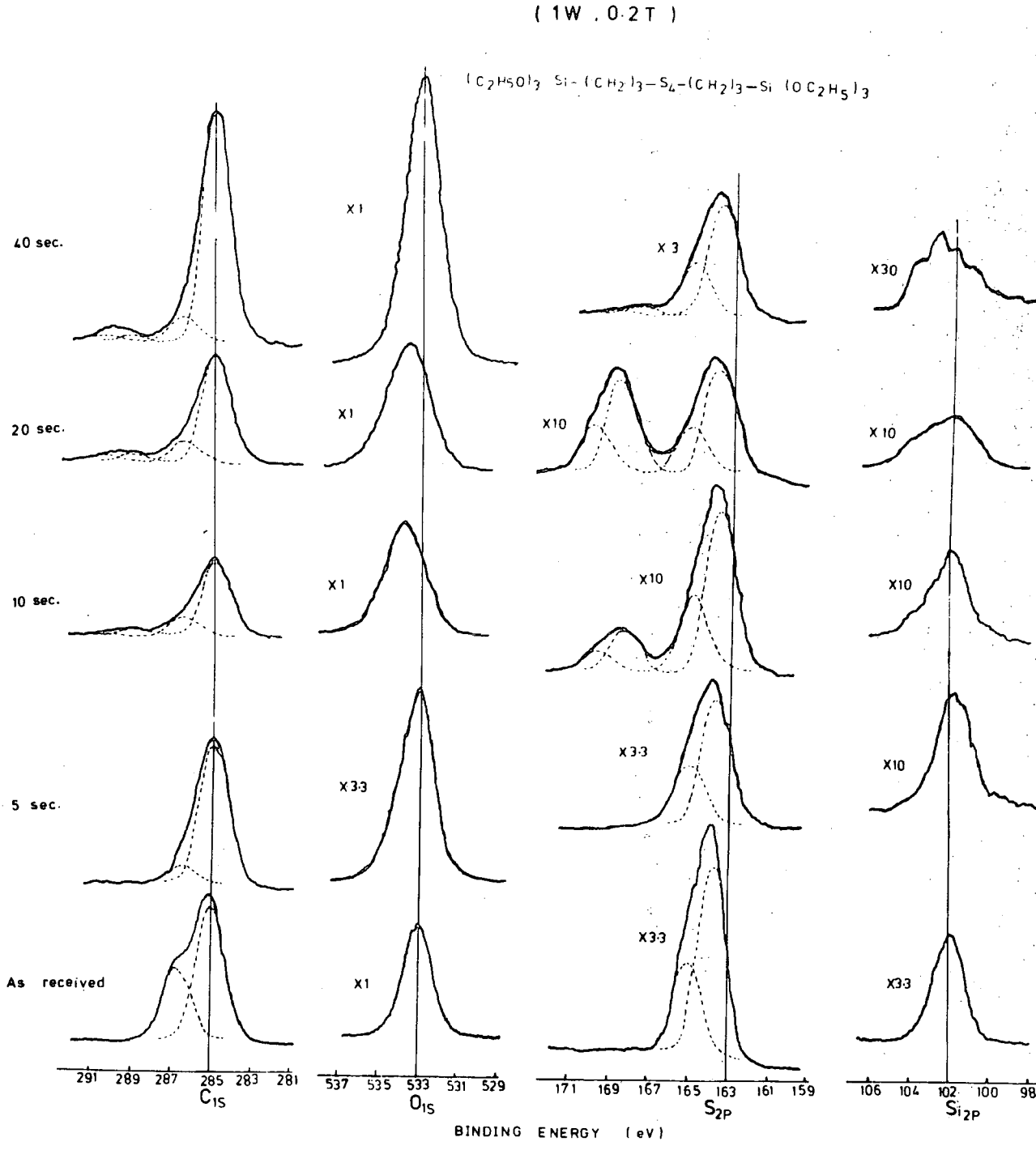

Figure 6.9. C_{1s}, O_{1s}, S_{2p} and Si_{2p} spectra of bis-n-propyl-γ-triethoxysilyl tetrasulphide versus time of exposure to an oxygen plasma (1 watt and 0.2 torr).

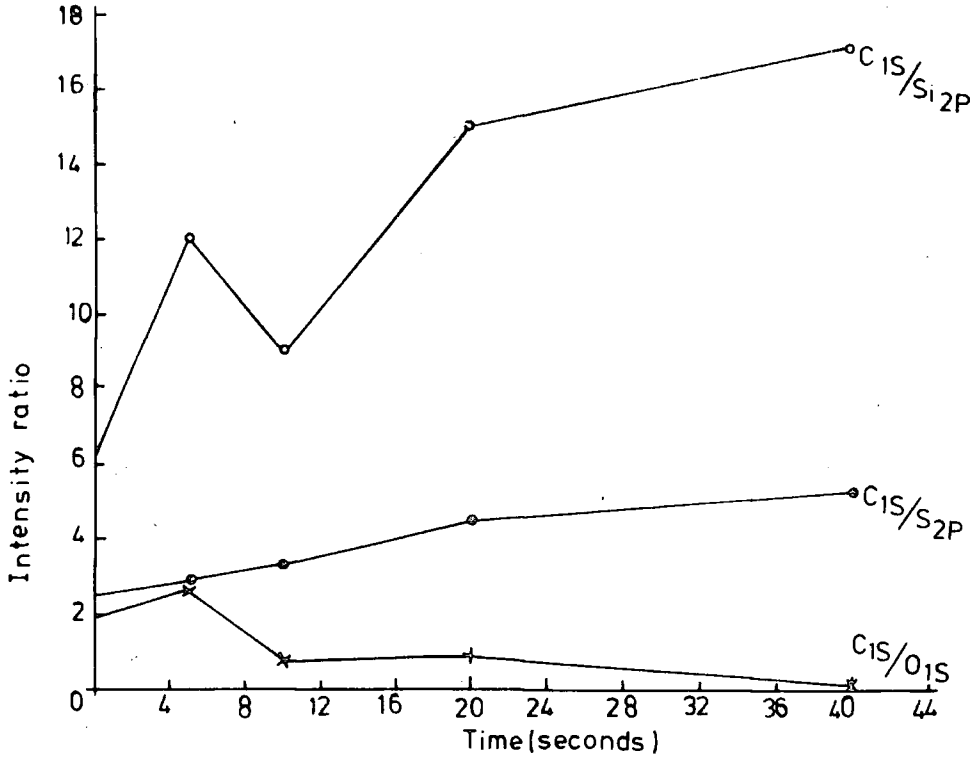

Figure 6.10a. Intensity ratios of the C_{1s}, O_{1s}, S_{2p} and Si_{2p} levels in the ESCA spectra of bis-n-propyl-γ-triethoxysilyl tetrasulphide vs. time of exposure to the oxygen plasma (1 watt, 0.2 torr).

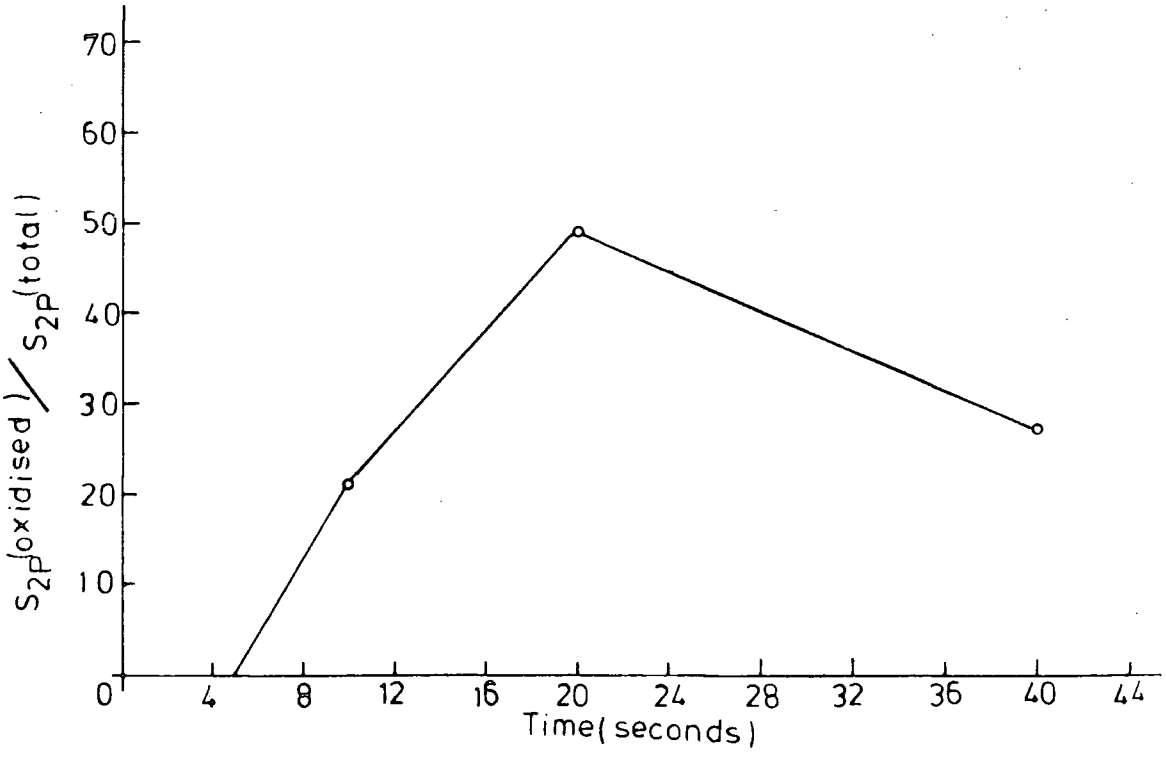

Figure 6.10b. Intensity ratio of the S_{2p} (oxidised) component of the S_{2p} spectrum of bis-n-propyl-γ-triethoxysilyl tetrasulphide relative to S_{2p} (total) vs. time of exposure to the oxygen plasma (1 watt, 0.2 torr).

linkage is accompanied by the loss of sulphur and the tetrasulphide linkage loses two sulphur atoms after 20 seconds reaction time, in contrast to lower rank sulphides. It can be stated that, with a knowledge of the mean free path of S_{2p}, 15Å, an electron take-off angle of 30° and the thickness of the modified layer, which is of the order one monolayer or so (assuming that the diffusion of oxygen atoms into the bulk is not significant under the employed conditions), for the estimation of the signal contributed from the modified surface that the oxidised sulphur after prolonged exposure time (20 - 40 seconds) is in the form of $-\overset{\overset{O}{\|}}{\underset{\underset{O}{\|}}{S}}-\overset{\overset{O}{\|}}{\underset{\underset{O}{\|}}{S}}-$, conceivably proceeding through the same sequences as those as illustrated for dinonyl trisulphide in reaction scheme 4 (it might be

Scheme 4

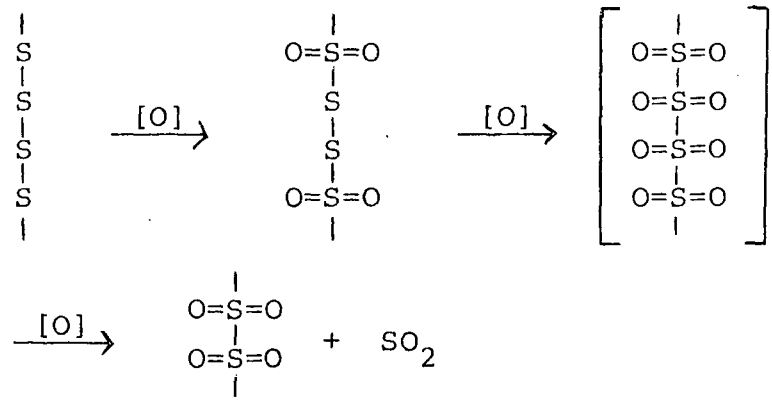

added here that the deviations seen in the separation of oxidised and unoxidised S_{2p} levels for dinonyl trisulphide, 5.6 eV, and bis-n-propyl-γ-triethoxysilyl tetrasulphide, 5.0 eV, could possibly be partly due to the hybridisation effect[239] requiring a higher electronegativity for the oxidised disulphide

bridge in scheme 4).

The data in Table 6.4, obtained at a power loading of 10 watts for 10 seconds and a total pressure of 0.2 torr, indicate very little change in the level of sulphur, which, in turn, may suggest that the treatment at a substantially higher power loading resulted in the ablation of the surface of bis-n-propyl-γ-triethoxysilyl tetrasulphide.

Table 6.4

The intensity ratios of the C_{1s}, O_{1s}, S_{2p} and Si_{2p} bands in the ESCA spectra of as received and plasma oxidised bis-n-propyl-γ-triethoxysilyl tetrasulphide $((EtO)_3Si-(CH_2)_3-S_4-(CH_2)_3-Si(EtO)_3$

Conditions: time = 10 seconds, pressure = 0.2 torr and temperature of a sample = 200K. After plasma treatment, the sample was further cooled to 170K before introducing into the spectrometer for an analysis at an electron take-off angle of 30^{o}.

	Power (watts)	C_{1s}/O_{1s}	C_{1s}/S_{2p}	C_{1s}/Si_{2p}
As received	0	1.9	2.5	6.3
	1	0.7	3.3	9.0
	10	0.4	3.2	21.0

(d) Ditertiododecyl pentasulphide in an oxygen plasma as a function of time

It is clearly evident from the data in Figure 6.12, pertaining to Figure 6.11 that the effect of iodine substitution distorts the overall reactivity such that the pentasulphide is no longer an adequate model for sulphur bridges in vulcanised rubbers. The most likely interpretation of these

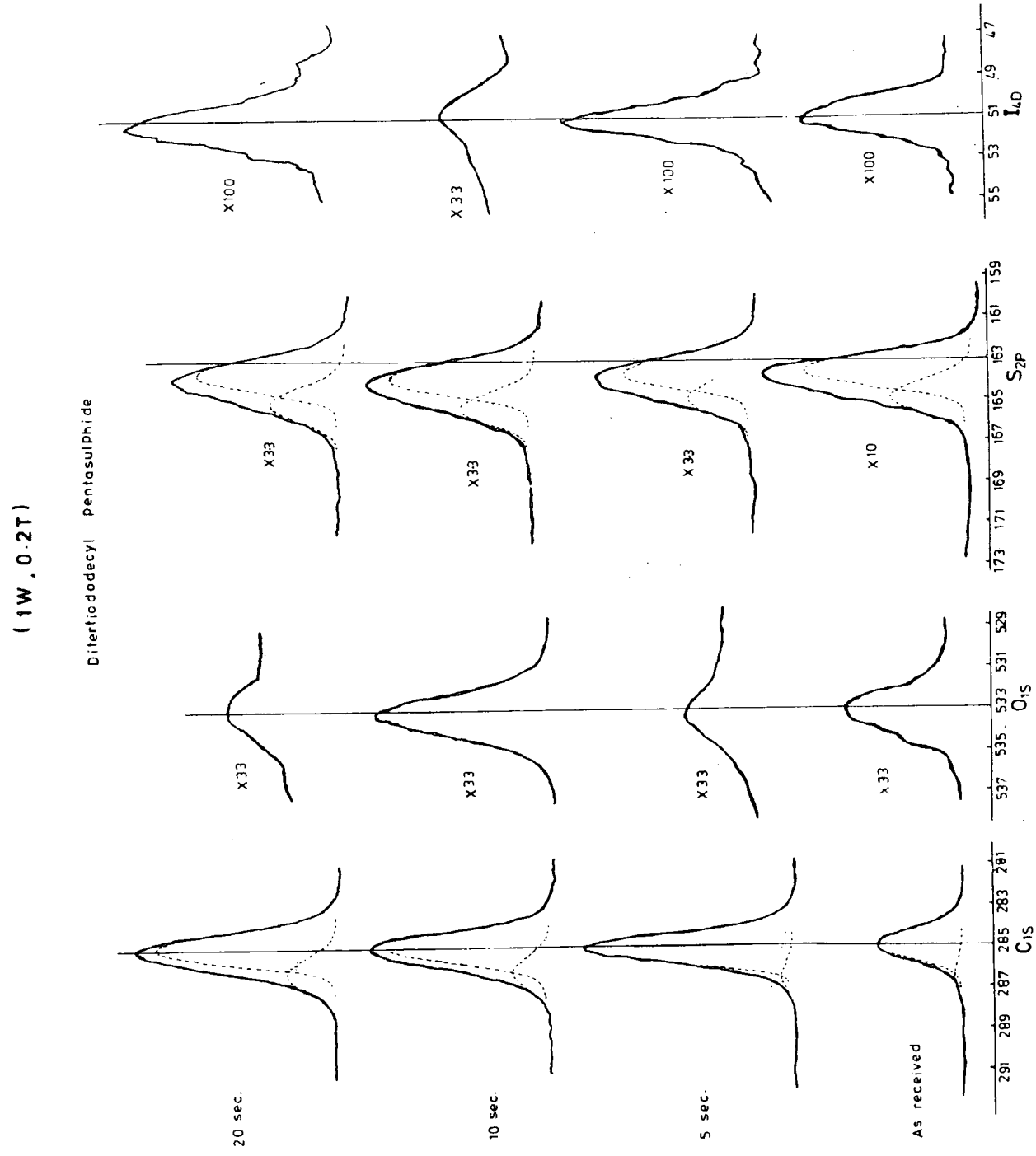

Figure 6.11. C_{1s}, O_{1s}, S_{2p} and I_{4D} spectra of ditertiododecyl pentasulphide versus time of exposure to an oxygen plasma (1 watt, 0.2 torr).

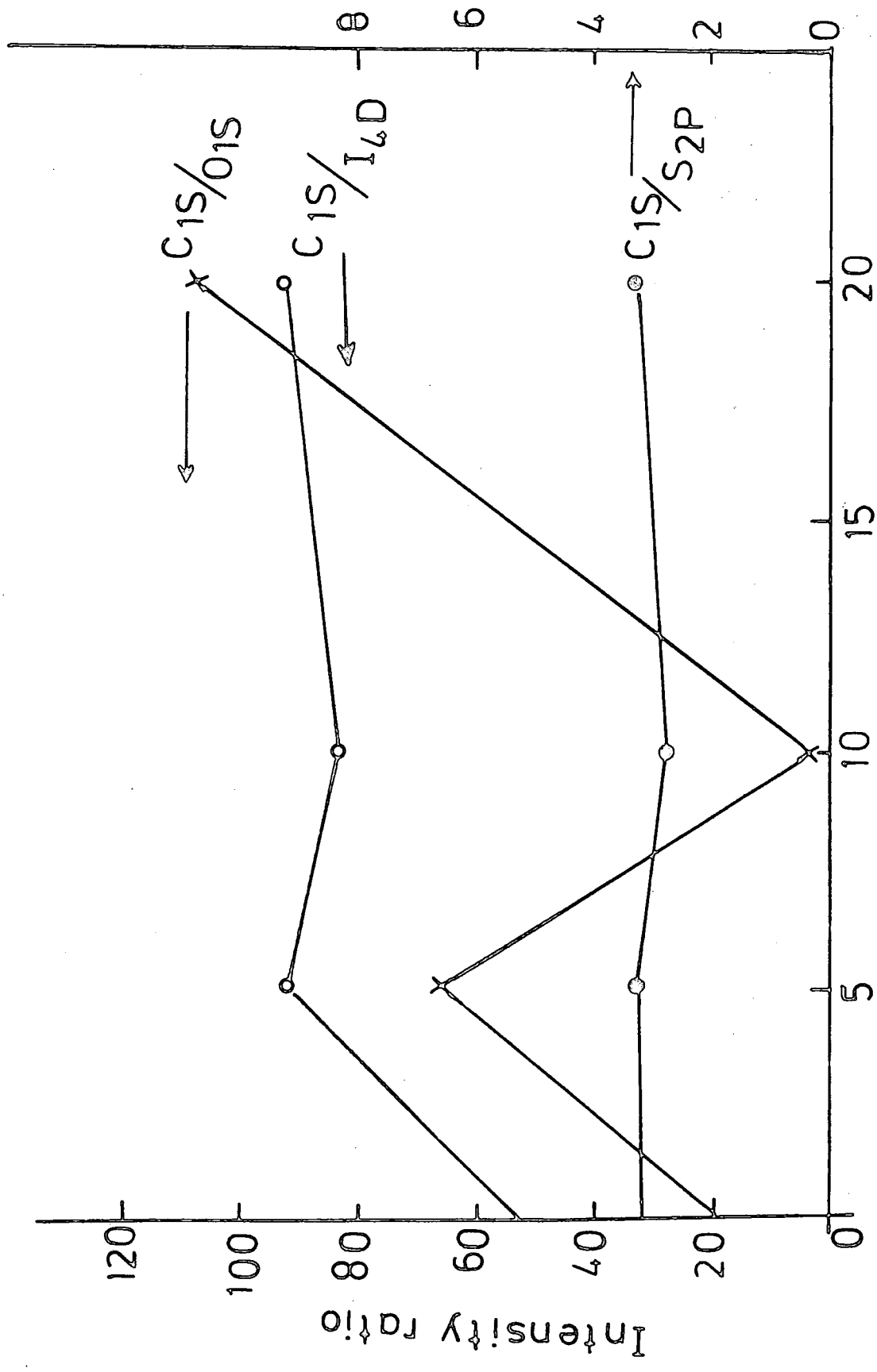

Figure 6.12. Intensity ratios of the C_{1s}, O_{1s}, S_{2p} and I_{4D} levels in the ESCA spectra of ditertiododecyl pentasulphide versus time of exposure to the oxygen plasma (1 watt, 0.2 torr).

data is that iodine effectively quenches the oxygen atoms (by recombination either directly or via iodoso and/or iodoxy derivatives) such that the level is reduced sufficiently for subsequent attack of reactive oxygen entities at the sulphide bridges to be relatively slow; and, therefore, the pentasulphide did not indicate any tendency for oxidation or desulphurisation,[240,241] under the conditions employed in this work.

6.3.3 Reactions of accelerators in an oxygen plasma

(a) Introduction

Since the levels of additives, employed in the formulation of elastomers, are substantially higher at the surface than in the bulk (chapter three), it is of great interest to investigate the ease and extent of oxidation by exposure to plasmas, excited in pure oxygen, before considering the ESCA data pertaining to elastomers treated in the oxygen plasma. Accelerators such as cyclohexylbenzthiazyl sulphenamide (CBS) and tetramethylthiuram disulphide (TMTD) used in Natsyn 2200 sample formulations have, therefore, been subjected to interrogation in 'situ', using ESCA, coupled with glow discharge techniques at a total pressure of 0.2 torr and a power loading of 1 watt for 10 seconds.

It should be noted that under comparable conditions, the extent of oxidation as evidenced by the higher binding S_{2p} component was $\sim$ 8%, 21% and $\sim$ 35% for the di-, tri- and tetrasulphide model systems respectively.

(b) Cyclohexylbenzthiazyl sulphenamide in an oxygen plasma

A comparison of the data in Table 6.5, extracted from the

Table 6.5

Cyclohexylbenzthiazyl sulphenamide in an oxygen plasma (1 watt, 0.2 torr)

Comparison of intensity ratios

Time (seconds)	C_{1s}/O_{1s}	C_{1s}/N_{1s}	C_{1s}/S_{2p}	S_{2p} oxidised (%)
As received	6.1	11	4.0	-
10	1.5	31	2.6	15

Comparison of C_{1s} components

	Total C_{1s}	C-H	C-O	C=O	O-C=O	O O-C-O
As received	100	82	16	2	-	-
10	100	71	21	2	5	1

raw spectra of as received and oxygen plasma treated CBS in 'situ' in Figure 6.13, clearly illustrates the dramatic effect on intensity ratios of different chemical environments, under the C_{1s} and S_{2p} envelopes and also on the N_{1s} and S_{2p} levels with respect to the C_{1s} signals.

A high level of total oxygen signal is associated with the development of various C_{1s} and S_{2p} components in an oxygen plasma at a power loading of 1 watt for 10 seconds and a total pressure of 0.2 torr. The unexpected increase in the S_{2p} level on exposure to the plasma may be explained by considering the cleavage of S-N bond in sulphenamide and then dimerisation of benzthiazyl, giving 2,2'-dithio-bis(benzothiazole); the possible overall reaction is as follows:

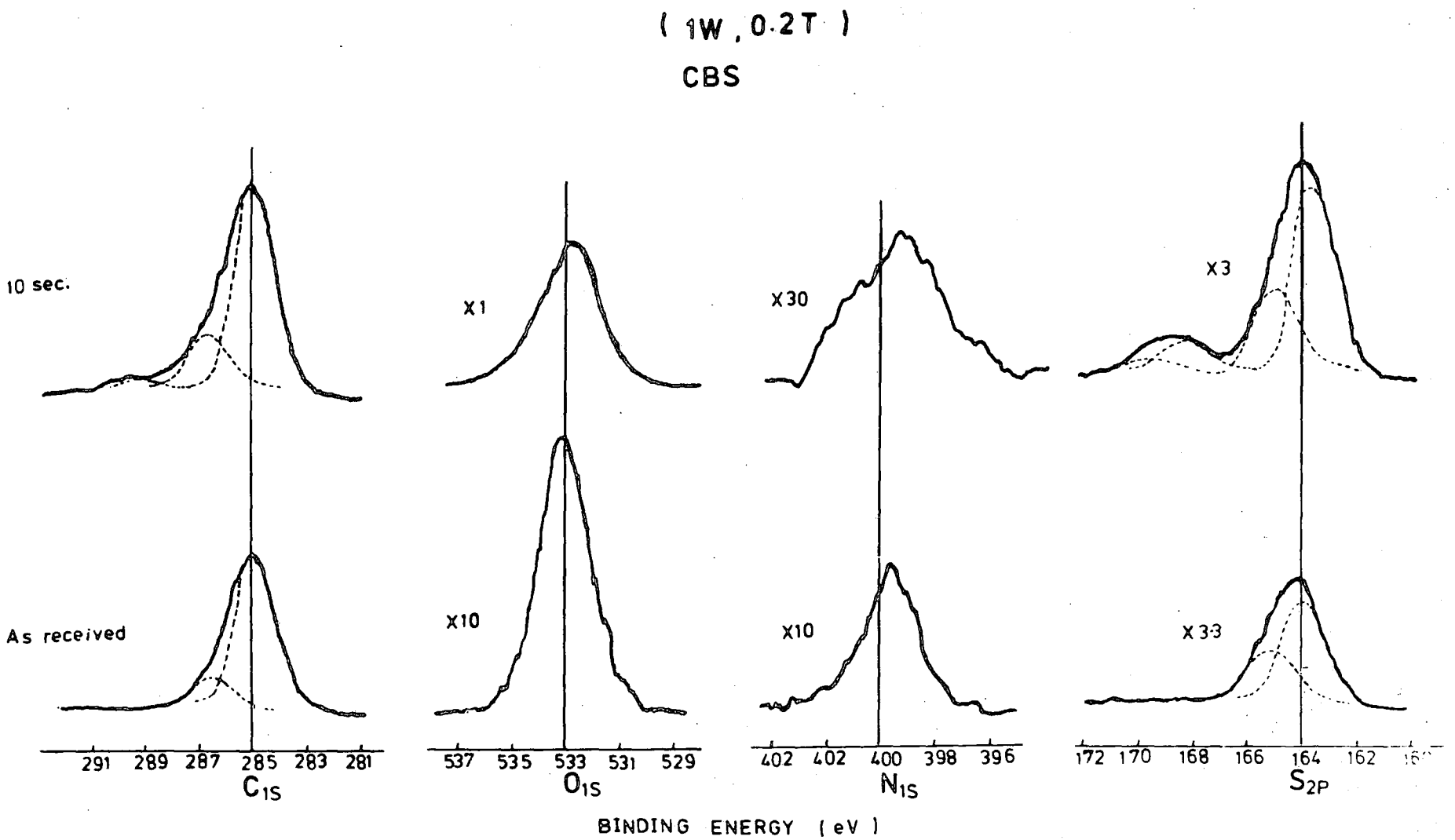

Figure 6.13. C_{1s}, O_{1s}, N_{1s} and S_{2p} spectra of cyclohexylbenzthiazyl sulphenamide exposed for 10 seconds in the oxygen plasma (1 watt, 0.2 torr).

Scheme 5

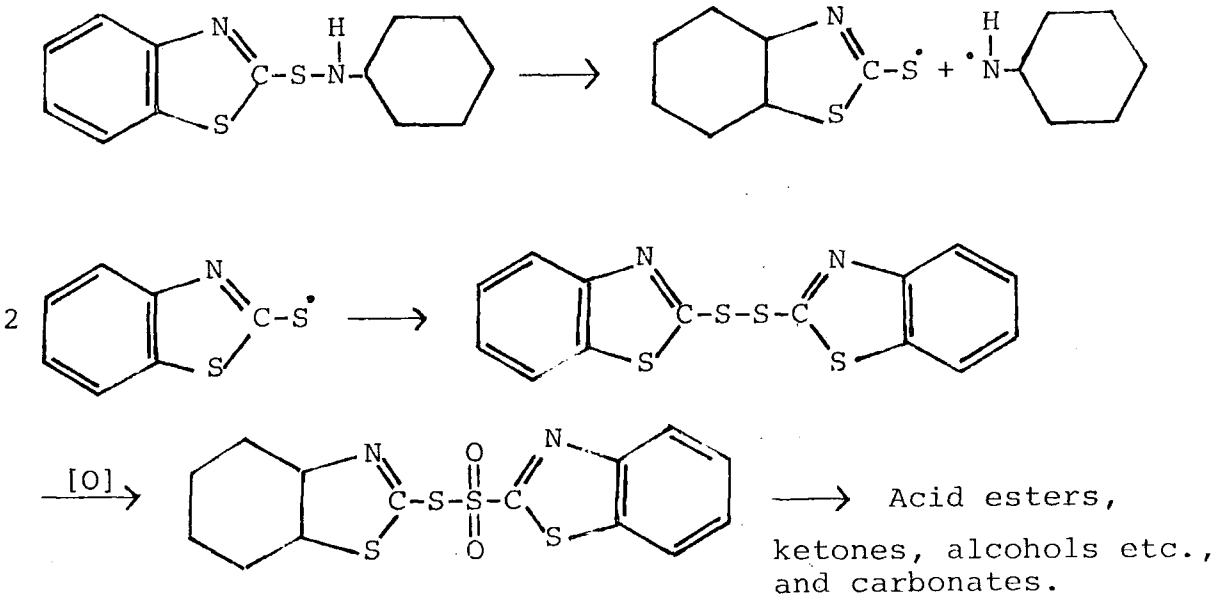

It is known from the related studies in these laboratories that the aromatic systems are particularly prone to oxidation compared with the aliphatic systems. The competition between the production of oxidised sulphur and carbon functionalities, which the data reveal, is, therefore, entirely reasonable.

A knowledge of an electron mean free path for S_{2p} and an extent of S_{2p} oxidation by 15% suggests the oxidised product is thiosulphonate $-S-\overset{\overset{O}{\|}}{\underset{\underset{O}{\|}}{S}}-$ (it should be noted that an electron take-off angle of 30^{o} in the equation 6.2 has been considered as zero, due to the surface topography of a powdered CBS sample).

(c) Tetramethylthiuram disulphide in an oxygen plasma

The ESCA data for TMTD are shown in Table 6.6, whilst the core level spectra are indicated in Figure 6.14 (oxygen plasma treatment:- a power loading of 1 watt for 10 seconds and a

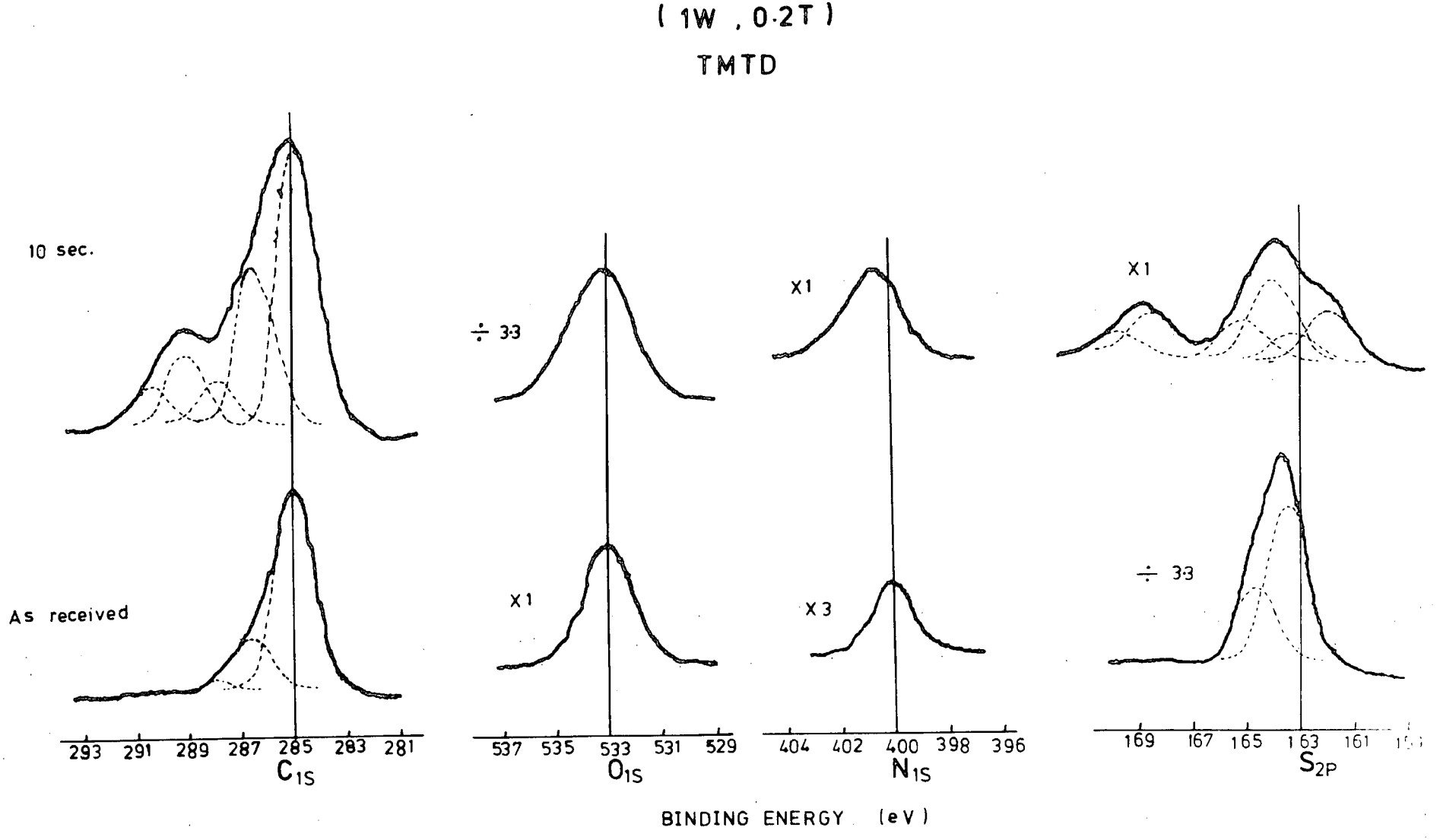

Figure 6.14. C_{1s}, O_{1s}, N_{1s} and S_{2p} spectra of tetramethylthiuram disulphide exposed for 10 seconds in the oxygen plasma (1 watt, 0.2 torr).

total pressure of 0.2 torr). The data clearly reveal distinct differences in the regions of the C_{1s} and S_{2p} spectra, corresponding to the oxygen-containing structural features.

Table 6.6

Tetramethylthiuram disulphide in an oxygen plasma (1 watt, 0.2 torr)

Comparison of intensity ratios

Time (seconds)	C_{1s}/O_{1s}	C_{1s}/N_{1s}	C_{1s}/S_{2p}	S_{2p} oxidised (%)
As received	1.7	10	0.31	-
10	0.9	5.2	2.1	26

Comparison of C_{1s} components

	Total C_{1s}	C-H	C-O	C=O	O-C=O	O O-C-O
As received	100	75	21	4	-	-
10	100	46	26	8	13	7

The data reveal that sulphur is very readily lost, whilst the stoichiometry with respect to nitrogen increase. The level of oxygen functionality increases also and the degree of charge asymmetry in the parent molecule (scheme 6) perhaps provides a basis for rationalising the facile loss of sulphur.[239]

Scheme 6

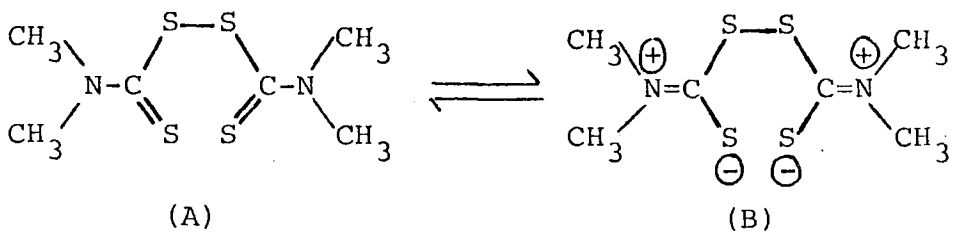

(A) (B)

The overlap between the C_{2p} orbital and S_{3p} is not favourable on both an energy or size basis, the C=S bond is rather unstable, and, in consequence, the net result is that TMTD can readily be oxidised. A large distribution of C_{1s} components and the appearance of S_{2p} level as a substantially broadened structure at a rather low binding (FWHM 4.0 eV compared with FWHM 2.3 eV for the as received material) provide some evidence for the very large contribution of mesomeric structure-(B) to the ground state valence bond description.

The difference in C_{1s}/S_{2p} intensity ratios is attributed to the loss of sulphur as SO_2 from the two doubly bonded sulphur to carbon on either side of a disulphide linkage; and, the disulphide linkage is oxidised at one of its sulphur atoms, whilst the other remains unaffected in the oxygen plasma, under the employed conditions. Thus, the overall oxidation of TMTD, analogous to the known procedures for the preparation of C-sulphonylformamides,[257] can be represented as follows:

Scheme 7

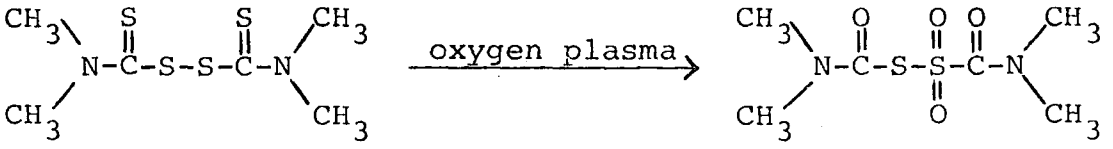

6.3.4 Overall features of organic sulphides

It is now possible to establish, with certainty, the overall gross picture of the chemistry of oxidation of different sulphides, which mirror the sulphide linkages in vulcanised rubbers, before a variety of Natsyn 2200 elastomers are exposed

sequentially to the oxygen plasma.

It has been stated in chapter one that the vulcanisation of natural and synthetic rubbers in the presence of sulphur and accelerators produces a mixed network structure of mono-, di- and polysulphides; and, these sulphides are anticipated to give the same products as models on exposure to the oxygen plasma, under the comparable conditions.

The overall features of oxidation for different sulphides, inferred from the models, as a function of time in the oxygen plasma, are as follows:

(i) A plot of initial rate of S_{2p} oxidation versus the number of sulphur atoms in the sulphur linkage, in Figure 6.15, clearly reveals that the relative reactivity for different sulphides falls in the order: mono-, < di-, < tri-, < tetrasulphide, indicating that the monosulphide is least reactive and the tetrasulphide is most reactive, under the employed conditions in this work.

(ii) The ultimate products resulting from the oxidation of sulphides in the oxygen plasma are as follows:

Monosulphide

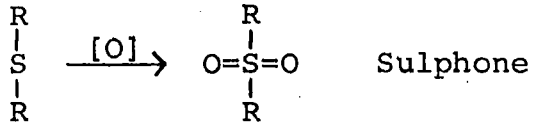

Sulphone

Disulphide

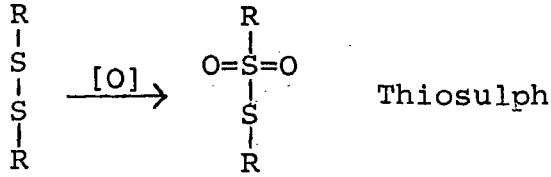

Thiosulphonate

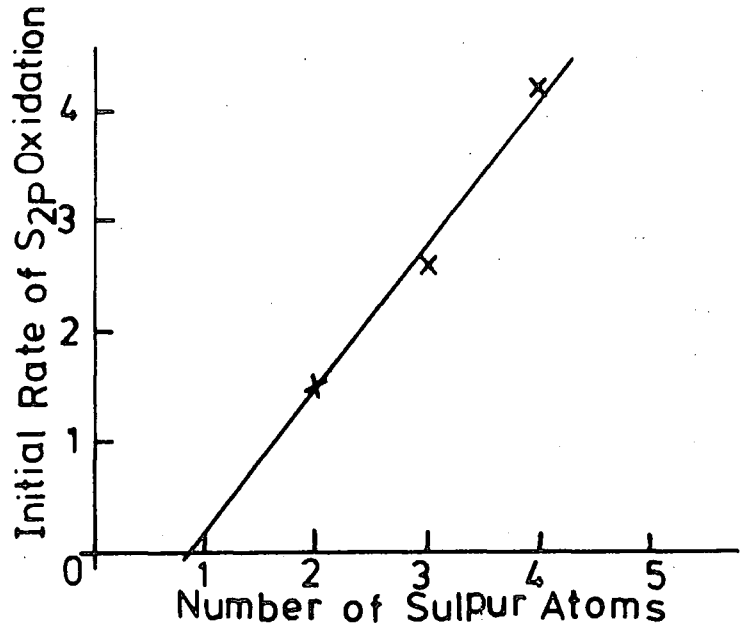

Figure 6.15. Initial rate of S_{2p} oxidation versus number of sulphur atoms in the sulphur linkage.

Trisulphide

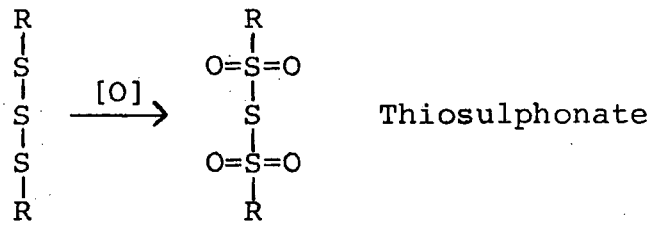

Tetrasulphide

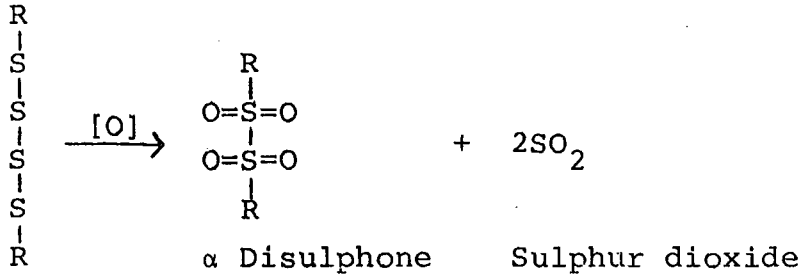

(iii) Mono-, di- and trisulphides oxidise without involving the cleavage of sulphur crosslinks, whereas the tetrasulphide indicated α-disulphone structure with the loss of sulphur as sulphur dioxide.

(iv) L.Cystine and dinonyl trisulphide indicate that oxidation of the sulphur functionalities occurs substantially faster than for the hydrocarbon overlayer.

It is clear from the study of bis-n-propyl-γ-triethoxysilyl tetrasulphide in an oxygen plasma that the reactive oxygen entities are selectively reacting initially with the triethoxy functional groups, attached directly to silicon, before the oxidation proceeds at the tetrasulphide bridge. The effect of iodine substitution distorts the overall reactivity of ditertiododecyl pentansulphide such that the pentasulphide is no longer an adequate model for sulphur bridges in 'sulphur-vulcanised' rubbers.

(v) The thickness of modified surface in an oxygen plasma depends on the physical form of the sample. The liquid samples indicated greater depth of modification than L.cystine (solid)

6.3.5 Surface modification of Natsyn 2200 elastomers in an oxygen plasma

(a) Introduction

The discussion to date in both this chapter and those previously presented highlights the complex nature of the elastomer surfaces, and their dependence on the initial bulk formulation and sample history. The reaction of the model systems with oxygen plasmas is also, by no means, straightforward; nonetheless, it is worthwhile now, considering the ESCA examination of plasma processed surfaces of the elastomers themselves.

The detailed composition of the bulk formulation in terms of weight and normalised mole % for type 1, Natsyn 2200, system in chapter three, clearly indicates that the C_{1s} signal should predominantly arise from the Natsyn (polyisoprene) framework, with smaller contributions from stearic acid, CBS and permanax B. N_{1s} signals would be expected from both CBS and permanax B, whilst the sulphur signal should predominantly derive from the added sulphur itself as opposed to the sulphur of CBS. Zinc is added to the formulation as the oxide to enhance the cure rate. Oxygen signals can conceivably arise from residual metal oxide (low binding energy), from carboxylate and oxygen in stearate and permanax B respectively, and from oxidative functionalisation of sulphur and the Natsyn surface, arising from oxidation in the oxygen plasma. In principle, the ESCA experiment provides C_{1s}, N_{1s}, O_{1s}, S_{2p} and Zn_{3p} core levels to define a surface stoichiometry.

On the basis of the complexities of the surface for the

as received samples, it is therefore, convenient to consider the proceeding ESCA data in detail for one particular case, and then provide a somewhat less detailed analysis for the other systems.

(b) Type 1, Natsyn 2200, elastomer in an oxygen plasma

In the light of the models investigated in the previous sections, an optimum cured type 1, Natsyn 2200, sample containing antioxidant has been studied at two different take-off angles for different periods of time exposed to an oxygen plasma, in reactor B, with a power loading of 2 watts and a total pressure of 0.2 torr at room temperature. The results of relative intensity ratios, together with the deconvoluted components of the C_{1s} and S_{2p} envelopes, corresponding to Figure 6.16 are shown in Table 6.7, clearly revealing the similarities and differences between them. In both cases of different times and angles, coupled with oxygen plasma, the reaction is very rapid and essentially complete after 5 seconds as far as the change in the surface composition is concerned. The extreme surface, an electron take-off angle of 70^{o}, shows a greater tendency for oxidation than that of sub-surface, an electron take-off angle of 30^{o}, together with very little or no loss of sulphur under the experimental conditions; and, therefore, this is manifested in the Zn_{3p}/S_{2p} ratios.

The relative intensity of the carbon and oxygen peaks exposed to oxygen plasma for 20 seconds is essentially the same at both electron take-off angles, indicating homogeneous sample on the ESCA depth scale; but this does not mean that

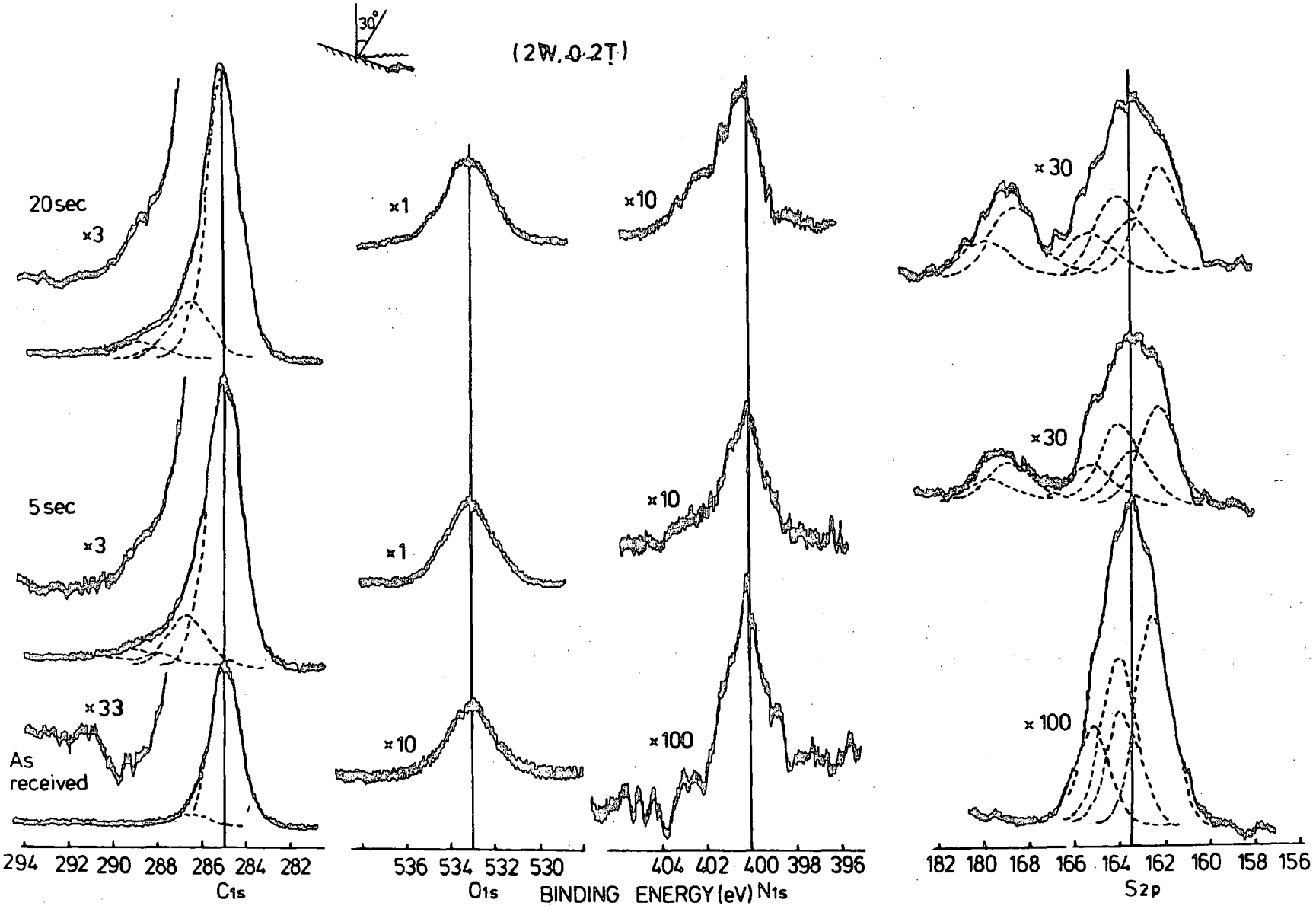

Figure 6.16. C_{1s}, O_{1s}, N_{1s} and S_{2p} spectra of an optimum cured type 1, Natsyn 2200, elastomer vs. time of exposure to an oxygen plasma (2 watt, 0.2 torr).

the surface modification has extended more than 50Å into the sample during plasma treatment. This statement can be easily substantiated by reconsidering the ESCA data of as received optimum cured type 1, Natsyn 2200, elastomer in chapter three, together with the plasma treated samples. The ESCA analysis of an optimum cured type 1 elastomer in chapter three gave ratios of 100:2.3 and 1.2 in moles % for Natsyn 2200 (polyisoprene), permanax B and CBS respectively, indicating higher levels of antioxidant and accelerator by a factor of approximately eight than in the bulk, whilst the level of zinc, arising from zinc oxide and sulphide, at the surface is approximately 1.5 mole %, less compared to that in the bulk (4.0 mole %); and, therefore, revealing that the level of zinc increases with increasing ESCA depth profile. Furthermore, an estimate of a number of sulphur atoms between the cross-linked points of two polymer chains, calculated from the use of 'swelling' data and analysis of S_{2p} envelope, is on average tetrasulphidic linkage for this optimum cured type 1, Natsyn 2200, system.

In view of the complexities of the surface of as received optimum cured type 1 elastomer, the ESCA data of such a sample, coupled with oxygen plasma is examined in greater detail by considering the C_{1s} and S_{2p} spectra. The total fraction of the C_{1s} and S_{2p} envelopes associated with oxygen environment is greater for the 70^{o} electron take-off angle compared to that of 30^{o} and, a greater proportion of singly bonded oxygen is produced in the very initial stages of reaction, under the C_{1s} envelope, as is evidenced by the data

in Tables 6.7a and b; and also, this is even clear from a distinct broadening of O_{1s} peak at a higher binding energy, as the reaction proceeds at an electron take-off angle of 70^{o} in Figure 6.16. The enhancement of the relative intensities of oxygen functionalities under the C_{1s} and S_{2p} envelopes at near grazing electron take-off angle (70^{o}), therefore, demonstrates the surface nature of the modification and, the structural features associated with oxygen are contained in a layer of thickness of the order of a monolayer or so, one monolayer being $\sim 5\text{Å}$. (It should be noted that the additional O_{1s} signal arising from the additives is opposed to the oxygen of plasma incorporated during treatment. The surface rich in permanax B by a factor of approximately 8 and stearate, in contrast to the level of zinc, partially arising from zinc oxide with the remaining contribution from zinc sulphide as revealed by Auger parameters in chapter three, compared to the bulk composition, conceals the O_{1s} contribution from plasma on the basis of total signal intensity ratios of carbon to oxygen. Thus, the net effect of oxygen contributing additives is that the C_{1s}/O_{1s} intensity ratio remains the same at both electron take-off angles.) Indeed, this situation can be further envisaged on the basis of C_{1s} and S_{2p} components associated with oxygen at both electron take-off angles. It is clearly evident from data in Table 6.7, a greater proportion of C_{1s} and S_{2p} envelopes is oxidised at an electron take-off angle of 70^{o} than at 30^{o}, and the oxidation of these envelopes is complete within 5 seconds of exposure to the oxygen plasma, whilst these envelopes at an electron take-off angle of 30^{o}

Table 6.7

The ratio of intensities of the C_{1s}, O_{1s}, N_{1s}, S_{2p} and Zn_{3p} bands in the ESCA spectra of optimum cured type 1, Natsyn 2200, elastomer containing antioxidant and plasma oxidised Natsyn 2200 elastomer

(2 watts, 0.2 torr)

(a) Electron take-off angle (70^{o})

Time (seconds)	C_{1s}/O_{1s}	C_{1s}/S_{2p}	C_{1s}/N_{1s}	C_{1s}/Zn_{3p}	% S_{2p} oxidised
As received	14	27	89	27	-
5	2.9	31	21	18	34
20	3.2	31	16	17	33

C_{1s} Components

	C-H	C-O	C=O	O-C=O
As received	96	4	-	-
5	71	20	2	7
20	71	17	6	6

(b) Electron take-off (30^{o})

Time (seconds)	C_{1s}/O_{1s}	C_{1s}/S_{2p}	C_{1s}/N_{1s}	C_{1s}/Zn_{3p}	% S_{2p} oxidised
As received	16	27	69	24	-
5	3.2	28	22	15	16
20	3.3	23	19	13	27

C_{1s} Components

	C-H	C-O	C=O	O-C=O
As received	95	5	-	-
5	80	14	2	4
20	77	16	2	5

are still in a process of oxidation, even after long plasma exposure time (20 seconds). A comparison of the S_{2p} envelopes, oxidised to the same extent at the extreme surface, an electron take-off angle 70° and, the different extent of oxidation at the sub-surface, take-off angle of 30°, for the different periods of time, therefore, clearly demonstrate the thickness of the modified layer being of the order of one monolayer or so. Additional evidence to support this argument can be found elsewhere.[246] The effect of oxygen plasmas at a substantially higher power loading (20 watts, 0.2 torr) with samples being exposed for 10 seconds is very similar to that of a lower power loading treated for longer time (20 seconds), as is evidenced by the distribution of C_{1s} components pertaining to oxygen as shown in Table 6.8. However, the S_{2p} envelope, monitored at an electron take-off angle of 70°, shows a greater tendency for oxidation at a higher binding ($\sim$ 168.0 eV) separated by approximately 5.7 eV from the unoxidised S_{2p} peak; and this, in conjunction with the oxidation of S_{2p} levels at a lower power loading exposed for longer time and, also together with the knowledge of model compounds, unambiguously reveals the nature of sulphur oxidation, being of the form

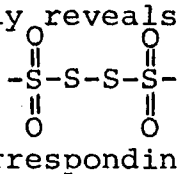

The nitrogen spectra, corresponding to the glow-discharge treated sample were broadened by the presence of at least two components but overlapping N_{1s} components approximately at 399 and 402 eV, indicating amine and protonated amine functionalities, respectively. The sharp decrease in C_{1s}/N_{1s}

Table 6.8

The ratio of intensities of the C_{1s}, O_{1s}, N_{1s} and Zn_{3p} bonds in the ESCA spectra of optimum cured type 1, Natsyn 2200, elastomer containing antioxidant and plasma oxidised Natsyn 2200 elastomer

(20 watts, 0.2 torr)

(a) Electron take-off angle (70^{o})

Time (seconds)	C_{1s}/O_{1s}	C_{1s}/S_{2p}	C_{1s}/N_{1s}	C_{1s}/Zn_{3p}	% S_{2p} oxidised
As received	14	27	89	27	0
10	3.4	31	19	19	42

C_{1s} Components

	C-H	C-O	C=O	O-C=O
As received	96	4	-	-
10	75	18	4	3

(b) Electron take-off angle (30^{o})

Time (seconds)	C_{1s}/O_{1s}	C_{1s}/S_{2p}	C_{1s}/N_{1s}	C_{1s}/Zn_{3p}	% S_{2p} oxidised
As received	16	27	69	24	-
10	3.1	25	15	14	26

C_{1s} Components

	C-H	C-O	C=O	O-C=O
As received	95	5	-	-
10	77	18	3	2

ratios in Table 6.7 with respect to as received samples suggests that nitrogen is either incorporated from the atmosphere after bringing the whole vacuum system to an atmospheric pressure for transfer into the spectometer (very unlikely), or more probably, the antioxidant has diffused to the surface after plasma treatment, or due to the continuous renewal of the surface by the evolution of small volatile molecules (e.g. CO, CO_2, H_2O etc.), which can not be detected directly by ESCA. It is, therefore, quite conceivable that the deconvoluted component for singly bonded oxygen under the C_{1s} envelope is slightly over-estimated as a result of the similarity in C-N bonding energy, however, this does not alter the overall argument.

The increase in Zn_{3p}/S_{2p} LBE ratios, (LBE: low binding energy, components under the S_{2p} envelopes), by a factor of approximately two at both electron take-off angles after oxygen plasma treatment, as is evidenced in Table 6.9, suggests that these ratios are manifested either by the increase in level of zinc after ablation of surface (it has been already mentioned in chapter three that the level of zinc at the surface is 1.5 mole % compared to that in the bulk, 4.0 mole %), or the sulphur contributing to low energy components has been lost under the conditions employed; the latter possibility seems improbable, as it has been indicated by the approximate constant level of sulphur, whereas the slight increase in ratios of zinc to total sulphur is most likely due to the removal of small volatile molecules containing carbon, thus increasing the level of zinc with ESCA

depth into the sample.

Table 6.9

Comparison of Zn_{3p}/S_{2p} LBE, before and after plasma treatments (2 watts, 0.2 torr)

Time (seconds)		30^{o}	70^{o}
0	As received	2.1	2.0
5		3.8	5.3
20		4.2	4.5

Additional experiments have also been carried out on the optimum cured type 1, Natsyn 2200, elastomers as a function of the time, the samples being left in the dark, before analysing the surface after oxygen plasma treatment at a power loading of 2 watts for 20 seconds and a total pressure of 0.2 torr to interrogate the extent of C_{1s} and S_{2p} oxidation in the presence and absence of antioxidant. The effect of antioxidant, a condensate of acetone and diphenyl amine, on the surface modification is fairly explanatory by the data set out in Table 6.10 in that the elastomer without antioxidant indicates a greater tendency for surface oxidation than that with antioxidant after long exposure to the atmosphere. The ESCA analysis immediately after oxygen plasma treatment revealed very little or no effect of antioxidant on the surface oxidation, which distinguishes the oxygen plasma treatment from the thermal oxidation described in chapter eight.

In the light of these results for the optimum cured type 1

Table 6.10

Comparison of C_{1s} and S_{2p} components for an optimum cured type 1, Natsyn 2200, elastomer with and without antioxidant

(2 watts, 0.2 torr)

Time (days)	C-H	C-O	C=O	O-C=O	$S_{2p_{1/2}}$	$S_{2p_{3/2}}$	$S_{2p_{1/2}}$	$S_{2p_{3/2}}$	$S_{2p_{1/2}}$	$S_{2p_{3/2}}$
2	75	20	3	2	7	13	10	20	17	33
4	83	15	1	1	3	7	13	25	17	35
					Without antioxidant					
2	71	22	3	4	4	9	13	26	16	32
4	77	18	2	3	5	9	11	23	17	35

elastomer studied under different conditions, a partially (50%) cured type 1, Natsyn 2200, elastomer containing antioxidant, which differs only in time of cure (15 minutes) compared to an optimum cured sample (25 minutes) has been investigated at 70^{o} and 30^{o} electron take-off angles, coupled with oxygen plasma at a power loading of 20 watts for 10 seconds and a total pressure of 0.2 torr in reactor B. The effect of an oxygen plasma on the relative intensity ratios, together with the deconvoluted components of C_{1s} and S_{2p} peaks, corresponding to Figure 6.17 in Table 6.11 can be envisaged by reconsidering the ESCA data of the as received sample, discussed in chapter three. The ESCA analysis of a partially cured type 1 elastomer gave on average ratios of 100:5:3 in mole % for Natsyn 2200 (polyisoprene) permanax B and CBS respectively, indicating higher levels of antioxidant and accelerator by a factor approximately eighteen times greater than in the bulk, whilst the level of zinc arising largely from ZnO and the remaining from ZnS, (as revealed by Auger data in chapter three), at the surface is on average 3.0 mole %, slightly less compared to that in the bulk (4.0 mole %), revealing very little increase of zinc level with increasing ESCA depth profile. An estimate of the number of sulphur atoms between the cross-linked points of two polymer chains, calculated from the use of 'swelling' data and analysis of S_{2p} envelope, is on average ten per sulphide linkage.

The differenc in intensity ratios and the development of various structural features under the C_{1s} and S_{2p} envelopes pertaining to oxygen are fairly self explanatory in the light

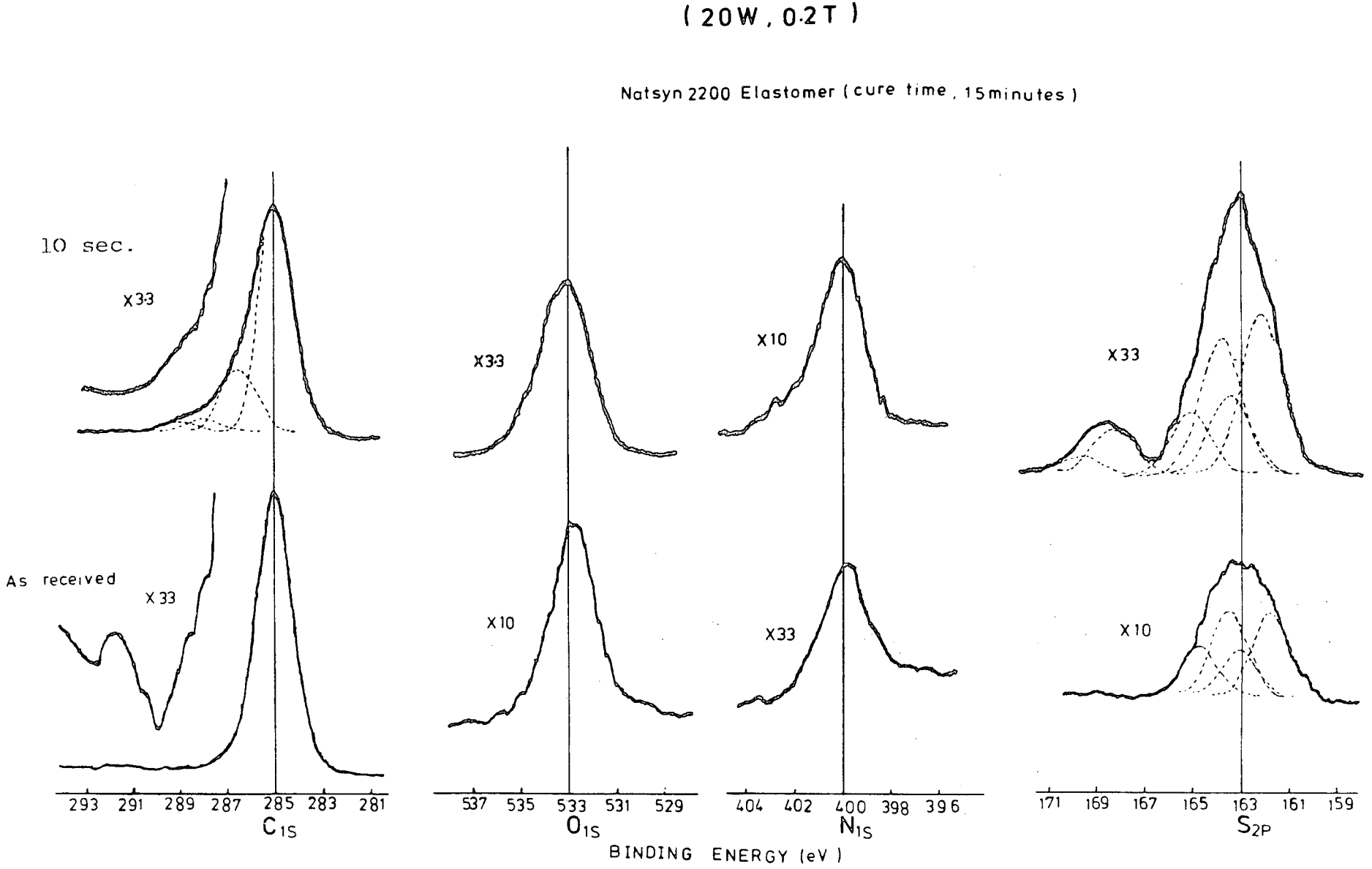

Figure 6.17. C_{1s}, O_{1s}, N_{1s} and S_{2p} spectra of a partially cured type 1, Natsyn 2200, elastomer exposed for 10 seconds in the oxygen plasma (20 watts, 0.2 torr)

Table 6.11

The ratio of intensities of the C_{1s}, O_{1s}, N_{1s}, S_{2p} and Zn_{3p} band in the ESCA spectra of as received partially (50%) cured type 1, Natsyn 2200, elastomer containing antioxidant and plasma oxidised Natsyn 2200 elastomer

(20 watts, 0.2 torr)

(a) Electron take-off angle (70^{o})

Time (seconds)	C_{1s}/O_{1s}	C_{1s}/S_{2p}	C_{1s}/N_{1s}	C_{1s}/Zn_{3p}	Zn_{3p}/S_{2p}	LBE % S_{2p} oxidised
As received	11	15	47	15	1.7	-
10	3.5	26	11	14	4.4	21

C_{1s} Components

	Total C_{1s}	C-H	C-O	C=O	O-C=O
As received	100	96	4	-	-
10	100	69	22	5	4

(b) Electron take-off angle (30^{o})

Time (seconds)	C_{1s}/O_{1s}	C_{1s}/S_{2p}	C_{1s}/N_{1s}	C_{1s}/Zn_{3p}	Zn_{3p}/S_{2p}	LBE % S_{2p} oxidised
As received	13	11	57	11	2.0	-
10	1.3	19.4	13	10	4.0	14

C_{1s} Components

Total C_{1s}	C-H	C-O	C=O	O-C=O
100	96	4	-	-
100	72	21	4	3

of discussion for the optimum cured elastomer with the exception of Zn_{3p}/S_{2p} LBE ratios, as is evidenced by the data in Table 6.11. The increase in Zn_{3p}/S_{2p} LBE ratios by a factor of approximately two at both take-off angles, also consistent with the optimum cured sample, suggests that these ratios for the partially cured elastomer are dictated only by the loss of sulphur at the surface. Indeed, the loss of sulphur by a factor of approximately two as evidenced by the increase of C_{1s}/S_{2p} ratios in Table 6.11 accounts for such an increase, which the latter after oxygen plasma treatment is contradictory to the situation observed for the optimum cured sample. For an optimum cured sample, the ratios of Zn_{3p}/S_{2p} LBE were, merely manifested by the increase of zinc level with increasing ESCA depth profile into the sample.

CHAPTER SEVEN

SURFACE MODIFICATION OF MODELS AND ELASTOMERS BY HYDROGEN PLASMA

PART II

7.1 Introduction

This chapter, as a logical extension of chapter six, describes the effect of hydrogen plasma on models (taken for the establishment of surface chemistry) and 'sulphur-vulcanised' elastomers by exposure to glow discharges, excited in pure hydrogen, as a function of reaction time. In addition, the surface modification affected by hydrogen plasmas, followed by further oxygen plasma treatment in reactor A (Figure 6.4 of chapter six), directly attached to the spectrometer, has also been investigated.

It has been demonstrated in chapter six that, for extensively treated samples in oxygen plasmas, the level of sulphur in di- and trisulphides remained unchanged and the tetrasulphide indicated a loss of sulphur by a factor of two, under the employed conditions. It is also clear that the well-resolved components under the S_{2p} envelopes (caused by spin orbit split) are attacked by the reactive entities of oxygen plasma after the oxidation of carbon-carbon double bonds. Indeed, the observation at substantially higher power loadings indicated the same trend of oxidation (resulting in the ablation of materials from the surface on prolonged treatments in oxygen plasmas).

The background information, in the literature, relates primarily to the reduction of simple sulphide compounds and arises predominantly from studies of reactions of a variety of reagents (lithium aluminium hydride and zinc/acetic acids, etc.) in solution phase.[242,243,249-251] The choice of method for the modification of the surface of thickness in the range

of a few monolayers is, therefore, of particular importance to obviate the reactions extending into the bulk of the sample.[235,252-254]

The prime objective in this chapter has been to establish the surface chemistry of models and hence to use this knowledge to elucidate the surface aspects of sulphur-vulcanised elastomers after treatment with hydrogen plasmas. Very little work has been done in the past on the use of plasmas for the investigation of sulphur containing systems.[240,241,255]

There is very little evidence for the existence of reactive hydrogen entities other than atomic hydrogen at a low pressure (0.2 torr), employed in this work. At a substantial higher pressure (30 - 300 torr), the reactive unstable entities in the plasma: hydrogen atoms (H), excited hydrogen atoms (H*) and molecules (H_2*), protons (H^+) and possibly unstable complexes (H_x*) resulting from three body-collisions of atomic hydrogen with hydrogen molecules, appear to retain a greater proportion of the energy of recombination and, may survive up to 10^8 collisions in the sustaining plasma state before proceeding chemical reactions.[221,256,258,259] Thus, one or more species may participate in the chemical reactions. Figure 7.1 illustrates the numerical solution of the Boltzmann equation for a typical hydrogen plasma, identified by the extent of ionisation value of ($^n/N$). It is clearly apparent that at very low energy, the $f(\varepsilon)$ value decreases with an increasing extent of ionisation. The distributions cross each other in the neighbourhood of 1 eV and the situation is reversed. At still higher energies, the distributions cross

each other twice before the population has increased with the degree of ionisation. The distribution function resembles that of Maxwellian at a very high degree of ionisation. The average energy expressed in the Boltzmann equation is a function of the power and the pressure.

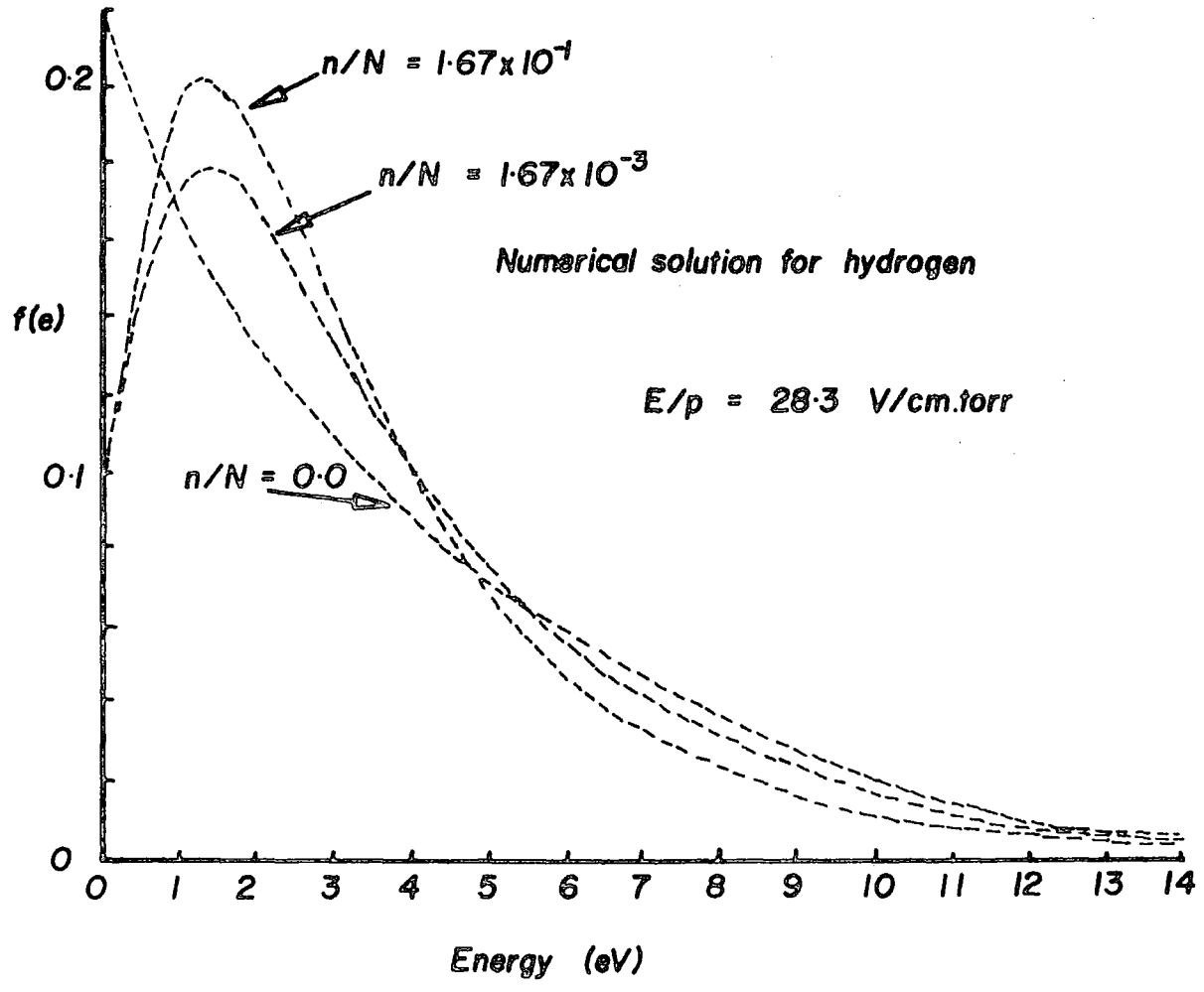

Figure 7.1. Effect of the extent of ionisation on the energy distribution function for a hydrogen plasma.

7.2 Experimental

7.2.1 Samples

The same samples (models as a function of time for the establishment of surface chemistry and Natsyn 2200 elastomers treated sequentially) as in chapter six were subjected to inductively coupled radio-frequency glow discharges excited in hydrogen. The technique of handling the samples and obtaining the spectra were as previously stated.

In chapter six, it has been shown that the level of sulphur was the same before and after plasma treatment (for the optimum cured sample); and, the oxidised sulphur moiety gave rise to a distinct band centred at binding energy $\sim$ 168.5 eV and the corresponding S_{2p} signal from the unoxidised organic sulphide at approximately 164 eV after the oxidation of carbon-carbon double bonds. The oxidation of unsaturated systems constitutes a very fast process, which is followed by the slow oxidation of di- and polysulphides. It will become apparent in the proceeding sections that the chemical nature of the final surface produced on exposure to a hydrogen plasma is largely dictated by the initial surface chemistry of the samples; and, therefore, both models and elastomers have been studied.

Standard laboratory cylinder hydrogen was used without further purification.

7.2.2 Instrumentation

The spectra of as received and plasma treated samples were obtained on the AEI ES200B spectrometer, under the same conditions employed in section 6.2.2 of chapter six; and,

therefore, it is unnecessary to repeat this here.

The potential for specific modification of surface properties by means of plasma techniques has already been elaborated in chapter six and the virtues of employing inductively coupled instrumentation are also well documented elsewhere.[220,228,246] The surfaces modified by hydrogen plasmas in this chapter were affected with both reactors A and B, as indicated schematically in Figure 6.4 of chapter six. Reactor A, particularly designed for the investigation of model systems, was directly attached to a spectrometer enabling considerable flexibility in terms of handling, in particular, liquid samples, without exposure to the atmosphere. Samples of L.cystine in the form of a powder, carefully mounted on Scotch tape to avoid erroneous signals (which would conceivably arise from the uncovered area of a tape), and Natsyn 2200 elastomers cut to a size (20 mm x 6 mm and 2.5 mm) appropriate for a probe tip were inserted into the bridge of the inverted T shaped reactor B by means of the flanged housing at one end of the reactor B. The hydrogen excitations were sustained using a Tegal Corporation Radio-frequency Generator, tuning being accomplished by varying the impedence of matching network. The effect of residual oxygen, which is more pronounced in a less efficient vacuum system, was minimised by producing a greater pumping speed from the modification of existing pumping mechanism.

7.2.3 Plasma reduction of model systems as a function of time

The experimental procedure for the investigation of the effect of hydrogen plasmas on the models was accomplished in the manner outlined in section 6.2.4. Precaution was taken to

minimise the residual effect of oxygen in the vacuum system.

The ESCA and radio-frequency equipment together with experimental procedures have previously been described.

7.3 Results and Discussion

7.3.1 Introduction

The main emphasis in this work, complementary in some respects to chapter six, has been to investigate the effect of hydrogen plasmas on both models and 'sulphur-vulcanised' elastomers, using ESCA as a tool.

It is convenient here to consider the ESCA data in less detail for models first, and then compare them with those of elastomers in the proceeding discussion (with regard to the situation of surface oxidation achieved by exposing to inductively coupled oxygen plasma, described in chapter six).

The important structural features of carbon (C_{1s}) and sulphur (S_{2p}), together with the method of deconvolution into their individual components, have also been outlined previously.

7.3.2 Reactions of models in hydrogen plasma

(a) L.cystine in a hydrogen plasma as a function of time

The core level spectra of as received and hydrogen plasma treated L.cystine, as a function of reaction time, are shown in Figure 7.2, and the relevant intensity ratios are presented in Figure 7.3.

The C_{1s}/O_{1s}, C_{1s}/N_{1s} and C_{1s}/S_{2p} intensity ratios of as received L.cystine reveal that the surface is not entirely representative of the bulk and the powdered sample must have a surface layer of hydrocarbon contamination (section 6.3.2a).

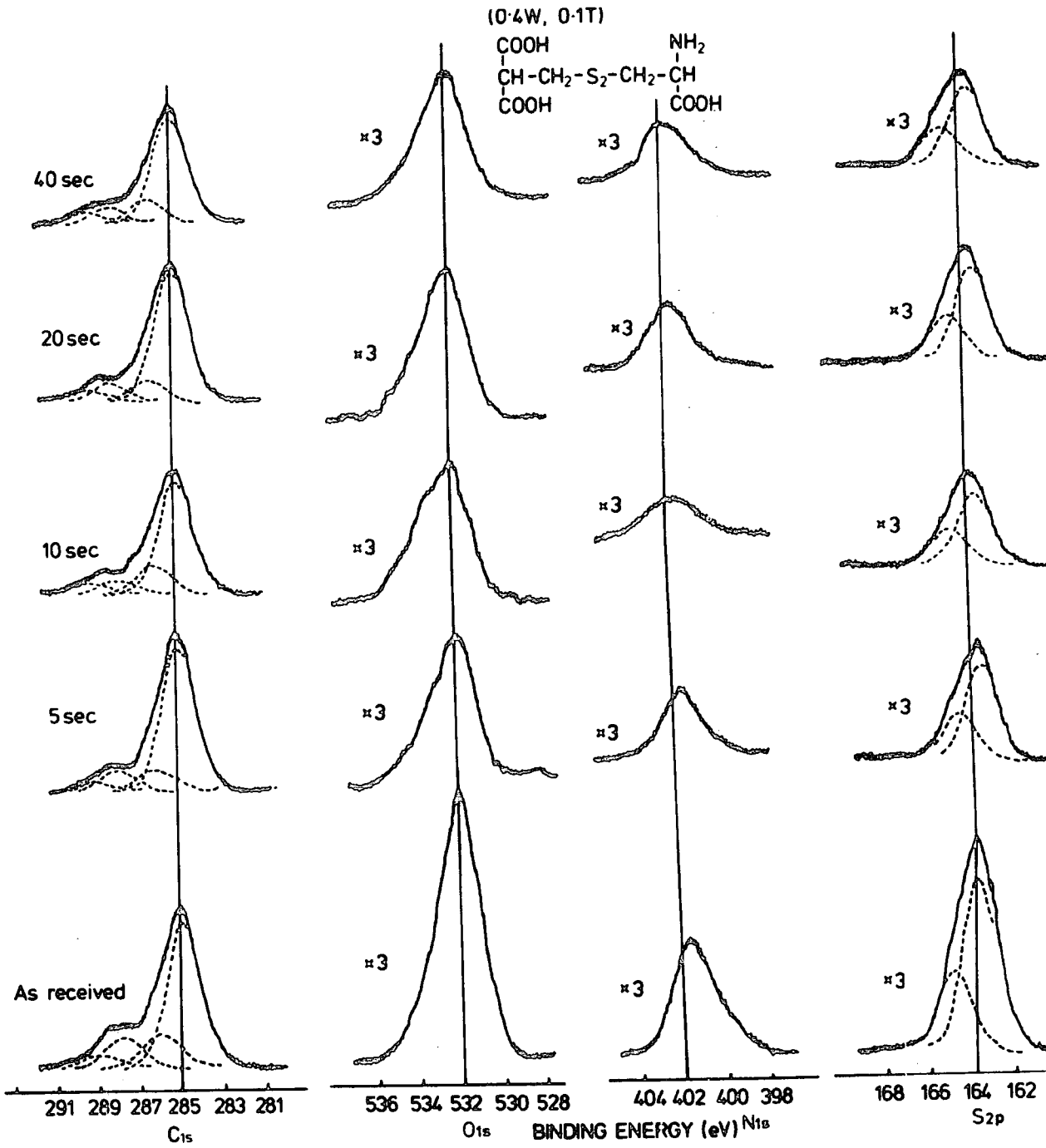

Figure 7.2. C_{1s}, O_{1s}, N_{1s} and S_{2p} spectra of L. cystine vs. time of exposure to a hydrogen plasma (0.4 watt, 0.1 torr).

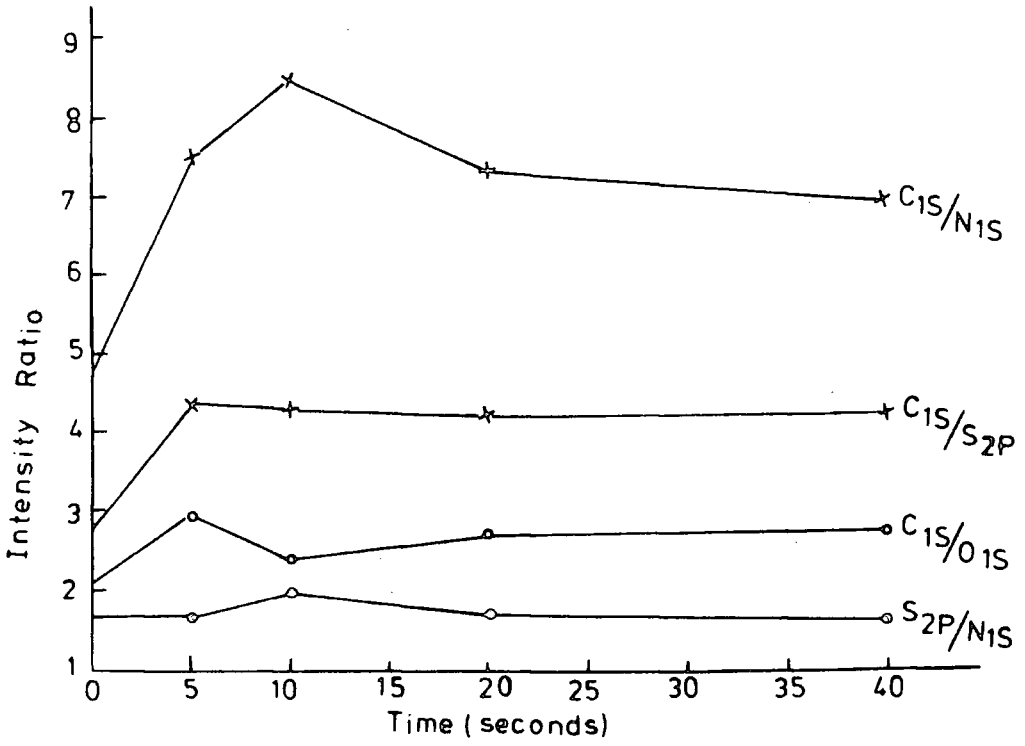

Figure 7.3. Intensity ratios vs. reaction time for L.cystine in a hydrogen plasma (0.4 watt and 0.1 torr).

The ratios of S_{2p}/N_{1s} as a function of reaction time in Figure 7.3 provide clear evidence that sulphur is not lost in the hydrogen plasma under the employed conditions or that both elements are lost at the same rate, whilst the C_{1s}/S_{2p} and C_{1s}/N_{1s} ratios vary significantly, which, in turn, may suggest a build up of a hydrocarbon overlayer. In view of the nature of the sample resulting from impurities, further

elaboration of the C_{1s} functionalities is not preferred; however, an examination of the C_{1s} components under the C_{1s} envelopes and broadening of the shoulder of the O_{1s} levels at binding energy $\sim$ 534 eV reveals that the carboxyl groups (COOH) are converted into hydroxyl functionalities (-OH).

The data in Table 7.1, obtained at a substantially higher power loading (20 watts for 10 seconds and 0.1 torr), also indicate that the level of sulphur remains unchanged in the surface regions.

Table 7.1

The ratio of intensities of the C_{1s}, O_{1s}, N_{1s} and S_{2p} bands in the ESCA spectra of as received and hydrogen plasma treated L.cystine

Conditions: time = 10 seconds, pressure = 0.1 torr and temperature of a sample in the spectrometer = 210K.

	Power (watts)	C_{1s}/O_{1s}	C_{1s}/N_{1s}	C_{1s}/N_{1s}
As received	0	2.1	4.8	2.8
	0.4	2.4	8.5	4.3
	20	2.7	7.3	5.7

The data would seem to be most readily interpretable in terms of reduction of the disulphide to the thiol, the level of sulphur being the same before and after hydrogen plasma treatment.

$$R\text{-}S\text{-}S\text{-}R \xrightarrow[\text{plasma}]{\text{Hydrogen}} 2RSH \qquad (7.1)$$

The study of model systems show that the S_{2p} binding energy for the thiol and disulphide are essentially the same. One may anticipate, therefore, that the reaction of disulphide crosslinks in vulcanised elastomers will lead to surface ($\sim$ 20Å) specific reduction with no loss of sulphur.

(b) Dinonyl trisulphide in a hydrogen plasma as a function of time

The C_{1s} and S_{2p} core levels for dinonyl trisulphide and for the hydrogen plasma treated samples at a power loading of 1 watt and a total pressure of 0.1 torr are indicated in Figure 7.4 as a function of time, and the data, derived from the relevant analysis, are presented in Figure 7.5. The results can be rationalised unambiguously by recalling the equation (6.2) in chapter six.

A knowledge of the mean free path of the photoemitted electrons $\sim$ 15Å for S_{2p} level using $Mg_{k\alpha_{1,2}}$ radiation, an electron take-off angle of 30° and the thickness of the modified layer $\sim$ 5Å suggests that the trisulphide bridge is cleaved under the conditions employed in this investigation and the reaction in the hydrogen plasma results in desorption of H_2S from the surface and formation of thiols, as illustrated in equation (7.2).

$$R\text{-}S\text{-}S\text{-}S\text{-}R \xrightarrow{[H]} 2RSH + H_2S \qquad (7.2)$$

The data in Table 7.2, obtained at a substantially higher power loading, is fairly self explanatory that the sulphur from trisulphide bridge is lost in the form of H_2S and the increase in level of sulphur at the surface is from

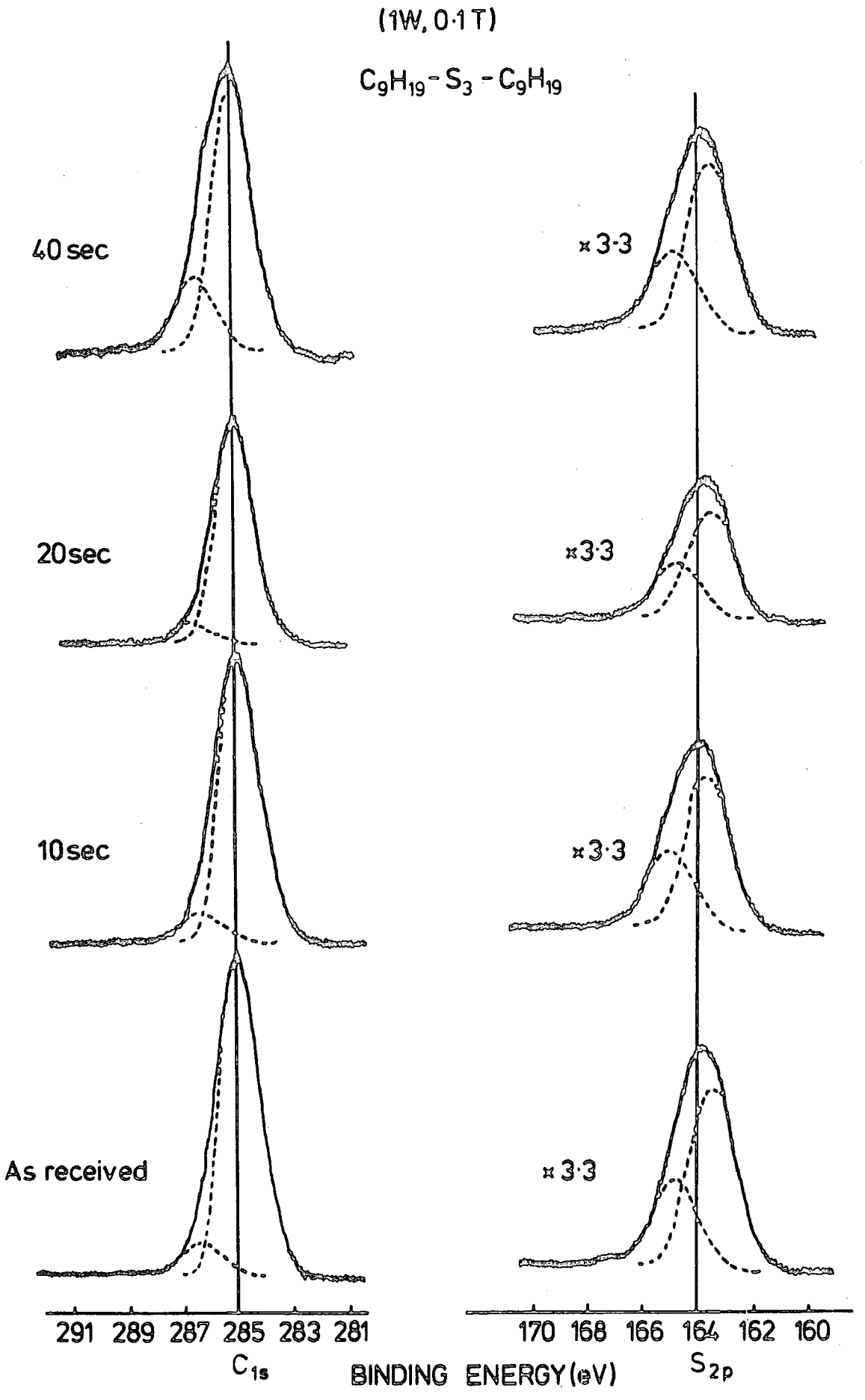

Figure 7.4. C_{1s} and S_{2p} spectra of dinonyl trisulphide vs. time of exposure to a hydrogen plasma (1 watt, 0.1 torr).

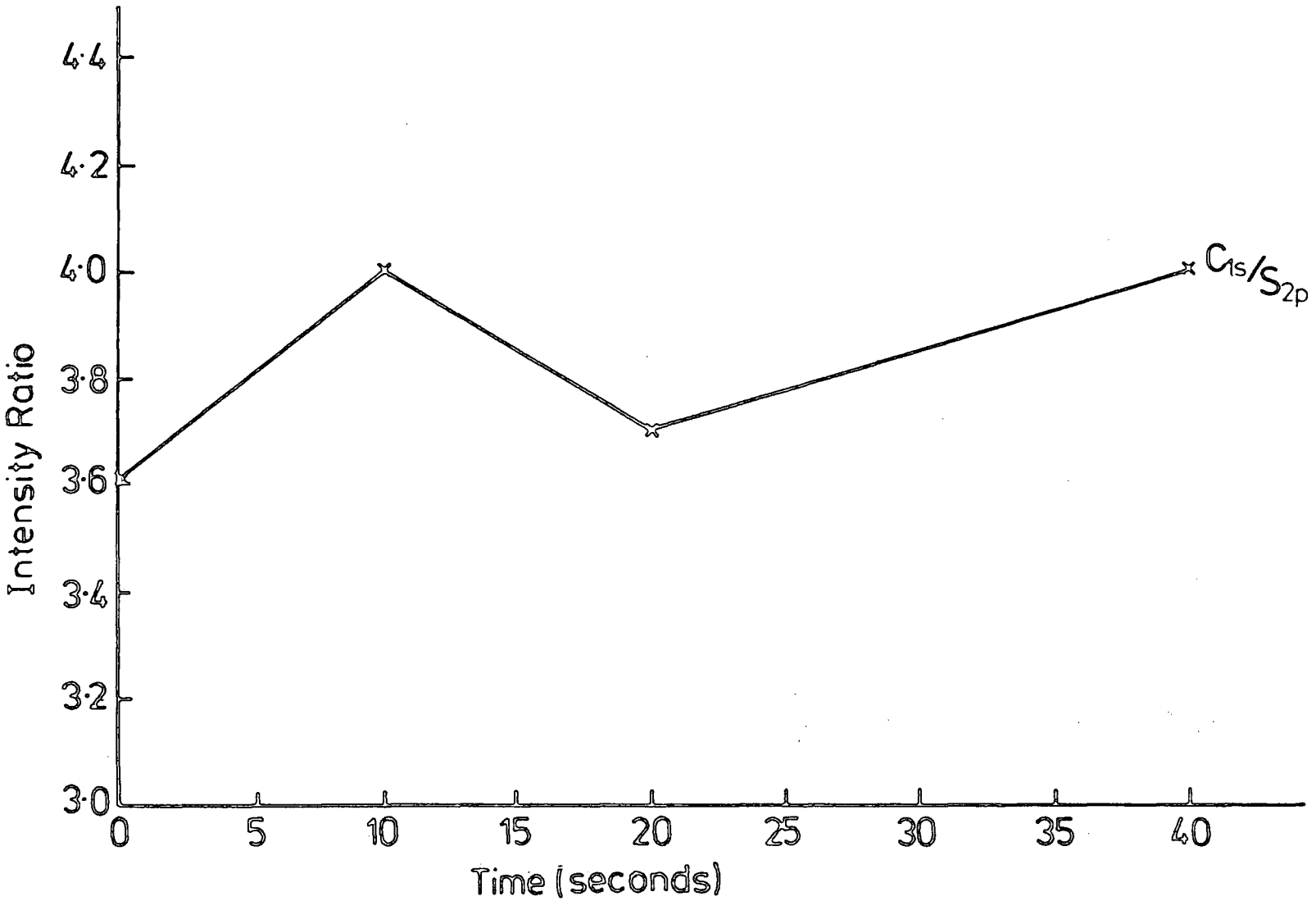

Figure 7.5. Intensity ratio of the C_{1s} and S_{2p} levels in the ESCA spectra of dinonyl trisulphide versus time of exposure to the hydrogen plasma (1 watt, 0.1 torr).

polymerisation of thiols.

Table 7.2

The ratio of intensities of the C_{1s} and S_{2p} bands in the ESCA spectra of as received and hydrogen plasma treated dinonyl trisulphide

Conditions: time = 10 seconds, pressure = 0.1 torr and temperature of a sample = 210K. After plasma treatment, the sample was further cooled to 170K before introducing into the spectrometer for an analysis at an electron take-off angle of 30^{o}.

	Power (watts)	C_{1s}/S_{2p}
As received	0	3.6
	1	4.0
	10	2.9

(c) Bis-n-propyl-γ-triethoxysilyl tetrasulphide in a hydrogen plasma

The effect of the hydrogen plasma on bis-n-propyl-γ-triethoxy tetrasulphide, as a function of time in reactor A, directly attached to the spectrometer, was so dramatic that it was not possible to obtain the data beyond 10 seconds of treatment at a power loading of 1 watt and a total pressure of 0.1 torr; although, several attempts at maximum cooling (150K) had been unsuccessful. The only possible obtainable data is set out in Table 7.3. The active entities, mainly hydrogen atoms in the hydrogen plasma, are selectively reacting initially with ethoxy functional groups and then with silicon before the reaction could proceed at the tetrasulphidic

Table 7.3

The ratio of intensities of the C_{1s}, O_{1s}, S_{2p} and Si_{2p} bands in the ESCA spectra of as received and hydrogen plasma treated bis-n-propyl-γ-triethoxysilyl tetrasulphide

Conditions: power = 1 watt, pressure = 0.1 torr and temperature of a sample in reactor A = 190K. After plasma treatment, the sample was further cooled to 150K before introducing into the spectrometer for an analysis at an electron take-off angle of 30^{o}.

	Time (seconds)	C_{1s}/O_{1s}	C_{1s}/S_{2p}	C_{1s}/Si_{2p}
As received	0	1.9	2.5	6.3
	10	1.7	2.4	6.0

bridge, and the possible overall reactions are as follows:

Scheme 1

$$(EtO)_3Si\text{-}(CH_2)_3\text{-}S_4\text{-}(CH_2)_3\text{-}Si(EtO)_3$$

$$\downarrow \text{ Hydrogen plasma}$$

$$6EtOH + 2SiH_4 + CH_3\text{-}(CH_2)_2\text{-}S_4\text{-}(CH_2)_2\text{-}CH_3$$

$$\longrightarrow 2CH_3(CH_2)_2\text{-}SH + 2H_2S$$

A comparison of the data in Table 7.3 and a knowledge of additional unsuccessful experiments beyond 10 seconds of exposure time in hydrogen plasmas indicates that the products upon such treatments were pumped away in the vacuum system and, the further treatment of a sample, coated onto a gold

substrate, resulted in complete ablation of the sample.

In the light of the discussion for dinonyl trisulphide, it follows that the tetrasulphide is cleaved in the hydrogen plasma, resulting in desorption of two molecules of H_2S and two molecules of thiols formation.

In view of the di-, tri- and tetrasulphide reactions in hydrogen plasmas, further investigation has not been carried on ditertiododecyl pentasulphide.

7.3.3 Reactions of accelerators in a hydrogen plasma

(a) Introduction

It is of interest to study the effect of hydrogen on additives by exposure to plasmas excited in pure hydrogen before examining the ESCA data pertaining to elastomers treated in the hydrogen plasma. Cyclohexylbenzthiazyl sulphenamide (CBS) and tetramethylthiuram disulphide (TMTD) employed in Natsyn 2200 sample formulations have, therefore, been investigated in 'situ', using ESCA, coupled with glow discharge techniques at a total pressure of 0.1 torr and a power loading of 1 watt for 10 seconds.

The samples were cooled to $\sim$ 180K prior to analysis on the ES200B spectrometer.

(b) Cyclohexylbenzthiazyl sulphenamide in a hydrogen plasma

The data in Table 7.4 pertaining to the raw spectra of as received and hydrogen plasma treated in 'situ' in Figure 7.6 indicate very little change in C_{1s}/N_{1s} and C_{1s}/S_{2p} intensity ratios, whilst the effect is dramatic on the FWHM of the N_{1s} peak (FWHM 4.5 eV compared with the untreated sample). The increase in level of oxygen by a factor of two is conceivably from residual oxygen present in the hydrogen plasma (it is

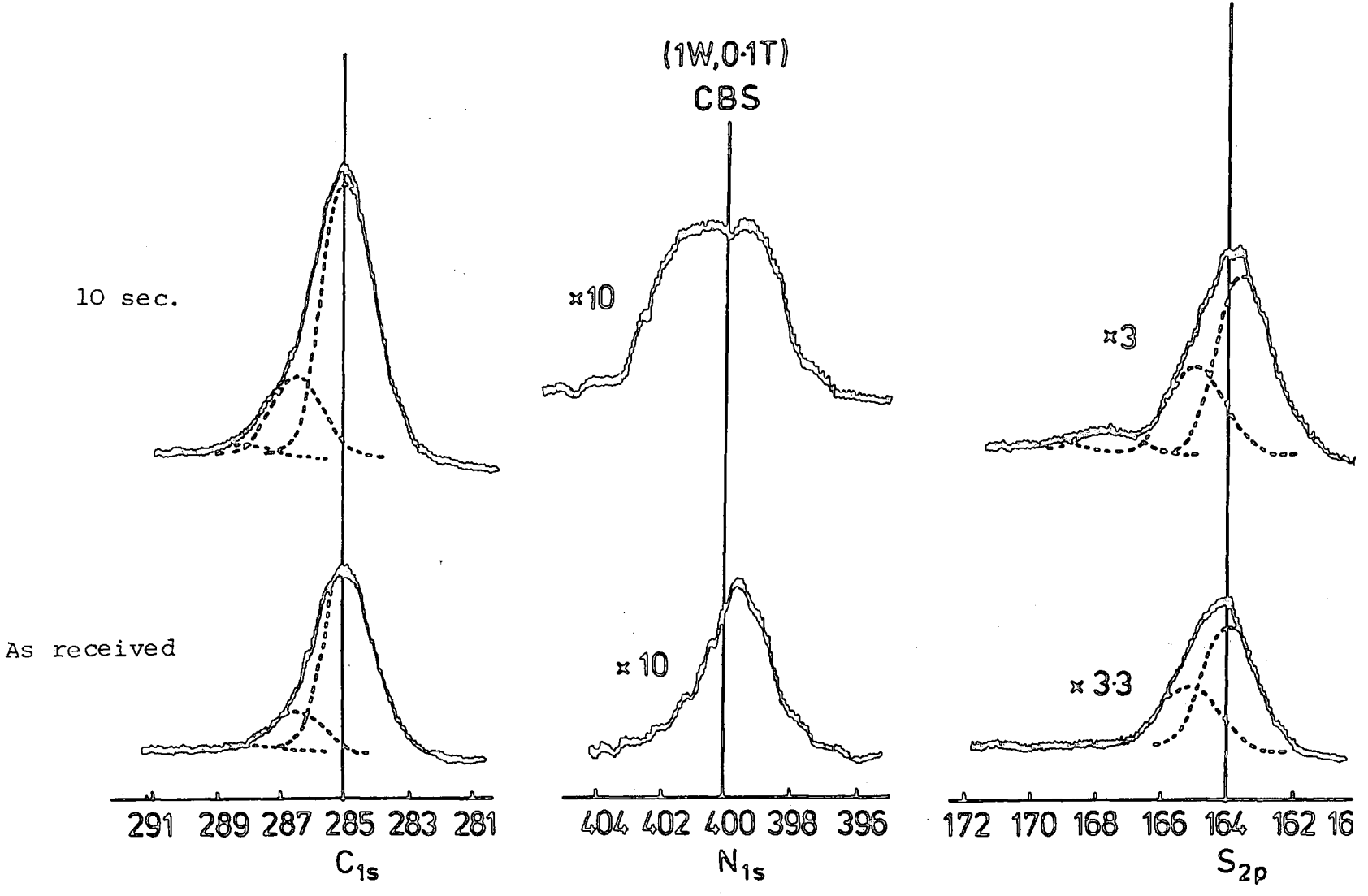

Figure 7.6. C_{1s}, N_{1s} and S_{2p} spectra for cyclohexylbenzthiazyl sulphenamide exposed to a hydrogen plasma (1 watt, 0.1 torr).

Table 7.4

Comparison of intensity ratios before and after plasma treatment

(1 watt, 0.1 torr)

	Time (seconds)	C_{1s}/O_{1s}	C_{1s}/N_{1s}	C_{1s}/S_{2p}
As received	0	6.1	11	4
	10	3.1	10.3	3.6

well known that aromatic systems are particularly prone to oxidation compared with the aliphatic systems). An examination of core level spectra in Figure 7.6 suggests that the carbon doubly bonded to nitrogen in a benzthiazyl is cleaved resulting in the formation of different amine environments and carbonyl functionalities, which the latter is reduced to hydroxyl functionality as is evidenced by the component at 286.6 eV under the C_{1s} envelope. As far as the chemistry of sulphur is concerned, the reactive entities in the hydrogen plasma have very little or no effect on the level of sulphur.

(c) Tetramethylthiuram disulphide in a hydrogen plasma

The ESCA data in Table 7.5 and the core level spectra for TMTD in Figure 7.7 (hydrogen plasma treatment:- a power loading of 1 watt for 10 seconds and a total pressure of 0.1 torr) clearly reveal the effect of reactive hydrogen entities on the intensity ratios of different chemical environments, under the C_{1s} and S_{2p} envelopes. It is clear from the data that sulphur is very readily lost, whilst the stoichiometry of nitrogen with respect to carbon remains unchanged. The

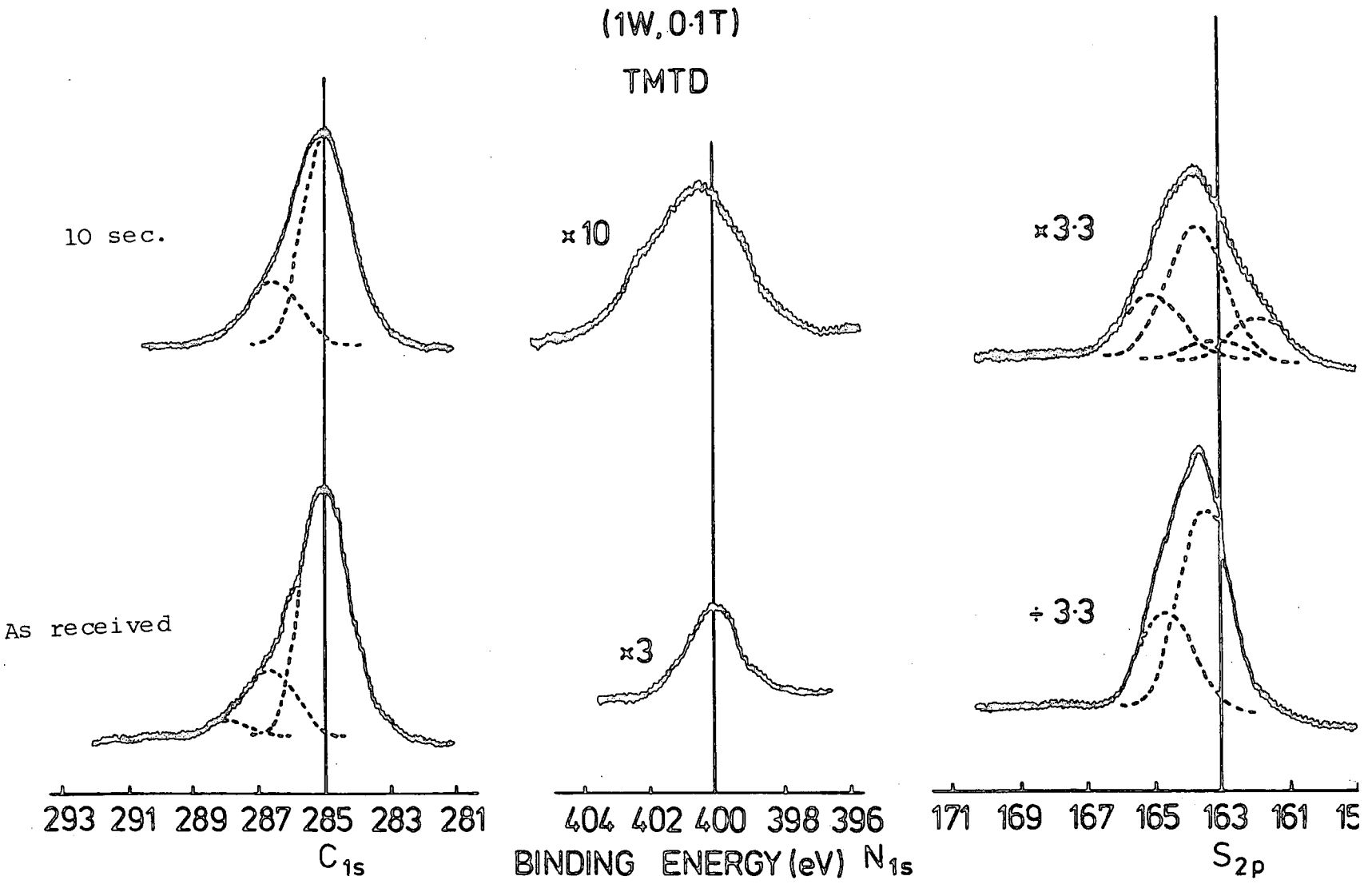

Figure 7.7. C_{1s}, N_{1s} and S_{2p} spectra for tetramethylthiuram disulphide exposed to a hydrogen plasma (1 watt, 0.1 torr)

level of oxygen decreases by a factor of three, conceivably in the form of H_2O and the degree of charge asymmetry in the parent molecule (as is indicated in scheme 6 of chapter six) perhaps provides a basis for rationalising the facile loss of sulphur in the hydrogen plasma. The C=S band is rather unstable, and, in consequence, the net result is that TMTD can readily lose sulphur under the conditions employed in this work.

Table 7.5

Comparison of intensity ratios

(1 watt, 0.1 torr)

Time (seconds)	C_{1s}/O_{1s}	C_{1s}/N_{1s}	C_{1s}/S_{2p}
As received	1.5	10	0.30
10	5.1	11	3.1

The large difference in C_{1s}/S_{2p} intensity ratios is attributed to the loss of sulphur as H_2S from the two doubly bonded sulphur to carbon on either side of a disulphide bridge and partially to the increase of a hydrocarbon layer. The disulphide linkage is conceivably cleaved and reduced to thiol (CH_3, CH_3 $>N-CH_2-SH$).

7.3.4 Surface modification of Natsyn 2200 elastomers in a hydrogen plasma

(a) Introduction

It is clear that the reactions of model systems with hydrogen plasmas are by no means simple; nonetheless, it is

worthwhile examining the ESCA data of hydrogen plasma processed surfaces of the elastomers themselves. Samples of type 1, Natsyn 2200, elastomer containing antioxidant (antioxidant - a condensate of acetone and diphenyl amine) have been subjected to sequential treatments with inductively coupled glow discharge, excited in pure hydrogen at a power loading of 2 watts and a total pressure of 0.1 torr. The detailed compositions of the bulk formulation in terms of weight and normalised mole % for type 1, Natsyn 2200, elastomer are given in chapter three.

(b) Type 1, Natsyn 2200, elastomer in a hydrogen plasma

The core level spectra for the as received and hydrogen plasma treated type 1, Natsyn 2200, elastomer are shown in Figure 7.8 and the pertaining ESCA data at 30^{o} and 70^{o} electron take-off angle are set out in Table 7.6.

The data, in conjunction with the model studies, suggest that the polysulphide crosslink is cleaved and the sulphur is lost in the form of H_2S and the resulting thiols polymerise such that the level of sulphur at the surface decreases slightly with reaction time, or the sulphur is not lost. The variation in C_{1s}/S_{2p} intensity ratios is due to different surface composition of elastomer, taken fresh for each hydrogen treatment from the same sheet and conceivably to build up of a hydrocarbon overlayer, whilst the stoichiometry of nitrogen increases with respect to carbon. An examination of the C_{1s}/Zn_{3p} intensity ratios (compared with the oxygen plasma treatments in chapter six) and the approximate constant ratios

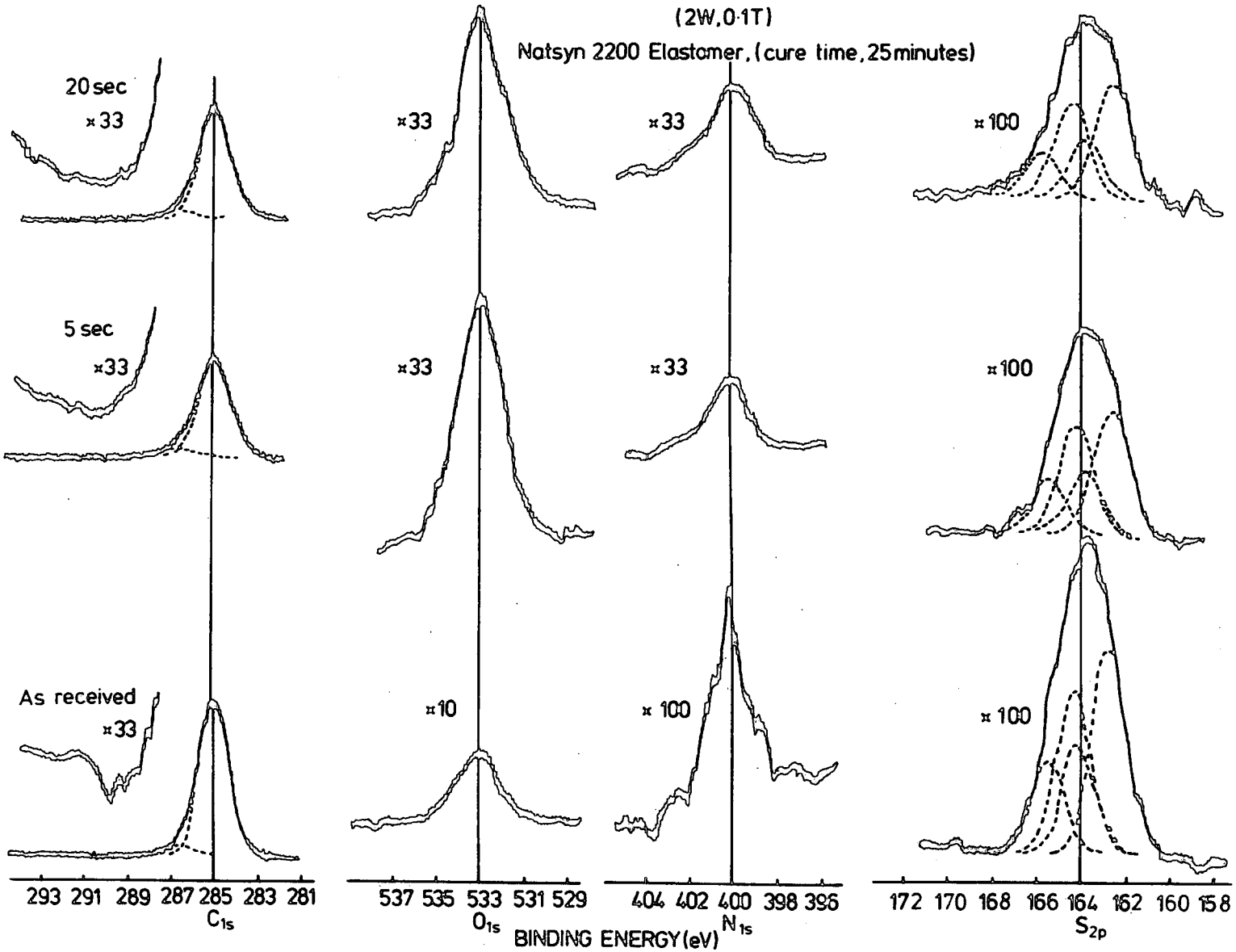

Figure 7.8. C_{1s}, O_{1s}, N_{1s} and S_{2p} spectra of an optimum cured type 1, Natsyn 2200 elastomer vs. time of exposure to a hydrogen plasma (2 watts, 0.1 torr).

Table 7.6

The ratio of intensities of the C_{1s}, O_{1s}, N_{1s}, S_{2p} and Zn_{3p} bands in the ESCA spectra of as received optimum cured type 1, Natsyn 2200, elastomer containing anti-oxidant and hydrogen plasma treated Natsyn 2200 elastomer

(2 watts, 0.1 torr)

Electron take-off angle (70^{o})

Time (seconds)	C_{1s}/O_{1s}	C_{1s}/S_{2p}	C_{1s}/N_{1s}	C_{1s}/Zn_{3p}
As received	14	27	89	27
5	13	37	42	30
20	12	38	35	45

Electron take-off angle (30^{o})

Time (seconds)	C_{1s}/O_{1s}	C_{1s}/S_{2p}	C_{1s}/N_{1s}	C_{1s}/Zn_{3p}
As received	16	27	69	24
5	11	29	41	23
20	15	34	37	31

of Zn_{3p}/S_{2p} suggests the latter statement that the level of sulphur remains essentially unchanged and sulphur is not desorbed from the surface as H_2S under the conditions employed in this part of the study.

The Zn_{3p}/S_{2p} LBE intensity ratios in Table 7.7 are approximately constant (two) at both electron take-off angles and a comparison with the data in Table 6.9 of chapter six implies that the ablation of the surface is not a dominant

factor under the conditions used during hydrogen plasma treatments. (It has previously been stated that the level of zinc at the surface is, approximately 1.5 mole %, less compared to that in the bulk, ∿ 4.0 mole %, and increases with increasing ESCA depth profile into the sample. The oxygen plasma processed surfaces revealed the increased level of zinc by a factor of two, suggesting that the ablation of materials from the surface is a dominant factor in oxygen plasmas).

Table 7.7

Comparison of Zn_{3p}/S_{2p} LBE before and after plasma treatments

(2 watts, 0.1 torr)

	Time (seconds)	30°	70°
As received	0	2.1	2.0
	5	2.4	2.2
	20	2.0	1.6

The nitrogen spectra in Figure 7.8 are broadened by the presence of at least two components (amine and protonated amino), and a sharp decrease in C_{1s}/N_{1s} intensity ratios in Table 7.6 with respect to as received sample indicates that the nitrogen in the form of amine is conceivably incorporated either from the atmosphere after bringing the whole vacuum system to atmospheric pressure for the transfer of the sample into the spectrometer (very unlikely) or more probably that the

antioxidant has diffused to the surface after plasma treatment (the oxygen plasma processed elastomers, under the comparable experimental procedure, also indicated amine and protonated amine functionalities at binding energies ∿ 399 eV and ∿ 402 eV respectively).

The immediate loss of unsaturation, ∿ 6.5 eV from the main C_{1s} photoionisation peak, is associated with the addition of reactive hydrogen entities to the carbon-carbon double bonds. The carboxyl groups are converted into hydroxyl functionalities, as is evidenced by the increase of a component at a binding energy of 286.6 eV under the C_{1s} envelope.

The data in Table 7.8 for 30^{o} and 70^{o} electron take-off angles, corresponding to the hydrogen plasma at a substantially higher power loading (20 watts for 10 seconds and 0.1 torr), indicate that the intensity ratios of C_{1s}/S_{2p} and Zn_{3p}/S_{2p} are increased by a factor of approximately two; which may imply that the sulphur at the surface of elastomer containing sulphur functionality of four on average is desorbed as H_2S and the subsequent reaction stops at thiols. The increase in Zn_{3p}/S_{2p} LBE intensity ratio, by a factor of approximately two at 30^{o} electron take-off angle in Table 7.8 indicates that the level of zinc increases with the ESCA depth profile into the sample. However, the rather low ratio of Zn_{3p}/S_{2p} LBE at the extreme surface is attributed to the low level of zinc, initially present in the extrme surface region as is evidenced by the high intensity ratio of C_{1s}/Zn_{3p} in Table 7.8. The high susceptibility of carbon-carbon double bonds to reactive

Table 7.8

The ratio of intensities of the C_{1s}, O_{1s}, N_{1s}, S_{2p} and Zn_{3p} bands in the ESCA spectra of as received optimum cured type 1, Natsyn 2200, containing antioxidant and hydrogen plasma treated Natsyn 2200 elastomer

(20 watts, 0.1 torr)

Electron take-off angle (70^{o})

Time (seconds)	C_{1s}/O_{1s}	C_{1s}/S_{2p}	C_{1s}/N_{1s}	C_{1s}/Zn_{3p}	Zn_{3p}/S_{2p} LBE
As received	14	27	89	27	2.0
10	10	49	45	51	1.8

Electron take-off angle (30^{o})

As received	16	27	69	24	2.1
10	10	52	38	30	3.9

entities of oxygen, either resulting from air bubbles in the elastomer or from the presence of residual oxygen in the sustaining hydrogen plasma, is evidenced by the increase of O_{1s} level.

In view of these results for the optimum cured type 1, elastomer, a partially (50%) cured type 1, Natsyn 2200, elastomer containing antioxidant, which differs only in time of cure (15 minutes) compared to an optimum cured sample (25 minutes) has been studied at 30^{o} and 70^{o} take-off angles, coupled with hydrogen plasma at a power loading of 20 watts for 10 seconds and a pressure of 0.1 torr; and, the relevant intensity ratios, derived from the raw spectra in Figure 7.9,

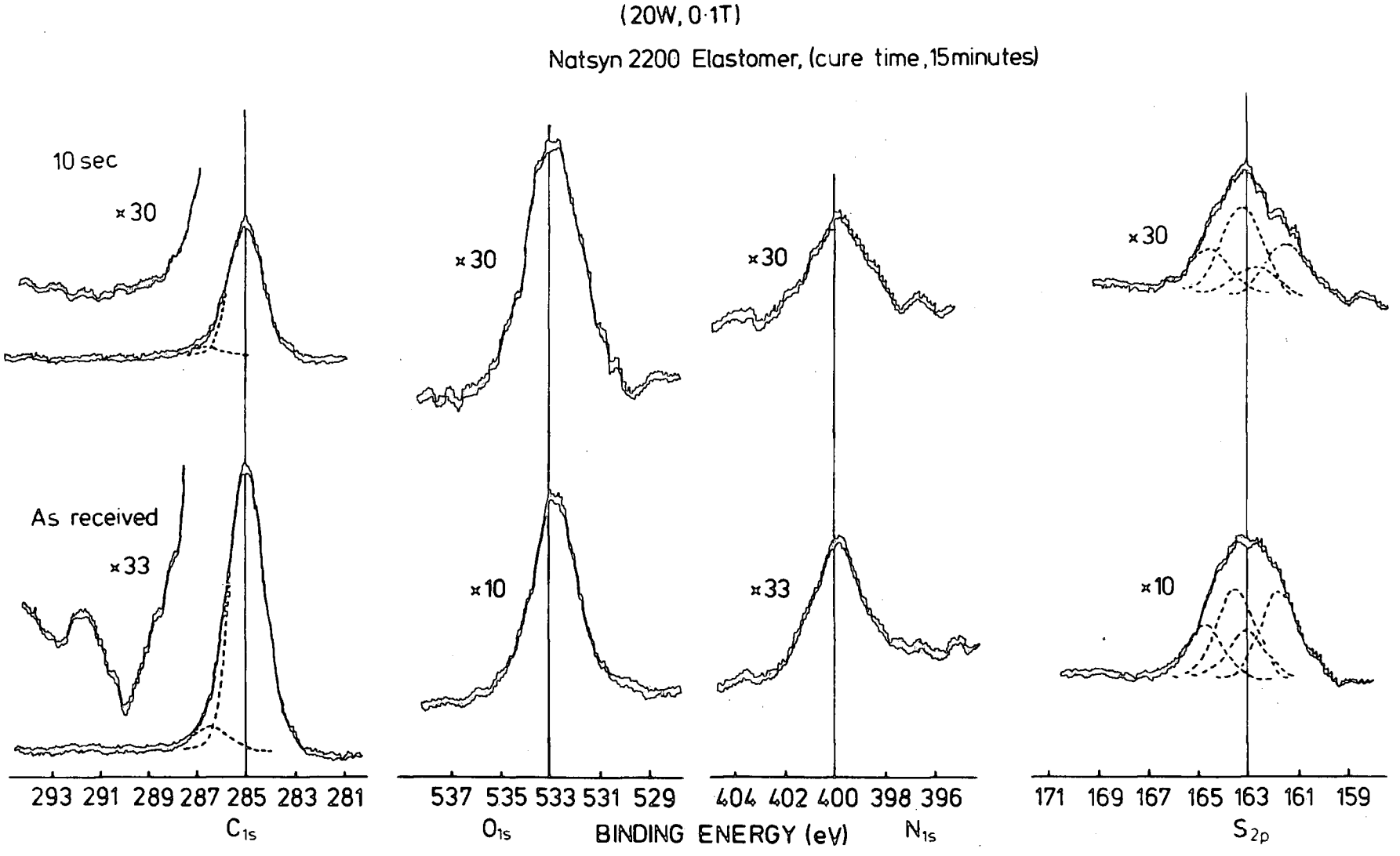

Figure 7.9. C_{1s}, O_{1s}, N_{1s} and S_{2p} spectra for a partially cured type 1, Natsyn 2200, elastomer exposed to a hydrogen plasma (1 watt, 0.1 torr).

are set out in Table 7.9.

The increase in C_{1s}/S_{2p} intensity ratios at both electron take-off angles after hydrogen plasma treatment suggests that half of the sulphur from the polysulphide crosslink (ten sulphur atoms per crosslink) is eliminated in the form of H_2S and the subsequent reaction stops at thiols, whilst the stoichiometry of nitrogen increases with respect to carbon. However, the intensity ratios of C_{1s}/Zn_{3p} are increased by a factor of approximately two and do not support the above statement that the level of sulphur is changed during the hydrogen plasma treatment.

The Zn_{3p}/S_{2p} LBE, intensity ratios remain essentially constant (two) at 30^{o} and 70^{o} electron take-off angles (it has been stated in chapter three that the level zinc at the surface, 3 mole %, is approximately the same as in the bulk, 4 mole %, and the angular dependent study has little effect on the Zn_{3p}/S_{2p} intensity ratios as far as the ESCA depth profile is concerned into the sample).

7.3.5 Surface modification by hydrogen/oxygen plasmas

(a) Introduction

In this part of the study, the surface chemistry of model and elastomer substrates has been specifically modified by means of inductively coupled plasmas, excited in hydrogen and oxygen, and the results of such treatment are elaborated by means of ESCA.

Dinonyl trisulphide as a model and an optimum cured type 1, Natsyn 2200, elastomer containing antioxidant were treated

Table 7.9

The ratio of intensities of the C_{1s}, O_{1s}, N_{1s}, S_{2p} and Zn_{3p} bands in the ESCA spectra of as received partially (50%) cured type 1, Natsyn 2200, elastomer containing antioxidant and hydrogen plasma treated Natsyn 2200 elastomer

(20 watts, 0.1 torr)

Electron take-off angle (70^{o})

Time (seconds)	C_{1s}/O_{1s}	C_{1s}/S_{2p}	C_{1s}/N_{1s}	C_{1s}/Zn_{3p}	Zn_{3p}/S_{2p} LBE
As received	11	15	47	15	1.7
10	11	25	35	36	1.7

Electron take-off angle (30^{o})

As received	13	11	57	11	2.0
10	11	18	27	25	1.9

in reactor A, directly attached to the spectrometer, at a power loading of 1 watt and a total pressure of 0.2 torr (as indicated pressure of 0.2 torr by a Pirani gauge for hydrogen gas is approximately equal to true pressure of 0.1 torr).

(b) Dinonyl trisulphide in hydrogen/oxygen plasmas

The spectra of dinonyl trisulphide in Figure 7.10a treated with hydrogen plasma for 10 seconds after a brief exposure (10 seconds) to oxygen plasma and the spectra in Figure 7.10b for 20 seconds in oxygen plasma followed by a further 10 seconds in hydrogen plasma at a power loading of 1 watt and a total pressure of 0.2 torr as indicated by the Pirani gauge, together with data in Table 7.10, tend to reveal a different

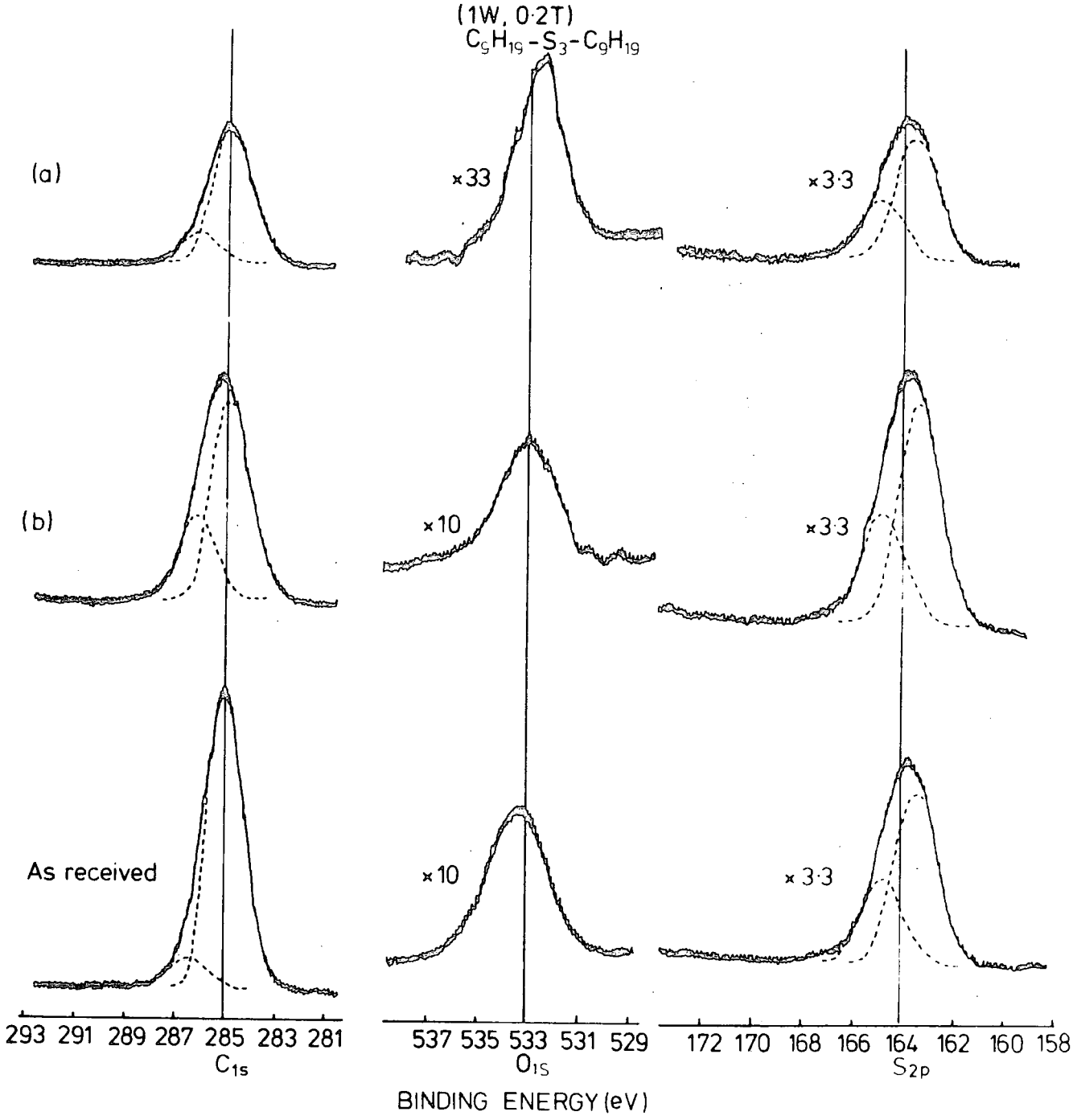

Figure 7.10. C_{1s}, O_{1s} and S_{2p} spectra for dinonyl trisulphide exposed to hydrogen/oxygen plasmas (1 watt, 0.2 torr).

Table 7.10

The ratio of intensities of the C_{1s}, O_{1s} and S_{2p} bands in the ESCA spectra of as received dinonyl trisulphide and hydrogen/oxygen plasmas treated dinonyl trisulphide

(1 watt, 0.2 torr as indicated by Pirani gauge)

Hydrogen plasma for 10 seconds, followed by an oxygen plasma for 10 seconds

	C_{1s}/O_{1s}	C_{1s}/S_{2p}
As received	12.3	3.6
Plasma treated	25	2.6

Oxygen plasma for 20 seconds, followed by a plasma for 10 seconds

	C_{1s}/O_{1s}	C_{1s}/S_{2p}
Plasma treated	5.2	2.7

situation compared with that of a sample treated in oxygen and hydrogen plasma alone. The intensity ratio of C_{1s}/S_{2p} of the order of 2.6 for both different treatments and a knowlege of the relative contribution of signals from the modified surface, derived using an equation 6.2 in chapter six, suggest that the alkyl trisulphide resulted in higher polysulphides, namely tetrasulphide, conceivably via free radical mechanism. One would also expect the same trend for a 'sulphur-vulcanised' elastomer, coupled with such conditions, if the above observation is genuine. The sulphur spectra do not indicate any propensity for oxidation to sulphates and, if any formed,

would have been reduced either to alkyl sulphides or thiols or the surface was ablated, the latter appearing more probable.

The increase in level of oxygen for these kinds of treatments are associated with the increase of carbon-oxygen functionalities, as is evidenced by the development of components under the C_{1s} envelopes in Figure 7.10.

(c) Type 1, Natsyn 2200, elastomer in hydrogen/oxygen plasmas

After having investigated the effect of the different exposure sequence of hydrogen and oxygen plasmas on the dinonyl trisulphide, an optimum cured type 1, Natsyn 2200, elastomer containing antioxidant has been subjected to hydrogen plasma for 20 seconds, followed by a further 20 seconds in oxygen plasma; and, also, with a sequence of oxygen and hydrogen plasma at a power loading of 1 watt and a total pressure of 0.2 torr, as indicated by the Pirani gauge on reactor A (configuration in chapter six). The reactor A, directly attached to the spectrometer, enabled the direct investigation of samples by obviating the effect of atmospheric exposure.

The core level spectra for an optimum cured type 1, Natsyn 2200, elastomer are presented in Figure 7.11 and the relevant intensity ratios are set out in Table 7.11. The data clearly illustrate the dramatic effect on the intensity ratios irrespective of the sequence of hydrogen and oxygen plasmas under the conditions employed in this part of the study. The C_{1s} and S_{2p} core level spectra in Figure 7.11 appear similar, irrespective of the sequence of hydrogen and oxygen plasmas used, without revealing any tendency for reduction of oxidised

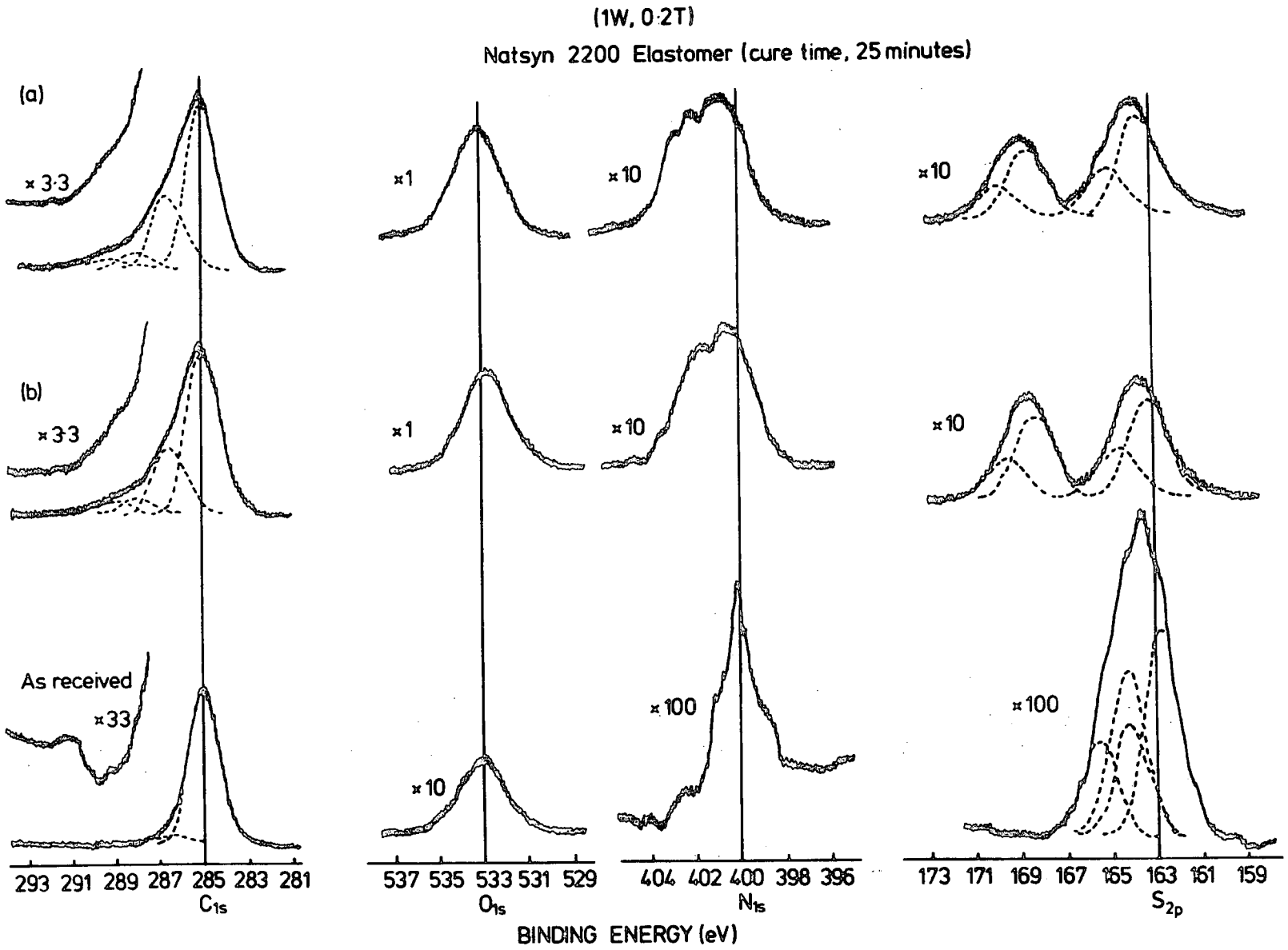

Figure 7.11. C_{1s}, O_{1s}, N_{1s} and S_{2p} spectra for an optimum cured type 1, Natsyn 2200, elastomer exposed to hydrogen/oxygen plasmas (1 watt, 0.2 torr).

Table 7.11

The ratio of intensities of the C_{1s}, O_{1s}, N_{1s}, S_{2p} and Zn_{3p} bands in the ESCA spectra of as received optimum cured type 1, Natsyn 2200, elastomer containing anti-oxidant and hydrogen/oxygen plasmas treated Natsyn 2200 elastomer

(1 watt, 0.2 torr as indicated pressure)

Hydrogen plasma for 20 seconds, followed by oxygen plasma for 20 seconds

	C_{1s}/O_{1s}	C_{1s}/S_{2p}	C_{1s}/N_{1s}	C_{1s}/Zn_{3p}
As received	16	27	69	24
Plasma treated	1.9	2.9	10.2	18.4

Oxygen plasma for 20 seconds, followed by hydrogen plasma for 20 seconds

	C_{1s}/O_{1s}	C_{1s}/S_{2p}	C_{1s}/N_{1s}	C_{1s}/Zn_{3p}
Plasma treated	2.0	7.7	9.7	16

organic sulphur, which distinguishes from the dinonyl trisulphide under such treatments; and, therefore, it is probable that the ablation of the dinonyl trisulphide surface may have been responsible for the disappearance of sulphone functionality.

It is clearly evident from the data in Table 7.11 that the levels of sulphur and nitrogen are much higher than for elastomers studied previously in oxygen and hydrogen plasmas alone. The sharp increase in sulphur level is either associated with the diffusion of sulphur from the bulk to the surface or the tetrasulphide linkages on average are cleaved via free

radical mechanism resulting in higher polysulphides; the latter seems more probable in conjunction with the knowledge of dinonyl trisulphide, subjected to similar conditions. The oxidised sulphur moiety gave a distinct peak of equal intensity to the corresponding unoxidised sulphur, occurring at binding energies of 168.5 (sulphonic acid) and 163.7 eV respectively. The distribution of carbon-oxygen functionalities is clearly evident from the spectra in Figure 7.11.

The dramatic rise in the level of nitrogen at the surface of an elastomer, monitored without exposure to the atmosphere, suggests that the antioxidant (a condensate of diphenyl amine and acetone) has diffused from the bulk to the surface after plasma treatments. (It has previously been stated that the increase in level of nitrogen at the surface is either associated with the diffusion of antioxidant from the bulk to the surface, or incorporated from the atmosphere by a reaction of nitrogen with the active sites on the surface of an elastomer after bringing the whole vacuum system to an atmospheric pressure for the transfer of the sample into the spectrometer. The active sites are created by plasmas.) The nitrogen (N_{1s}) spectra are consistent with the distinct overlapping components of amine and protonated amine appearing at binding energies of $\sim$ 399.0 and 402.0 eV respectively.

7.4 Conclusion

The ESCA data of models and elastomers, coupled with hydrogen plasmas at both modest and substantially higher power loadings, have highlighted the following

(i) The level of sulphur in L.cystine remains essentially the same before and after hydrogen plasma treatments, whereas the dinonyl trisulphide indicated a loss of sulphur as H_2S and the subsequent reaction either ceased at thiols or the thiols polymerised to give higher sulphides depending upon the conditions.

(ii) The effect of hydrogen plasma on bis-n-propyl-γ-triethoxy tetrasulphide is so dramatic that it was not possible to obtain the data beyond 10 seconds of treatment at a power loading of 1 watt and a total pressure of 0.1 torr.

(iii) Type 1, Natsyn 2200, elastomer suggests a loss of sulphur in the form of H_2S.
The intensity ratios of Zn_{3p}/S_{2p} LBE are approximately constant (2) at a modest power loading and the increase of these ratios by a factor of two at a substantially higher loading for the optimum cured elastomer is associated with an increase of zinc level with increasing depth into the sample (i.e. as the surface is ablated).

(iv) Irrespective of the sequence of hydrogen/oxygen plasma treatments in section 7.3.5, the surface of dinonyl trisulphide and elastomer indicated an increase of sulphur level, and the S_{2p} peak for the optimum cured, Natsyn 2200 sample is oxidised by 50% compared to the oxidation in oxygen plasma alone ($\sim$ 30%), in chapter six.

CHAPTER EIGHT

THERMAL OXIDATION OF NATSYN 2200 ELASTOMERS

8.1 Introduction

A very large body of knowledge on the thermal oxidation of polymers has been accumulated in the last fifty years, the motivation being the great technological importance of rubbers.[260-283] The predominant emphasis in these studies has been bulk analysis by the usual chemical and physical methods, however, there has been little work on the surface oxidation of elastomers.[284] This has been mainly due to the lack of a suitable analytical technique for analysing a very thin surface layer in the range 10 - 50Å. ESCA offers the possibility of undertaking such surface studies, although it may be anticipated that the complexity of the materials might lead to difficulties or ambiguities of interpretation. The large volume of ESCA background information, which is now available at Durham, however, on both carbon and sulphur containing systems make an investigation of the changes in surface chemistry, as a function of thermal oxidation worthwhile at this time, if only from an empirical basis because of the paucity of alternative data in the literature.

The general features of the bulk oxidation mechanism are well documented,[260-288] and they have been developed primarily from work on model systems largely because of the difficulties involved in analysing small amounts of chemical changes in polymers; and, therefore, it is to this problem, the ESCA work is addressed; to investigate the surface aspects of 'sulphur-vulcanised' systems. The choice of method used to oxidise the sample surface is also of considerable importance. For example, thermal oxidation by simply heating in air at

100°C, as has been used in this work, is not readily controlled and generally causes oxidation into the bulk of the sample.[235,252-254,289] Solution techniques, for example chromic acid etching,[290] also suffer from similar difficulties and, in addition, the loss of low molecular weight fragments cannot be discounted. The work here, complements that on plasma oxidation in chapter six, where the emphasis has been on a consideration of plasma techniques for delineating cross-link functionality.

Drastic changes in tensile strength, dielectric constant, elongation, hardness and other properties at an elevated temperature can be caused by a few percent of oxygen absorption.[291-306] The essence of degradation is a change in structure, and bonding that may permeate the surface, sub-surface, and bulk; inhomogeneities usually result in these regions. Thermal oxidation, therefore, extends from the surface into the bulk. However, the initial interaction of oxygen at 100°C with 'sulphur-vulcanised' polyisoprene, at least as far as the surface regions are concerned, is dominated by the production of peroxides resulting in a wide range of free-radicals. Attempts at identification and quantification of individual rate processes in the thermal oxidation study have not been made; instead, attention has been focussed on examining the broad outlines of the oxidative degradation.

8.2 Experimental

8.2.1 Samples

Samples of an optimum cured type 1, Natsyn 2200, elastomer

with and without antioxidant (size of 20 mm x 6 mm x 2.5 mm), mounted on microscope slides, were heated in an oven at 100 ± 2°C, as a function of time and, then were studied by ESCA immediately after the heat processing.

Direct handling of the actual samples was avoided to prevent contamination, which could conceivably give rise to extraneous signals.

8.2.2 Instrumentation

ESCA spectra were recorded on an AEI ES200B spectrometer, using $Mg_{K\alpha_{1,2}}$ radiation of energy 1253.7 eV and $Au_{4f_{7/2}}$ level at 84 eV binding energy for calibration had a full width at half maximum (FWHM) of 1.15 eV, under the employed conditions. The spectra were deconvoluted and integrated on a DuPont (model 310) Curve Resolver, with binding energies being referenced to the hydrocarbon component at 285.0 eV.

A B and T Unitemp Oven (model BS2648) with a forced air ventilation rate of 3,000 litres per hour was used for thermal oxidation of elastomers at 100 ± 2°C. The radial fan impeller at the base draws the air from various levels over the heater elements and forces the hot air into the chamber, thus minimising the thermal gradient.

8.3 Results and Discussion

8.3.1 Introduction

The main emphasis of this chapter, with the application of ESCA, has been to study the surface oxidation of elastomers and to investigate the efficiency of antioxidant. Samples of an optimum cured type 1, Natsyn 2200, elastomer with and

without antioxidant (a condensate of acetone and diphenyl amine added as a thermal antioxidant) were oxidised by simply heating in air at 100 ± 2°C.

In view of the complexities presented by the many factors, such as the type, the degree of cure, presence of non-rubber components, vulcanisation ingredients, antioxidants, and by the behaviour of oxidation of polyisoprenes and sulphides separately, it is convenient to divide the discussion into two parts, namely the chemistry of polyisoprenes and sulphides. The vital role of sulphides to act as preventive antioxidant are also discussed along with the added antioxidant.

The detailed compositions of type 1, Natsyn 2200, elastomers with and without antioxidant, as indicated in chapter three, are identical.

8.3.2 An optimum cured type 1, Natsyn 2200, elastomer in air at 100°C, as a function of time

Figure 8.1 shows the C_{1s}, O_{1s}, N_{1s} and S_{2p} photoionisation levels for the optimum cured type 1, Natsyn 2200, elastomer measured at an electron take-off angle of 30° after having been heated in air at 100°C as a function of time, and the corresponding results for both 30° and 70° take-off angles are represented pictorially in Figures 8.2 - 8.6 (partial results of a higher take-off angle are included, where appropriate).

A comparison of Figures 8.2 and 8.3 pertaining to oxidative functionalities of carbon and sulphur respectively, as a function of time, clearly demonstrates that the carbon-carbon double bonds react with oxygen at a much faster rate

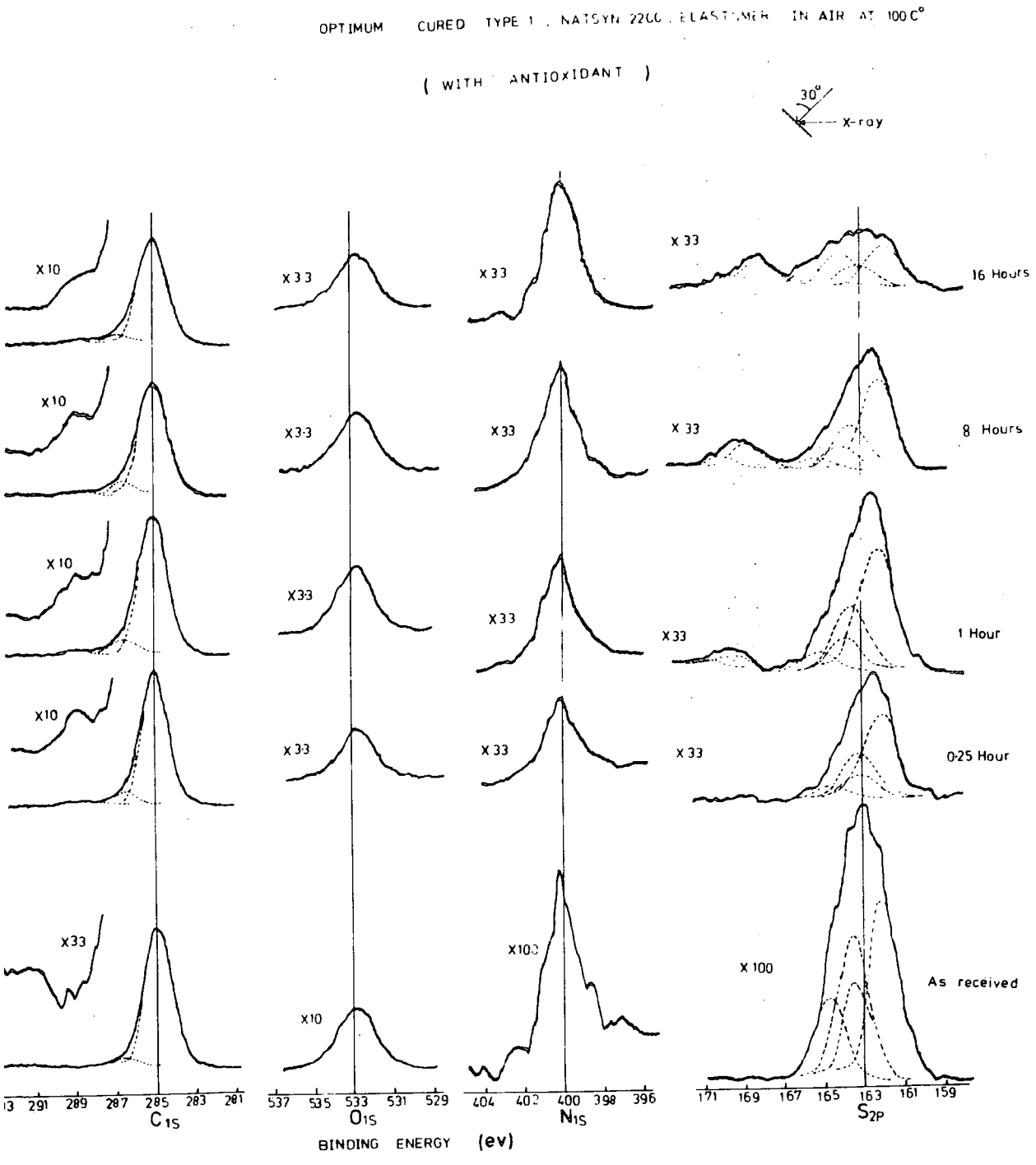

Figure 8.1. C_{1s}, O_{1s}, N_{1s} and S_{2p} spectra of an optimum cured type 1, Natsyn 2200, elastomer versus time of heat processing in air at 100°C.

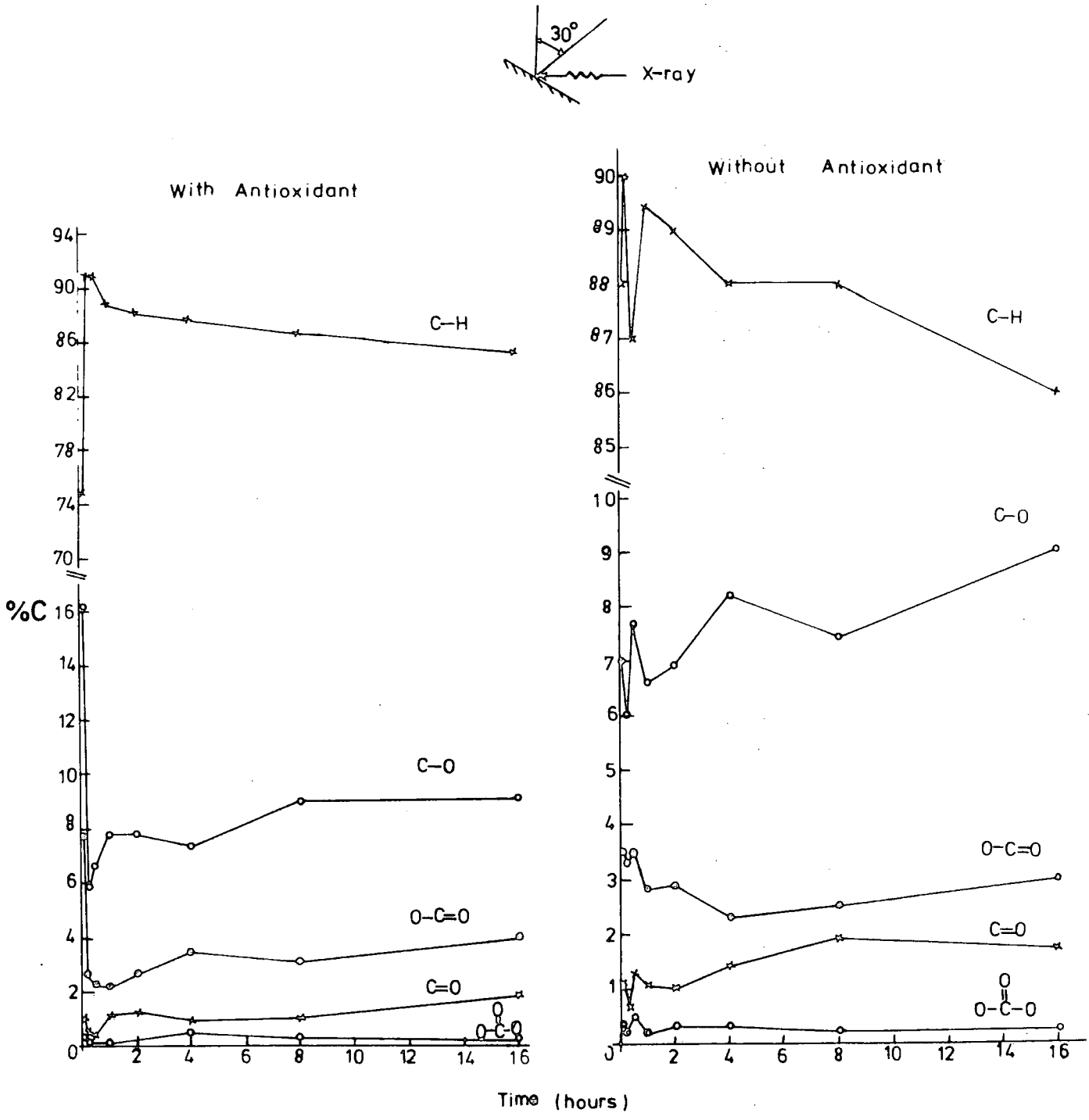

Figure 8.2. Intensity of the various components of the C_{1s} spectrum of an optimum cured type 1, Natsyn 2200, elastomer in relation to C_{1s} (total) versus time of heat processing in air at 100°C.

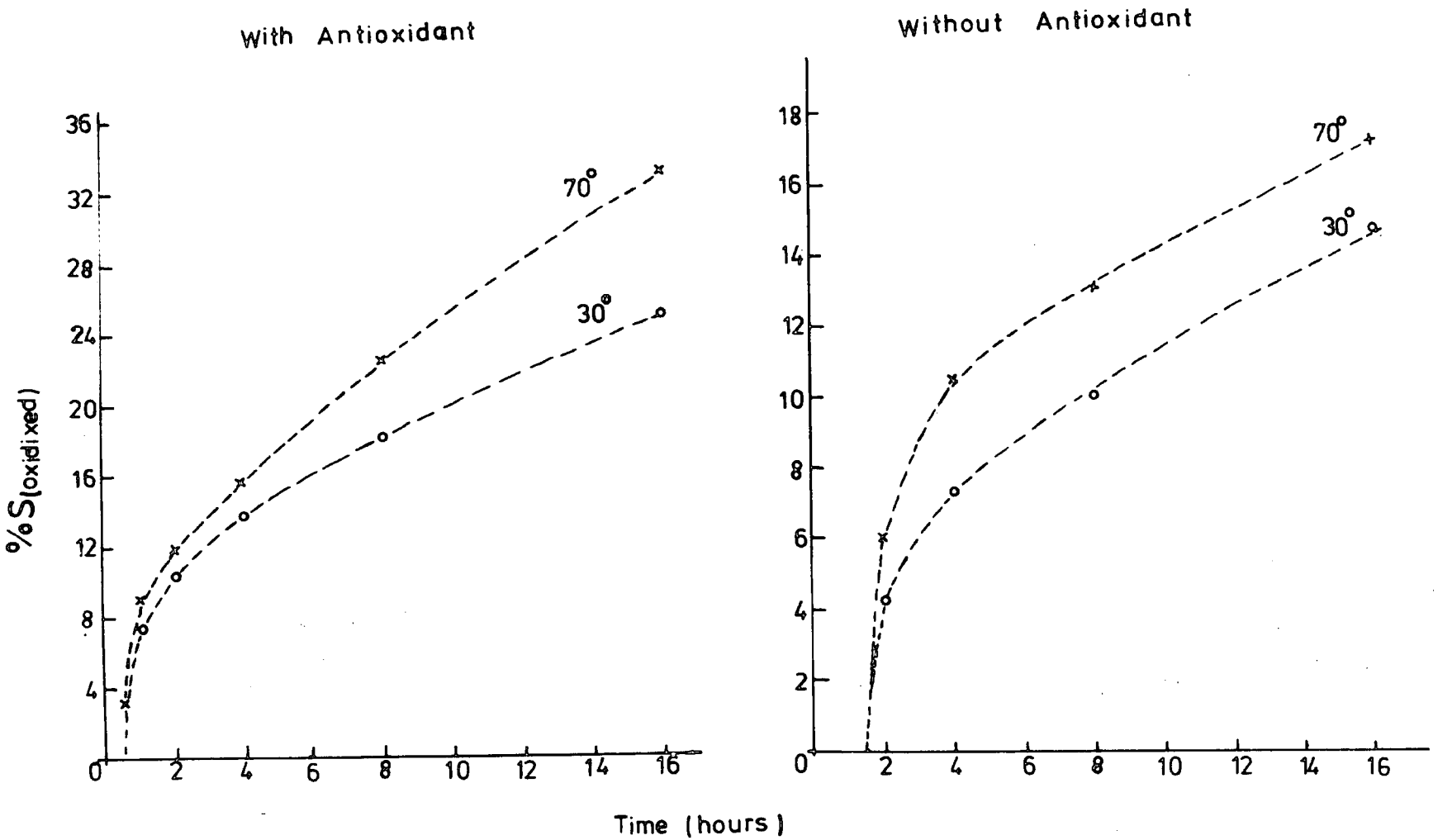

Figure 8.3. Intensity of the S_{2p} (oxidised) component of the S_{2p} spectrum of an optimum cured type 1, Natsyn 2200, elastomer relative to S_{2p} (total) versus time of heat processing in air at 100°C.

than the crosslinked sulphur (organic sulphur). This observation also receives support from the complete immediate absence of shake-up phenomenon approximately 6.5 eV from the main C_{1s} photoionisation peak on thermal treatment in Figure 8.1. The asymmetrical C_{1s} peak (FWHM 1.7 eV compared with 1.5 eV of without additives) is associated with C-O, C=O/O-C-O and O-C=O oxidative functionalities at approximate binding energies of 286.6 eV, 288 eV and 289.1 eV respectively, and these features tend to attain a limiting value after approximately four hours of exposure at 100°C. The direct attack of oxygen at the double bond resulting in loss of unsaturation compared with the formation of peroxide and chain scissions occurring in the polyisoprene can be explained by Grassie's scheme,[300] as follows:

Scheme 1

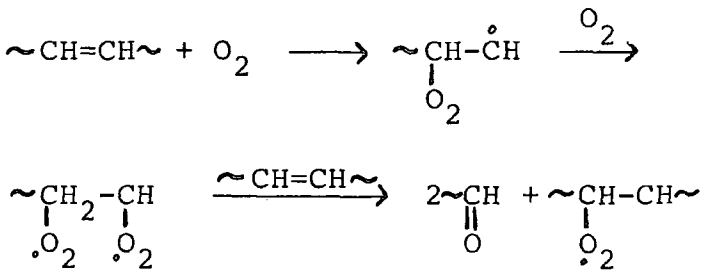

The mechanism for chain scission of polyisoprene is much more complicated than the attack of oxygen at the double bond. Thermal oxidation of polyisoprene is always accompanied by some scission and the formation of volatile products.[273] The yield of volatile products is a direct measure of scission in both raw and vulcanised rubber.[263,264]

In oxidation of a mixture of rubber and non-rubber

components with different polymer units (RH and R'H etc.), the amount of each which will react depends directly on their relative stabilities and concentrations, provided that the respective peroxy radicals (RO_2 and $R'O_2$) are of the same reactivity (in reactions (8.3, (8.5) and (8.6)) as outlined in scheme 2 for uninhibited autoxidation.[275,285,286,301]

Scheme 2

Initiation Step	Proproduction of R° or RO_2° radicals		(8.1)
Propagation Step	$R^\circ + O_2 \longrightarrow RO_2^\circ$		(8.2)
	$RO_2^\circ + RH \longrightarrow RO_2H + R^\circ$		(8.3)
Termination Step	$2R^\circ \longrightarrow$	non-chain carriers	(8.4)
	$R + RO_2^\circ \longrightarrow$		(8.5)
	$2RO_2^\circ \longrightarrow$		(8.6)

According to the above scheme, the primary product of autoxidation, hydroperoxide, is probably associated with enhanced carbon-carbon bond fission in the back-bone of polyisoprene,[302] thus indicating intimate connection with autoxidation. The fall in hydroperoxide concentration can be explained from another point of view that peroxy radicals propagate the reaction chain solely by abstracting labile hydrogen atoms. However, as this process decreases, another mode of peroxy radical attack on the double becomes possible. In other words, both hydroperoxide and diperoxide formation proceed consecutively in the same molecule.[304] A molecule of polyisoprene has four sites, which are vulnerable to attack by

a peroxy radical, as is shown in scheme 3. The peroxy radicals formed by combination with oxygen may react intramolecularly by addition to an adjacent double bond to form a cyclic peroxide,

Scheme 3

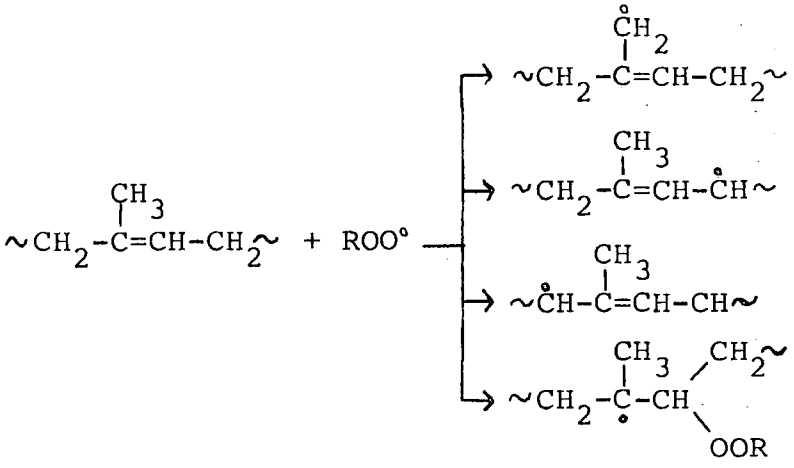

which would react with another molecule of oxygen to form a new peroxy radical, as is illustrated in the following reaction sequence:

Scheme 4

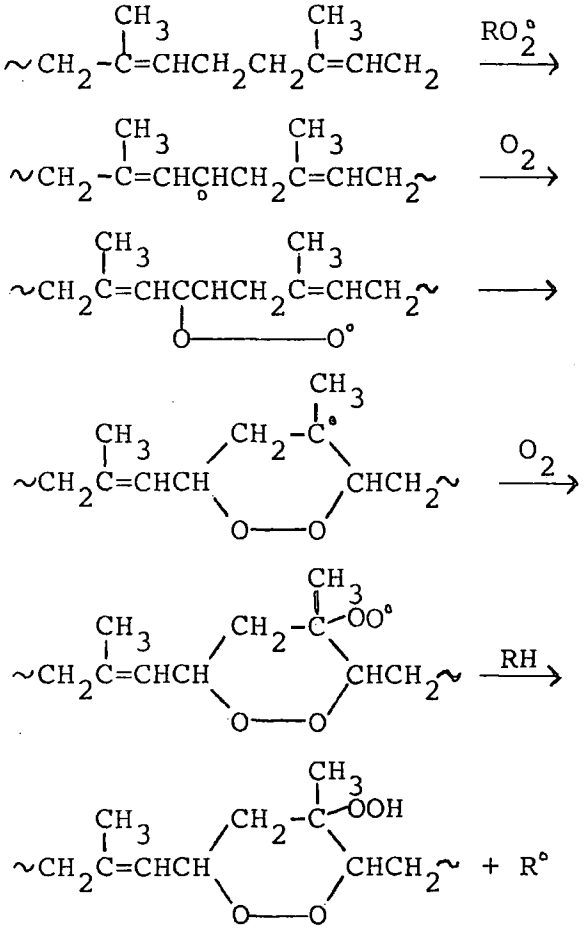

Several alternative structures for the formation of cyclic peroxidic intermediates have been postulated,[267,269,304-306] and it is likely that more than one is involved. It has been generally accepted that the actual scission involves decomposition of tertiary alkoxy radicals, derived from peroxy radicals of the type as is indicated in the scheme 4. The type of cleavage believed to be involved to account for the observed products is as follows:

Scheme 5

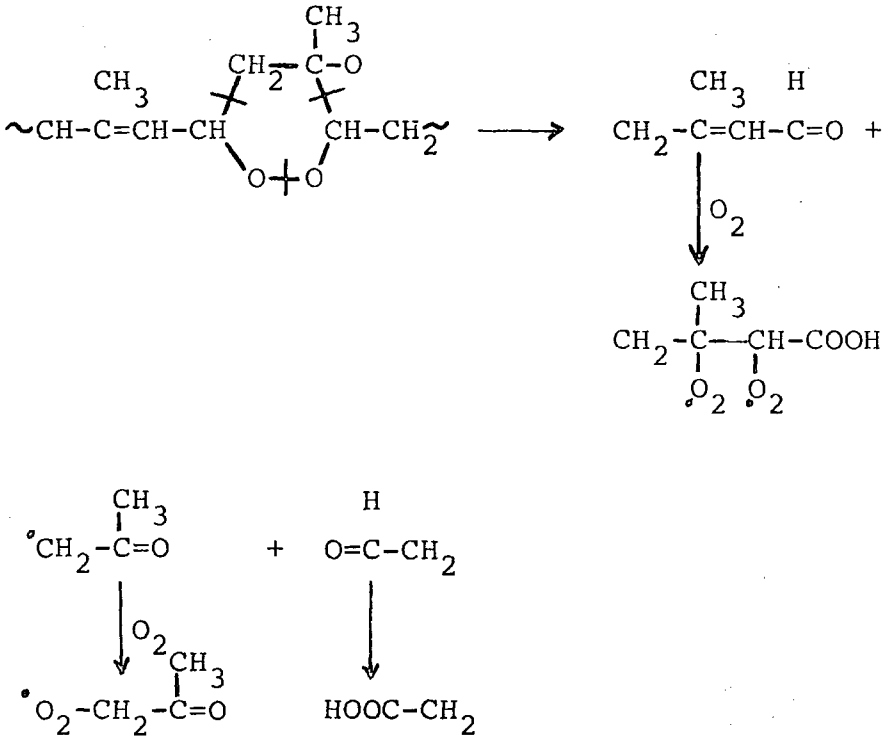

It is not yet clear, as to how carbonates are formed from the oxidation of polyisoprene.

The chemistry of polyisoprene oxidation has been further complicated by the addition of acetone/diphenylamine condensate as a thermal antioxidant and the varieties of sulphur functionalities occurring in a conventional sulphur

accelerated type 1, Natsyn 2200, elastomer, namely mono-, di- and polysulphides. It has been established in chapter three that this optimum cured elastomer had on average a functionality of four, indicating tetrasulphidic linkage between two polyisoprene molecules. This sulphide linkage occurs after every approximately 100 monomer repeat unit. Since, the relative reactivities of different sulphide is in the order di- < tri- < tetrasulphide on exposure to oxygen plasma in chapter six (the literature indicates the reverse order of relative reactivities in more conventional liquid phase oxidations[307]), it is, therefore, imperative to consider the smaller linkages in details as tetrasulphide. The various sulphide linkages are oxidised from reaction with hydroperoxides,[308-313] as are formed in subsequent oxidative treatments at 100°C.

An examination of S_{2p} peaks and plots of S_{2p} (oxidised)/ S_{2p} (total) in Figures 8.1 and 8.3 respectively reveals the oxidation of organic sulphides to a final product sulphate with binding energy of approximately 168.8 eV. Although, an attempt has not been made to deconvolute the S_{2p} peak into sulphoxide components ($\sim$ 166.5 eV), it was detectable in the range 0 - 1.5% under the S_{2p} envelope throughout the subsequent thermal treatments. Since sulphoxide is many times more reactive than sulphone, it follows that sulphoxide formed in the early stages of oxidation and present in a very small concentration on the surface of an elastomer is an active inhibitor.[303-308] This fact clearly implies that it is not the sulphides, which show the inhibitory effect only after

the very small amount of oxygen absorption, but are one or more oxygenated derivatives produced in the autoxidising medium. These could be the sulphoxides or thiosulphinates or a mixture of both, resulting from the reaction of sulphides with hydroperoxides. The antioxidant activity results from a rapid conversion of sulphoxides into sulphone functionalities by interacting with hydroperoxides. The lost peroxides are replenished from the oxidation of polyisoprene at decreasing rate, as indicated by the gradual rise of C_{1s}-oxygen functionalities and a slow oxidation rate of S_{2p} levels in Figures 8.2 and 8.3 respectively. The dramatic fall of C-O component in the very initial stage of oxidation in the presence of added antioxidant in Figure 8.2 is conceivably associated with the interference of propagating cycle by the antioxidant. Although, the active sulphoxides are effective in suppressing the autoxidation in concentration much smaller than their respective parent sulphides, their action is short lived as a result of instability at an elevated temperature and, the further oxidation leads ultimately to sulphonic acids through series of intermediates,[315] as are shown below:

Scheme 6

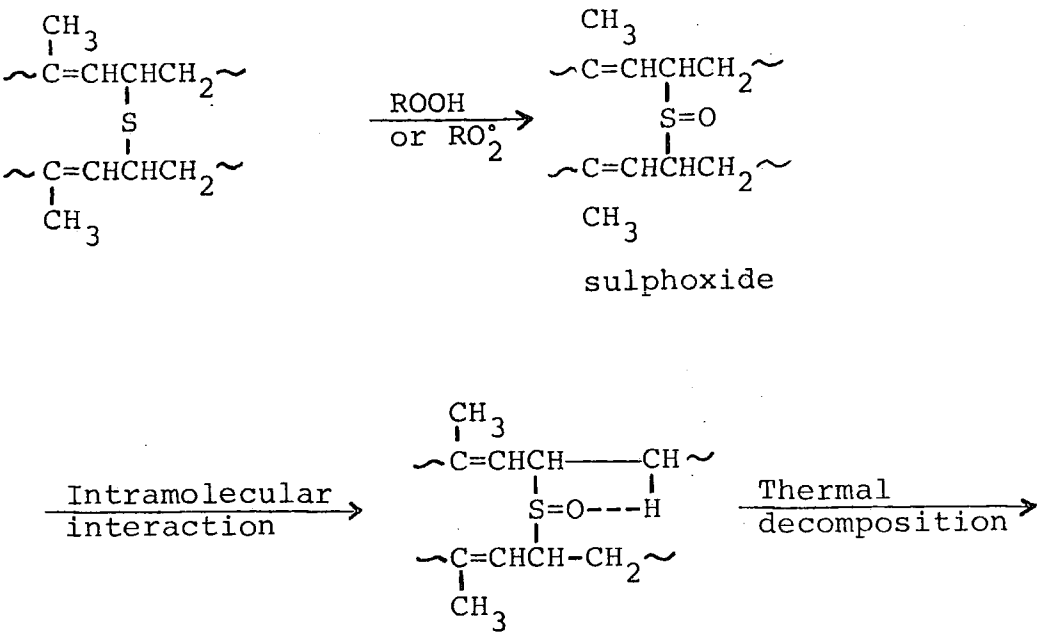
ROOH
or RO2°
sulphoxide
Intramolecular
interaction
Thermal
decomposition
X2
Sulphenic acid
ROOH
or ROO°
Thiolsulphinate
Thiolsulphonate
ROOH
or RO2°
Sulphinyl sulphone
α-Disulphone
ROOH
Sulphonic acid

The net result of decomposition of oxidised monosulphide linkage is the loss of half the original crosslinks, the monosulphides being converted into disulphide bridges and these are further oxygenated to give various derivatives. The new thiolsulphinate crosslink formed from monosulphides undergoes scission by a similar mechanism to that illustrated for the monosulphide linkage in scheme 6, probably through a free-radical disproportionation, is as follows:

Scheme 7

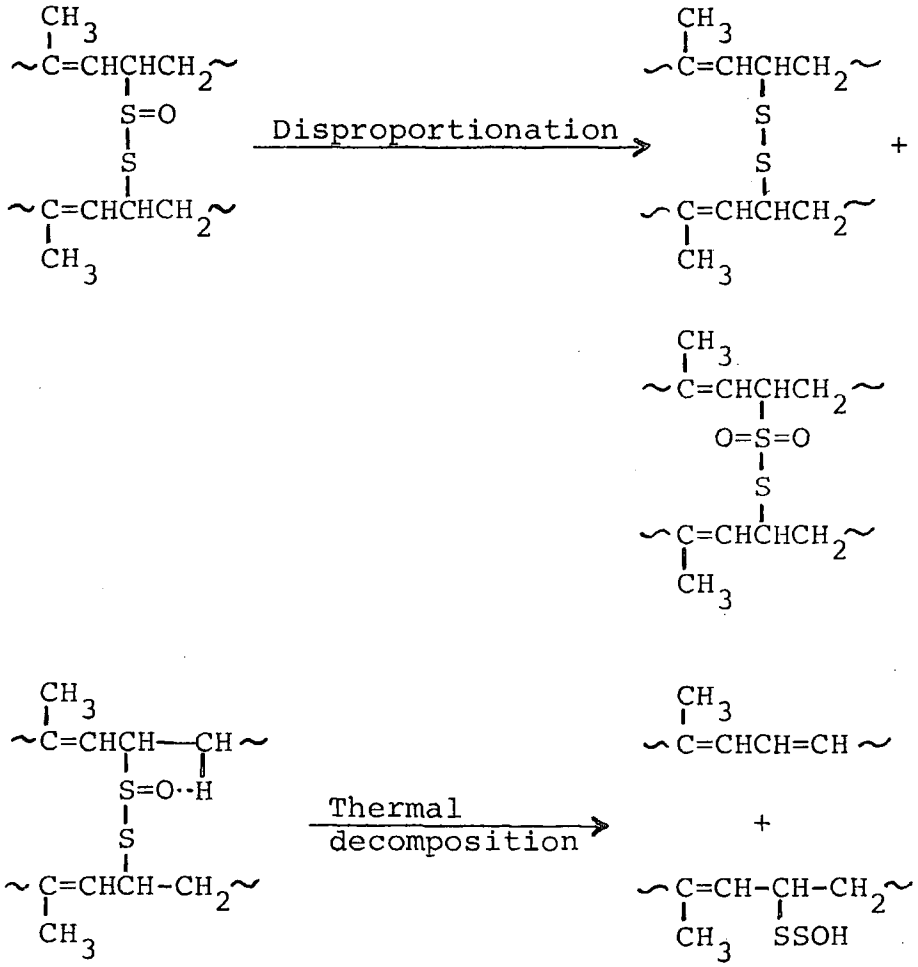

Polysulphides, tetrasulphide linkages present in a very large proportion, also oxidise in a similar manner as disulphide in scheme 7 to give various intermediates before the further oxidation leads ultimately to sulphonic acid. The reaction processes believed to occur, are as follows:

Scheme 8

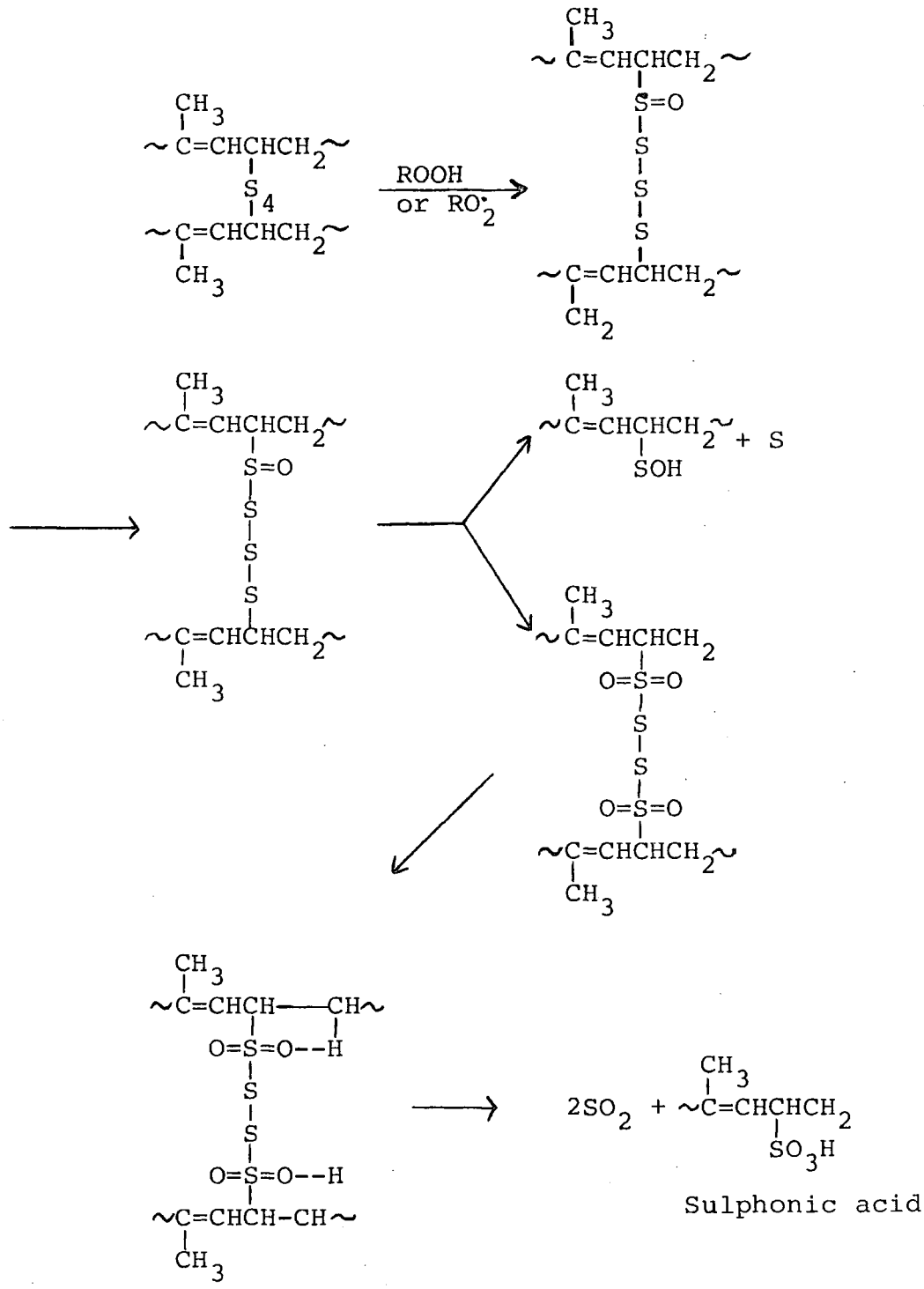

The presence of sulphur dioxide in scheme 8 is susceptible to further rapid oxidation to SO_3 and H_2SO_4 on reaction with hydroperoxides, which may exhibit as an effective anti-oxidant,[313,314] or the SO_2 may be lost from the surface. The fact that the plot of C_{1s}/S_{2p} intensity ratios in Figure 8.4 did not provide an evidence for the loss of sulphur from the surface; instead, an increase of sulphur is observed with increasing oxidation time, suggesting that the sulphur from the bulk has diffused to the surface. The deviations in C_{1s}/S_{2p} intensity ratios in the presence and absence of antioxidant are attributed to different surface composition of each fresh sample taken for an investigation.

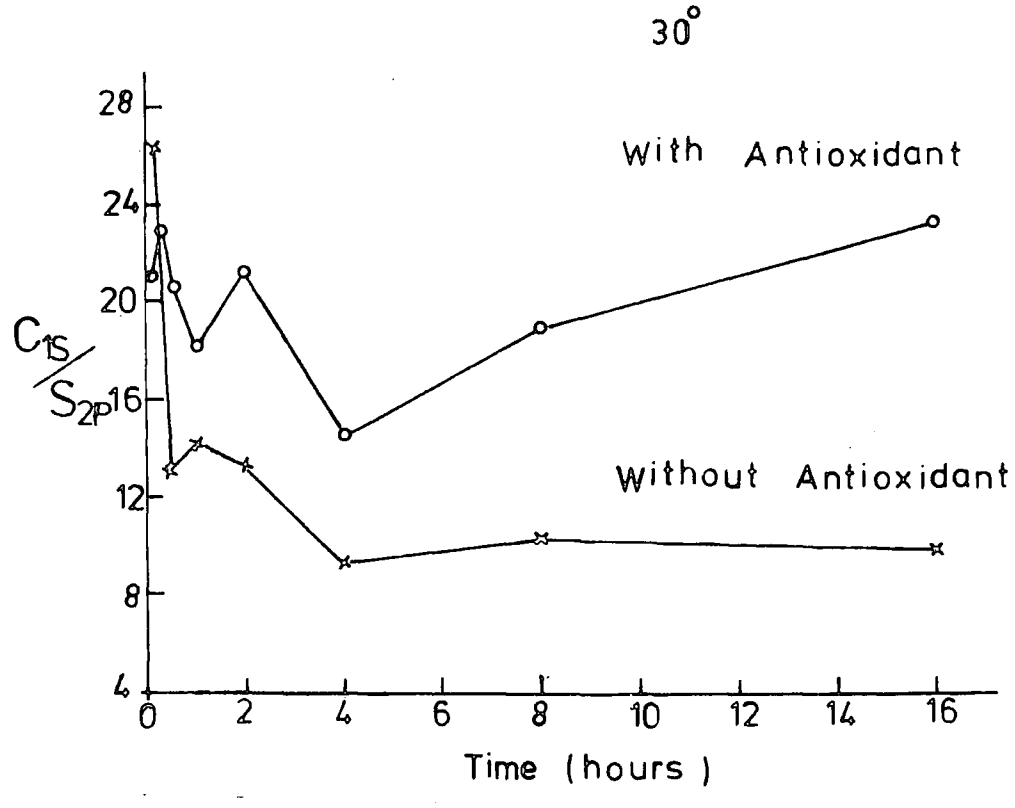

Figure 8.4. C_{1s}/S_{2p} as a function of thermal oxidation time for an optimum cured type 1, Natsyn 2200, elastomer in air at 100°C.

The sulphenic (RSOH), sulphinic (RSO_2H), sulphonic (RSO_3H), thiosulphoxylic (RSSOH) and thiosulphur ($RSSO_3H$) acids formed from various types of sulphide linkages react with hydroperoxides to give non-radical products. The sulphide cross-links, together with the pendent and cyclic groups containing sulphur, are thus a reservoir of potential oxidised sulphur compounds, which mainly function as preventive and to a lesser extent as chain-breaking antioxidants.[320,321]

The plot of S_{2p} (oxidised)/S_{2p} (total) as a function of time in Figure 8.3 reveals the quite distinctive features of organic sulphides that there is a certain time lag before the oxidation of sulphides proceeds autocatalytically and this soon slackens and, the autoretardation becomes progressively more severe as most of the hydroperoxides are consumed by reacting with organic sulphides after a very short period of oxidation. The differences in relative rates of oxidation of sulphides at take-off angles of 30° and 70° are most likely due to the availability of oxidising species (the concentration of peroxides is greater at 70° take-off angle as a consequence of greater availability of oxygen in contact with the atmosphere) rather than to the diffusion process.[298] It has been suggested that the diffusion phenomenon is negligible in the range < 50Å of the ESCA profile depth. The inhibition period demands further study at a much lower temperature for its validity, which the time lag, if it is true, would prolong. However, the evidence of Figure 8.3 with the absence of antioxidant indicates a longer time lag than for systems containing added antioxidant.

It has been shown[310,316,317] that the presence of zinc mercaptobenzthiazole and its hydrate as in the type 1, Natsyn 2200, elastomer give a very good ageing resistance. The mechanism of the antioxidant of zinc complex has been investigated[318] and has been shown to involve the formation of the stable zinc benzthiazole sulphinate, which acts as a reservoir for sulphur trioxide and hence H_2SO_4 for an effective non-radical decomposition of hydroperoxides,[314] as is illustrated in scheme 9.

Scheme 9

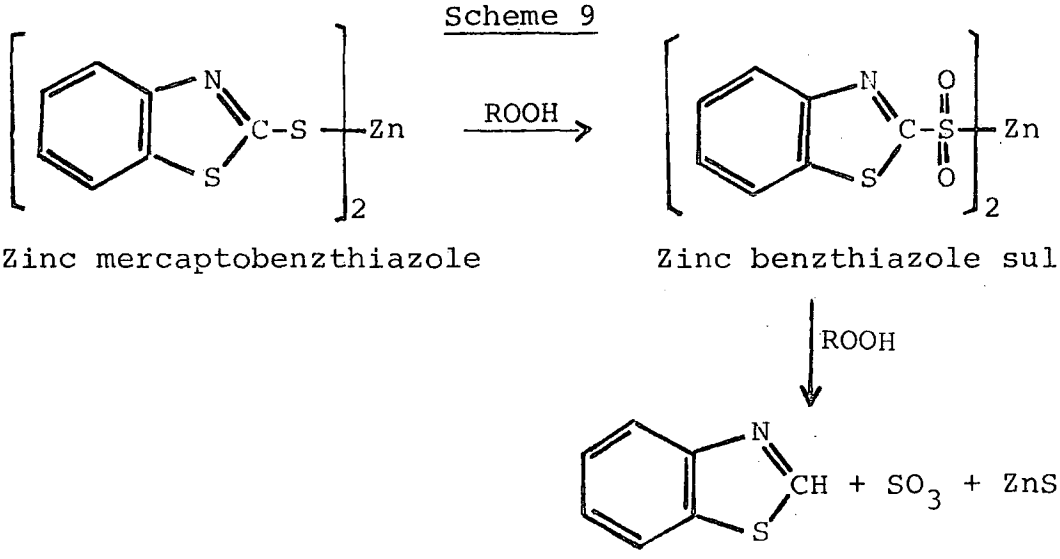

Zinc mercaptobenzthiazole

Zinc benzthiazole sulphinate

A condensate of acetone/diphenylamine added as a thermal antioxidant from the industrial point of view to prevent, or at least to retard the deterioration of physical properties has a substantial effect on the rate of oxidation and on the induction period of organic sulphides, as are evidenced in Figure 8.3. The relative rate of oxidation after autoxidation period (4 hours) is approximately three-fold higher than in the absence of antioxidant, suggesting that the added anti-oxidant interrupted the propagation cycle by reacting with

either R° or RO_2° free-radicals. The chain breaking antioxidant, thus, retarded the oxidation, as is shown in Figure 8.5. The mechanism is believed to involve the abstraction of a hydrogen from the aromatic ring resulting in formation of radical ion on the aromatic ring, which, in turn, is stabilised

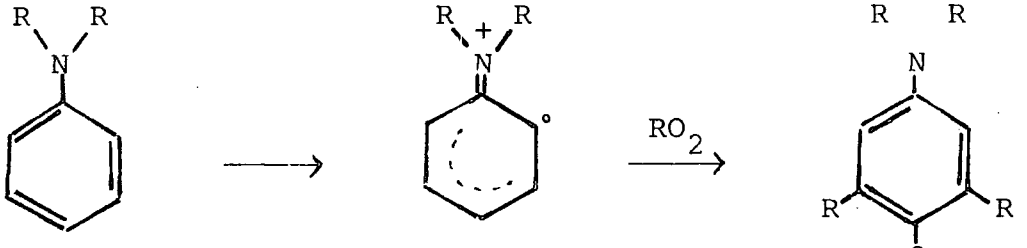

⟶ Various products

(A structure,

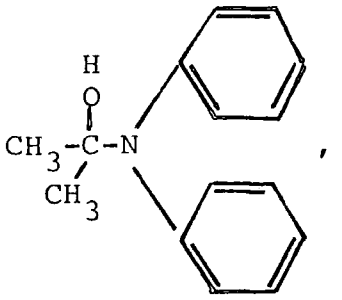

of acetone/diphenyl amine condensate has been supported by the ESCA investigation described in chapter three.)

The effect on the C_{1s}/O_{1s} (total) is less pronounced as a result of oxygen contribution made from antioxidant (a condensate of acetone/diphenyl amine) to the total O_{1s} signal and this contribution increased with increasing oxidation time, as is evidenced indirectly by the increase of N_{1s} signal in Figure 8.6. The increase of a N_{1s} signal implies that the antioxidant has diffused from the bulk to the surface.[322] The high level of antioxidant at the surface, is, therefore, responsible for the retarded autoxidation, as is indicated by C-H component in Figure 8.2. The increase in level of anti-

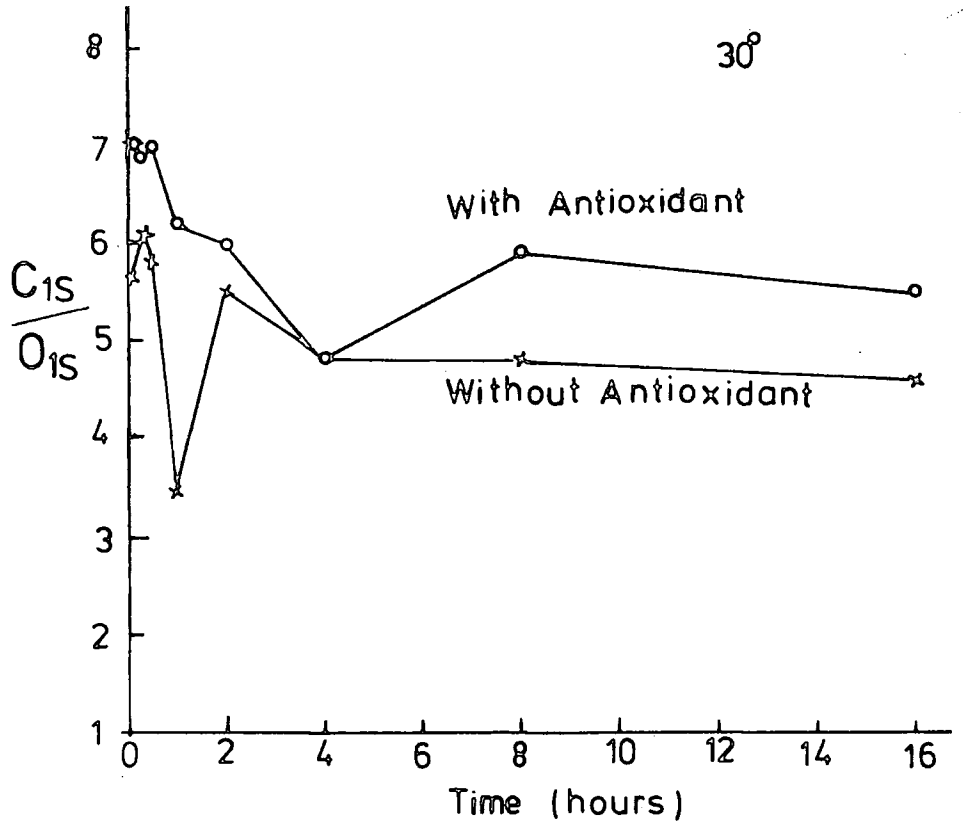

Figure 8.5. C_{1s}/O_{1s} as a function of thermal oxidation time for an optimum cured type 1, Natsyn 2200, elastomer in air at 100°C.

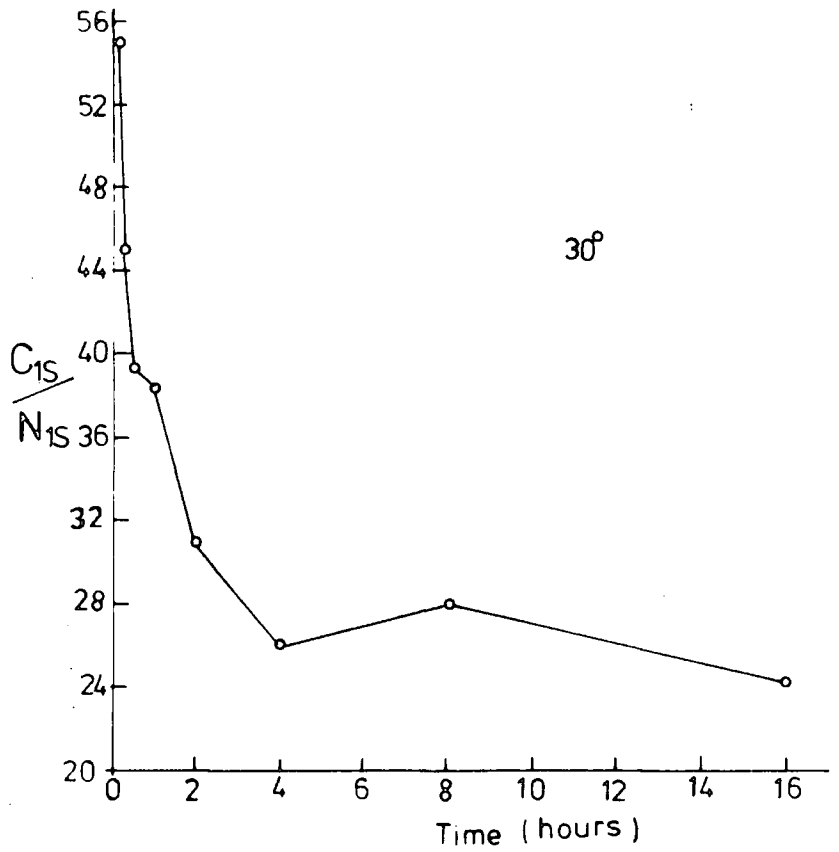

Figure 8.6. C_{1s}/N_{1s} as a function of thermal oxidation time for an optimum cured type 1, Natsyn 2200, elastomer containing antioxidant in air at 100°C.

oxidant at the surface is probably associated with the renewal of the surface layer, depleted by erosion, etc. or with the restructuring of the partially degraded rubber network. However, the compounds as antioxidant are frequently capable of reacting in more than one way, including prooxidant effects in addition to the desired antioxidant action. The following reaction sequence includes four ways, in which, antioxidants may participate in the mechanism of retarded thermal autoxodation:[279,311,319]

Scheme 10

(i) Prevention of peroxide initiation by decomposing hydroperoxides to form stable products rather than free radicals (preventive antioxidant being oxidised products of organic sulphides in type 1, Natsyn 2200 elastomer).

(ii) Initiation by direct attack of oxygen on the antioxidant to produce chain-initiating radicals.

(iii) Chain transfer with the antioxidant, in which the radical derived from the antioxidant reacts in some way to reform a propagating free radical.

(iv) Termination by hydrogen donation to RO_2° as in the first step of chain transfer, followed by reactions of the antioxidant radical with a second RO_2, thus terminating two kinetic chains per molecule of antioxidant consumed.

Peroxide Destruction: (preventive antioxidant)	$ROOH + AH \longrightarrow$ nonradical products	(8.7)
Initiation: (peroxide decomposition)	$nROOH \longrightarrow RO^{\bullet}, RO_2^{\bullet},$	(8.8)
O_2 (attack on antioxidant)	$AH + O_2 \longrightarrow A^{\bullet} + HO_2^{\bullet}$	(8.9)
Propagation: (same as unhibited)	$RO_2^{\bullet} + RH \longrightarrow ROOH + R^{\bullet}$	(8.10)
	$R + O_2 \longrightarrow RO_2^{\bullet}$	(8.11)
Chain Transfer: (with antioxidant)	$RO_2^{\bullet} + AH \longrightarrow ROOH + A^{\bullet}$	(8.12)
Termination: (by antioxidant)	$A^{\bullet} + RH \longrightarrow AO_2H + RO_2^{\bullet}$	(8.13)
	$RO_2^{\bullet} + AH \longrightarrow ROOH + A^{\bullet}$	(8.14)
	$AO_2^{\bullet} + A \longrightarrow RO_2A$	(8.15)
	$2A^{\bullet} \longrightarrow A\text{-}A$	(8.16)
(as in uninhibited)	$2RO_2^{\bullet} \longrightarrow$ nonradical products $+ O_2$	(8.6)
	$RO_2^{\bullet} + R \longrightarrow RO_2R$	(8.5)
	$2R^{\bullet} \longrightarrow R\text{-}H$	(8.4)

The mechanism of retarded autoxidation of elastomers in the presence of antioxidants thus includes the same fundamental free radical reaction as uninhibited autoxidation in scheme 2. However, the initiation, propagation, and termination processes are altered by reactions with the antioxidant.

It is clearly evident that the addition of antioxidant into the Natsyn 2200 formulation results in a shorter inhibition period for the oxidation of organic sulphide than in the absence of antioxidant; which, in turn, implies that the earlier the sulphides are oxidised, better is the ageing of the elastomer. The oxidised products of organic sulphide

act as nonradical decomposure of hydroperoxides.[314]

It has already been seen in chapter six that plasma oxidation, unlike thermal oxidation, was unaffected by the antioxidant and, the elastomer with and without antioxidant showed the same extent of oxidation immediately after oxygen plasma treatment. Thermal and plasma treatments differ in the initial steps of oxidation processes. The initial steps for thermal oxidation in (8.1), (8.8) and (8.9) are driven by the thermal energy and proceed on a time scale of hours; whereas, the initial steps for the oxygen plasma in scheme 11 involve the dissociation of bonds by inelastic collisions of high energy species with the polymer surface and, at a greater depth, dissociation is from absorption of UV radiation. Once the oxidation has initiated, the ensuing reactions are

Scheme 11

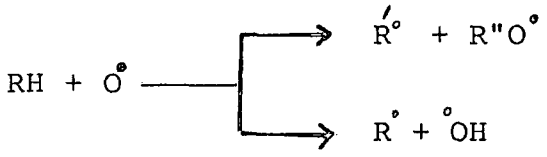

(8.17)

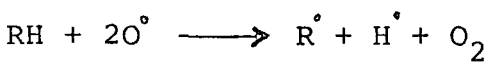

(8.18)

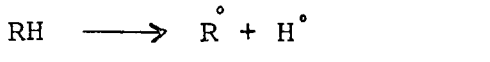

(8.19)

similar for both plasma and thermal oxidation. The production of free radicals in thermal oxidation is a chain process but being very slow. The polymer free radicals, after initiation, are generated through the oxidation process itself. The antioxidant terminates the reaction through a series of steps, as indicated in (8.13) - (8.16) of scheme 10.

In plasma oxidation, the antioxidant still terminates the oxidation chain reactions but, does not decrease the oxidation rate. The polymer free radicals generated by (8.17), (8.18) and (8.19) steps differentiate from the thermal oxidation.

8.4 Conclusion

An optimum cured type 1, Natsyn 2200, elastomer in the presence and absence of antioxidant (a condensate of acetone/diphenylamine) studied with the application of ESCA after heat processing in air at 100°C has highlighted the following points:

(i) The carbon-carbon double bonds of polyisoprene are very rapidly oxidised, as is evidenced by the immediate complete loss of shake-up phenomenon, approximately 6.5 eV from the main C_{1s} photoionisation peak.

(ii) There is very rapid build up of hydroperoxide concentration at the surface in the first few minutes of thermal treatments and this resulted in oxidation of organic sulphides.

(iii) The oxidation of organic sulphides revealed a certain time lag before the oxidation could proceed. The presence and absence of antioxidant gave inhibition period of approximately half an hour and one and a half hours respectively.

(iv) The products of oxidised organic sulphides, but not their parent sulphides, have been found to be an

effective antioxidant in conjunction with the added thermal antioxidant. The behaviour of oxidised organic sulphides is attributed to the catalytic decomposition of hydroperoxides. The thermal antioxidant and the oxidised organic sulphides, thus, indicated the dual characteristics in protecting from deterioration of a sample.

CHAPTER NINE

STRUCTURAL CHARACTERISATION

OF VULCANISATES

9.1 Introduction

As has already been stated in chapter one, the most important aspect of current interests in the chemistry of vulcanisation is the problem of determining the structure of rubber vulcanisates and, hence, the relative proportions of different types of crosslinks. The thermal and mechanical properties of vulcanised rubbers are strongly dependent on the different types of crosslinks.[2,45,295,297] The direct methods for estimation of the structural properties of vulcanisates include measurements of physical properties[96] such as swelling,[64] creep[369] and stress-strain relaxation.[40,41] Specific degradation with chemical reagents (so-called chemical probes), which react and break crosslinks of particular types, are employed in combination with the stress-strain measurements[64,95] for determining the relative proportions of different types of crosslinks. The physical assessment before and after treatment with reagents, therefore, allows the estimation of different types of crosslinks. Despite the existing methods, there is still a demand for improving the procedures to determine the types and distribution of sulphidic bridges, especially in filled vulcanisates.[96]

The approach to characterisation of a vulcanisate network in terms of the relative proportions of the different types of chemical crosslinks, in this chapter, is based on treatment with a solution of propane-2-thiol (0.4M) and piperidine (0.4M) in heptane to cleave the polysulphide linkages only, leaving di- and monosulphide crosslinks intact in the sulphur vulcanisate. The treatment involves an exposure time of two

hours at room temperature and the use of a second solution of n-hexanethiol (1.0M) in piperidine - which cleaves both di- and polysulphide bridges, leaving only monosulphides intact.[91,95] The treatment of 'sulphur-vulcanised' elastomers with a solution of propane-2-thiol and piperidine in heptane assumes that the polysulphides are orders of magnitude more reactive than disulphides and, the concentration of disulphides remains essentially the same, under the conditions employed. The use of this reagent in conjunction with the other solution and the difference in chemical reactivity allow mono-, di-, and polysulphides to be determined in this way at least for the bulk.

It is anticipated that, in the treatment of vulcanisates with solutions, the mobility of surface functional groups[370] and the high sensitivity of ESCA may seriously affect the interpretation of the surface chemistry of the treated elastomers. Nevertheless, it is worthwhile considering the ESCA examination of the elastomers treated in solutions for comparison with bulk studies reported in the literature.

9.2 Experimental

(i) Natural rubber vulcanisates of two formulations, with sulphur/N-cyclohexylbenzthiazyl sulphenamide (CBS) and tetramethylthiuram disulphide (TMTD), respectively, have been analysed by ESCA, as a function of cure time.

(ii) The formulations of the samples, all cured on a calendering system at 150°C in air, with a 2 mm

nip setting to draw into sheets, as a function of time are shown in Table 9.1. The samples were received in paper envelopes and stored in the dark.

Table 9.1

Natsyn 2200 Sample Formulations

	1		2	
	weight (%)	moles (%)	weight (%)	moles (%)
Natsyn 2200 (cis-polyisoprene)	90	90.3	89.3	94.3
Zinc oxide	4.54	4.1	4.44	3.91
Stearic acid	2.72	0.69	2.72	0.72
CBS	0.54	0.14	-	-
Sulphur	2.2	4.8	-	-
TMTD	-	-	3.53	1.08

Cure time (minutes) at 150°C

Type 1	14	16	20	25
Type 2	5	10	15	25

(iii) The effects of propane-2-thiol and piperidine solvents alone on the particular vulcanisate have been investigated as a function of reaction time, before carrying out specific cleavage of sulphide crosslinks with the solution of the thiol-amine reagent.

(iv) The type 1 and type 2 vulcanisates were treated with a solution of propane-2-thiol (0.4M) and

piperidine (0.4M) in heptane for ∿ 3 hours to cleave the polysulphide crosslinks and a solution of n-hexanethiol (1.0M) in piperidine for ∿ 15 hours to break both polysulphide and disulphide crosslinks.

For a given cure time, separate specimens from the same vulcanisate sheet were used for the determination of (a) total chemical crosslink density, (b) chemical crosslink density after treatment with propane-2-thiol (0.4M) and piperidine (0.4M) in n-heptane solution, and (c) chemical crosslink density after treatment with n-hexanethiol (1.0M) in piperidine solution. The concentration of monosulphides is obtainable directly from (C) after hexanethiol treatment, on the assumption that the S_{2p} signal was only from the sulphide crosslinks and the thiols did not react with the rubber network. The concentration of disulphide crosslinks is attributed to the difference of (b) and (c) treatments and the concentration of polysulphide crosslinks is related to the difference of (a) and (b) (total chemical crosslink density minus chemical crosslink density after treatment with propane-2-thiol reagent).

(v) In all cases, the samples have been treated at room temperature. The samples were cut to an appropriate size (20 mm x 6 mm x 2.5 mm), with a pair of scissors, for mounting onto the spectrometer probe tip.

The rubber sample and reagent solution (or pure solvent) were placed in separate limbs of an apparatus (Figure 9.1) consisting of two glass tubes connected near their upper ends by a short transverse tube. The solution was degassed in one limb

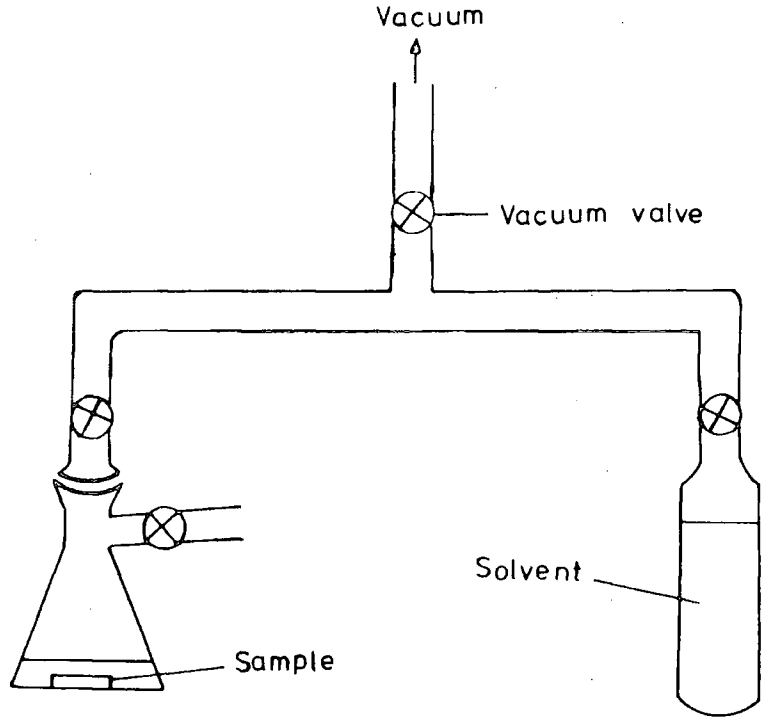

Figure 9.1. Schematic representation of an apparatus, used for specific degradation of sulphide crosslinks at room temperature.

and the rubber in the other limb, the apparatus sealed in vacuum and the solution then transferred onto the sample in the dark, through the transverse tube. This was achieved by tilting the solution tube by 90^{o}. The whole apparatus was left

in the dark, with the sample lying horizontal in the solution (40 cm^3 of reagent solution per gram of rubber) to avoid mechanical distortion. This is particularly important during chemical treatment and subsequent extraction and/or solvent removal. After a standard reaction time (section 9.3.2), the sample was removed from the reagent solution in the dark, and quickly dried to constant weight in vacuum ($\sim 10^{-3}$ torr) at room temperature, before obtaining the ESCA spectra.

(vi) The ESCA examinations have been carried out on an AEI ES200B spectrometer using $Mg_{K\alpha_{1,2}}$ radiation and $Au_{4f_{7/2}}$ level at 84 eV binding energy for calibration purposes had a FWHM of $\sim$ 1.2 eV. The spectra were resolved and integrated with a DuPont curve resolver.

(vii) The high binding energy components under the S_{2p} envelopes after deconvolution are attributed to the organic sulphur (i.e. mono-, di- and poly-sulphides, and also S_8) and the low binding energy components to inorganic sulphur (zinc sulphide).

9.3 Results and Discussion

9.3.1 Introduction

The treatment of elastomers with thiol solutions is based on nucleophilic displacement reactions by alkanethiols on sulphur atoms of poly- and disulphides to give cleavage of sulphur-sulphur bonds, as depicted in scheme 1. The relative

Scheme 1

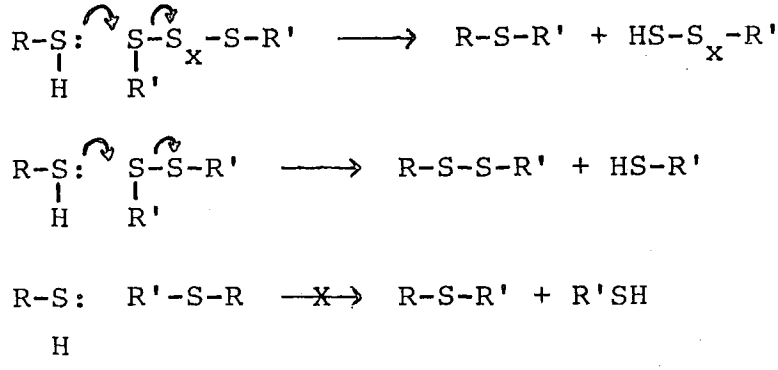

rates of the three displacement reactions depend on the selectivity of the nucleophiles. The reaction with polysulphides ($x \geq 3$) is a more rapid process than with disulphides occurring quantitatively within two hours,[96] and the corresponding disulphides react at least 1000 times more slowly and are essentially unaffected in the time required for the complete decomposition of polysulphides. The carbon-sulphur linkage in monosulphides is highly resistant to such nucleophilic displacement.

The reaction with polysulphides becomes extremely fast in a more polar solvent and the reaction with disulphide is sufficiently fast to be experimentally useful. Such marked increase in reaction rate has been reported to be achieved by using a solution of n-hexanethiol (1.0M) in piperidine for combined di- and polysulphide cleavage instead of a solution of propane-2-thiol (0.4M) and piperidine (0.4M) in heptane, which the latter cleaves polysulphides only, leaving di-, and monosulphides intact.[96] These reagents are widely used in this chapter for the treatment of 'sulphur-vulcanised' networks.

9.3.2 Effect of reagents on elastomers

(a) Introduction

The main emphasis in this preliminary work has been to investigate the effect of solvents and solutions on the particular type of vulcanisate, as a function of reaction time to provide a basis for the interpretation of the ESCA data. It is anticipated that the mobility of surface functional groups, the incorporation of thiol-amine reagent into the rubber network, and the high surface sensitivity of ESCA may lead to unambiguous interpretation of vulcanisates after treatment with propane-2-thiol and piperidine in n-heptane and hexanethiol in piperidine for cleavage of poly-sulphides only and for combined cleavage of di- and poly-sulphides respectively.

The ESCA investigation of as received elastomers (chapters three, four and five) highlighted the complex nature of the elastomer surfaces and their dependence on the initial bulk formulation and sample history. The reactions of elastomers with plasma treatment are also by no means straightforward; nevertheless, it is, worthwhile, now considering the ESCA examination of elastomers treated with chemical reagents.

(b) Type 1, Natsyn 2200, elastomer in piperidine

The core level spectra at an electron take-off angle of 30^{o} for the type 1, Natsyn 2200, elastomer (cured for 14 minutes) treated with piperidine as a function of time are presented in Figure 9.2 and the relevant intensity ratios are set out in Table 9.2.

The data clearly indicate that piperidine has no effect

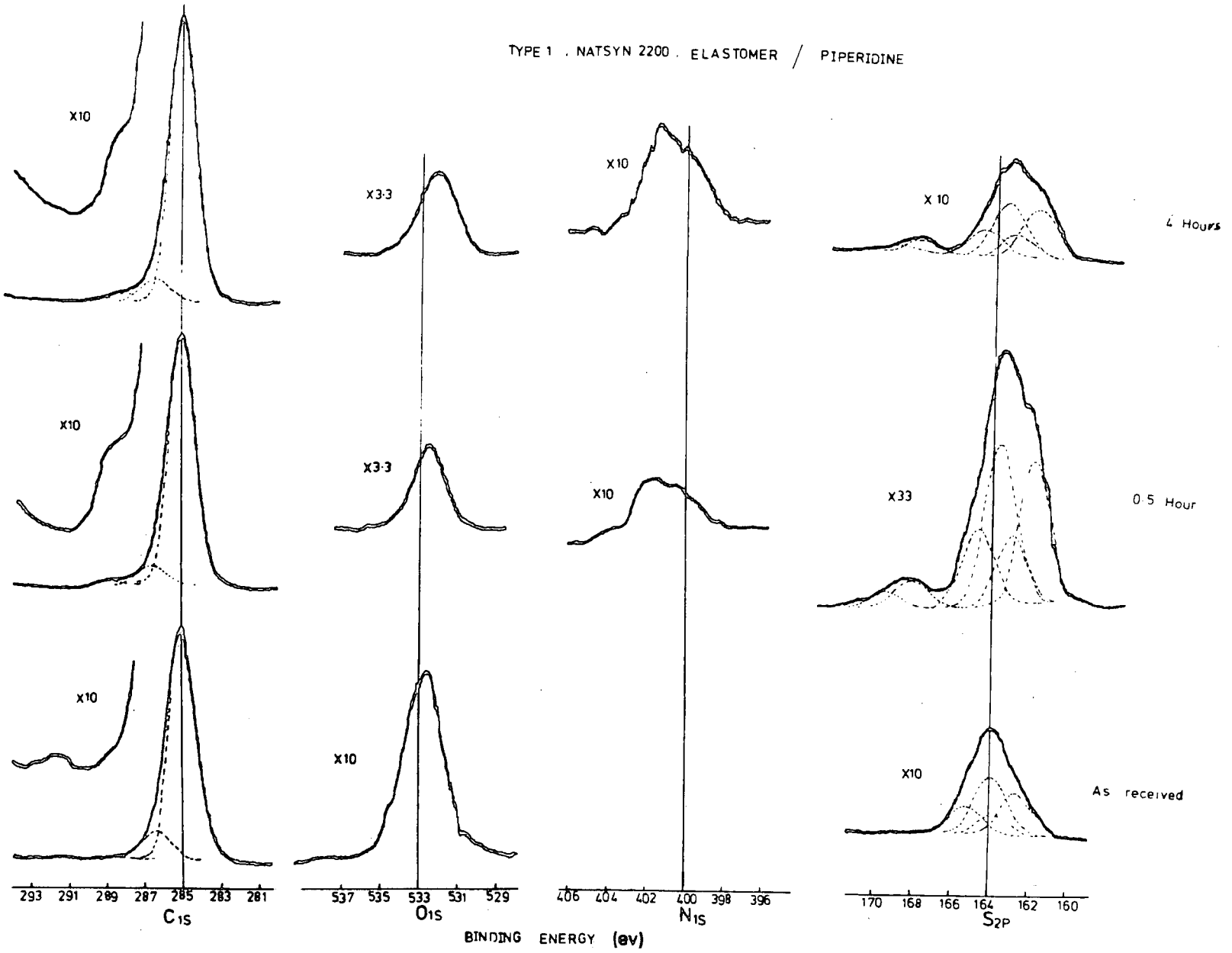

Figure 9.2. C_{1s}, O_{1s}, N_{1s} and S_{2p} spectra of a type 1, Natsyn 2200, elastomer (cured for 14 minutes) versus time of treatment with piperidine.

Table 9.2

Type 1, Natsyn 2200, elastomer (cured for 14 minutes) treated with piperidine at room temperature

Intensity ratios

	Reaction time (hours)	C_{1s}/O_{1s}	C_{1s}/N_{1s}	C_{1s}/S_{2p}	C_{1s}/Zn_{3p}	C_{1s}/S_{2p} HBE
As received	0	10.0	-	17	26	30
	0.5	9.0	25	17	17	30
	4	9.0	16	14	23	25

on the level of sulphur, whilst the level of nitrogen increases with reaction time and, this is most likely associated with the formation of complexes between sulphur and piperidine under the employed conditions. Analogous behaviour of this genre is the action of piperidine at room temperature on dialkyl tetrasulphide in removing a considerable proportion of the polysulphidic sulphur in the form of complex, the tetrasulphide being largely converted into disulphide. It is, therefore, conceivable that the removed sulphur from the polysulphide bridge is retained in the surface region such that the level of sulphur remains essentially unaffected.

A very slight increase in oxygen level (arising from trapped air bubbles) is associated with the development of various carbon-oxygen, and sulphur-oxygn functionalities, as are evidenced from the spectra in Figure 9.2.

The nitrogen peaks indicate the presence of at least two components, namely protonated amine at $\sim$ 402 eV and amine at $\sim$ 399.0 eV. The C-O, C=O and $\overset{O}{\overset{\|}{C}}$=O functionalities are evident

at C_{1s} binding energies of 286.1 eV, 288.0 eV and 289.2 eV respectively. A broad development of a S_{2p} peak in the region ∿ 168.0 eV is indicative of $-\overset{\overset{O}{\|}}{\underset{\underset{O}{\|}}{S}}-$ sulphone structure.

(c) Type 1, Natsyn 2200, elastomer in propane-2-thiol

The data in Table 9.3, pertaining to Figure 9.3, for the type 1, Natsyn 2200, elastomer cured for 14 minutes, reveal a substantial amount of loss of organic sulphur on treatment with propane-2-thiol at room temperature, as is evidenced by the C_{1s}/S_{2p} HBE intensity ratios.

Table 9.3

Type 1, Natsyn 2200, elastomer (cured for 14 minutes) treated with propane-2-thiol at room temperature

Intensity ratios

	Reaction time (hours)	C_{1s}/O_{1s}	C_{1s}/N_{1s}	C_{1s}/S_{2p}	C_{1s}/Zn_{3p}	C_{1s}/S_{2p} HBE
As received	0	10.0	-	17	26	30
	0.5	8	53	19	17	47
	4	9	85	22	13	60

The overall loss of sulphur from the sulphide linkages may be summarised, as follows:

Scheme 2

$$RSH + R'SSR' \rightleftharpoons RSSR' + R'SH$$

$$RSH + RSSR' \rightleftharpoons RSSR + R'SH$$

$$RSH + R'SS_xSR' \rightleftharpoons RSSR' + HS_xSR'$$

$$(2x-1)RSH + HS_xSR' \rightleftharpoons RSSR' + H_2S + (x-1)RSSR$$

$$RSH + RSSR' \rightleftharpoons RSR + R'SH$$

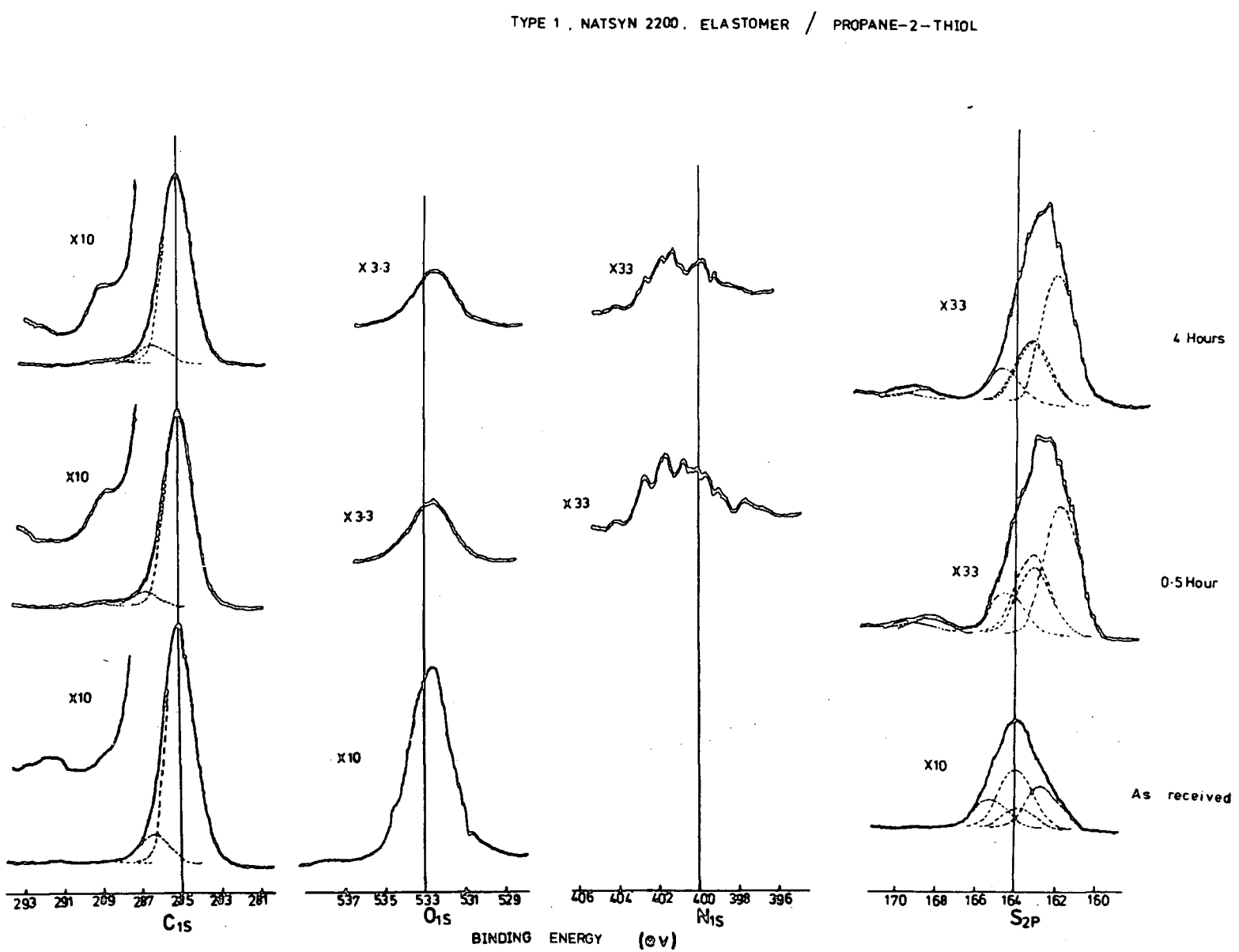

Figure 9.3. C_{1s}, O_{1s}, N_{1s} and S_{2p} spectra of a type 1, Natsyn 2200, elastomer (cured for 14 minutes) versus time of treatment with propane-2-thiol.

The requirement of a satisfactory chemical reagent for selective cleavage of sulphide crosslinks in vulcanisate has been described by Saville and Watson.[96] It can be concluded from the known relative reactivities of polysulphides and disulphides towards propane-2-thiol and piperidine in n-heptane solution that the reaction conditions, which result in the cleavage of disulphide crosslinks at an experimentally useful rate, will also cause extremely rapid cleavage of polysulphides under the same conditions.

The nitrogen signal arises as contaminant and is broadened by the presence of amine and protonated amine functionalities at binding energies ∿ 399.0 eV and ∿ 402 eV respectively. The air bubbles, trapped during the curing process on a calendering system at 150°C in air, are conceivably involved in oxidative functionalisation, as is evidenced by the high energy tail of C_{1s} envelope and by the development of a broad band at ∿ 168.0 eV in the S_{2p} regions.

(d) Type 1, Natsyn 2200, elastomer, in a solution of propane-2-thiol (0.4M) and piperidine (0.4M) in heptane, as a function of time

On the basis of preliminary examination for the reactions between organic sulphides in vulcanisates and piperidine and propan-2-thiol solvents, a reaction of vulcanisates with a solution of propane-2-thiol (0.4M) and piperidine (0.4M) in heptane has been chosen for further study, as a function of reaction time. The data in Figure 9.5, pertaining to the raw spectra in Figure 9.4, illustrate the effect of the thiol-amine reagent on the type 1, Natsyn 2200, elastomer (cured for 14 minutes on a calendering system at 150°C in air).

TYPE 1, NATSYN 2200, ELASTOMER/THIOL-AMINE

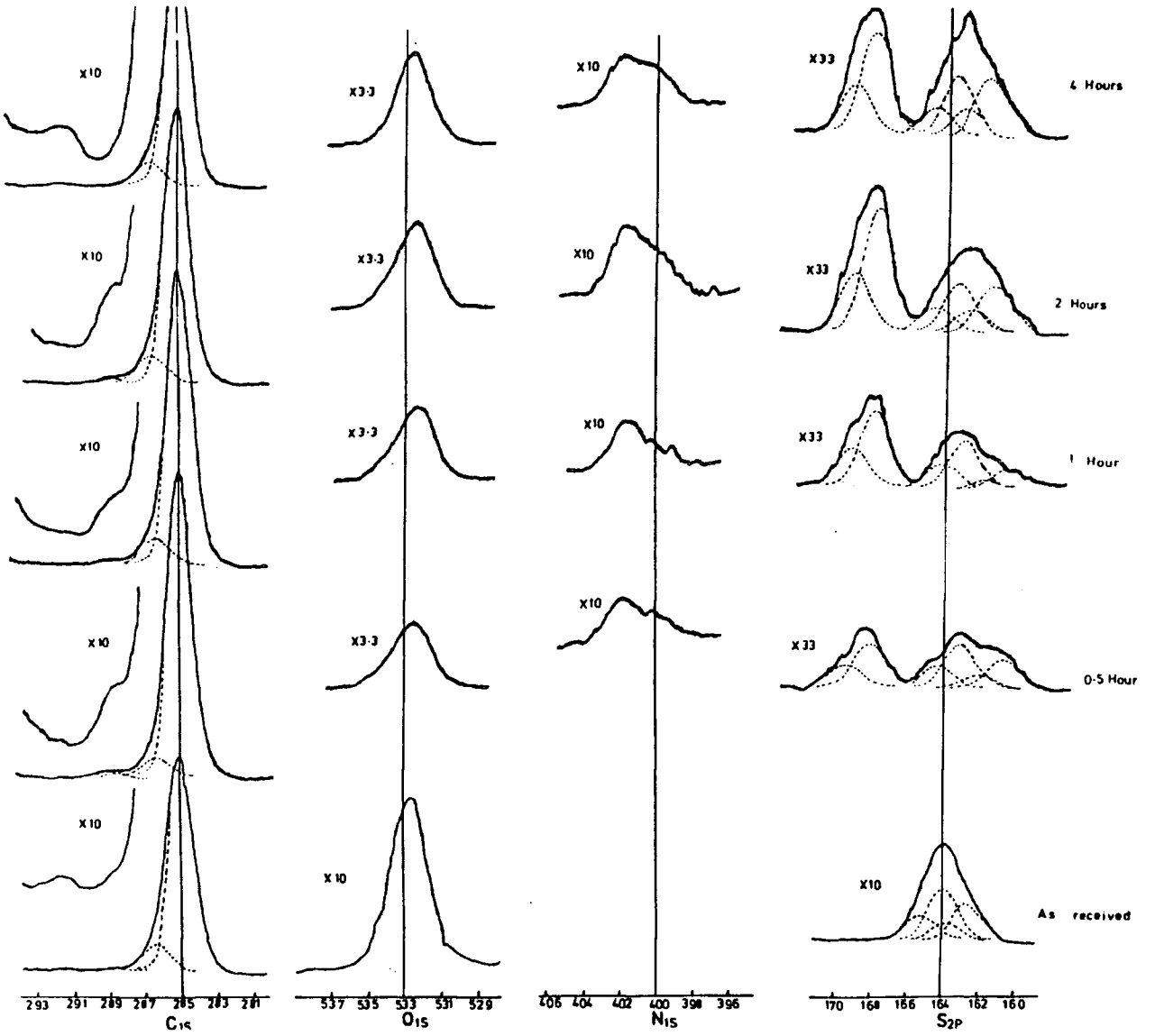

Figure 9.4. C_{1s}, O_{1s}, N_{1s} and S_{2p} spectra of a type 1, Natsyn 2200, elastomer (cured for 14 minutes) versus time of treatment with a solution of propane-2-thiol (0.4M) and piperidine (0.4M) in heptane.

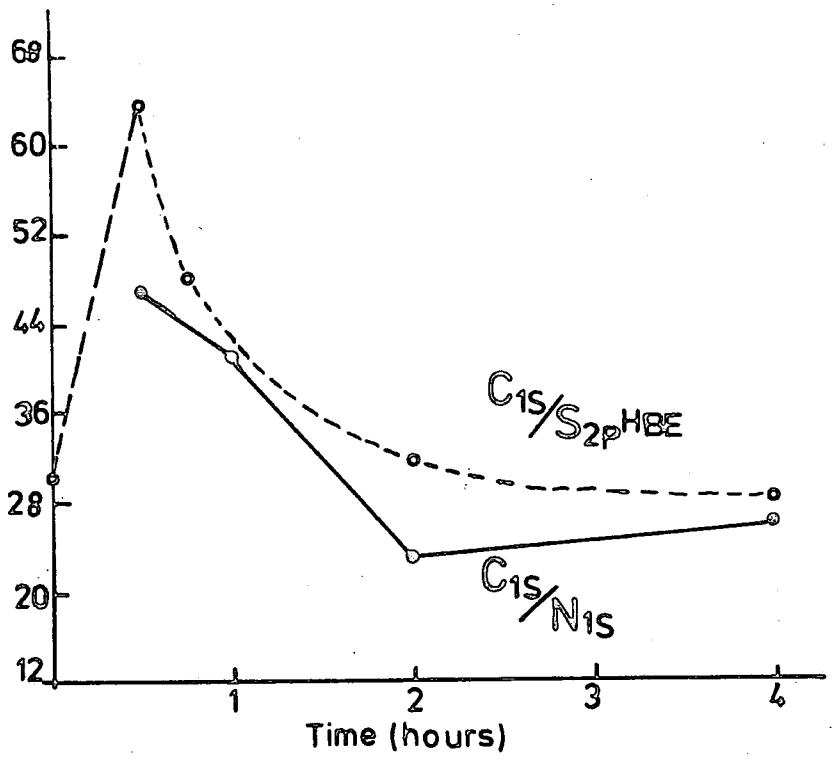

Figure 9.5a. Intensity ratios of the C_{1s}, N_{1s} and S_{2p} levels in the ESCA spectra of a type 1, Natsyn 2200, elastomer (cured for 14 minutes) versus time of treatment with a solution of propane-2-thiol (0.4M) and piperidine (0.4M) in n-heptane.

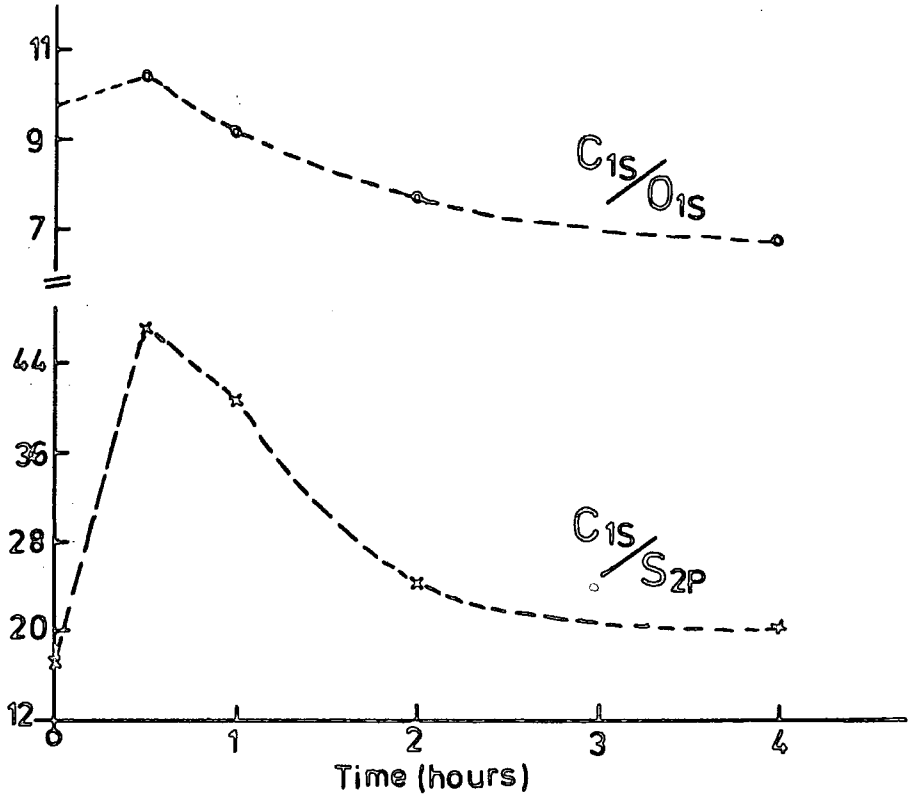

Figure 9.5b. Intensity ratios of the C_{1s}, O_{1s} and S_{2p} levels in the ESCA spectra of a type 1, Natsyn 2200, elastomer (cured for 14 minutes) versus time of treatment with a solution of propane-2-thiol (0.4M) and piperidine (0.4M) in heptane.

The C_{1s}/S_{2p} intensity ratio passes through a maximum before the level of sulphur increases with the reaction time and, an equilibrium between the organic sulphides in vulcanisates and thiols is finally established after reaction time of two hours at room temperature. The rate of sulphur loss from the surface is very fast in the initial stages of reaction time (< 30 minutes), as far as the ESCA depth profile is concerned into the sample. The level of nitrogen in the surface region also increases with reaction time and levels after two hours. The existence of an equilibrium of the rubber network with thiol-amine reagent in n-heptane is not of experimental significance for determining the relative proportions of mono-, di- and polysulphides, because rubber-bound thiol groups are formed during the treatment, as is evident by the decrease of C_{1s}/S_{2p} intensity ratios after reaction time of 30 minutes. The increase in S_{2p} level is conceivably brought about by the addition of thiols to the double bonds of rubber chains, which, in the presence of oxygen (oxygen is from air bubbles trapped during processing of elastomers on a calendering system) could lead to disulphide crosslinks.

The background information, in the literature, pertaining to the bulk, indicates that the addition of alkanethiols to natural rubber is a slow process,[371] even in the presence of peroxide catalyst or UV light, and isomerisation of NR by alkanethiols does not occur in the absence of free radical catalysts, but, as far as the ESCA depth profile is concerned into the sample, the effect of thiols addition to NR is

substantially significant and is possibly much more enhanced by the mobility of sulphur groups. The cleavage reaction by the thiol-amine reagent in n-heptane, occurring in the very initial stage of treatment, may be best understood by considering the trisulphide in scheme 3.

Scheme 3

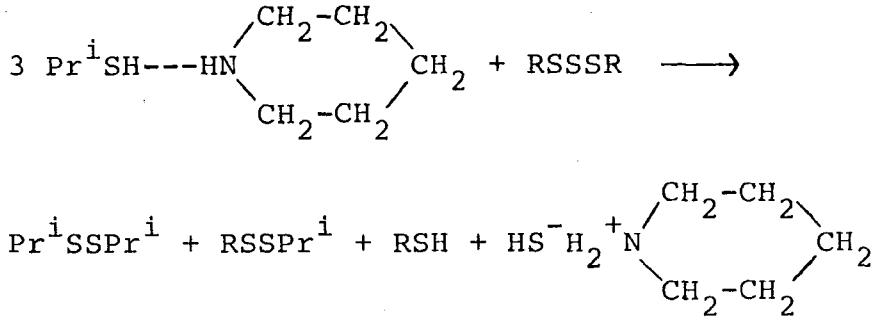

$Pr^i \equiv$ iso-propyl

The thiol-amine combination is thought to yield an associate, piperidinium propane-2-thiol ion pair, in which the nucleophilicity of the sulphur atom has been enhanced, and this is capable of cleaving organic polysulphides within reaction time of 30 minutes (Figure 9.5), while reacting one thousand-fold more slowly with the corresponding disulphides.

A plot of C_{1s}/O_{1s} intensity ratios as a function of reaction time in Figure 9.5b reveals the same trend as for the C_{1s}/S_{2p} that the level of oxygen increases with increasing reaction time and, this is associated with the oxidation of organic sulphides and polyisoprene chains, as is evidenced by the development of oxidative functionalisation under the high binding energy tail of the C_{1s} envelope and by the appearance of a broad band at binding energy $\sim$ 168 in the S_{2p} regions.

Cluff and Gladding have reported[372] that the oxidation of rubber-bound thiols in polyurethane elastomers by atmospheric oxygen is involved in reformation of disulphide crosslinks. However, oxidative degradation of rubber networks was impossible to avoid in this part of the study since the elastomer had a large number of voids. The air bubbles were trapped during curing process on a calendering system at 150°C in air. Despite the degassing of elastomers and thiol-amine reagent at a pressure of $\sim 10^{-3}$ torr and also of carrying out the treatments in vacuum did not obviate the oxidation degradation of the type 1, Natsyn 2200, elastomer at room temperature.

It is clear from the preceding discussion that the incorporation of sulphur from the thiol-amine reagent and of oxygen in the surface region have additionally complicated the ESCA examination of solution treated elastomers; and, therefore, it is not possible, with the application of ESCA, to determine the relative proportion of different sulphides in the surface regions, using thiol-amine reagent.

9.3.3 ESCA data of as received elastomers as a function of cure time

The review in chapter one highlights the fact that the sulphur is bound in vulcanised rubbers as different types of sulphide crosslinks and also as cyclic sulphides which do not participate in crosslinking polymer chains. The two 'sulphur-vulcanised' systems are taken to represent materials with different composition of sulphide crosslinks.

The ESCA data of as received elastomers, as a function of cure time, are shown in Figures 9.6 and 9.7. It is clearly

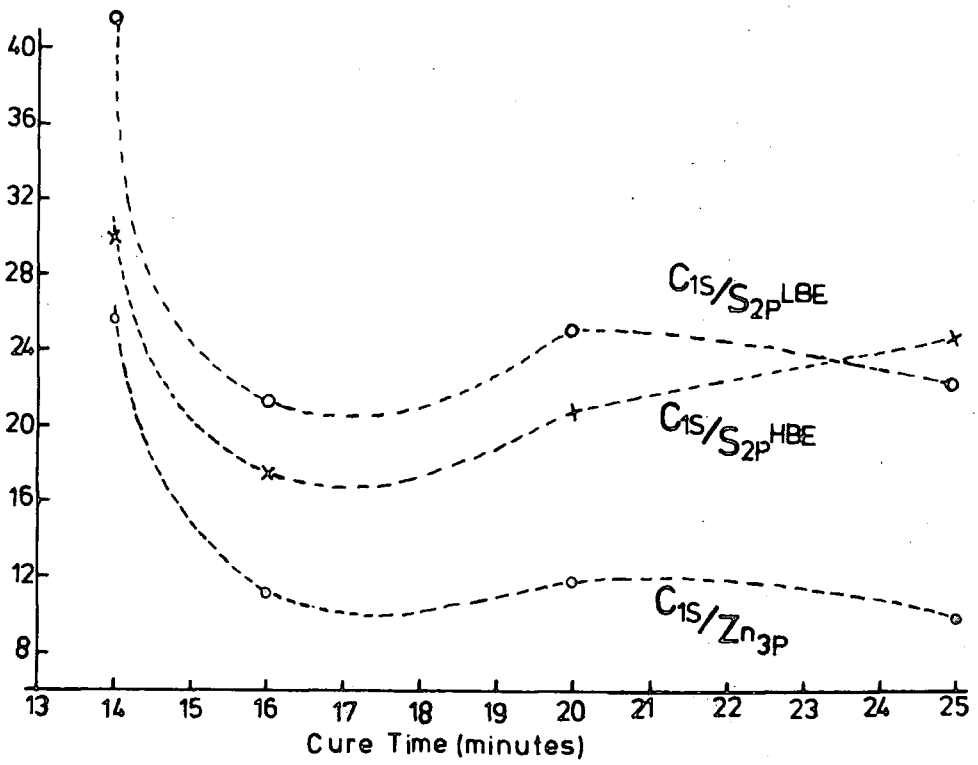

Figure 9.6. Intensity ratios of the C_{1s}, S_{2p} and Zn_{3p} levels in the ESCA spectra of a type 1, Natsyn 2200, elastomer versus time of cure.

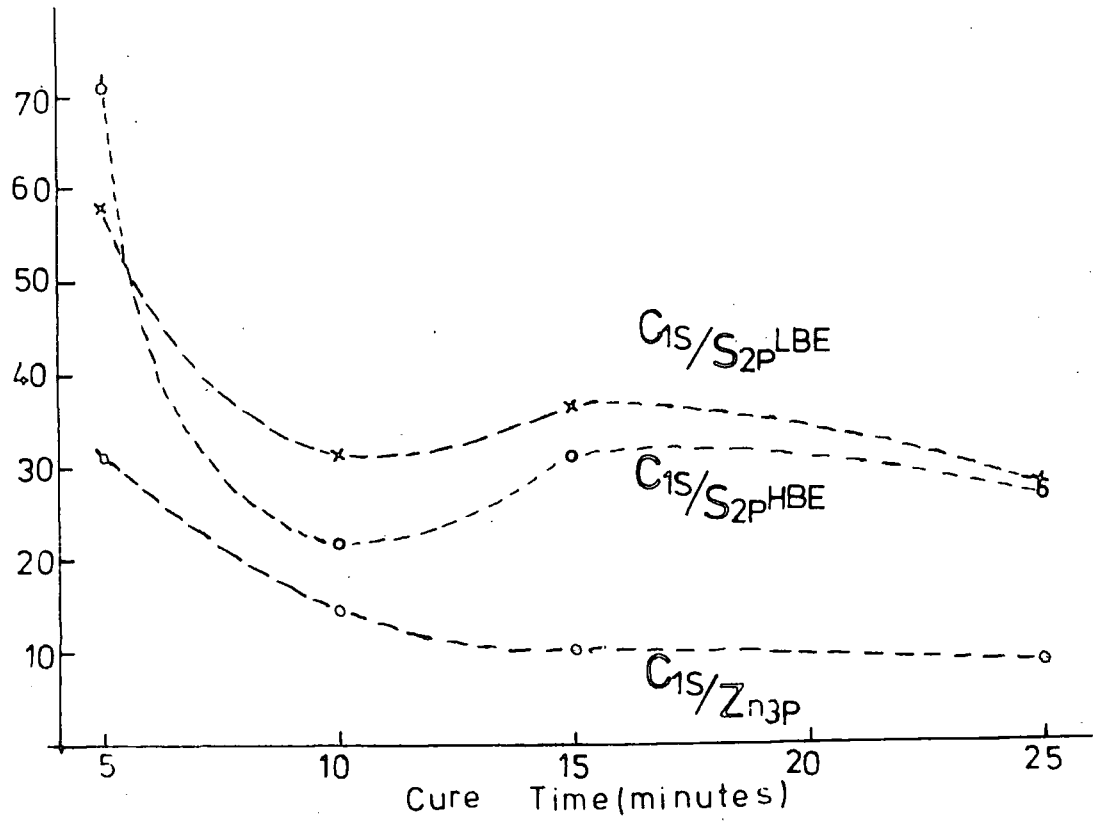

Figure 9.7. Intensity ratios of the C_{1s}, S_{2p} and Zn_{3p} levels in the ESCA spectra of a type 2, Natsyn 2200, elastomer versus time of cure.

evident that both types of vulcanisates (with sulphur/cyclohexylbenzthiazyl sulphenamide and tetramethylthiuram disulphide respectively) reveal the same trend that the distribution of sulphur in the total sulphide crosslinks passes through a maximum with the cure time. (The samples were cured on a calendering system at 150°C in air, with a 2 mm nip setting to draw into sheets).

The competing nature of two opposing reactions is also evident from the shapes of the C_{1s}/S_{2p} intensity ratio curves in Figures 9.6 and 9.7. The ESCA results appear complex but may be rationalised on the assumption that the opposing factors determine the course of the polysulphide concentration in the system. The shape of the C_{1s}/S_{2p} curves also support the prevalent concept of maximum polysulphide formation in the earlier stage of curing reaction and these polysulphide crosslinks are subsequently desulphurised to more stable structures on prolonged curing time, which contain less sulphur per crosslink, and also into cyclic sulphides which do not contribute to crosslinks.

9.4 Conclusion

It is clear that the ESCA results have been additionally complicated by the incorporation of thiol and amine into the elastomers, and it is not possible, with the application of ESCA, to determine the relative proportion of different sulphides in the surface regions, using thiol-amine reagents.

APPENDIX I

Lectures and Seminars Attended During the Period 1980-1983

7 October 1980

Professor T. Fehlner (University of Notre-Dame, U.S.A.),
"Metalloborane Cages or Coordination Compounds?".

16 October 1980

Dr. D. Maas (University of Salford),
"Reactions a Go-Go".

30 October 1980

Professor N. Grassie (University of Glasgow),
"Inflammability Hazards in Commercial Polymers".

6 November 1980

Professor A.G. Sykes (University of Newcastle upon Tyne),
"Metallo-Proteins: An Inorganic Chemists' Approach".

12 November 1980

Dr. M. Gerloch (University of Cambridge),
"Magnetochemistry is about Chemistry".

13 November 1980

Professor N.N. Greenwood (University of Leeds),
"Metalloborane Chemistry".

19 November 1980

Dr. T. Gilchrist (University of Liverpool),
"Nitroso-olefins as Synthetic Intermediates".

4 December 1980

Reverend R. Lancaster,
"Fireworks".

18 December 1980

Dr. R. Evens (University of Brisbane, Australia),

"Some Recent Communications to the Editor of the Australian Journal of Failed Chemistry".

29 January 1981

Mr. H. Maclean (I.C.I. Ltd.),

"Managing in the Chemical Industry in the 1980s".

18 February 1981

Professor S. Kettle (University of East Anglia),

"Variations in the Molecular Dance at the Crystal Ball".

25 February 1981

Dr. K. Bowden (University of Essex),

"The Transmission of Polar Effects of Substituents".

17 March 1981

Professor W. Jencks (Brandeis University, Massachusetts),

"When is an Intermediate not an Intermediate?".

7 May 1981

Professor M. Gordon (University of Essex),

"Do Scientists have to Count?".

10 June 1981

Dr. J. Rose (I.C.I. Plastics),

"New Engineering Plastics".

21 September 1981

Dr. P. Plimmer (Dupont),

"From Conception to Commercialisation of a Polymer".

14 October 1981

Professor E. Kluk (University of Katawice),

"Some Aspects of the Study of Molecular Dynamics - Simple Molecular Liquids".

22 October 1981

Dr. P.J. Corish (Dunlop Ltd.),

"What would life be like without Rubber".

6 November 1981

Dr. W. Moddeman (Monsanto Ltd., U.S.A.),

"High Energy Materials".

12 November 1981

Professor A.I. Scott (University of Edinburgh),

"An Organic Chemist"s View of Life in the N.M.R. Tube".

26 November 1981

Dr. W.O. Ord (Northumbrian Water Authority),

"The Role of the Scientist in a Regional Water Authority".

2 December 1981

Dr. G. Beamson (University of Durham),

"Photoelectron Spectroscopy in a Strong Magnetic Field".

20 January 1982

Dr. M.R. Bryce (University of Durham),

"Organic Metals".

28 January 1982

Professor I. Fells (University of Newcastle upon Tyne),

"Balancing the Energy Equations".

3 February 1982

Dr. D. Parker (University of Durham),

"Modern Methods for the Determination of Enantiomeric Purity".

10 February 1982

Dr. D. Pethrick (University of Strathclyde),

"Conformational Dynamics of Small and Large Molecules".

17 February 1982

Professor D.T. Clark (University of Durham),
"Structure, Bonding, Reactivity and Synthesis of Surfaces as revealed by ESCA".

3 March 1982

Dr. P. Bamfield (I.C.I. Organics Division),
"Computer Aided Synthesis Design: A View from Industry".

19 May 1982

Professor R.D. Chambers (University of Durham),
"Fluorocarbanions - some 'Alice in the Looking Glass' Chemistry".

28 June 1982

Professor D.J. Burton (University of Iowa),
"Some Aspects of the Chemistry of Fluorinated Phosphonium Salts and Phosphonates".

13 September 1982

Professor R. Neidlein (University of Heidelberg),
"New Aspects and Results of Bridged Annulene Chemistry".

27 September 1982

Dr. W.K. Ford (Xerox Research Centre, Webster, New York),
"The Dependence of the Electronic Structures of Polymers on their Molecular Architecture".

13 October 1982

Dr. W.J. Feast (University of Durham),
"Approaches to the Synthesis of Conjugated Polymers".

28 October 1982

Professor M.F. Lappert, F.R.S. (University of Sussex),
"Approaches to Asymmetric Synthesis and Catalysis Using Electron-Rich Olefins and Some of Their Metal Complexes".

15 November 1982

Dr. G. Bertrand (University of Toulouse),

"Curtius Rearrangement in Organometallic Series: A Route for New Hybridised Species".

24 November 1982

Professor G.G. Roberts (University of Durham),

"Langmuir-Blodgett Films".

24 November 1982

Professor F.R. Hartley (R.M.C.S. Shrivenham),

"Supported Metal Complex Hydroformylation Catalysts: A Novel Approach Using γ-radiation".

2 December 1982

Dr. G.M. Brooke (University of Durham),

"The Fate of the Ortho-Fluorine in 3,3-Sigmatropic Reactions Involving Polyfluoro-aryl- and -heteroaryl Systems".

9 February 1983

Dr. P. Moore (University of Warwick),

"Mechanistic Studies in Solution by Stopped Flow F.T. NMR and High Pressure NMR Line Broadening".

2 March 1983

Dr. D. Bloor (Queen Mary College, University of London),

"The Solid-State Chemistry of Diacetylene Monomers and Polymers".

11 March 1983

Professor H.G. Viehe (University of Louvain),

"Oxidations on Sulphur".

16 March 1983

Dr. I. Gosney (University of Edinburgh),

"New Extrusion Reactions: Organic Synthesis in a Hot Tube".

25 March 1983

Professor F.G. Baglin (University of Newark),
"Interaction Induced Raman Spectroscopy in Supracritical Ethane".

21 April 1983

Professor J. Passmore (University of New Brunswick),
"Novel Selenium-Iodine Cations".

4 May 1983

Professor P.H. Plesch (University of Keele),
"Binary Ionisation Equilibria Between Two Ions and Two Molecules. What Ostwald Never Thought Of".

10 May 1983

Professor K. Berger (University of Munich),
"New Reaction Pathways from Trifluoromethyl-Substituted Heterodienes to Partially Fluorinated Heterocyclic Compounds".

11 May 1983

Dr. N. Isaacs (University of Reading),
"The Application of High Pressures to the Theory and Practice of Organic Chemistry".

13 May 1983

Dr. R. de Kock (Calvin College, Grand Rapids, Michigan),
"Electronic Structural Calculations on Organometallic Cobalt Cluster Molecules: Implications for Metal Surfaces".

APPENDIX II

Conferences Attended During the Period 1980-1983

(1) Polymer Characterisation Symposium, July 1981, Durham.

(2) Graduate Symposium, Durham, 1982.

(3) Graduate Symposium, April 1983, Durham.

REFERENCES

1. I.J. Sjothan and G. Alliger, in 'Vulcanisation of Elastomers', Eds., G. Alliger and I.J. Sjothan, Reinhold, New York (1978).
2. W. Hofman, 'Vulcanisation and Vulcanising Agents', Maclaren, London (1967).
3. L. Bateman, J.I. Cunneen, C.G. Moore, L. Mullins and A.G. Thomas, p.715, ref. 301.
4. E.H. Farmer and F.W. Shipley, J. Polym. Sci., 293, 1 (1946).
5. E.H. Farmer, J. Chem. Soc., 1519 (1947).
6. E.H. Farmer, J. Chem. Ind., 86, 66 (1947).
7. G.F. Bloomfield and R.F. Naylor, Int. Congr. Pure Appl. Chem., 11th, London, 7, 2 (1947).
8. L. Bateman, C.G. Moore and M. Porter, J. Chem. Soc., 2866 (1958).
9. E.M. Bevilacqua, Rubber Chem. Technol., 721, 32 (1959).
10. M. Porter, 'The Chemistry of Sulphur Vulcanisation of Natural Rubber', in 'The Chemistry of Sulphides', Ed., A. Tabolsky, Interscience, New York (1968), p.168.
11. M. Porter, in 'Organic Chemistry of Sulphur', ref. 243.
12. B. Milligan, J. Chem. Soc., 34, A (1966).
13. J.G. Lichty, U.S. Patent No. 2, 129, 621 (1938).
14. G. Spacu and C.G. Macarovici, Bull. Sec. Sci. Acad. Roumanie, 173, 21 (1938).
15. G. Spacu and C.G. Macarovici, Chem. Abst., 4007, 34 (1940).
16. G.M.C. Higgins and B. Saville, J. Chem. Soc., 2812 (1963).

17. E. Coates, B. Rigg, B. Saville and D. Skelton, J. Chem. Soc., 5613 (1965).

18. S.K. Gupta and T.S. Srivastava, J. Inorg. Nuclear Chem., 1611, 32 (1970).

19. B.C. Barton and E.J. Hart, Ind. Eng. Chem., 2444, 44 (1952).

20. B. Milligan, Rubber Chem. Technol., 1115, 39 (1966).

21. A.Y. Coran, Rubber Chem. Technol., 679, 37 (1964).

22. A.Y. Coran, Rubber Chem. Technol., 1, 38 (1965).

23. J.P. Fackler, D. Coucouvanis, J.A. Fetchin and W.C. Seidel, J. Amer. Chem. Soc., 2784, 90 (1968).

24. J.P. Fackler, J.A. Fetchin and J.A. Smith, J. Amer. Chem. Soc., 2910, 92 (1970).

25. J.P. Fackler and J.A. Fetchin, J. Amer. Chem. Soc., 2912, 92 (1970).

26. R.E. Davis and H.F. Nakshbendi, J. Amer. Chem. Soc., 2085, 84 (1962).

27. W.G. Hodgson, S.A. Buckler and G. Peters, J. Amer. Chem. Soc., 543, 85 (1963).

28. R. MacColl and S. Windwer, J. Phys. Chem., 1261, 74 (1970).

29. Y. Sasaki and F.P. Olsen, Can. J. Chem., 283, 49 (1971).

30. J.P. Fackler, J.A. Fetchin and D.C. Fries, J. Amer. Chem. Soc., 7323, 94 (1972).

31. L. Bateman, C.G. Moore, M. Porter and B. Seville, in 'The Chemistry and Physics of Rubber-like Substances', Ed., L. Bateman, MacLaren, London, p.451 (1963).

32. J.R. Dunn, J. Scanlan, J. Appl. Polym. Sci., 84, 1 (1959).

33. C.G. Moore and A.A. Watson, J. Appl. Polym. Sci., 851, 8 (1964).

34. T.D. Skinner, Rubber Chem. Technol., 182, 45 (1972).

35. D. Banard, T.H. Houseman, M. Porter and B.K. Tidd, Chem. Commun., 371 (1969).

36. B.K. Tidd, Int. J. Sulphur Chem., 101, C6 (1971).

37. A.A. Watson, Ph.D. Thesis, University of London (1965).

38. D.S. Campbell, J. Appl. Polym. Sci., 1013, 13 (1969).

39. M.L. Studebaker, Rubber Chem. Technol., 1359, 39 (1966).

40. C.G. Moore, L. Mullins and P. McL. Swift, J. Appl. Polym. Sci., 293, 5 (1961).

41. C.G. Moore and B.R. Trego, J. Appl. Polym. Sci., 299, 5 (1961).

42. T.D. Skinner and A.A. Watson, Rubber Chem. Technol., 404, 42 (1969).

43. R.M. Russell, T.D. Skinner and A.A. Watson, Rubber Chem. Technol., 418, 42 (1969).

44. J.R. Dun, C.G. Moore and B.R. Trego, J. Appl. Polym. Sci., 723, 8 (1964).

45. B.A. Dogadkin, Z.N. Tarasova and I.I. Golberg, Proc. of the 4th Rubber Technol. Conf. London, 65, 7 (1962).

46. C.M. Blow and C.T. Loo, Polymer, 205, 16 (1975).

47. C.T. Loo, Polymer, 729, 15 (1974).

48. C.T. Loo, Polymer, 357, 15 (1974).

49. J. Scanlan and D.K. Thomas, J. Polym. Sci., 1015, Part A1, (1963).

50. E.H. Farmer and S.E. Michael, J. Chem. Soc., 513 (1942).

51. E.H. Farmer and C.G. Moore, J. Chem. Soc., 131 (1951).

52. E.H. Farmer and C.G. Moore, J. Chem. Soc., 142 (1951).

53. L.D. Loan, Rubber Chem. Technol., 149, 40 (1967).

54. L.D. Loan, J. Appl. Polym. Sic., 2259, 7 (1963).

55. D.M.E. Van der Hoff, Ind. Eng. Chem., Prod. Res. Dev., 273, 2 (1963).

56. D.K. Thomas, J. Appl. Polym. Sci., 613, 6 (1962).

57. C.R. Parks and O. Lorenz, J. Polym. Sci., 287, 50 (1961).

58. K.W. Scott, J. Polym. Sci., 517, 58 (1962).

59. R. Rado and D. Simunkova, Vgsokmol. Soedin., 1277, 3 (1961).

60. D.K. Thomas, Trans. Faraday Soc., 511, 57 (1961).

61. L.D. Loan, J. Polym. Sci., 2127, Part A2 (1964).

62. J.O. Harris and C.D. Trivette, in 'Vulcanisation of Elastomers', Ed., G. Alliger and I.K. Sjothan, New York (1978).

63. C.M. Blow, Rubber Technology and Manufacture, Butterworth, London (1971).

64. P.J. Flory, 'Principles of Polymer Chemistry', Cornell University Press, Ithaca, New York (1978).

65. A. Ciferri, J. Polym. Sci., 149, 54 (1961).

66. K.H. Meyer, G. Von Susich and E. Valko, Kolloid Z., 208, 59 (1932).

67. L.R.G. Treloar, 'The Physics of Rubber Elasticity', 2nd Ed., Clarendon Press, Oxford (1958).

68. Ref. 64, p.464.

69. M. Mooney, J. Appl. Phys., 582, 11 (1940).

70. R.S. Rivlin and D.W. Saunders, Phil. Trans. Roy. Soc., 251, A243 (1951).

71. L. Mullins, J. Appl. Polym. Sci., 1, 2 (1959).

72. S.M. Gumbrell, L. Mullins and R.S. Rivlin, Trans. Faraday Soc., 1495, 49 (1953).

73. P.J. Flory and J. Rehner, J. Chem. Phys., 512, 11 (1943).

74. P.J. Flory and J. Rehner, J. Chem. Phys., 521, 11 (1943).

75. P.J. Flory, J. Chem. Phys., 108, 18 (1950).

76. L. Mullins, J. Polym. Sci., 225, 19 (1956).

77. G.M. Bristow and W.F. Watson, Trans. Faraday Soc., 1567, 54 (1958).

78. G. Crespi and M. Bruzzone, Chim. Ind. (Milan), 741, 41 (1959).

79. W.J. Bobear, Ind. Eng. Chem. Prod. Res. Dev., 277, 3 (1964).

80. C.G. Moore and B.R. Trego, J. Appl. Polym. Sci., 1957, 8 (1964).

81. C.G. Moore and W.F. Watson, J. Polym. Sci., 237, 19 (1956).

82. G.M. Bristow, C.G. Moore and R.M. Russell, J. Polym. Sci., 3893, A3 (1965).

83. M.L. Studebaker and L.G. Nabors, Proc. Intern. Rubber Conf., Washington, D.C. (1959), p.

84. M.L. Studebaker and L.G. Nabors, Rubber Chem. Technol., 941, 32 (1959).

85. M.L. Studebaker, Kautschuk Gummi, WT177, 14 (1961).

86. M.L. Studebaker and L.G. Nabors, Proc. 4th Rubber Technol. Conf., (1962) p.300.

87. A.Y. Coran, Rubber Chem. Technol., 668, 37 (1964).

88. S. Chakravarty, P.K. Chatterjee and A.K. Sircar, J. Appl. Polym. Sci., 1395, 9 (1965).

89. W. Scheele and T. Kadibelban, Kautschuk Gummi, 363, 21 (1968).

90. C.G. Moore, in 'Proc. Nat. Rubber Producers' Res. Assoc. Jubilee Conf., Cambridge, Ed., L. Mullins (1964) p.167.

91. D.S. Campbell and B. Saville, Proc. Intern. Rubber Conf., Brighton (1967), p.1.

92. G. Butenuth and H. Westlinning, Rubber Chem. Technol., 311, 37 (1964).

93. G. Butenuth, Rubber Age, 737, 94 (1963-1964).

94. C.G. Moore and B.R. Trego, J. Chem. Soc., 4205 (1962).

95. D.S. Campbell, J. Appl. Polym. Sci., 1201, 13 (1969).

96. B. Saville and A.A. Watson, Rubber Chem. Technol., 100, 40 (1967).

97. M.B. Evans and B. Saville, Proc. Chem. Soc., 18 (1962).

98. G.A. Blokh, Gummi Asbest., 610, 10 (1957).

99. G.A. Blokh, Rubber Chem. Technol., 1035, 31 (1958).

100. B.A. Dogadkin, Kautschuk Gummi, WT5, 12 (1959).

101. W. Scheele and W. Triebel, Kautschuk Gummi, WT127, 11 (1958).

102. W. Scheele and W. Triebel, Rubber Chem. Technol., 208, 32 (1959).

103. E.C. Gregg, J. Polym. Sci., 303, 24 (1968).

104. C.G. Moore and B.R. Trego, Tetrahedron, 205, 18 (1962).

105. A.A. Watson, J. Chem. Soc., 2100 (1964).

106. J. Haslam, H.A. Willis and D.C. Squirrell, Identifications and Analysis of Plastics (2nd Ed.), Iliffe (1972).

107. C.J. Henniker, Infrared Spectroscopy of Plastics and Rubbers, Chapman and Hall (1966).

108. G.L. Clark, 'Encyclopedia of Spectroscopy', Reinhold Publishing Corp., New York (1960).

109. S. Krimm, Fortschr. der Hochpolymeren Forschung, 51, 2 (1960).

110. F. Ciampelli, D. Morero and M. Cambini, Makromol. Chem., 250, 61 (1963).

111. P.J. Corish, Spectrochimica Acta, 598 (1959).

112. P.J. Corish, Rubber Chem. Technol., 975, 33 (1960).

113. J.L. Binder, J. Polym. Sci., 47, A1 (1963).

114. J. Kiji and M. Iwamoto, J. Polym. Sci., 53, B6 (1968).

115. Y. Tanaka and Y. Takenchi, J. Polym. Sci., A2, 13, 9 (1971).

116. Y. Tanaka and H. Sato, Polymer, 113, 17 (1976).

117. Y. Tanaka and H. Sato, Polymer, 413, 17 (1976).

118. W. Gronski, N. Murayama and H.J. Cantow, Polymer, 358, 17 (1976).

119. H. Sato, A. Ono and Y. Tanaka, Polymer, 580, 18 (1977).

120. Y. Tanaka, Y. Takeuchi, M. Kobayashi and H. Tadokoro, J. Polym. Sci., A2, 43, 9 (1971).

121. J.P. Kistler, G. Friedmann and B. Kaemph, Bull. Soc. Chim. France, 4759 (1967).

122. F. Schve and J.P. Dole-Robbe, Bull. Soc. Chim. France, 975 (1963).

123. E.R. Santee, V.D. Mochel and M. Morton, J. Polym. Sci. Polym. Lett. Ed., 453, 11 (1973).

124. K. Hatada, Y. Tanaka, Y. Terawaki and H. Okuda, Polym. J., 327, 3 (1973).

125. Y. Tanaka, H. Sato, K. Katada, Y. Terawaki and H. Okuda, Makromol. Chem., 1823, 178 (1977).

126. M.W. Duch and D.M. Grant, Macromolecules, 165, 3 (1970).

127. Y. Tanaka and H. Sato, J. Polym. Sci. Polym. Lett. Ed., 473, 16 (1978).

128. J. Schaefer, E.O. Stejskal, 'High Resolution ^{13}C NMR of Solid Polymers, in 'Topics in Carbon-13 NMR Spectroscopy', Ed., G. Levy, p.283 (1979).

129. N. Uri, in 'Autoxidation and Antioxidants', Ed., W.O. Lundberg, Interscience, New York (1962), p.65.

130. R. Criegee, Abstracts of papers presented at the 120th Meeting of the Amm. Chem. Soc., Sept. (1951), p.22M.

131. P.S. Bailey, Chem. Rev., 925, 58 (1958).

132. D.J. Carlsson and D.M. Wiles, Macromolecules, 587, 597, 2 (1969).

133. F.R. Mayo, J. Polym. Sci., 921, B10 (1972).

134. L.H. Lee, G.L. Stacy and R.G. Engel, J. Appl. Polym. Sci., 1699, 1717, 10 (1966).

135. L. Reich and S.S. Stivala, J. Appl. Polym. Sci., 2033, 12 (1968).

136. J.F. Rabek, in 'Comprehensive Chemical Kinetics', Ed., C.H. Bamford and C.F.H. Tipper, 425, 14 (1975) Elsevier Scientific Publishing Co., Amsterdam.

137. J.H. Adams and J.E. Goodrich, J. Polym. Sci., 1269, A1, 8 (1970).

138. J.C.W. Chien, E.J. Vandenburg and H. Jabloner, J. Polym. Sci., 381, A1, 6 (1968).

139. N.J. Harrick, Internal Reflectance Spectroscopy, Wiley-Interscience, New York (1967).

140. D.T. Clark, in 'Electron Emission Spectroscopy', Ed., W. Dekyser and D. Reidel, D. Reidel Publishing Co., Dordrecht, Holland, 373 (1973).

141. W. Hallwachz, Wied. Ann., 301, 33 (1888).

142. P. Leanard, Ann. Physik, 359, 2 (1900).

143. A. Einstein, Ann. Physik, 132, 17 (1905).

144. H. Robison, Phil. Mag., 241, 50 (1925).

145. M. de Broglie, Compt. Rend., 274, 172 (1921).

146. K. Siegbahn and K. Edvardson, Nucl. Phys., 137, 1 (1956).

147. C. Nordling, E. Sokolowski and K. Siegbahn, Phys. Rev., 1676, 105 (1957).

148. C. Nordling, E. Sokolowski and K. Siegbahn, Proc. Roy. Soc., 420, A161 (1937).

149. S. Hagström, C. Nordling and K. Siegbahn, Phys. Lett., 235, 9 (1964).

150. C. Nordling, S. Hagström and K. Siegbahn, Z. Physik, 433, 178 (1964).

151. K. Siegbahn, C. Nordling, A. Fahlman, R. Nordberg, K. Hamrin, J. Hedman, G. Johansson, T. Berkmark, S.E. Karlsson, I. Lidgren and B. Linberg, 'ESCA Atomic, Molecular and Solid State Structure Studied by Means of Electron Spectroscopy', Almquist and Wiksells, Uppsala (1967).

152. K. Siegbahn, C. Nordling, G. Johansson, J. Hedman, P.F. Heden, K. Hamrin, U. Gelius, T. Berkmark, L.D. Warme, R. Manne and Y. Bear, 'ESCA Applied to Free Molecules', North Holland Publishing Co., Amsterdam (1969).

153. A.D. Baker and C.R. Brundle, 'An Introduction to Electron Spectroscopy', in 'Electron Spectroscopy. Theory, Techniques and Applications', Vol. 1, Eds., C.R. Brundle and A.D. Baker, Academic Press, London (1977).

154. T.N. Rhodin and J.W. Gadzuk, 'Electron Spectroscopy and Surface Chemical Bonding', in 'The Nature of the Surface Chemical Bond', Eds., T.N. Rhodin and G. Erti, 112, North Holland Publishing Co., Amsterdam (1979).

155. D.T. Clark,'Structure and Bonding in Polymers as Revealed by ESCA', in 'Electronic Structure C.f. Polymers and Molecular Crystals', Eds., J. Ladik and J.M. Andre, Plenum Press, New York (1975).

156. H.B. Culien, Handbook of Physics, Section 8, Chapter 2, McGraw-Hill (1967).

157. A. Rosen and I. Lindgren, Phys. Rev., 114, 176 (1968).

158. P.S. Bagus, Phys. Rev. A., 619, 139 (1965).

159. D.A. Shirely, in 'Advances in Chem. Phys.', Eds., I. Prigogini and S.A. Rice, J. Wiley and Sons Ltd., New York, 85, 23 (1973).

160. U. Gelius and K. Siegbahn, Faraday Discuss. Chem. Soc., 257, 54 (1972).

161. L.C. Snyder, J. Chem. Phys., 95, 55 (1971).

162. D.B. Adams and D.T. Clark, Theoret. Chim. Act., 171, 31 (1973).

163. M.F. Guest, I.H. Hillier, V.R. Saunders and M.W. Wood, Proc. Roy. Soc., 201, A333 (1973).

164. D.T. Clark, I.W. Scanlan and J. Müller, Theoret. Chim. Act. (Be), 341, 35 (1974).

165. D.T. Clark and I.W. Scanlan, J. Chem. Soc. Farad. Trans., 11, 1222, 70 (1974).

166. D.T. Clark, in 'Advances in Polymer Science', Ed., H.J. Cantow, Ipringer Verlag, Berlin, 125, 24 (1977).

167. R. Manne and T. Aberg, Chem. Phys. Lett., 282, 7 (1970).

168. D.T. Clark, B.D. Adams, A. Dilks, J. Peeling and H.R. Thomas, J. Elec. Spec. Rel. Phenom., 51, 8 (1976).

169. D.T. Clark and A. Dilks, J. Polym. Sci. Polym. Chem. Ed., 533, 14 (1976).

170. D.T. Clark and A. Dilks, J. Polym. Sci. Polym. Chem. Ed., 15, 15 (1977).

171. P. Auger, J. Phys. Radium, 205, 6 (1925).

172. P. Auger, Compt. Rend., 180, 65 (1925).

173. J.J. Lander, Phys. Rev., 1382, 91 (1953).

174. C.f. T.A. Carlson, 'Photoelectron and Auger Spectroscopy', Plenum Press, New York (1975).

175. D. Coster and R. de L. Kronig, Physica, 13, 2 (1935).

176. E.H.S. Burhop, 'The Auger Effect and Radiationless Transitions', Cambrige University Press (1952).

177. O. Keski-Rahkonen and M.I. Krause, At. Data Nucl. Data Tables, 139, 14 (1974).

178. J.P. Coad, M. Gettings and J.G. Riviere, Faraday Discuss. Chem. Soc., 269, 60 (1975).

179. C.D. Wagner, Discuss. Faraday Soc., 291, 60 (1975).

180. S.P. Kowalcyzk, F.R. McFeely, R.S. Pollak, L. Ley and D.A. Shirley, Phys. Rev., 3583, B8 (1973).

181. L. Ley, S.P. Kowalczyk, F.R. McFeely, R.A. Pollak and D.A. Shirley, Phys. Rev., 2392, B8 (1973).

182. S.P. Kowalczyk, L. Ley, F.R. McFeely, R.A. Pollak and D.A. Shirley, Phys. Rev., 2387, B8 (1973).

183. S.P. Kowalczyk, L. Ley, F.R. McFeely, R.A. Pollak and D.A. Shirley, Phys. Rev., 381, B9 (1974).

184. C.D. Wagner, Anal. Chem., 1650, 44 (1972).

185. C.D. Wagner and P. Bilden, Surface Sci., 82, 35 (1973).

186. C.D. Wagner, Faraday Discuss. Chem. Soc., 291, 60 (1975).

187. C.D. Wagner, L.H. Gale and R.H. Raymond, Anal. Chem., 466, 51 (1979).

188. A.E. Sandström, in 'Handbook of Physics', Vol. XXX, 'X-rays', 164 Ed., S.F. Flügge, Springer-Verlag, Berlin (1957).

189. T.A. Koopmans, Physics, 104, 1 (1933).

190. W.L. Jolly and D.N. Hendrickson, J. Amer. Chem. Soc., 1863, 92 (1970).

191. J.N. Murrel and B.J. Ralston, J. Chem. Soc., Faraday Trans., 11, 68, 1393 (1972).

192. M.E. Schwartz, Chem. Phys. Lett., 631, 6 (1970).

193. D.A. Shirley, Chem. Phys. Lett., 325, 15 (1972).

194. C.S. Fadley, 'Basic Concepts of X-ray Photoelectron Spectroscopy' in 'Electron Spectroscopy, Theory, Techniques and Applications', Vol. 2, 1, Eds., C.R. Brundle and A.D. Baker, Academic Press (1978).

195. R.E. Watson and A.J. Freeman, in 'Hyperfine Interactions' Eds., A.J. Freeman and R.B. Frankel, Academic Press, New York (1967).

196. C.S. Fadley, D.A. Shirley, A.J. Freeman, P.S. Bagus and J.V. Mallow, Phys. Rev. Lett., 1397, 23 (1969).

197. J.V. Van Vleck, Phys. Rev. Lett., 405, 45 (1934).

198. C.S. Fadley, in 'Electron Spectroscopy', Ed. D.A. Shirley, 781, North Holland Publishing Co. (1972).

199. D.W. Davis and D.A. Shirley, J. Chem. Phys., 669, 56 (1972).

200. P.M. Hay, in 'Chemical Reactions in Electrical Discharges', Ed., R.F. Gould, Am. Chem. Soc. Pubs. (1969).

201. M. Hudis, 'Plasma Treatment of Solid Materials' in 'Techniques and Applications of Plasma Chemistry', Ed., J.R. Hollahan and A.T. Bell, J. Wiley and Sons, New York (1974).

202. G.A. Byrne and K.C. Brown, J. Soc. Dyers and Colourists, 113, 88 (1972).

203. J.R. Hall, C.A.L. Westerdahl, A.T. Devine and M.J. Bodnar, J. Appl. Polym. Sci., 2085, 13 (1969).

204. M. Hudis, J. Appl. Polym. Sci., 2397, 16 (1972).

205. H. Schonhorn and R.H. Hansen, J. Appl. Polym. Sci., 1461, 11 (1967).

206. H. Yasuda, J. Macromol. Sci-Chem., 383, A10 (1976).

207. H. Schonhorn, Proceedings of 'Durham Polymer Surfaces Symposium', Ed., D.T. Clark and W.J. Feast, J. Wiley and Sons, London, in press (1977).

208. A.K. Sharma, F. Millich and E.W. Hellmuth, J. Appl. Polym. Sci., 2205, 26 (1981).

209. A.K. Sharma, F. Millich and E.W. Hellmuth, Ibid., 2197, 26 (1981).

210. N. Inagaki and H. Yasuda, Ibid., 3333, 26 (1981).

211. S. Yamakawa and F. Yamamoto, Ibid., 41, 25 (1980).

212. L.C. Jackson, Adhesive Age, 34, 9 (1978).

213. D. Briggs, in 'Surface Analysis and Pretreatment of Plastics and Materials', Ed., D.M. Brewis, Appl. Sci. Pubs. (London).

214. W.W. Balwanz, Surf. Contam. Genesis (Proc. Symposium), 225 (1979).

215. S.L. Degisis and C.H. Smith, SPE ANTEC papers, 675 (1978).

216. R.J. Chang, A.N. Gent, C.C. Hsu and K.C. Sehgal, J. Appl. Polym. Sci., 163, 25 (1980).

217. S. Yamakawa and F. Yamamoto, Ibid., 25, 25 (1980).

218. H. Yasuda, H.C. Marsh, S. Brandt and C.N. Reilley, J. Polym. Sci., Polym. Chem. Ed., 991, 15 (1977).

219. H.A. Willis and V.J.I. Zichy, Chapter 15, in 'Polymer Surfaces', Eds., D.T. Clark and W.J. Feast, Wiley, New York (1978).

220. D.T. Clark and A. Dilks, J. Polym. Sci., Polym. Chem. Ed., 1233, 18 (1980).

221. C.f. A.T. Bell, 'Fundamentals of Plasma Chemistry', ref. 201.

222. D.T. Clark, A. Dilks and D. Shuttleworth, Proceedings of 'Durham Polymer Surfaces Symposium', Ed., D.T. Clark and W.J. Feast, J. Wiley and Sons, London, in press (1977) and references therein.

223. G. Francis, 'Ionisation Phenomena in Gases', Butterworth Publications Ltd., London (1960).

224. E.O. Johnson and L. Malter, Phys. Rev., 58, 80 (1950).

225. J.D. Swift and M.J.F. Schwar, 'Electrical Probes for Plasma Diagnostics', Iliffe Books Ltd., London (1970) and references therein.

226. D.T. Clark and A. Dilks, A.C.S. Centennial Meeting, New York, April 1976, 'Internal Symposium on Advances in Characterisation of Metal and Polymer Surfaces', Ed., L.H. Lee, 101, 2, Academic Press, New York (1976).

227. D.T. Clark and A. Dilks, J. Polym. Sci., Polym. Chem. Ed., 2321, 15 (1977).

228. D.T. Clark and A. Dilks, Ibid., 911, 16 (1978).

229. D.T. Clark, 'ESCA Applied to Polymers' in 'Advances in Polymer Science', Springer-Verlag, Berlin, in press (1977).

230. D.T. Clark and W.J. Feast, J. Macromol. Sci., Reviews in Macromol. Chem., 191, C12 (1975).

231. D.T. Clark, in 'Structural Studies of Macromolecules by Spectroscopic Methods', Chapter 9, Ed., K. Ivin, J. Wiley and Sons, London (1976).

232. D.T. Clark, in 'Advances in Polymer Friction and Wear', Vol. 5A, Ed., L.H. Lee, Plenum Press, New York (1975).

233. D.T. Clark, 'Some Chemical Applications of ESCA' in 'Molecular Spectroscopy', Ed., A.R. West, Heydon and Sons, London (1976).

234. D.T. Clark, in 'Advances in Characterisation of Polymer and Metal Surfaces', Ed., L.H. Lee, Academic Press, New York (1976).

235. D.T. Clark and H.R. Thomas, J. Polym. Sci., Polym. Chem. Ed., 1671, 14 (1976).

236. D.T. Clark and A. Harrison, J. Polym. Sci. Chem. Ed., 1945, 19 (1981).

237. D.T. Clark, B.J. Cromarty and A. Dilks, J. Polym. Sci., Polym. Chem. Ed., 3173, 16 (1978).

238. J. Mitchell and L.R. Perkins, Appl. Polym. Symp., 167, 4 (1967).

239. B.J. Lindberg, K. Hamrin, G. Johansson, U. Gelius, A. Fahlman, C. Nordling and K. Siegbahn, Physica Scripta, 286, 1 (1970).

240. R.G. Boisiso, D. Klvana, P. Khosraviani and B. Damlaj, J. Microwave Power, 57, 16(1) (1981).

241. R.M. Jimeson and L.W. Richardson, AICHE Symp. Ser. No. 148, 199, 71 (1975).

242. E.E. Reid, 'Organic Chemistry of Bivalent Sulphur', Vol. 3, Chemical Publishing Co., New York (1960) p.362.

243. L. Field, in 'Organic Chemistry of Sulphur', Ed., S. Oae, Plenum Press, New York (1977).

244. W.E. Savige and J.A. MacLaren, in 'The Chemistry of Organic Sulphur Compounds', Ed., N. Kharasch and C.Y. Meyers, Vol. 2, Pergamon Press Inc. (1966) p.367.

245. G. Capozzi and G. Modena, in 'The Chemistry of the Thiol Group', Part 2, Ed., S. Patai, Interscience Publication (1974) p.785.

246. D.T. Clark and A. Dilks, J. Polym. Sci., Polym. Chem. Ed., 957, 17 (1979).

247. H.D. Hagstrum, in 'Technique of Metals Research', Ed., R.F. Bunshak, J. Wiley and Sons, New York (1972).

248. E.E. Muschlitz, Jr. Science, 599, 159 (1968).

249. D. Landini and F. Montanari, Tetrahedron Letters, 269, No. 38 (1964).

250. Chao-Tung Chen and Sou-Jen Yan, Tetrahedron Letters, 3855, No. 44 (1969).

251. F.G. Bordwell and W.H. McKellin, J. Am. Chem. Soc., 2251, 73 (1951).

252. D.T. Clark, A. Dilks and D. Shuttleworth, J. Mater. Sci., 2547, 12 (1977).

253. D.T. Clark, W.J. Feast, W.K.R. Musgrave and I. Ritchie, in Advances in Polymer Friction and Wear, Ed., L.H. Lee, Plenum, New York, Vol. 5A (1975).

254. D.T. Clark, W.J. Feast, W.K.R. Musgrave and I. Ritchie, J. Polym. Sci., Polym. Chem. Ed., 857, 13 (1975).

255. P. Henne and H. Suhr, 'Plasma Desulphurisation of Petroleum', Plasma Chemistry Conference, Limogers, July 12-15 (1977).

256. F.K. McTaggart, Plasma Chemistry in Electrical Discharges, Elsevier, Amsterdam (1967).

257. S.J. Skorini and A. Senning, Phosphorous and Sulphur, 193, 9 (1980).

258. B. Chapman, Ed., Glow Discharges Processes-Sputtering and Plasma Etching, J. Wiley and Sons (1980).

259. G. Francis, Ed., Ionisation Phenomena in Gases, Butterworths Scientific Publications (1960).

260. F.M. Bevilacqua, J. Amer. Chem. Soc., 5394, 5396, 77 (1955).

261. E.M. Bevilacqua, J. Org. Chem., 369, 21 (1956).

262. E.M. Bevilacqua, J. Amer. Chem. Soc., 2915, 79 (1957).

263. E.M. Bevilacqua, Ibid., 5364, 80 (1958).

264. E.M. Bevilacqua, Ibid., 5071, 81 (1959).

265. E.M. Bevilacqua, J. Appl. Polym. Sci., 364, 4 (1960).

266. E.M. Bevilacqua, Ibid., 55, 6 (1962).

267. E.M. Bevilacqua and E.S. English, J. Polym. Sci., 495, 49 (1961).

268. E.M. Bevilacqua, E.S. English and E.E. Philipp, J. Org. Chem., 1276, 25 (1960).

269. E.M. Bevilacqua, E.S. English, J.S. Gall and P.M. Norling, J. Appl. Polym. Sci., 1029, 8 (1964).

270. E.M. Bevilacqua, E.S. English, J.S. Gall and P.M. Norling, Rev. Gen. Caoutchouc Plastiques, 357, 43 (1966).

271. E.M. Bevilacqua, J. Polym. Sci. B. Letters, 1109, 5 (1967).

272. E.M. Bevilaqua, Ibid., 285, C(24) (1968).

273. E.M. Bevilacqua, in 'Thermal Stability of Polymers', Vol. I, R.T. Conley, Ed., Marcel Dekker, New York (1970) p.189.

274. P.M. Norling, T.C.P. Lee and A.V. Tobolsky, Rubber Chem. Technol., 1198, 38 (1965).

275. J.I. Cunneen, Rubber Chem. Technol., 182, 41 (1968).

276. C.L.M. Bell and J.I. Cunneen, J. Appl. Polym. Sci., 2201, 11 (1967).

277. T. Colclough, J.I. Cunneen and G.M. Higgins, J. Appl. Polym. Sci., 295, 12 (1968).

278. D. Barnard, M.E. Cain, J.I. Cunneen and T.H. Houseman, Rubber Chem. Technol., 381, 45 (1972).

279. J.R. Shelton, Rubber Chem. Technol., 359, 45 (1972).

280. J.A. Howard, Rubber Chem. Technol., 976, 47 (1974).

281. D.L. Allara and D. Edelson, Rubber Chem. Technol., 437, 45 (1972).

282. J.R. Morand, Rubber Chem. Technol., 1094, 47 (1974).

283. A.B. Mathur and G.N. Mathur, Polymer, 54, 23 (1982).

284. L. Smith, C. Doyle, D.E. Gregonis and J.D. Andrade, J. Appl. Polym. Sci., 1269, 26 (1982).

285. J.L. Bolland, Quart. Review, 1, 3 (1949).

286. J.L. Bolland, Ibid., 147, 8 (1958).

287. J. Hrivikova, A. Blazkova and L. Lapcik, J. Appl. Polym. Sci., 761, 25 (1980).

288. A. Hoff and S. Jacobsson, J. Appl. Polym. Sci., 3409, 26 (1981).

289. D. Briggs, D.M. Brewis and M.B. Konieczko, J. Mater. Sci., 429, 12 (1977).

290. D. Briggs, D.M. Brewis and M.B. Konieczko, J. Mater. Sci., 1270, 11 (1976).

291. Yu. S. Zuev and A.S. Kuzminskii, Rubber Chem. Technol., 593, 29 (1956).

292. J.R. Dunn, J. Scanlan and W.F. Watson, Trans. Faraday Soc., 667, 55 (1959).

293. A.S. Kuzminskii, Rubber Chem. Technol., 88, 39 (1966).

294. M.L. Studebaker and J.R. Beatty, Rubber Chem. Technol., 450, 45 (1972).

295. B.L. Chan, D.J. Elliot, M. Holley and J.F. Smith, J. Polym. Sci., 61, Symposium No. 48 (1974).

296. M.A. Golab, M.S. Hsu and L.A. Wilson, Rubber Chem. Technol., 953, 48 (1975).

297. B. Stenberg and J.F. Jansson, J. Macromol. Sci-Phys., 143, B19(1) (1981).

298. N.C. Billingham and P.D. Calvert, in 'Development in Polymer Stabilisation-3', Ed., G. Scott, Applied Science Ltd., London (1981).

299. S.L. Malhotra, C. Baillet and L.P. Blanchard, J. Macromol. Sci-Chem., 1427, A12(10) (1978).

300. N. Grassie, 'Chemistry of High Polymer Degradation Processes', Butterworth, London (1956).

301. D. Barnard, L. Bateman, J.I. Cunneen and J.F. Smith, in 'Chemistry and Physics of Rubber-like Substances', Ed., L. Bateman, Maclaren, London, p.593 (1963).

302. C.G. Moore and J. Scanlan, J. Polym. Sci., 23, 43 (1960).

303. N. Grassie, Encyclopedia of Polymer Science and Technology, Interscience, 647, 4 (1966).

304. J.L. Bollan and H. Hughes, J. Chem. Soc., 492 (1949).

305. A.V. Tobolsky and A. Mercurio, J. Amer. Chem. Soc., 5535, 81 (1959).

306. F.R. Mayo, Ind. Eng. Chem., 614, 52 (1960).

307. L. Bateman and J.I. Cunneen, J. Chem. Soc., 1596 (1955).

308. C. Armstrong and G. Scott, J. Chem. Soc. (B), 1747 (1971).

309. N.R. Neureiter and D.E. Bown, I.E.C. Product Res. and Develop., 367, 1, No. 4 (1962).

310. C. Armstrong, F.A.A. Ingham, J.G. Pimblott, G. Scott and J.E. Stuckey, Proc. Int. Rubb. Conf. Brighton, Part F2.1 (1972).

311. J.R. Shelton, in 'Dev. Polym. Stab.', Ed., G. Scott, 23, 4 (1981).

312. C. Armstrong, M.A. Plant and G. Scott, Eur. Polym. J., 161, 11 (1975).

313. C. Armstrong, M.J. Husbands and G. Scott, Ibid., 241, 15 (1979).

314. M.J. Husbands and G. Scott, Ibid., 249, 15 (1979).

315. B.A. Marshall, in 'Stabilisation of Polymers and Stabiliser Process', Ed., R.F. Gould, American Chemical Society, Washington, D.C., 140, 85 (1968).

316. F.A. Ingham, G. Scott and J.E. Stuckey, Eur. Polym. J., 783, 11 (1975).

317. J.E. Stuckey, in 'Developments in Polymer Stabilisation-1', Ed., G. Scott.

318. M.J. Husband and G. Scott, Eur. Polym. J., 879, 15 (1979).

319. J.R. Shelton, in 'Polymer Stabilisation', Ed., W.L. Hawkins, Wiley, New York (1972).

320. J.R. Shelton and E.R. Harrington, Rubber Chem. Technol., 147, 49 (1976).

321. J.R. Shelton, Rubber Chem. Technol., 949, 47 (1974).

322. A.A. Katbab and G. Scott, Polymer Degradation and Stability, 221, 3 (1981).

323. C.f. P.W. Atkins, 'Molecular Quantum Mechanics', Oxford University Press, London (1970).

324. C.f. F.A. Cotton and G. Wilkinson, 'Advanced Inorganic Chemistry', John Wiley, New York (1972).

325. G.M. Bancroft, I. Adams, H. Lampe and T.K. Sham, Chem. Phys. Lett., 173, 32 (1975).

326. R.P. Gupta and S.K. Sen, Phys. Rev. Lett., 1311, 28 (1972).

327. T. Novakov and J.M. Hollander, Phys. Rev. Lett., 1133, 21 (1968).

328. T. Novakov and J.M. Hollander, Bull. Amer. Phys. Soc., 524, 14 (1969).

329. G.K. Wertheim, Mössbaur Effect: Principles and Applications', Academic Press, New York (1964).

330. P. Ascarelli and G. Missoni, J. Elec. Spec., 417, 5 (1974).

331. A. Dilks, Ph.D. Thesis, University of Durham, U.K. (1977).

332. H.R. Thomas, Ph.D. Thesis, University of Durham, U.K. (1977).

333. C.f. R.S. Swingle and W.M. Viggs, CRC Crit. Rev. Anal. Chem., 267, 5 (1975), CRC Press, Cleveland.

334. D.A. Huchital and R.T. McKeon, Appl. Phys. Lett., 158, 20 (1972).

335. D.T. Clark, A. Dilks, D. Shuttleworth and H.R. Thomas, J. Polym. Sci., Polym. Chem. Ed., 627, 17 (1979).

336. D.T. Clark, Physica Scripta (Sweden), 307, 16 (1977).

337. T.A. Carlson and G.E. McGuire, J. Elec. Spec., 161, 1 (1972).

338. C.S. Fadley, R.J. Baird, W. Siekhaus, T. Novakov and S.A.L. Bergström, J. Elec. Spec., 93, 4 (1974).

339. J.H. Scofield, Lawrence Livermore Laboratory Report UCRL, 51326, Jan. (1973).

340. J.H. Scofield, J. Elec. Spec. Rel. Phenom., 129, 8 (1976).

341. J. Cooper and R.B. Zare, J. Chem. Phys., 942, 48 (1968).

342. F.O. Ellison, J. Chem. Soc., 507, 61 (1974).

343. J.J. Huang, J.W. Rabalais and F.O. Ellison, J. Elec. Spec. Rel. Phenom., 85, 6 (1975).

344. D.R. Penn, J. Elec. Spec. Rel. Phenom., 29, 9 (1976).

345. D.T. Clark and D. Shuttleworth, J. Polym. Sci. Polym. Chem. Ed., 1093, 16 (1977).

346. D.T. Clark and H.R. Thomas, J. Polym. Sci. Polym. Chem. Ed., 2843, 15 (1977).

347. C.f. D. Shuttleworth, Ph.D. Thesis, University of Durham, U.K. (1978).

348. C.D. Wagner, L.H. Gale and R.H. Raymond, J. Vac. Sci. Tech., 518, 15 (1978).

349. A.F. Carley and R.M. Joyner, J. Elec. Spec. Rel. Phenom., 1, 16 (1979).

350. R.M. Eisenberg, in 'Fundamentals of Modern Physics', Chapter 14, J. Wiley and Sons, New York (1981).

351. B.L. Henke, Adv. X-ray Analysis, 1, 13 (1969).

352. E.M. Purcell, Phys. Rev., 818, 54 (1938).

353. J.C. Helmer and N.H. Weichert, Appl. Phys. Lett., 268, 13 (1968).

354. C.f. H. Seigbahn, L. Asplund, P. Kelfve and K. Seigbahn, J. Elec. Spec. Rel. Phenom., 411, 7 (1975).

355. K. Seigbahn, J. Elec. Spec. Rel. Phenom., 3, 5 (1974).

356. G.M. Bristow and W.F. Watson, Trans. Faraday Soc., 1731, 54 (1958).

357. R.J. Chang and A.N. Gent, J. Polym. Sci. Polym. Physics Ed., 1619, 19 (1981).

358. R.J. Chang and A.N. Gent, J. Polym. Sci. Polym. Physics Ed., 1635, 19 (1981).

359. W.V. Chang, J. Appl. Polym. Sci., 1759, 26 (1981).

360. A. Pines, M.G. Gibby and I.S. Waugh, J. Chem., 569, 59 (1973).

361. S.R. Hartmann and E.L. Hahn, Phys. Rev., 2042, 128 (1952).

362. W.J. Van Ooij and A. Kleinhesselink, Applications of Surface Science, 342, 4 (1980).

363. H.Y. Chen. Anal. Chem., 1134, 34 (1962).

364. H.Y. Chen, Anal. Chem., 1793, 34 (1962).

365. H.Y. Chen, J. Polym. Sci., Part B, 891, 4 (1966).

366. W. Hofmann, 'A Rubber Review for 1963, Nitrile Rubber', Rubber Chem. Technol., XXXVII, Part 2 (1964).

367. T.C.P. Lee and S.H. Morrell, 'Network Changes in Nitrile Rubber at Elevated Temperatures', RAPRA Research Report 201, May 15 (1972).

368. D.C. Coulthard and W.D. Gunter, 'New Compounding Approaches to Heat Resistant NBR', presented at a meeting of the Rubber Division, American Chemical Society, October 7-10 (1975).

369. B.A. Dogadkin, K.G. Kuanyshev and V.E. Gul, Koll. Zh., 310, 25 (1963).

370. D.S. Everhart and C.N. Reiley, Surface and Interface Analysis, 126, 3, No. 3 (1981).

371. J.I. Cunneen, J. Appl. Chem., 353, 2 (1952).

372. E.J. Cluff and E.K. Gladding, J. Appl. Polym. Sci., 290, 3 (1960).